01 Jan 2004

Opportunities for Undergraduate Research Experiences (OURE) Research Papers 2004-2005 Volume III

Sandeep Pedam

Bren Phillps

Eric Pieper

Andrew Ricke

et. al. For a complete list of authors, see https://scholarsmine.mst.edu/oure/160

Opportunities for Undergraduate Research Experiences (OURE)

Research Papers

2004 -2005

Volume III

(Pe – Z)

Opportunities for Undergraduate Research Experience (OURE)
Research Papers – 2004-2005
Volume-III
INDEX (Pe - Z)

This volume includes 2004-2005 OURE research papers authored by the following students (listed alphabetically by student's last name)

Study of the Dynamic Response of Human Skull Impact on Laminated Automotive Glazing

ABSTRACT

During vehicle accident, occupants head impacting on windshield or side window is commonly observed. It is estimated that over 40,000 people are killed annually in vehicle related accidents in the United States. Use of laminated glass which consists of two soda lime glass plies adhered by a polyvinyl butyryl (PVB) interlayer on automotive windshields and side windows can reduce the possibility of body injury and property damage caused by flying glass fragments. Most of the previous work on laminated glass under head impact has primarily concerned the dynamic response of head rather than the laminated glazing. Any attempt to design glazing that minimizes injury to and death of occupants during a vehicle accident requires a thorough understanding of the mechanical behavior of automotive glazing subjected to head impact loads.

A 3-D nonlinear dynamic finite element model is developed to study the dynamic response of a laminated glazing subjected to simulated head impact. An analytical solution based on the large-deflection plate theory is presented to compare with the FEA result. The crack initiation time and location are determined using a finite element method based on the energy release rate criterion (*J*-integral criterion). A constitutive model based on the continuum damage mechanics (CDM) is employed and implemented into the finite element model to study the failure and impact resistance of laminated automotive glazing. The damage patterns and zone size are predicted. The CDM based constitutive model has been extended to investigate the failure behavior of a laminated architectural glazing subjected to blast loading.

Notations:

a	glass panel length (m)
b	glass panel width (m)
E	Young's modulus (MPa)
Go	Short time shear modulus (MPa)
Gω	long time shear modulus (MPa)
G(t)	Stress relaxation modulus (MPa)
h	total thickness of glass panel (m)
hi	impact side glass ply thickness (m)
ho	non-impact side glass ply thickness (m)
hp	PVB thickness (m)
hs	skin thickness (m)
K	bulk modulus (MPa)
Ks	spring constant for the plate
P(t)	surface pressure (MPa)
P	contact force (N)
Po	maximum contact force (N)
Ro	maximum radius of contact area (m)
R	radius of aluminum skull (m)
T	time (s)
2to	impact duration (s)
Vo	initial impact velocity (m/s)
w	plate bending deformation (m)
wo	plate maximum bending deformation (m)
β	decay factor (s-1)
v	poisson's ratio
ρ	density (kg/m3)

Introduction:

In 1995, The National Highway Traffic Safety Administration (NHTSA) documented research establishing the problem size and the potential benefits of preventing occupant ejection through front side windows during accidents. A prototype system made of a modified door and glazing materials was built and tested for this research. This research was primarily concerned with the dynamic response of the head during impact.
Further study was conducted at the University of Missouri-Rolla in this subject which is mentioned in detail in this report. 3-d models were simulated using finite element software (ABAQUS) and results were obtained on different simulated specimens.

Finite Element model:

Dr. Dharani and Ji developed a 2-D axisymmetric model to simulate the human head, in which a solid aluminum sphere (skull) is covered with a viscoelastic skin. The skull density is 2150 kg/m3 and comparable to that of aluminum which is 2700 kg/m3. So the skull is modeled as

aluminum. In this paper, a three dimensional featureless headform model is developed to simulate the occupant's head impacting on the automotive glazing.
Same two-phase headform model is used in which the solid aluminum sphere representing the skull is covered with a viscoelastic skin. Both the skull and skin are deformable. The viscoelastic parameters of the skin used by Dr. Dharani and Ji are also used in the present work. A typical three layer glazing system, consisting of two soda lime glass plies separated by PVB interlayer glazing system, consisting of two soda lime glass plies separated by a PVB interlayer is considered. The interlayer bond is assumed to be perfect with no slipping between the layers during impact. The idealized impact problem under consideration is one where ho is the non-impact side glass ply thickness, hi is the impact side glass ply thickness, hp is the thickness of PVB interlayer, a is the length of the plate and b is the width of the plate. R is the radius of the aluminum skull, hs is the thickness of viscoelastic skin on the skull Vo is the initial velocity of impact. The laminated glass plate is simply supported along its entire perimeter to simulate the service condition. The impact problem is solved by using dynamic nonlinear finite element package ABAQUS.
The glass plies and aluminum sphere are modeled as linear elastic materials. The skin is modeled as linear viscoelastic material the stress relaxation modulus G(t) is assumed to be of the form
$G(t) = G\omega + (Go-G\omega)e^{-\beta t}$
Where e is the base of the natural logarithm, Gω is the long time shear modulus, Go is the short time shear modulus, β determines how fast G(t) decays from Go to Gω.
In the previous study, the PVB interlayer was modeled as a linear viscoelastic material. The impact duration is in range of milliseconds, the stress relaxation modulus G (t) of PVB changes very little during this short duration. In this short time, PVB behaves like a glass solid. PVB could be modeled as a linear elastic material. This assumption would not only make the problem amenable for a close-form solution but also results in significant reduction in computing time. Therefore, PVB is modeled as linear elastic in the present study with a shear modulus Go and with bulk modulus K. The elastic modulus E and poisson's ratio v are given by:

$E = (9KGo/(3K+Go))$ (1)
$V=((3K-2Go)/(6K+2Go))$ (2)

Objective:

This study was based on the dynamic response of a laminated glazing subjected to simulated head impact. Using 3-d nonlinear dynamic final models to response of a laminated glazing subjected to simulated head impact, results were procured and have been presented in this report. Tests were conducted on three different cases – 2D head impact, 3D head impact with a monolithic glass and a 3D head impact with a laminated glass.

Designing the model:

Using the finite element analysis software, the model was designed. It was split into two parts – the head and the laminated glass. Alternatively, the head was modeled out of a hollow sphere, not taking into account the brains of the specimen since that is not of primary concern in this report. The head was modeled out of two layers – the outer layer comprising the skin and the inner layer being the skull itself.

The laminated glass had three parts to it, the outer and innermost layers being the laminated glass itself and a layer of polyvinyl butyryl (PVB) in between them.

Assembly:

The head was modeled out of a solid revolution part the skin and the skull was assigned a "tie" constraint to each other. This way the software would treat both parts as one and would react as one single unit while performing the finite element analysis. Similarly, the three glass layers (in case of a laminated glass setup) were tied to one another for the same reason. In case of a monolithic glass setup, there was only one glass layer and hence there was no need of assigning a tie constraint to the glass setup. The head is place atop the glass setup and tests are run on this assembly.

Results and Discussions:

A baseline case representing a typical automotive glazing impact situation was set. Various parameters were varied from the baseline value (while holding all the other parameters fixed) to determine their effectiveness in reducing the magnitude of stress in the laminate.
The tensile strength of common glass objects (bulk glass) is relatively low and varies from 20 to 100 Mpa. But the compressive strength is substantially higher, by almost a factor of 10 or even more. The tensile strength of car windows can be increased from 300-500 MPa with special processes involving thermal or chemical toughening. The duration of stress during impact loading is normally 10^{-2} to 10^{-5} s. The glass strength under these conditions is increased by a factor of 2. The tensile strength of the laminated automotive glazing under head impact loading conditions could be as high as 1 GPa.

Laminated glass vs. monolithic glass
The thickness of monolithic panel was the same as that of a laminated panel which is 4.76 mm. All these parameters have been described in Table 1. The maximum principal stress and central deflection of laminated glass were greater than those of the monolithic glass. This is because the PBV interlayer had almost negligible stiffness when compared to that of the glass ply.

Parametric study:

When considering the effect of a parameter on the maximum principal tensile stress only this parameter was varied while keeping all other parameters same as the baseline configuration. The initial impact velocity varied from 3.34 m/s to 20 m/s. The proper law fit showed that the maximum principal stress is almost proportional to V.
The effects of impact side glass ply thickness on the maximum principal tensile stress. As expected, the thicker impact side ply meant lower maximum principal tensile stress. Increasing the non-impact side glass poly thickness beyond 2 mm decreased the maximum principal tensile stresses at crucial points.
The effects of thickness ratio of impact side ply to non-impact side ply on the maximum principal tensile stress. The total thickness of the plate is the same as the baseline value (h=4.76 mm). The maximum stress corresponds to hi/ho=0.6. For thin laminate with h=4.76 mm and hp=0.76mm, the worst combination would be hi=1.5mm and ho=2.5 mm. After the peak value,

the stress is reduced significantly with increasing thickness ratio. It indicated that reducing the non-impact side ply thickness and increasing the thickness to the impact side ply while keeping the total glass thickness as a constant is a good way to increase the impact resistance of the glazing system without increasing the total glass thickness.
The effect of PVB thickness on the maximum principal tensile stress was also studied. The results indicate that PVB thickness has no significant effect on the maximum principal tensile stress. There is no additional benefit by using PVB interlayer in the laminated automotive glazing.
In the baseline case, the panel area is 600 X 400 mm. In order to study the effect of panel area on the dynamic response, another glass panel with area 700 X 500 mm is now compared with the baseline case. Incerase in the plate area results in lower maximum principal stress This means that the larger plate would suffer less damage than a smaller plate with all other parameters held constant. When subjected to the same impact load, since the larger plate is more flexible, the central deflection is larger than that of the smaller panel. The stresses in the larder plate are therefore lower.
Three different laminate configurations with same panel area are used to study the effect of laminate aspect ratio a/b on the dynamic response. The laminate aspect ratio has negligible effect on the dynamic response.

Table 1. Baseline headform, material, impact and panel parameters.

	Parameter and Properties
Skull	(Aluminum)E=70GPa, ρ = 2700kg/m^3, v=0.29
Skin	Go=6 GPa, Gω =1 GPa, K = 540GPa, ρ =1100kg/m^3, β = 3800s^{-1}
Glass	E=72 GPa, ρ = 2500 kg/m3, v= 0.25
PVB	Go=0.33GPa, Gω=0.69X10^{-3} GPa, K=20GPa, ρ=1100Kg/m^3, β=12.6 s^{-1}
Configuration	Panel dimensions (a X b): 600 mm X 400 mm Laminated panel: h = 4.76 mm, ho=h1=2mm, hp=0.76 mm Monolithic panel: h =4.76 mm Head form: R=72.3 mm, head mass = 4.5 kg, skin thickness hs = 3mm Initial impact velocity Vo=6.67 m/s

Acknowledgements

I would like to express my gratitude to the following people for their support and assistance during the course of this project:

Dr. Dharani,Lokeswarappa R
Professor of Mechanical and Aerospace Engineering
1870 Miner Circle
229 Mechanical engineering building
Rolla, MO 65409

Shuangmei Zhao
Graduate Research Assistant
Materials Research Center
1870 Miner Circle
101 Straumanis Hall
Rolla, MO 65409

Determination of Cadmium and Gold Concentrations Utilizing Neutron Activation Analysis

Bren Phillips
OURE 2004-2005
Nuclear Engineering Department
4 April 2005

Executive Summary

The purpose of this experiment was to build a baseline for comparison for cadmium and gold concentrations using neutron activation analysis. This baseline can be used in the future to find the concentration of cadmium and gold in samples with unknown concentrations such as determining the amount of these elements in aerogels that are being used to absorb these metals out of solution.

Neutron Activation Analysis was used by bombarding samples of known concentrations of cadmium and gold with neutrons using the UMR reactor. Then the radiation emitted from the activated isotopes could be measured using a germanium detector and a trend established for various concentrations of these elements.

The samples were solutions of cadmium and gold ranging from 5E-5 molar to 1.0 molar solutions. These samples were packaged using centering devices in the vials to ensure that the samples were irradiated in the same manner time after time. The samples were then irradiated at 20 kW or in a thermal flux of approximately 1.86E11 n/cm^2/s. The irradiation time varied depending on the metal – 15 seconds for cadmium and 30 seconds for gold.

The samples were then counted on a germanium detector again using centering devices to ensure consistent placement of the samples relative to the detector. The samples were counted for 10 minutes of live time. Live time counts compensate for the time the detector is busy from detecting a previous count.

The gold samples consisted of two different chemical formulas. The first was HAuCl4 and the second was KAuCl4. These two different sets created different results, which was not expected because NAA is independent of the chemistry of the substance. The conclusion was that one of the sample sets was incorrectly prepared but at this point, which set was incorrect has not been determined, but both samples followed the same linear trend.

Cadmium and gold were both easily detectable using NAA. The trend for both of these materials was linear which agrees with the theory for short irradiations such as these. The standard deviation of most of the sample sets was between 2.5% and 5.0%. The only sets that did not fall within this range had too few samples to create an acceptable statistical base.

NAA should be able to be used to detect cadmium and gold in unknown samples without difficulty. The baseline created here can be used in the future to determine the concentration of these elements in unknown samples.

Table of Contents

Introduction

The purpose of this project is to show that neutron activation analysis (NAA) can be used to quantitatively determine the amount of various metals in a sample. This project specifically addresses Cadmium and Gold and their detection using NAA.

This project has the goal of building a baseline comparison from samples containing Cadmium and Gold in known concentrations. The results from this project may be used to determine the amount of Gold and Cadmium collected in aerogels that are being used to trap metals such as cadmium and gold out of solution.

Background

Neutron activation analysis (NAA) is a qualitative and quantitative method of identifying elements that make up a sample. The elements present can be identified by the types of radiation they emit, the energy of the radiation, its intensity, and the half-life. For this research gold and cadmium were irradiated to create a benchmark for their detection[1].

The first step is to determine the nuclear reaction that will take place and be measured. In this case the University of Missouri Rolla Reactor was used as a neutron source for irradiation so (n,γ) reactions were used. In this reaction the sample is bombarded by neutrons in the reactor and some of the sample atoms absorb neutrons and are activated to an excited state. The two reactions used are shown below in Eq. 1 and Eq. 2[2].

$$^{110}Cd(n,\gamma)^{111m}Cd \qquad \text{(Eq. 1)}$$

$$^{197}Au(n,\gamma)^{198}Au \qquad \text{(Eq. 2)}$$

The sample is packaged and irradiated in the reactor as specified in the procedure. The sample is irradiated and the excited nuclei then release their energy by giving off gamma radiation that can then be measured using a high purity germanium detector attached to a Multi-Channel Analyzer. Each isotope has specific energies that it emits, and the energy and intensity can be recorded by the gamma spectroscopy system.

When a sample is irradiated the activation of the sample is given by the activation equation as shown in Eq.3. This equation assumes that a small number of the target nuclei are transmutated so that the total number of target atoms stays essentially the same. This also assumes that the isotope formed is destroyed by decay only and not by neutron absorption. Finally, this formula also assumes that the flux is uniform throughout the target.

$$A(t_0) = a_i N_i \sigma_i \phi (1 - e^{-\lambda_{i+1} t_0}) \qquad \text{(Eq. 3)}$$

Where:

$A(t_0)$ = Activity after irradiation
a_i = Weight fraction of an isotope of interest
N_i = Number of atoms of the element of interest in the sample
σ_i = Cross section for the reaction of interest
ϕ = Thermal neutron flux
λ_{i+1} = Decay constant for element created
t_0 = Irradiation time

Equipment Used

The Equipment used to take the measurements is shown in Table I along with their electronic settings. The equipment shown in the table is the equipment used with the germanium detector at the UMRR.

Table I: Type, Manufacturer, Model and Settings of Equipment Used

Instrument	Type	Manufacturer and Model	Electronic Setting	Remarks
Detector	Ge	CANBERRA		
HVPS		CANBERRA Model 3105	+4400 V	
Preamplifier		CANBERRA		
Amplifier	Fast Spectroscopy	CANBERRA 2024		
Analog to Digital Converter (ADC)		Canberra 8077	0.3 V discrimination	
NIM Bin		CANBERRA Model 2000		
Data Acquisition Software		CANBERRA Genie 2000 Version 1.3, May 15, 1999		

The system at the reactor is constantly setup with the high voltage applied and the detector cooled with liquid nitrogen. The signal originates from the Ge crystal where a gamma interaction creates an electron and a hole. The electron and hole then move under the influence of the electric field and are collected. The pulse is then amplified about 10

times and impedance matched to the amplifier by the preamplifier. The amplifier then amplifies the signal about 1000 times. The signal then goes to the Analog to Digital Converter (ADC) that changes the pulse into a channel number and then a count is stored in that channel by the Genie 2000 program. Figure 1 shows a diagram of the experimental setup.

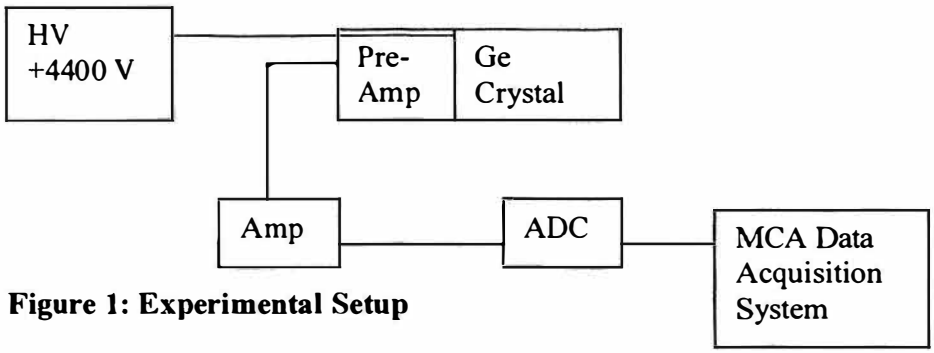

Figure 1: Experimental Setup

Procedure

The first step is to have the solutions to be irradiated prepared. Different concentrations of both cadmium and gold were prepared and irradiated. Concentrations tested for both Cadmium and gold are shown in Table II.

Table II: Concentrations of Gold and Cadmium Irradiated

	Chemical Form	**Concentrations Tested (M)**	**Irradiation time**
Cadmium	$CdNO_3$	0.001, 0.01, 0.1, 0.25, 0.5, 1.0	15 seconds
Gold	$HAuCl_4$ & $KAuCl_4$	5E-5, 1E-4, 5E-4, 1E-3, 2E-3, 1E-2	30 seconds

After the solutions are prepared the next step is to package the sample. NAA is very sensitive to contamination so this step is very sensitive requiring very careful handling to ensure that neither the sample nor the packaging gets any foreign substances on them. The packaging was mostly made of thermoelastic polymers, most of which were composed of polyethylene. This makes an excellent packaging material because it absorbs very few neutrons and is very light which makes it capable of being used in the reactor's pneumatic transfer system for irradiation. Problems arose with consistency of the results so a centering device was created for use in the vial used in the pneumatic transfer system and kept the sample centered in the vial at all times. Figure 2 shows the different packaging used, but does not show the centering device.

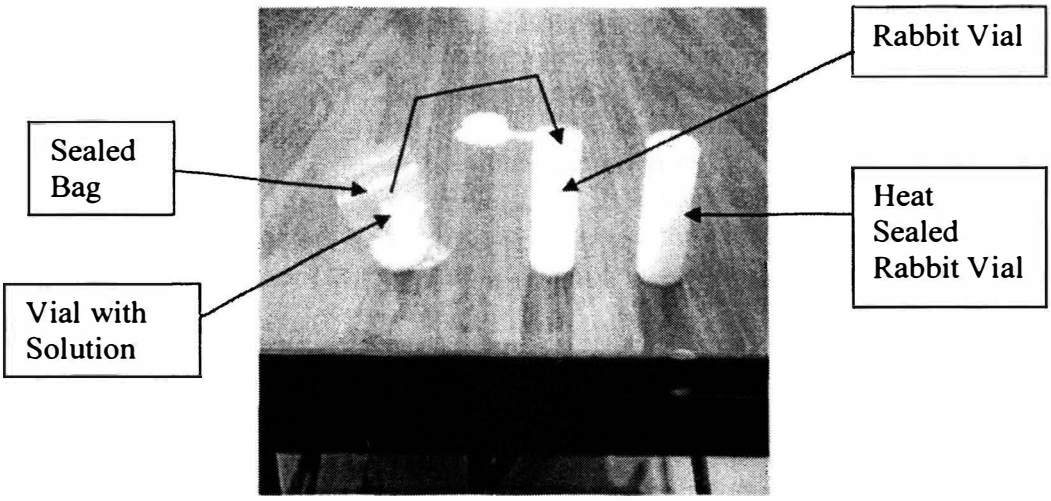

Figure 2: Sample Irradiation Configuration

Each of the small vials with the solution was filled with 1.0 ml of the solution to be irradiated and then sealed in the plastic bag shown. This was then placed in the centering device that is not shown, which was then placed in the rabbit vial and heat-sealed. The centering device for the rabbit vial was deemed necessary after consistent results could not be obtained without it. The centering device keeps the small vial centered in the rabbit vial at a consistent height. This way no matter how the vial is placed next to the reactor, the sample will always be the same distance away from the core. Each of the different pieces of packing are thoroughly cleaned with rubbing alcohol and handled with gloves prior to being packaged to ensure that there is a minimum of contamination on the packaging that could be activated and produce unwanted activity.

This vial can then be sent to the core using the pneumatic transfer system. This pneumatic transfer system has several advantages. First it allows for the sample to be inserted and removed very quickly, which allows for accurate irradiation times. Also, the tube is not much larger than the vial so samples can be irradiated with a consistent geometry sample after sample.

After the sample is prepared and labeled it is then irradiated at 20 kW, or a thermal flux of 1.86E11 n/cm^2/s, for the appropriate amount of time – 15 seconds for the Cadmium samples and 30 seconds for the gold samples. During all of the irradiations the shim rods of the reactor were kept as close as possible to 21.7 inches with the regulating rod being positioned where necessary to maintain criticality. Also, the power indication display on the picoammeter was kept as close to 10.26 as possible while the irradiation was taking place.

When the sample returned from the core and was determined safe to handle it was placed in an overpack, which also had a centering device designed for the rabbit vial. The overpack was used so that the contaminated sample could be handled and counted easily without spreading contamination.

The overpack was then placed on the detector, which has yet another centering device designed to keep the overpack centered on the detector. Then two minutes after the return of the sample the sample was counted for 10 minutes of live time. A live time count counts for extra time to make up for the amount of time the system misses counting

radiation because it is recovering from the last count. In a gamma spectroscopy system most of this time is taken by the multichannel analyzer to store the data in the appropriate channel. The dead time increases as the activity level of the sample increases. For samples that have a long half-life this approximation for making up for dead time is very accurate. The gold nuclide being measured has a half-life of about 2.7 days so the dead time is not even a consideration. The cadmium has a half-life of about 48.5 minutes so as long as the dead time correction is a small percentage of the counting time the error is small. When the count is completed the data is saved and the next sample can be irradiated.

Data and Observations

A typical gamma spectrum for the Cadmium is shown is Figure 3. The radioactive nuclide of cadmium that was measured is Cd-111m, which is a metastable isotope of Cadmium that has the same mass as the stable nuclide of Cd-111, but the nucleus has extra energy. The nucleus releases this extra energy in the form of gamma rays and then becomes the stable Cd-111 nuclide. This nuclide releases two prominent gamma rays. The first is at 150.81 keV with a probability of 30.9% and the second is at 245.39 keV with a probability of 94.0%. The second peak is more probable and therefore is used in all the calculations.[3]

A typical gamma spectrum for the Gold is shown in Figure 4. The radioactive gold nuclide that is being measured is Au-198. This isotope only has one prominent gamma ray and it has an energy of 411.8 keV with a probability of 95.5%. This nuclide eventually decays by beta minus emission into Hg-198, which is a stable isotope.

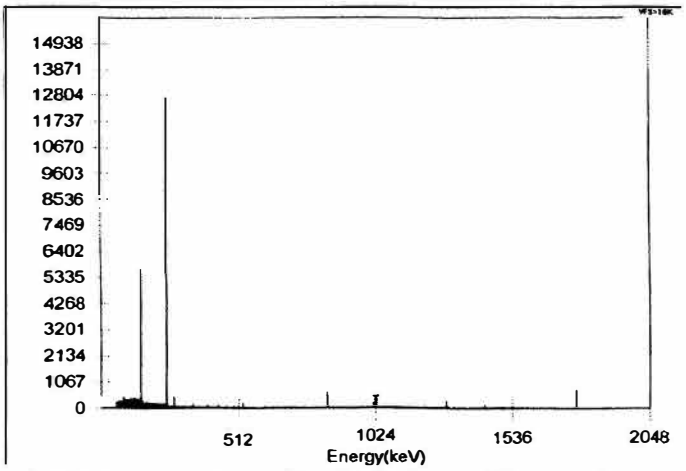

Figure 3: A typical gamma spectrum for Cadmium. The two large peaks are both from the radioactive Cadmium isotope.

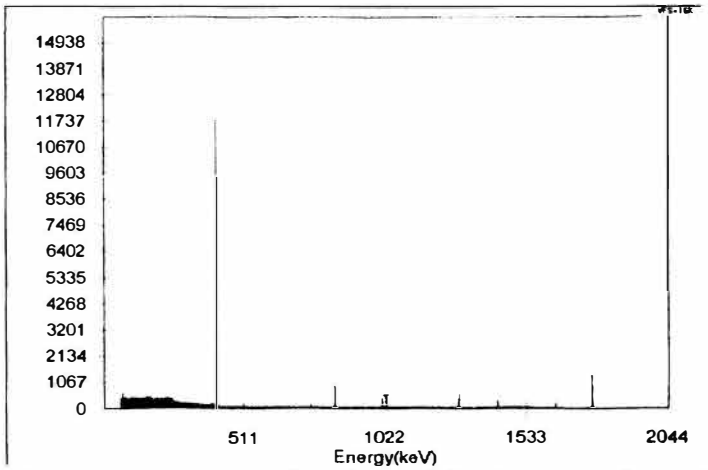

Figure 4: A typical gamma spectrum for Gold. The large peak on the left is the peak for the radioactive gold isotope.

The data is then reduced to a set of x-y data points of channel and counts. The following formula is then used to calculate the net peak area for the count. This formula sums the counts within three full widths at half maximum (FWHM) and then subtracts the counts at 1.5 times the FWHM (also denoted as Γ) on either side of the peak. This removes the extra gross radiation from the peak that is not caused by the isotope of interest. This is also depicted in Figure 5[1].

$$NPA = G - B_L - B_R \qquad \text{(Eq. 4)}$$

Where:

NPA	= Net Peak Area
G	= Gross counts within three times the FWHM
B_L	= Background levels to the left of peak within 1.5 times FWHM
B_R	= Background levels to the right of peak within 1.5 times FWHM

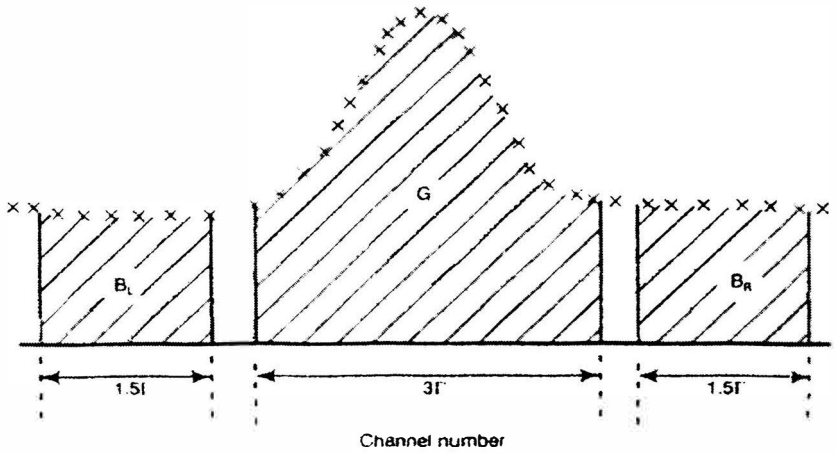

Figure 5: Determination of the net area under the peak using Eq. 3.[1]

At this point the regular background radiation when the sample is not present could also be subtracted out. However, the background level is so low because of excellent shielding that background without the sample was ignored. The background would only amount to 10 or less counts over a 10-minute period and when dealing with thousands of counts this level is negligible. Also, the background radiation spectrum is relatively flat without peaks so the net peak area calculation method takes care of the background.

After the net peak counts is calculated for each of the samples, then the data can be plotted and the standard deviation of each of the sample sets calculated. Table III shows the cadmium data and Figure 6 shows the plot of the cadmium data.

Table III: CdNO3 net peak areas.

Sample for Concentration	0.001 Molar	0.01 Molar	0.10 Molar	0.25 Molar	0.50 Molar	1.00 Molar
1	38	759	6988	17880	31772	53886
2	18	722	7280	19183	30562	52871
3		708	6770	18798	33509	48176
4		723	7207	18944	30710	53684
5		772	7342	18013	33352	48956
6					33071	57653
7					33288	56936
8					32060	54801
9					30782	54957
10					34263	54868
11						53489
12						55072
13						52181
14						55327
15						57514
16						53215
17						55645
18						54689

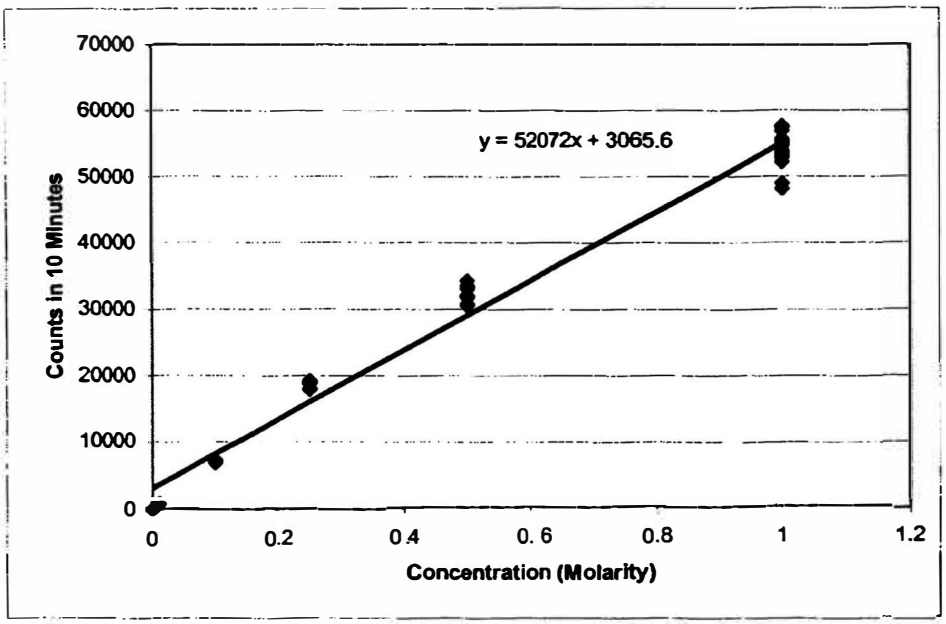

Figure 6: Cadmium data plotted for the various concentrations.

From Table III and Figure 6 it can be seen that the standard deviation for the different sample sets is relatively low and this is shown in Table IV. The only concentration that has a high error is the 0.001 molar solutions and this is because there were only 2 samples done for this concentration and this is at the lower limit of the detection threshold for cadmium.

Table IV: CdNO3 standard deviation data.

	0.001 Molar	0.01 Molar	0.10 Molar	0.25 Molar	0.50 Molar	1.00 Molar
Standard Deviation	34.96%	3.31%	2.96%	2.80%	3.93%	4.65%

The same reduction was done for the data for the Gold solutions. However, two different chemical forms of gold were used – $HAuCl_4$ and $KAuCl_4$. These yielded different results and the reason for this is not yet known. Presumably, one of the sets of solutions was prepared incorrectly but it has not yet been determined which one was incorrectly prepared. Additional solutions will have to be prepared to determine which one is correct. The $HAuCl_4$ data is shown in Table V plotted in Figure 7 and the $KAuCl_4$ data is in Table VII and plotted in Figure 8.

Table V: HAuCl4 net peak areas.

Sample for Concentration	5E-4 Molar	1E-3 Molar	2E-3 Molar
1	23209	39734	82175
2	22949	40358	81080
3	22170	39862	83198
4	23495	38860	78665
5	23521	41281	85040
6		40802	
7		38569	

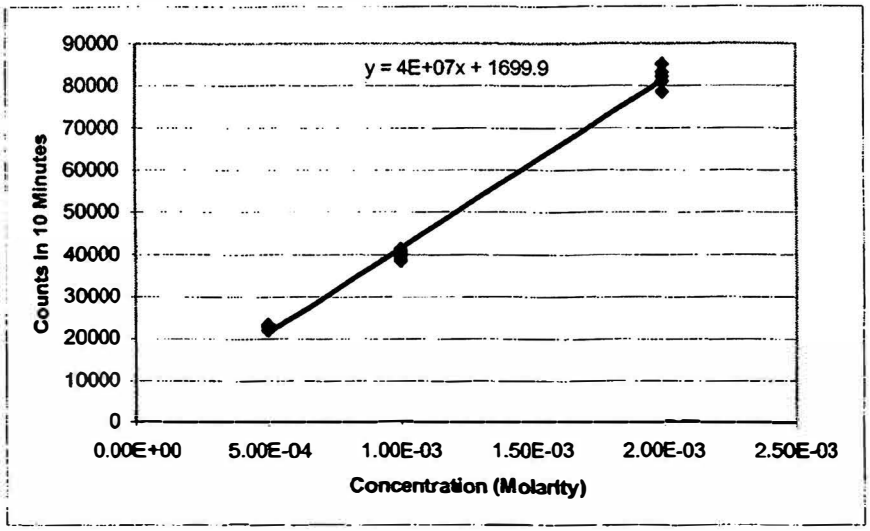

Figure 7: Gold data for HAuCl4 for various concentrations.

Again the standard deviation is quite small for the HAuCl4 samples and is shown in Table VI.

Table VI: HAuCl4 standard deviation data.

	5E-4 Molar	1E-3 Molar	2E-3 Molar
Standard Deviation	2.15%	2.28%	2.60%

Table VII: KAuCl4 net peak areas.

Sample for Concentration	5E-5 Molar	1E-4 Molar	1E-3 Molar	1E-2 Molar
1	483	1046	8998	81924
2	574	845	9790	85241
3	518	869	8849	86212
4	508	887	9592	
5	532		8953	
6			9479	

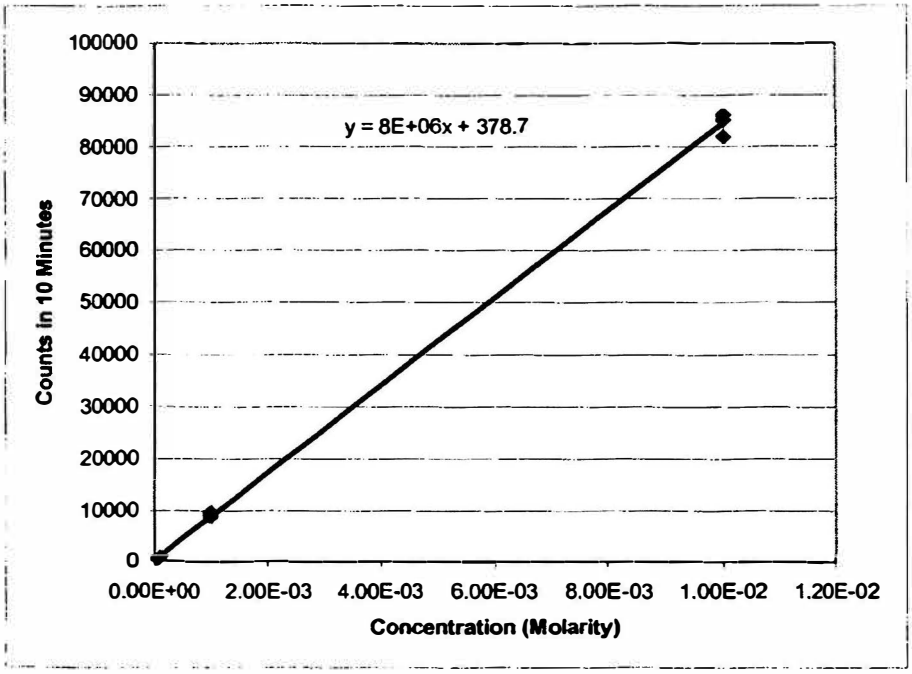

Figure 8: Gold data for KAuCl4 for various concentrations.

The standard deviation data for the different concentrations is shown in Table VIII.

Table VIII: KAuCl4 standard deviation data.

	5E-5 Molar	1E-4 Molar	1E-3 Molar	1E-2 Molar
Standard Deviation	5.76%	8.66%	3.86%	2.17%

The two gold solutions can also be plotted together to see the difference in the counts recorded for the same molarity.

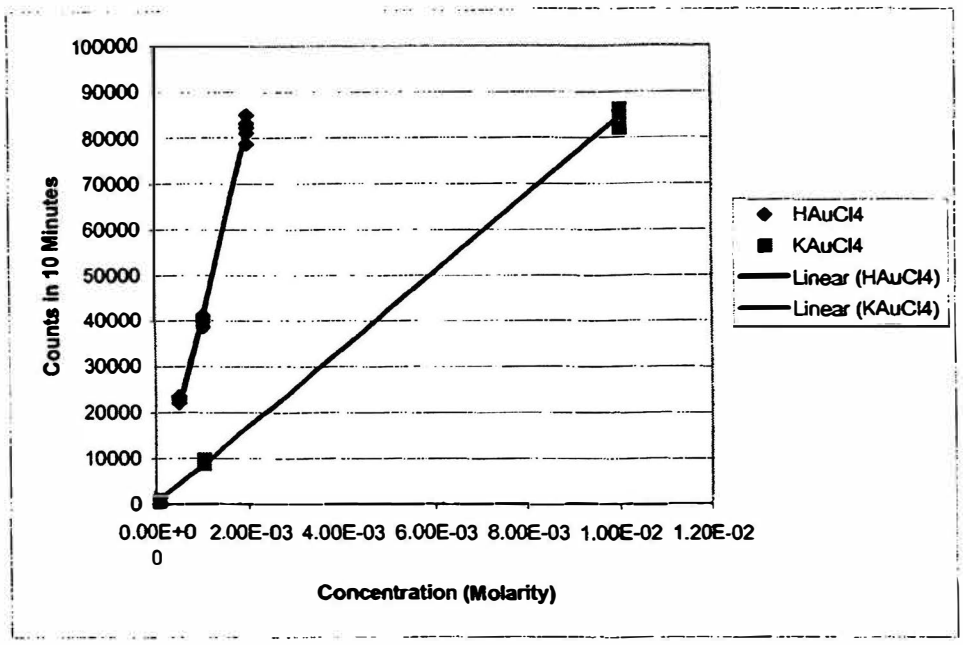

Figure 9: $HAuCl_4$ and $KAuCl_4$ data plotted together.

Conclusions

The counts recorded for the Cadmium and the Gold were both linear. This was theoretically predicted since the irradiation time is short compared to the half-lives of the isotopes and because such a small number of the target nuclei are transmutated into radioisotopes.

This method of using NAA should be able to be used to determine amounts of these metals in other samples. A baseline can be established using these known solutions and from that an unknown solution's concentration should be able to be determined based on the number of counts recorded under the same circumstances as the known solutions.

Acknowledgements

I would like to thank Dr. Massimo Bertino and Dr. Akira Tokuhiro for their guidance on this project and all of their help. Chuck Williams also deserves thanks for all of his help on collecting much of this data. Finally, I would like to thank the staff of the UMR reactor for operating for me for the many hours it took to gather all of this data.

References

1) Tsoulfanidis, Nicholas. Measurement and Detection of Radiation. Washington D.C.: Taylor & Francis, 1995.

2) Baum, Edward; Harold Knox; Thomas Miller. Chart of the Nuclides 16th Edition. KAPL 2002.

3) Hacker, Charles. *Radiation Decay*. Software, Ver 3.6. May 4, 2001.

High Strength Epoxy as an Alternative to Welding

Eric Pieper
University of Missouri-Rolla

Abstract

This research was performed to explore the possibility of using epoxy joint connections in place of welded connections in a tube frame structural design. Welded connections work very well when the frame is made of steel, aluminum or titanium. Carbon fiber tubes are available and have a higher strength-to-ratio than the metal tubes, but the connections cannot be welded. The long term goal of this research is to be able to use carbon fiber tubing to construct the solar car chassis.

A junction made using high strength epoxy to bond an insert into the adjoining tubes can be almost as strong as a tube that has not been cut. Using a 6061-T6 aluminum tube, an insert of the same material, and Araldite 2015 two-part epoxy the junction was almost as strong as a welded connection in two different types of tests. In a 3-point bending test a sample with the glued joint yielded at bending stresses of 10 to 20 ksi. In a torsion test the glue yielded at shear stresses of 4.5 to 10 ksi. A welded connection will typically yield at 16 ksi in bending and 8 ksi in shear. Since the results are so close to the strength of welded connections, this method may be examined as an alternative to welding in some instances.

Introduction

At present the best way of joining metal tubes into a space frame structure is through welding. This method works fine when using similar metals and metals that have properties suitable to welding. If neither of these are these are the case it becomes very

difficult to join the materials. Many times a specialized welding machine must be used to join the metals. Regardless of how many parts are to be manufactured, the welding machine has to be used for each.

When looking for a lightweight material with high strength properties it is very possible to find several different materials that do not have the ability to be welded. It may also be that a combination of materials needs to be used throughout the structure to achieve the greatest strength while maintaining the lightest weight. For these instances an acceptable and affordable substitute is not always available.

Epoxies have been used in the aerospace industry for several decades. Despite this, not much testing has been done for using glued joints as a replacement to the welded joints. Epoxy allows the user to be more flexible with materials used. Many epoxies will bond to a variety of materials. This makes it much less expensive to join materials that would have previously required large setup costs. For small production runs the parts can be glued by hand however, if the number of parts to be produced is large then an automated machine can be purchased to apply the epoxy.

Experimental Setup

For the experiment two different tests were conducted to determine the strengths of the samples. The first test was a three-point bending test. This was used to determine the stress at which the glue bond would break while in bending. The second test was a torsion test. This was used to determine the shear stress the bonded portion of the tube could withstand.

Samples made of 6061-T6 aluminum were used since it is often utilized in lightweight structures and the properties of welded samples were assumed to be that of

the original tube. The materials used for the tests were prepared in the following manner. A tube with outer diameter of 1.125 inches and wall thickness of 0.125 inches was cut into 4 inch segments. A tube with outer diameter of 0.875 inches and wall thickness of 0.125 inches was machined slightly to fit inside the larger tube and then cut into 1.5 inch segments. Each sample consisted of two of the 4 inch segments joined with one of the 1.5 inch segments.

To prepare the samples for bonding, the insides of the 4 inch segments and the outsides of the 1.5 inch segments were etched using 100 grit sandpaper. This rough surface was then cleansed using acetone. With the surface clean Araldite 2015 two part epoxy was applied to the outer surface of the small tube and the inner surface of the large tube as specified by the manufacturer. The process is illustrated in figure 1.

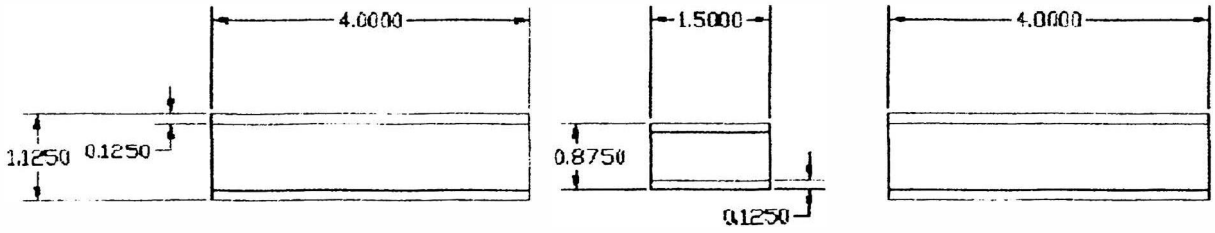

Figure 1 – Aluminum pieces for each sample

The three-point bending test tested a sample over a span of 7.0866 inches with the force applied at the junction of the sample as illustrated in figure 2. This test was done on three different samples. The test continued until the piece had failed. The data was recorded by computer.

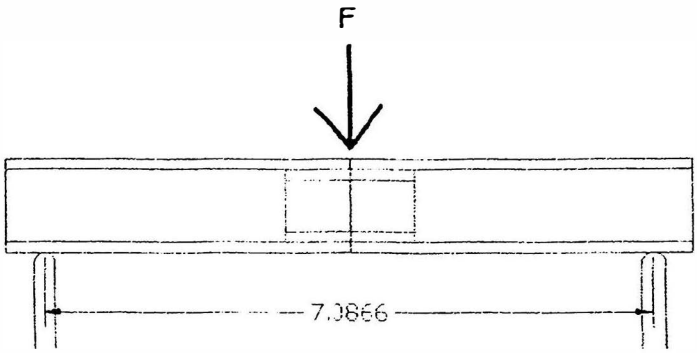

Figure 2 – Three-point bending test setup

The torsion test was completed by gripping the ends of the tubes and twisting one end as illustrated in figure 3. This test was also performed on three samples. The data was monitored as the test proceeded and the high value recorded by hand. The test was stopped when the value was no longer increasing.

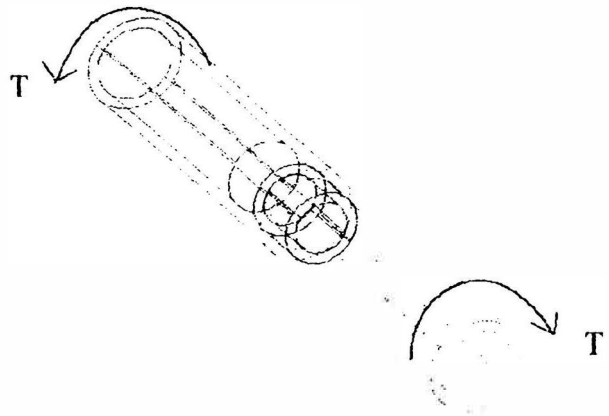

Figure 3 – Torsion test setup

Results

The data was all compared to the properties of 6061-T6 aluminum tubing with an outer diameter of 1.125 inches and a wall thickness of 0.125 inches. This gives a good comparison of the strength of the joint.

Bending Stress

The maximum stress achieved by each sample in the three-point bending test was calculated using the following equations.

$I = \frac{\pi}{64}(OD^4 - ID^4) = 0.049854 in^4$, where I is the moment of inertia, OD is the outer diameter of the tube, and ID is the inner diameter of the tube.

$M = \frac{PL}{4}$, where M is the moment, P is the load, and L is the span distance.

$\sigma = \frac{M(\frac{OD}{2})}{I}$, where σ is the bending stress. Using the numbers associated with the samples with these equations they were simplified to be $\sigma = 19.99P$.

The force used in the calculations was the point at which the force first started to drop, as illustrated in figure 4. This was assumed to be the point at which the glue yielded. After this point the insert provide even more strength by being wedged into the two sections of tube. Results of the tests are shown in table 1.

Sample #	Force	Stress(psi)
1	1048.6	20961.51
2	540.4102	10802.8
3	808.8599	16169.11

Table 1 – Bending stresses

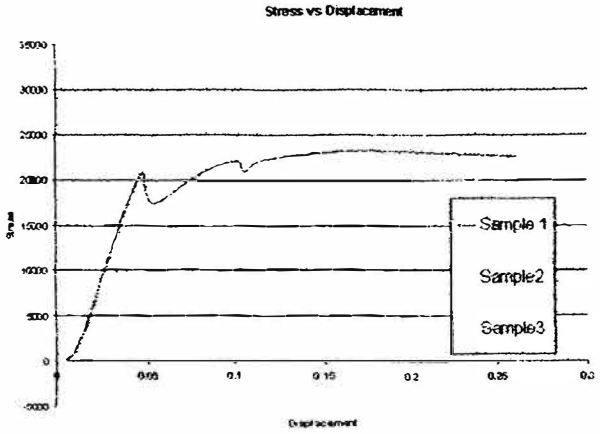

Figure 4 – Bending stress vs. displacement

Shear Stress

The shear stress of the bonded area was determined using the following formulas.

$$Area = \pi(0.875)(0.75) = 2.06167in^2$$

$$Force = \frac{T}{radius} = (2.2857)T \text{ , where T is the torque}$$

$$Stress = \frac{Force}{Area} = (1.1087)T$$

The stress in each of the samples is shown in table 2 below.

Sample #	Torque	Stress(psi)
4	1800	10154.58
5	800	4513.144
6	1440	8123.66

Table 2 – Shear stresses

Conclusions

As can be seen from the data above, the bonded tubes did not perform as well as the tube would have if it were in its original state. One sample did come close in the bending and one in the torsion test. Overall, the adhesive performed fairly well. While the

test results are not quite as good as a regular tube, the adhesive did come close on several of the tests.

It was originally thought that the tube/insert junctions were the same in all instances, some of the tolerances between the two were a little larger. This may have caused more stress to be placed on the adhesive instead of the insert. The difference in the test results is most likely due to inconsistent application of the adhesive. For further testing it would be good to try and standardize the application of the adhesive and the tolerances of the insert for more uniform results.

With a more reliable setup for the samples it should be possible to consistently see results closer to the theoretical limits of the plain tube. Knowing this, it will be possible to design structures that are glued instead of welded. Since some materials cannot be welded, this method of construction may be an acceptable substitute.

Acknowledgments

I would like to thank Dr. Douglas Carroll for his guidance for this report. His experience with the material analysis and testing were invaluable.

OURE Final Report

2005

Andrew Ricke

Advisor: Dr. David Spurlock 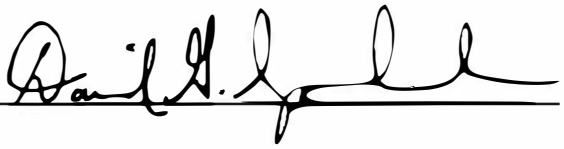

Student Time Management: Student Characteristics Comparison Between Traditional Coursework and Extracurricular Activities

Abstract

The trend that extracurricular activities and organizations are important to a college student is increasing. Many students are active in at least one activity or organization outside of class. These activities at the University of Missouri-Rolla range from design competition teams, to professional societies, to non-varsity sports, and to special interests groups Do students who have a high interest in education and learning find these activities more important than their coursework? What other traits could affect preference away from traditional coursework towards non-traditional extracurricular activities? Examination of selected traits could lead us to finding trends of preferences.

Introduction

To current students, there is a wide range of pressures put on them to do well in coursework and classes, while at the same time, a large pressure to join extracurricular activities. The pressure to do well in course work can come from many sources: parents, professors, potential employers, or a personal desire to succeed and achieve. On the other hand, extracurricular activities offer benefits of socialization, new challenges, hands-on experience, new and unique educational experiences, and various types of other rewards (Such as: awards, material prizes, job networking.). In addition, an increasing number of employers and school officials promote such activities as being beneficial to students. With only a finite amount of time available to participate

in such activities, as well as, time available to focus on school work, students are forced to make priorities. The biggest question is: What do students place as their top priority? This, of course, is dependent on many factors for each student. In this study, we focus on five constructs that may show a trend in preference. We wish to observe if they still prefer the more traditional coursework and classes, or if they now prefer to achieve their desires of learning though the non-traditional means of extracurricular activities.

Through personal experience and observation, I see a high number of students struggle to find a happy balance between coursework and extracurricular activities. Many students will try to do well in both their class and extracurricular pursuits. This makes predictions based on personality traits or constructs difficult to make. No confident hypothesis can be given based on casual observation, leaving us to wait on the results from each construct.

Model Components

To determine more about the preferences of engineering students, a set of variables needed to be defined. First set of measures that seem necessary are intrinsic and extrinsic motivation. The extrinsic motivation measures are based on a mixed set of extrinsic motivation constructs (Deci & Ryan[1], 1985; Ryan and Deci[2], 2000). The particular subtype relevant to this analysis is extrinsic introjection which describes one's feelings of consequences or guilt. The intrinsic motivation measures are based on the set of subtypes proposed by Vallerand, Pelletier, Blais, Briere, Senecal, & Vallieres[3]

(1992). The relevant subtype used here is intrinsic motivation to know, which relates to one's personal desire to learn.

The second set of measures is general personality traits. Need for cognition (Cacioppo & Petty[4], 1982), organization (International personality Item Pool[5], 2001), and activity level (International Personality Item Pool[5], 2001) each provide use for this report. Need for cognition refers to the need to think, learn, and analyze. Organization describes ability to plan, order, and provide structure with one's resources to accomplish one's goal. Activity level refers to how many tasks one will take on and handle.

Method

A survey was distributed at the University of Missouri-Rolla to the members of several campus organizations. During the Fall Semester of the 2004-2005 academic year, they were distributed by contacting the officers of each for permission. If they could not conveniently participate in the questionnaire during their meetings, an online version was made available to the members. Respondents completed informed consent forms prior to completing the questionnaire and received debriefing sheets at the conclusion. Due to the variety of organizations asked to participate, the respondents make a good representation of the students who actively participate in organizations on the campus.

The questionnaire consisted of five sections. The first section collected basic demographics, such as: academic major, class, gender, local residence, and ethnicity.

In addition, a 5-point scale was set up to rate their range of GPA, with "<2.00" at the low end and "3.50-4.00" at the high end.

The second section collected information about their participation in organizations, including leadership positions. It also asked about how many hours per week they spent on specific activities: extracurricular organizations, in class attendance, work on classes outside normal class time, and paid work. Also, they were asked for their current academic credit hours for the semester.

The third section contained 28 items to measure intrinsic and extrinsic motivation. Respondents had to rate answers to the questions "Why did you go to college?" with a five-point rating scale ranging from 1= Strongly Disagree to 5 = Strongly Agree.

The fourth section included 56 items to measure the personality construct measures mentioned above: Organization (10 items), Activity Level (10 items), Need for Cognition (10 items), Social Assurance (8 items), Social Connectedness (8 items), and Generalized Self-Efficacy (10 items). The same five-point scale used with the motivation items was used to measure the items in either a positive or negative manner. Only Organization, Activity Level, and Need for Cognition were used for this analysis.

The final section gave 26 statements about participation and preference in extracurricular activities and coursework. Respondents used another five-point rating scale ranging from 1 = Very Rarely to 5 = Very Often. Certain statements displayed

favor for coursework over extracurricular activities while other statements did the opposite. For this analysis, four statements in favor for coursework were grouped to compare with four equivalent statements favoring extracurricular activities. A ninth statement directly asked for preference towards extracurricular activities or not.

Results

Out of those returned, 147 were used for the data analysis. Median values were used to determine the split for High and Low categories for each construct. The values are show in Table 1 below. Also, a High GPA variable was created based on giving those who responded with a 3.5-4.0 GPA a 2, while all others received a 1. Given in each table are the most significant factors based on their p-values. Significant for our purposes is defined as $p < .05$. However, a few factors had values above $p = .05$, yet still near 05, and because their large mean differences are notable, they are included in the tables. With a larger sample study, improved significance is likely for these factors.

	Count	Maximum	Minimum	Median
Intrinsic Motivation (To Know)	147	5.00	1.00	4.00
Activity Level	147	5.00	1.60	3.80
Organization	147	4.90	1.40	3.30
Need For Cognition	147	4.70	2.30	3.60
Extrinsic Motivation (Introjected)	147	5.00	1.00	3.75

Table 1. Median values for the selected constructs.

With intrinsic motivation to know, none of the statements produced any significance in the difference in their means, which is shown in Table 2. However, the higher group reported slightly more high GPA's and worked nearly 2 hours more.

	Intrinsic Motivation to Know	Mean	Std. Dev.	Significance (P-Value)	Mean Difference (High - Low)
High GPA	High	1.61	0.490	0.035	0.176
	Low	1.44	0.500		
I. How many hours do you currently work per week for pay?	High	4.43	6.918	0.053	1.913
	Low	2.52	4.949		

Table 2. Significant variables for intrinsic motivation to know.

Activity level, displayed in Table 3, presents a few predictable results. The more activity group had a small increase of high GPA's, but also had over 2 more hours spent on extracurricular organizations. They also showed in statement 90 that higher activity respondents were less likely to miss their extracurricular activities for due to coursework.

	Activity Level	Mean	Std. Dev.	Significance (P-Value)	Mean Difference (High – Low)
High GPA	High	1.62	0.488	0.040	0.170
	Low	1.45	0.501		
Hours spent for extracurricular organizations	High	10.40	8.012	0.061	2.426
	Low	7.97	7.518		
90. I miss deadlines with my university extracurricular activities because I am working on my courses	High	1.89	1.117	0.061	-0 382
	Low	2.27	1.326		

Table 3. Significant variables for activity level.

In Table 4, organization shows the most effect on the preference for this report. Again, the high GPA is slightly more for the higher group, but this time the lower group shows to work for pay about 2 hours more. In statements 90, 85, 89, and 97, the higher organization group rated each statement less than the lower organization group. For the first three, this represents favor neither for coursework nor for extracurricular activities. However, statement 97 directly shows that the lower organization group reported more benefit in their extracurricular activities.

	Organization	Mean	Std. Dev.	Significance (P-Value)	Mean Difference (High - Low)
89. I miss homework deadlines because of my university extracurricular activities	High	1.45	0.920	0.001	-0.561
	Low	2.01	1.028		
85. I put less effort into my course work so that I have more time for my university extracurricular organization activities	High	2.24	1.354	0.026	-0.468
	Low	2.71	1.168		
High GPA	High	1.63	0.487	0.027	0.182
	Low	1.44	0.500		
I. How many hours do you currently work per week for pay?	High	2.61	4.647	0.047	-2.060
	Low	4.67	7.402		
97. In general, I feel I benefit more from my involvement in university extracurricular activities than from what I learn in my courses	High	2.67	1.212	0.052	-0.361
	Low	3.03	1.021		
90. I miss deadlines with my university extracurricular activities because I am working on my courses	High	1.89	1.226	0.059	-0.384
	Low	2.28	1.224		

Table 4. Significant variables for organization.

Need for cognition, shown in Table 5, has a few unique differences. First, need for cognition has been the only construct that did not show a significant relationship in the high GPA category. Four statements showed a relationship, though 3 were only near significance ($p \approx< .05$). For statements 90 and 93, the higher cognition group shows favor towards extracurricular activities, but statements 91 and 92 express that they will not sacrifice the quality or challenge in either their coursework or extracurricular activity.

	Need for Cognition	Mean	Std. Dev.	Significance (P-Value)	Mean Difference (High - Low)
90. I miss deadlines with my university extracurricular activities because I am working on my courses	High	1.86	1.064	0.021	-0.481
	Low	2.34	1.377		
91. I try to take easier classes so that I have more time for my university extracurricular activities	High	1.86	1.111	0.054	-0.391
	Low	2.25	1.295		
92. I choose university extracurricular activities that won't take too much time away from my course work	High	2.25	1.298	0.060	-0.422
	Low	2.67	1.375		
93. I expect my instructors to understand when I have to miss class because of my university extracurricular activities	High	2.76	1.380	0.061	0.449
	Low	2.31	1.479		
High GPA	High	1.58	0.497	0.322	0.082
	Low	1.49	0.504		

Table 5. Significant variables for need for cognition.

Finally, Table 6 shows extrinsic motivation (introjected) and how, besides a negative effect on the high GPA rating, no other significant changes to variables occurred.

	Extrinsic Motivation (Introjected)	Mean	Std. Dev.	Significance (P-Value)	Mean Difference (High - Low)
High GPA	High	1.47	0.502	0.052	-0.162
	Low	1.63	0.486		

Table 6. Significant variables for extrinsic motivation (introjected).

Discussion

The results demonstrate the difficulty in forming any predictions based on observation. None of the examined traits truly showed major change in affecting the preferences between coursework and extracurricular activities. Need for cognition and organization were notably close. Need for cognition may show that educationally minded students wish to increase their range of learning by adding extracurricular activities to their schedules. Organization, as could be predicted, shows that such students are more capable of handling both extracurricular activities and coursework, and tend to not make sacrifices of one for the other.

The high GPA category became an interesting factor to examine. GPA is a traditional way of judging performance and attitude towards the traditional coursework. Most of the traits showed increase in the high GPA category with the high category of each trait. Exceptions: need for cognition differences were insignificant, which seems unusual; and extrinsic motivation (introjected) showed a reduction of the high GPA. Could this be a sign that guilt reduces cheating, but cheating truly improves scores?

Organization, being the easiest trait to manipulate and improved with training, may be worth following up on. With improving organization of students, issues between professors and students dealing with coursework and class commitments can be solved. Proof may be found in the lower organization group responses that extracurricular activities are more beneficial to them. The time commitments plus real and diverse experience force such low organized students to make improvements in their organization skills in addition to other their other skills.

Acknowledgements

I would first like to acknowledge my advisor to this project, Dr. David Spurlock, Assistant Professor in the Engineering Management Department at the University of Missouri-Rolla. He guided me through my first entire research process: from preliminary readings to data collection and analysis. His work for the 2006 ASEE Annual Conference was the basis for my work.

I also would like to acknowledge Dan Bailey, a graduate student of the Engineering Management Department. His current research work with Dr. Spurlock was the overlaying basis to my research. He collected and provided the data used for this report. In addition, he also gave a crash course on how to use SPSS, the statistical software used for this report.

References

1. Deci, E. L. and Ryan, R. M. (1985). *Intrinsic motivation and self-determination in human behavior.* New York: Plenum.

2. Ryan, R. M., and Deci, E. L. (2000). Self-determination theory and the facilitation of intrinsic motivation, social development, and well-being. *American Psychologist*, 55, pp. 68-78.

3. Vallerand, R. J., Pelletier, L. G., Blais, M. R., Briere, N. M., Senecal, C. and Vallieres, E. F. (1992). The academic motivation scale: A measure of intrinsic, extrinsic, and amotivation in education. *Educational and Psychological measurement*, Vol. 52, pp. 1003-1017.

4. Cacioppo, J. T., & Petty, R. E. (1982). The need for cognition. *Journal of Personality and Social Psychology*, 42, 116-131.

5. International Personality Item Pool (2001). A scientific collaboratory for the development of advanced measures of personality traits and other individual differences (http://ipip.ori.org/). Internet Web Site.

Geological Research Regarding a Well in Mutare, Zimbabwe

March, 2005

Laura Ruf
University of Missouri-Rolla
Department of Geological Engineering

Abstract:

The purpose of this project was to collect information regarding the geology and hydrogeology of the area surrounding Mutare, as well as any other information that would be needed for determining a water supply for a well that will be built there. Unfortunately, much of this information could not be found. The two water sources that seem to be the most easily provided are building a well on spot or extending pipes to the Pungwe project. Determining which is the better choice would require a geologist or geological engineer to survey the site planned for the orphanage.

Introduction:

The average citizen of Sakubva, a southern suburb of Mutare, gets his water from communal ablution blocks. Washing is done in 'bays' that can accommodate three people. One person gets clean water from the tap while the other two gets the water as it runs down the bay. The toilet consists of a hole in the middle of the communal block, which is split as a wall separates the men from the women. Above the toilet is the shower, which is a separate room with a pipe of running water. Typically, this room has two water outlets. The lack of resources that often have to cater to 50-100 people causes these communal ablution blocks to be dirty and disease-ridden. Often people will rise at four in the morning in order to use a slightly cleaner block as the cleanliness deteriorates throughout the day. It is also from these blocks that people get their drinking water and water used in food preparation. (1. Mukheli, A. et al., 2001)

It is an area close to this that Samaritan Hands wants to build an orphanage. Though the city is attempting to remedy the situation described, the likelihood that they would be able to raise enough money to make the communal ablution more sanitary before Samaritan Hands wants to build the orphanage is low. No communal ablution block would be able to sustain an increase of twenty to thirty more people attempting to use its water. The government is attempting to provide water for overextended communal blocks and would have difficulties trying to provide the amount of water necessary to run an orphanage. For this reason, it is important that Samaritan Hands provides a water source for the orphanage with the building of the orphanage.

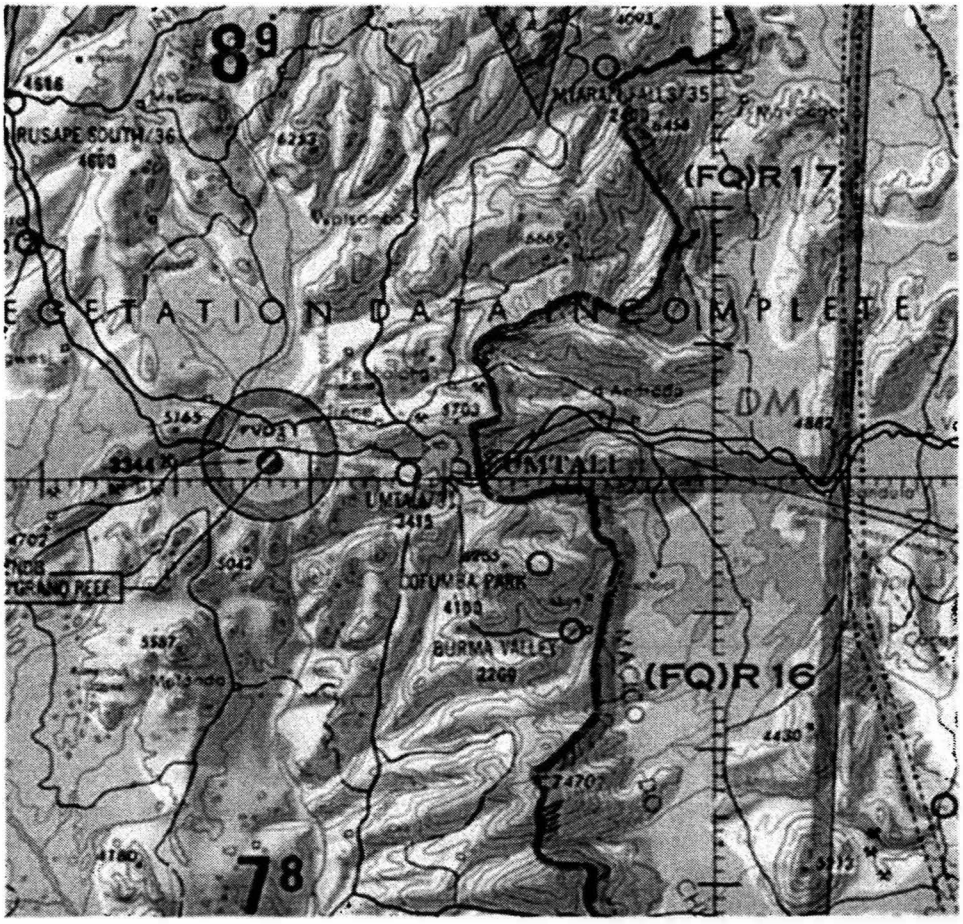

Figure 1: Topographical Map of the area around Mutare (labeled Umtali) (2. Beira)

Geology:

Mutare lies in a region known as the Eastern Highlands in Zimbabwe. Though in a relatively high elevation, the city is in a valley between two mountain ranges; the Bvumba to the south and the Nyanga to the north. Both ranges are made of greenstone granite containing dikes and other intrusions of dolerite. The city of Mutare, however, is sitting on mostly gneiss and in the area of which this project is most concerned, serpentine. While there are faults and dikes within the Nyanga Mountains, it is uncertain whether there are faults and dikes running through the city of Mutare. A determination of the volcanic activity of the area should also be checked as volcanic rock might also be in the area. Though the information collected will be important, it is still critical that rock samples from the area are collected and studied. Faults and the thickness of different layers will make a difference in how difficult it would be to drill a well or where groundwater can flow. (3. Samimi, n.d.) (4. Love, 2002)

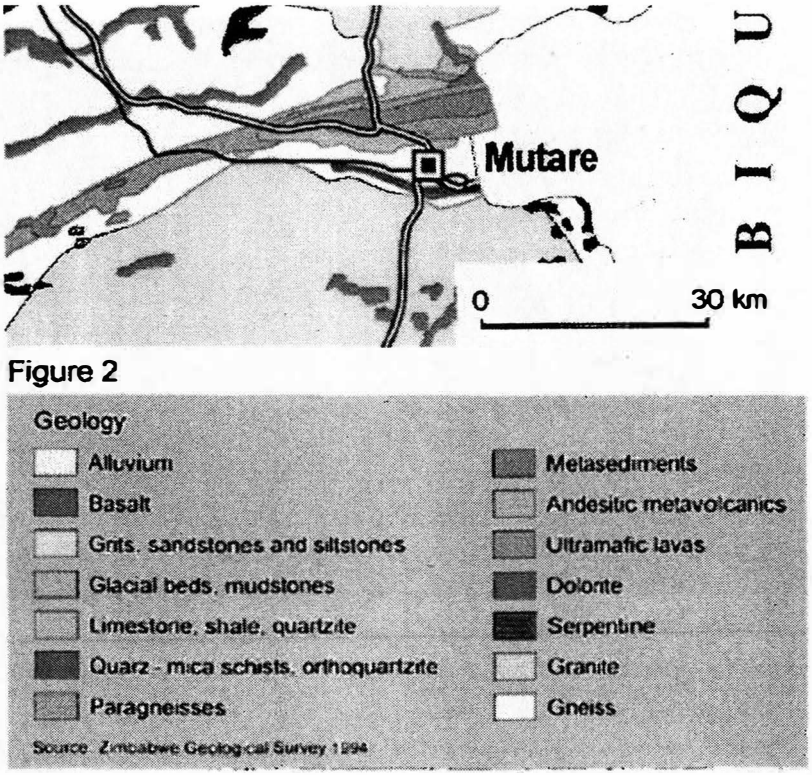

Figure 2

Figure 2: Map of the Geology of Mutare (3. Samimi, n.d.)

Greenstone Gneiss: Gneiss, in general, is a high-grade metamorphic rock. It can be formed from a variety of different rocks, but in this case is most likely to be formed from the greenstone granite found in the surrounding mountains. They could also be formed out of the andesitic metavolcanics or the ultramafic lavas as the greenstone granite rose as diapers from the earth's crust. As both were formed during the Achaean period, it is likely that there are several fractures within any layers of these rocks. (5. Precambrian Time)

Serpentine: Serpentine is a rock consisting of any number of the different minerals found in the Serpentine group. Unfortunately, this also includes chrysotile, a well-known asbestos mineral. While chrysotile is the most harmless of the asbestos minerasl, it still would be preferable that it not be released into the air. Within the serpentine soil, two heavy metals, nickel and chromium, are present. While these metals may not be in high enough quantities to be considered hazardous to people, they can be present in levels that are toxic to plants. This causes the soils to become thin and unable to retain water well except when forming the clay mineral montmorillite that binds water to itself so that vegetation cannot access it. (6. TrackRock Gap) (7. Serpentine Rock, 1994)

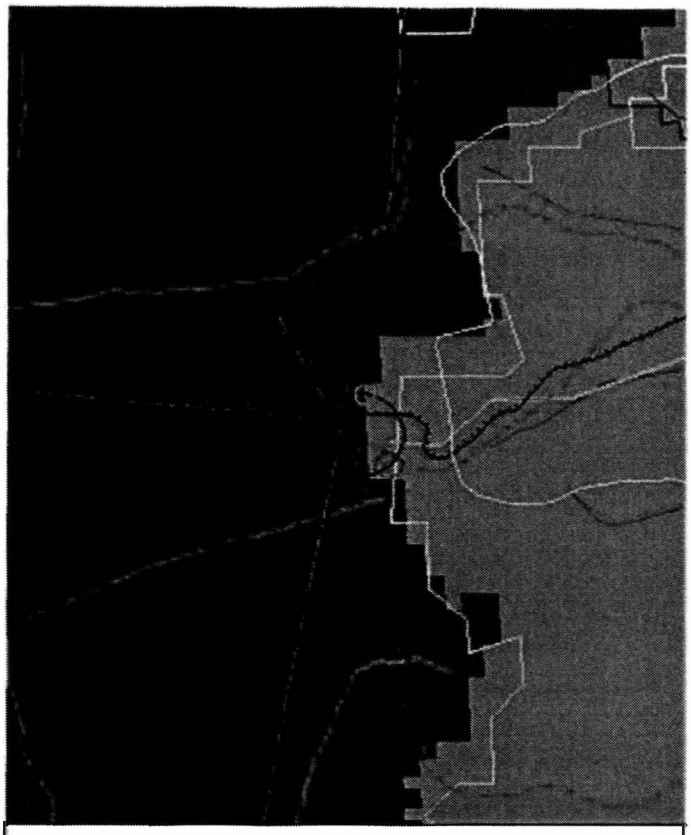

Figure 3:Map Showing the Drainage (light blue line) and River (opaque background) Basins around Mutare (black circle); Pungwe pipes (bright yellow line), and electricity wires (black outlined brown lines) are also shown; Christmas Pass is approximately at the purple circle; the orphanage would be built around the area of the red circle. (8. Hearn et al. 2001)

Water Resources:

Hydrology & Hydrogeology: Unfortunately, according to David Love, M.S., a geologist in Zimbabwe and a professor at the University of Zimbabwe, no work was done on this subject before Mutare was founded. As far as the Pungwe project is concerned, very little work was done toward the hydrology. There was little need for the pipeline and a pump was never investigated as a free-flowing pipe-line was, according to Per Renman, cleaner, cheaper, and more environmentally friendly.

Sakubva River: As the closest river to Mutare, the Sakubva River gets a lot of pollution as people dump waste and contaminated runoff flows into the river. This river also seems to be losing water - one city engineer had estimated that ninety percent of water that flows into the Sakubva is lost by one form or another. (1. Mukheli, A. et al., 2001)

Pungwe Project: In 1997, the city of Mutare began construction on a pipeline project connecting the Pungwe River to Mutare in order to help the problems of water scarcity in the area. In 1999, the pipes were completed and included a special tunnel-water purification system and internal and external regular checkups. (9. Pungwe, n.d.) Although this system has provided water in abundance to the Christmas Pass Reservoirs, Mutare is still lacking in adequate water. The executive mayor stated in 2004 that this was caused by a bottleneck of the pipes from the pass into the city and that these pipes are now too small due to city growth. Several companies also complained that the water problems they were experiencing caused financial losses for their company. (10. Mutare, 2004) It is also estimated that about fifty percent of the water that gets to Mutare is lost through vandalism and leakage. (11. Water Losses, 2004)

Pollution Problems:

Asbestos: Ultramafic rocks typically contain 1-25% chrysotile, the most common of the asbestos minerals. (12. Naturally-Occurring Asbestos, n.d.) Though chrysotile is thought of as the least harmful of all asbestos minerals, exposure to high levels of this mineral is still regarded by the American Lung Association as increasing the risk of lung cancer, mesothelioma (a cancer of the lining of the chest and the abdominal cavity), and asbestosis (in which the lungs become scarred with fibrous tissue). (13. Asbestos, 2005)

While any drilling might cause the asbestos to be released, it is possible to keep the majority of the asbestos from being released into the air by keeping the serpentine rock wet. (7. Serpentine Rock, 1994)

Nickel and Chromium: While I have found nothing that suggests that there is a high concentration of either of these metals in the soil around Mutare, serpentine soil is related to such metals. In order to make certain that these metals do not find their way into the water, the soil must be tested.

Sewage: Though Mutare is attempting to upgrade the sewage system, there are still problems created from the inadequate sewage disposal. In Sakubva, a suburb of Mutare found approximately 5 kilometers to the south of the city, much of the water provided is provided in communal ablution blocks. These blocks often have continuous running water, which drain into the main drainage. However, the pipes often get clogged as they are not always cleaned regularly and the shear number of people overstresses the system. This leads to stagnant water that often hold disease-carrying organisms. (1. Mukheli, A. et al, 2001)

Options:

Pungwe Pipes: One option is to extend pipes to connect to the Pungwe pipes. However, this might not be a good idea at this time as the pipes going into Mutare need to be replaced and the city of Mutare is struggling to find the money to do so. (10. Mutare, 2004) There is also the possibility of clogged or contaminated water pipes from the communal ablution blocks. (1. Mukheli, A. et al, 2001) The pipes would also have to be underground as anything above ground would have trouble with piracy. (11. Water Losses, 2004)

Hand-dug well: While this is always an option, the level of the water table is unknown at this point in time. A hand-dug well may not be deep enough to provide enough water to the orphanage as was seen in the Guatemala project. (14. Sommers, 2003)

Drilled well: At this point in time, it is also unknown if the groundwater is contaminated with any pollutants. Also the amount of asbestos within the serpentine rock is unknown, but can be contained through the use of water.

Borehole: The area of which is of concern is a suburban area and so contains many individuals as well as farmers. Boreholes have a tendency to pull the water table of the surrounding area down which would affect surrounding wells and farmland.

Importation of Water: While this is an option, it is likely that it would get to be expensive and the amount of money for the orphanage would probably not cover it, which can also been seen with the orphanage in Guatemala. (14. Sommers, 2003)

Research:

Most of the work I have done for this report has been done over the internet. I have attempted to contact several people who might have been able to give me more information about Mutare and in most cases, these people actually live in the city of Mutare. Given the lack of information I found on the area around Mutare, I turned to information about similar rocks within the United States. In no way will this guarantee that the rock descriptions are the same in Zimbabwe. However, it will give a better idea of what we can expect when rock samples and soil testing can be done in Mutare.

Conclusion:

Without looking at the site and talking with the city engineer, it would seem that the best options would either be to drill a well for the orphanage or to extend pipes to the Pungwe project. Both of these options have possible long- and short-term problems, such as the possible contamination of either. In the long-term, it would probably be more useful to have pipes extending to the Pungwe project. However, at this point, the Pungwe pipes need a lot of work in order to be a good constant source of water.

Field research must be done before beginning any sort of drilling and it would be necessary in determining the financial difference between drilling a well and extending pipes to the Pungwe pipeline and whether the possibility of drilling a well is acceptable to United States standards.

Acknowledgements:

Elmore, Curt. P.E., Ph.D., Professor of Geological Engineering and Project Advisor, University of Missouri – Rolla

Environment Africa, http://www.eafrica.utande.co.zw/ Retrieved on March 31, 2005

Hogan, John. Ph.D., Associate Professor of Geology, University of Missouri-Rolla

Love, David. M.S., Professor of Geology, University of Zimbabwe

Renman, Per, Civil Engineer, Contractors Environmental Manager for Skanska

References:

1. Mukheli, A., Mosupye, G., Swatuk, L. (2001) *Is the Pungwe Water Supply Project a solution to water accessibility and sanitation problems for the households of Sakubva, Zimbabwe?* Retrieved March 20, 2005 from http://www.waternetonline.ihe.nl/aboutWN/pdf/mukheli.pdf
2. "Beira to the Zimbabwe Border." University of Texas. Retrieved February 7, 2005 from http://www.lib.utexas.edu/maps/africa/beira_83.jpg
3. Samimi, C., Wagenseil, H. "Geology of the Eastern Highlands (Zimbabwe)." (n.d.) Retrieved February 19, 2005 from http://www.geographie.uni-erlangen.de/csamimi/podzol/Geologie_Umgebung.html
4. Love, David. "The Geology of the Country Around Nyangani Mountain: A Preliminary Report." (2002) Retrieved February 10, 2005 from http://www.uz.ac.zw/science/geology/davidlove/Nyangani-prelim%20abs.pdf
5. "Precambrian time." Encyclopædia Britannica. Retrieved March 30, 2005, from Encyclopædia Britannica Premium Service. http://www.britannica.com/eb/article?tocId=69795
6. Articles-Places: Track Rock Gap. (2004) The Georgia Botanical Garden. Retrieved February 19, 2005 from http://www.gabotsoc.org/articleTrackrock.htm
7. "Serpentine Rock Information." (1994) Silver Creek Country Club. Retrieved March 20, 2005 from http://silvercreekonline.com/silver-creek-valley-country-club-documents/Serpentine_Rock_Information.htm
8. Hearn, P. et al. *Global GIS database: Digital atlas of Africa* (2001) Flagstaff, AZ : USGS Flagstaff Field Survey ; Denver, CO.
9. "Pungwe - Carefully built pipeline that supplies water to a major city." (n.d.) Retrieved March 7, 2005 from http://www.skanska.com/skanska/templates/page.asp?id=3630

10. *Mutare Seeks $1.5 billion for Sewer System:* The Zimbabwe Situation. (2004, February 3) Retrieved March 24, 2005 from http://www.zimbabwesituation.com/feb3_2004.html
11. *Water Losses Worry Mutare*: Zimbabwe Standard (2004, April 18) Retrieved March 24, 2005 from http://www.queensu.ca/msp/pages/In_The_News/2004/April/47.htm
12. Naturally-Occurring Asbestos General Information. (n.d.) California Environmental Agency: Air Resources Board. Retrieved March 24, 2005 from http://www.arb.ca.gov/toxics/Asbestos/general.htm
13. Asbestos. (2004, March) American Lung Association. Retrieved March 24, 2005 from http://www.lungusa.org/site/pp.asp?c=dvLUK9O0E&b=35368
14. Sommers, E. (March, 2003) Humanitarian Groundwater Development and Geologic Study in Lemoa, Guatemala. Unpublished OURE paper, University of Missouri - Rolla.

OURE FINAL REPORT

Kristin L. Russell

4/11/05

Effects of Nitric Oxide Inhibitors and Scavengers on Gravitropism in *Arabidopsis thaliana*

Kristin Russell, Jennifer Jacobi, Jacob Elmer
University of Missouri – Rolla, Biological Sciences Department, Rolla, MO

Plant roots are gravitropic meaning they detect and respond to changes in orientation with respect to gravity. Pagnussat et al.(2003)[1] suggests that this response is initiated by nitric oxide and results in cGMP production. Here we investigate the effects of the removal of nitric oxide (NO) or the inhibition of nitric oxide-sensitive guanylate cyclase to show that such a cGMP producing cycle exists in plants. We also want to determine the exact effects of NO on gravitropism in *Arabidopsis thaliana*. Removal of NO with the NO scavenger 2-Phenyl-4,4,5,5-tetramethylimidazoline-1-oxyl 3-oxide (PTIO) showed unexpected results. Reorientation was expected to be delayed, however it occurred within the same time period as the controls. Inhibition of NO synthesis using 1H-[1,2,4]Oxadiazolo[4,3-a]quinoxalin-1-one (ODQ) behaved as expected. It delayed the degree of gravitropic bending, indicating that NO synthesis was required for the gravitropic response. Although the results from the tests with ODQ support our hypothesis, the results from PTIO contradict it.

Plant growth and development are strongly influenced by gravity. When roots are gravistimulated by horizontal orientation, instead of the usual vertical, they respond by bending downward with respect to gravity. This bending is due to differential growth at the root tip. The differential growth at the tip is probably caused by mechanosensing in the root cap and changes in calcium and pH. This results in relocation of auxin efflux carriers and subsequent downward transport of auxin, thus inducing the differential growth and downward bending [2,3,4] The cycle proposed by Pagnussat et al. suggests that it begins with NO and results in the production of cGMP. Our experiments tested for the existence of this proposed cycle.

NO occurs naturally in *A. thaliana*, as in other plants and animals, and is produced by a species-specific nitric oxide synthase (NOS) complex. Nitric oxide activates the guanylate cyclase. The guanylate cyclase then converts GTP into cGMP causing the transport of auxin. The effects of NO and cGMP donors as well as phosphodiesterase inhibitors was documented by two colleagues, Jacobi and Elmer. Their results show that NO and cGMP are strongly tied to the root reorientation of *A. thaliana*, heavily supporting our hypothesis. This report focuses on the effects of a NO scavenger and a guanylate cyclase inhibitor. In theory, if the NO scavenger, PTIO, was present, it would remove free NO and the guanylate cyclase wouldn't be able to convert GTP to cGMP fast enough thus causing delayed root

reorientation. The guanylate cyclase inhibitor, ODQ, is supposed to inhibit the NO/cGMP pathway at the guanylate cyclase and prevent GTP from forming cGMP. The plants showed a delayed reorientation rate when exposed to ODQ, however we received opposite, unexpected results for PTIO. These results both support and contradict the idea that NO is a major signaling molecule involved with root growth and the idea of a NO/cGMP cycle involved with growth, as proposed by Pagnussat et al. More testing is needed to confirm these results. The proposed cycle can be seen in Figure 1.

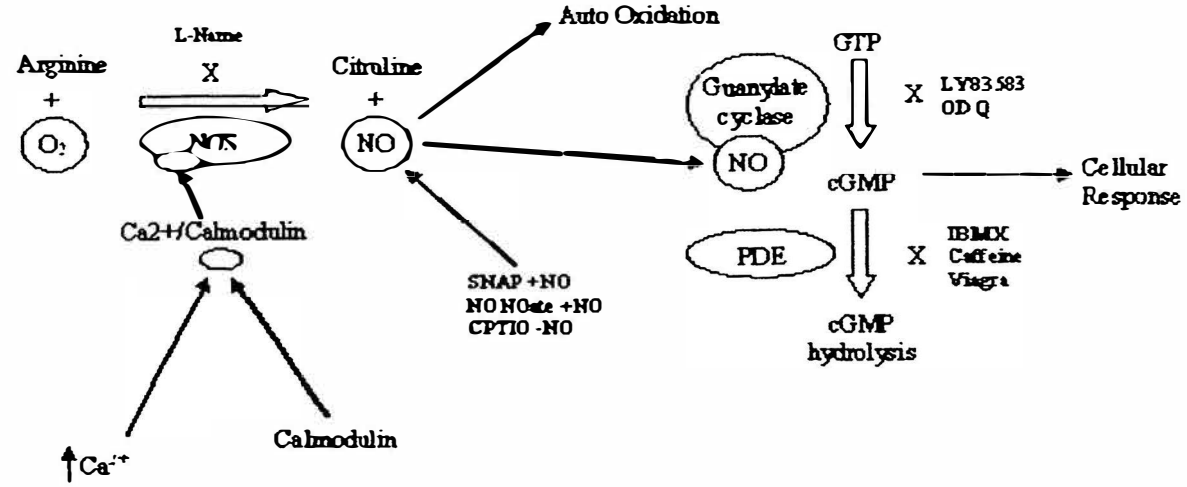

Figure 1. (Above) NO/cGMP Cycle
This pathway is documented in mammals. However, the goal of our project is to prove there is a similar pathway in plants. The NOS is signaled to run when there is an increase in calcium and calmodulin in the cell. The NOS then produces NO which goes on to the guanylate cyclase or is auto-oxidized. The guanylate cyclase then converts GTP into cGMP. The cGMP goes on to produce a cellular response, such as root reorientation. In addition to PTIO and ODQ, L-Name, SNAP, NONOate, LY83583, IBMX, Caffeine, and Viagra are common drugs used to probe this pathway. Their location in the diagram suggests where they inhibit the pathway.

Results

Effects of ODQ (Figures 2 and 6)
1H-[1,2,4]Oxadiazolo[4,3-a]quinoxalin-1-one, known as ODQ, is a selective inhibitor of the NO sensitive, guanylate cyclase. The results from ODQ behaved as expected. The roots had a delayed reorientation time when compared to the controls. See figure 3. As you can see from the graphs, there is no significant difference between the results from the different concentrations. Six day old seedlings were transferred to plates containing 10 μM, 25 μM, and 50 μM of ODQ.

Effects of PTIO (Figures 3 and 7)
2-Phenyl-4,4,5,5-tetramethylimidazoline-1-oxyl 3-oxide, known commonly as PTIO, is a stable radical scavenger for NO. It affects NO without affecting NOS. It has been documented that PTIO has significant inhibitory activity against NO biological actions. This however is not supported by the results we obtained. The seedlings exposed to PTIO actually reoriented faster

than the controls. This result was extremely unexpected. Further testing is needed to confirm these results. Six day old seedlings, germinated on plates without drugs, were transferred to new agar plates containing 50 μM, 100 μM, and 150 μM of PTIO.

Control Plates (Figures 4, 5 & 8)
Two types of controls were used, a 90-degree rotated control and a clinostat control. The clinostat control eliminates the effect of gravity by continuously rotating the seedlings. The 90 degree control roots showed no reorientation response until approximately two hours had passed. The clinostat plants showed slight curvature in two directions, indicating that they had no sense of gravity.

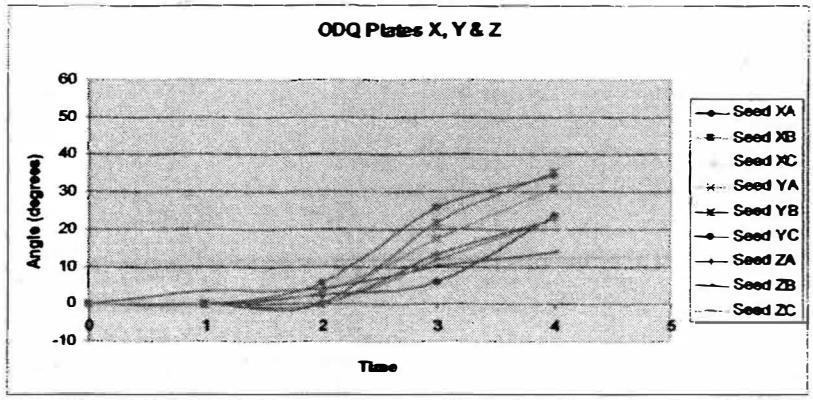

Figure2. ODQ Results
As can be seen from the graph, when exposed to ODQ, the roots didn't really begin to reorient until between two and three hours after being exposed to the drug. And, when compared to the control, the rate and degree of reorientation was much less. Seeds XA, XB, and XC were on plates containing 50μM of ODQ. Seeds YA, YB, and YC were on plates containing 25 μM of ODQ. Seeds ZA, ZB, and ZC were on plates containing 10 μM of ODQ.

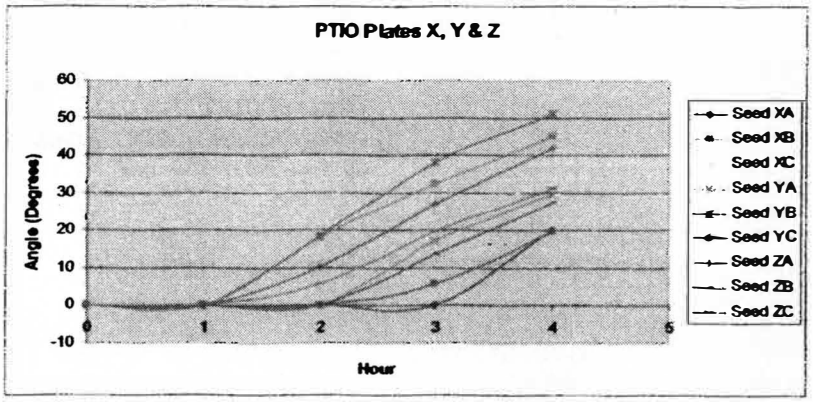

Figure 3. PTIO Results
As can be seen from the graph, the seedlings started to reorient between one and two hours after being exposed to PTIO. Seeds XA, XB, and XC were on plates containing 50 μM of PTIO. Seeds YA, YB, and YC on plates containing 100 μM of PTIO. Seeds ZA, ZB, and ZC were on plates containing 150 μM of PTIO. As you can tell from the graph, there is no significant, consistent difference between the different concentrations.

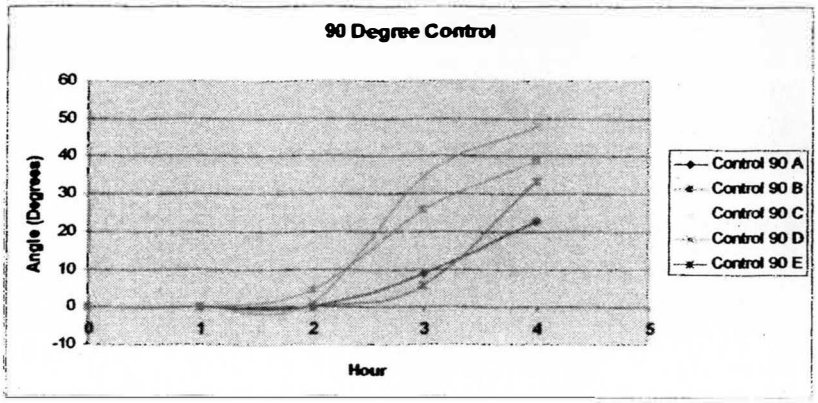

Figure 4. 90 Degree Control
According to the results, and as can be seen in the graph, the seedlings started to reorient downward between two and three hours after being transplanted to new plates.

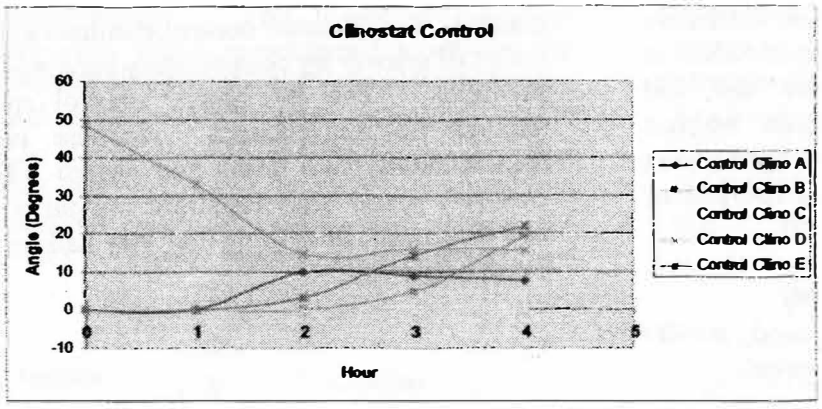

Figure 5. Clinostat Controls
The clinostat control is used to eliminate the effect of gravity. It does this by constantly rotating the seeds at 1 RPM. As can be seen from the graphs, the seedlings had no perception of gravity and grew randomly.

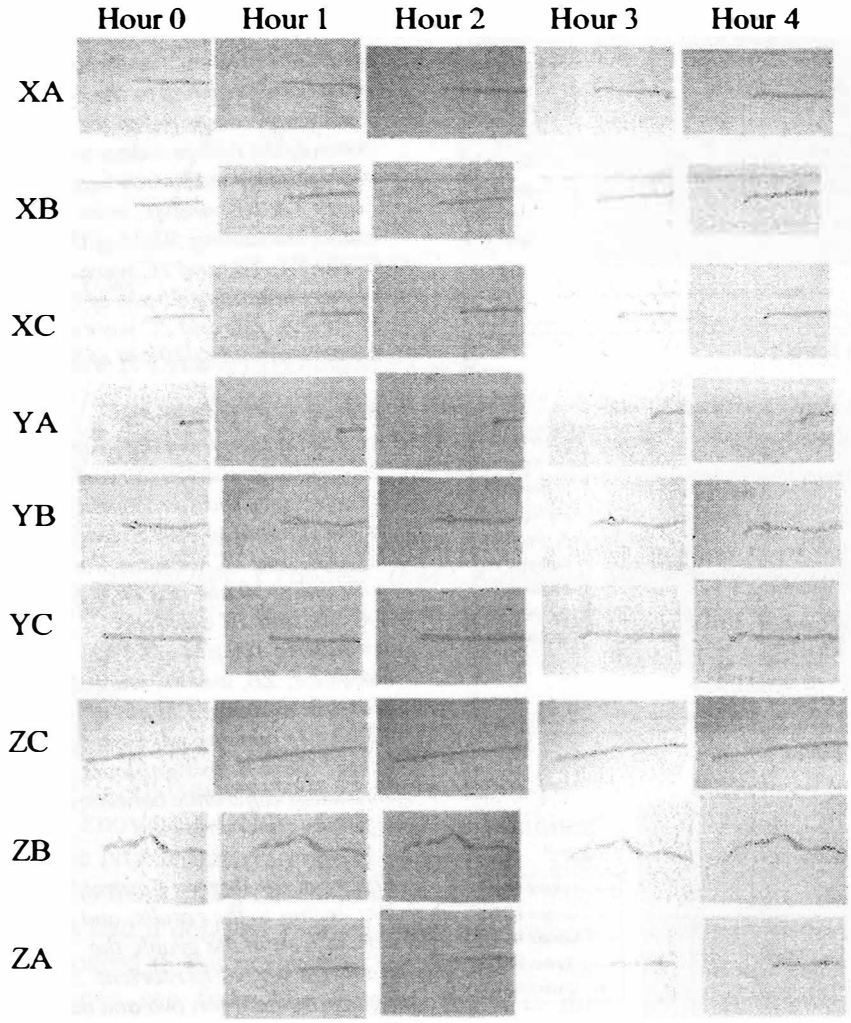

Figure 6. ODQ Images
As can be seen from the images, ODQ has a significant effect on the root reorientation. Seeds XA, XB, and XC were put on plates containing 50μM of ODQ. Seeds YA, YB, and YC were put on plates containing 25 μM of ODQ. Seeds ZA, ZB, and ZC were transferred to plates containing 10 μM of ODQ. The higher concentrations of ODQ definitely affected the roots more.

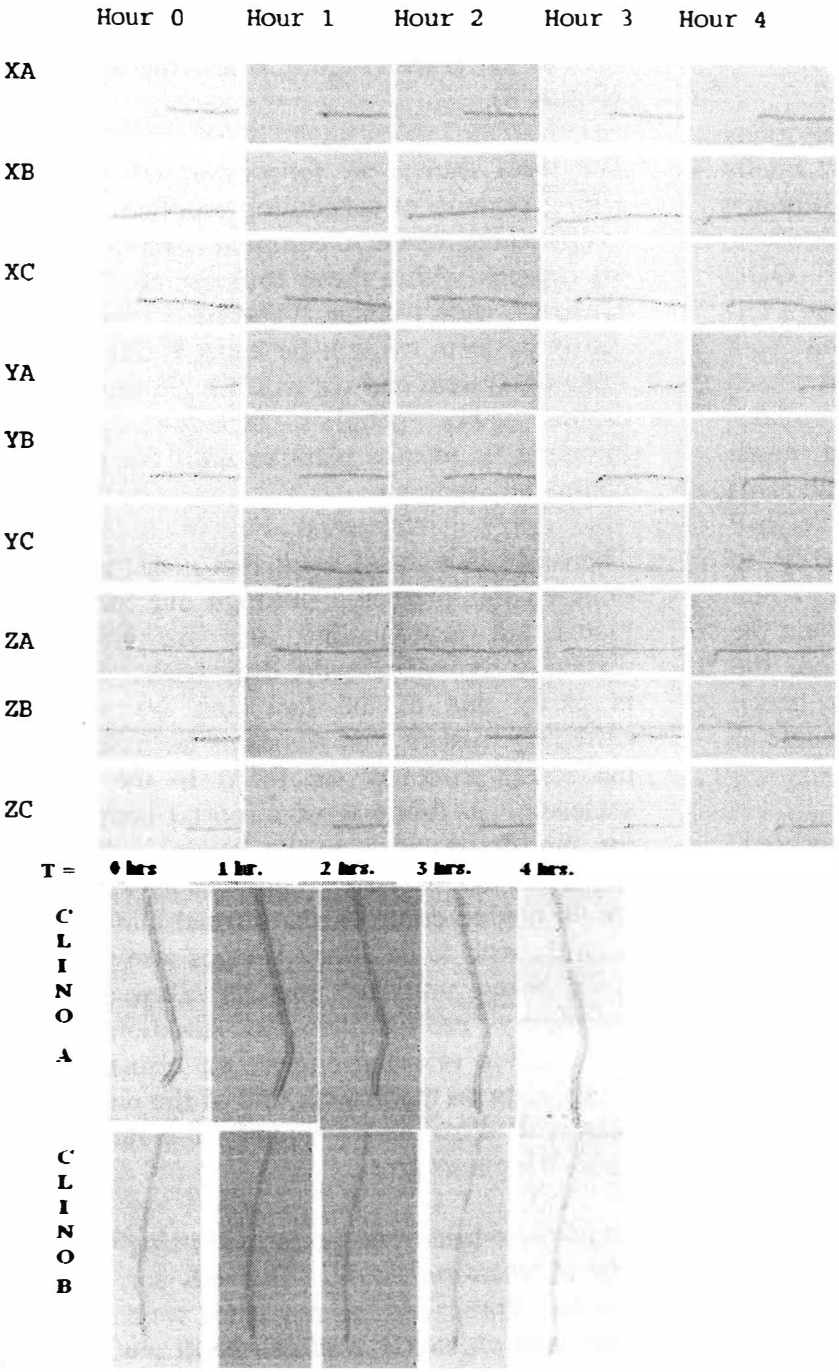

Figure 7. PTIO Images
As can be seen from the images, the roots exposed to PTIO begin to reorient fairly quickly. This was very unexpected. hours after being exposed to PTIO. Seeds XA, XB, and XC were transferred to plates containing 50 μM of PTIO. Seeds YA, YB, and YC were transferred to plates containing 100 μM of PTIO. Seeds ZA, ZB, and ZC were transferred to plates containing 150 μM of PTIO.

Figure8. Clinostat Controls
These images show the reorientation of the clinostat controls.

Plate	Deg/s
ODQ X (50 μM)	0.1151
ODQ Y (25 μM)	0.1485
ODQ Z (10 μM)	0.0831
PTIO X (50 μM)	0.1351
PTIO Y (100 μM)	0.1396
PTIO Z (150 μM)	0.1400

Figure 9. Reorientation Rate
From the table, you can tell the optimal concentration for ODQ was 25 μM. Of the ones tested, the optimal concentration of PTIO was 150 μM. The optimal concentration is defined as the concentration of drug that gives the highest rate of reorientation.

Discussion

In the beginning, this project had many roadblocks and complications. We finally got things underway in January. Although all plants showed a response to both drugs, the results weren't quite as expected. ODQ behaved as predicted but PTIO did not. The control plants and ODQ plants on both started to reorient between hours two and three. However, the control plates reoriented more slowly and at a much smaller angle than the ODQ plants did. This indicates that ODQ inhibited the NO/cGMP pathway at the conversion from GTP to cGMP. This, therefore, limited the amount of cGMP available to be used to reorient the roots. Once all the ODQ was used, the plants were able to reorient quickly, hence the significant jump in reorientation angle at about hour three.

The results for PTIO were not as expected. In mammals, it is documented that PTIO removes the NO that is produced by the NOS. This causes less NO to be available to be sent to the guanylate cyclase and therefore GTP cannot be converted to cGMP. These plants should have showed delayed reorientation like the ODQ trial, but it actually showed a faster reorientation than the controls. These results could possible be from expired drugs or human error. More trials will be preformed next semester to retest PTIO.

The control results worked out to our expectations. Multiple trials were performed on different days, and each time we received similar control results. This was a sign of the reproducibility of the project.

The clinostat controls were as expected. With the elimination of gravity on the roots, they grew multiple directions. This can be seen in the graph (Figure 5) and the images (Figure 8).

We were limited to four hours of photo taking because of scheduling conflicts. We expected the results to completely reorient to 90 degrees within those four hours. This, however, didn't occur. The next time we run these tests we will be using a different imaging system and we won't have to work around other people's schedules, thus allowing us to take pictures until the roots completely reorient.

There is still a lot of work that needs to be done on this project. Although our control plates are reproducible, we are having difficulty reproducing the drug trials. This is partly due to the fact that we were extremely rushed this semester because of the many problems we faced in the fall semester. In future tests, clinostat controls for the drugs need to be made. Also, additional trials for the drug plates as well as the 90 degree controls and normal clinostat controls need to be done. Images also need to be taken until the root is allowed to completely reorient. In addition to reorientation rate and angles, we also need to take data on the growth rate of the plants. This will allow us to quantify the rate at which the plants grow.

All of these tests were performed using wild type *A. thaliana* seeds. Our advisor, Dr. Marshall Porterfield has requested we do the same tests on two *A. thaliana* NOS mutants as well.

Material and Methods

Seed Preparation

All seeds were purchased from the Carolina Seed Company. Prior to planting, seeds were sterilized in a 50% bleach, 45% dH_2O, and 5% Tween20 solution for 10 minutes.

minutes. After 10 minutes in the sterilization solution, they were rinsed in ethanol for one minute followed by a one minute rinse in dH_2O.

Planting

The sterilized seeds were grown on an agar media composed of 1.1g MS+gamborg vitamins, 0.25g MeS, 2.5g sucrose, and 2g phytagel per 500mL of water. The mixture was pHed to 5.75 and then autoclaved for 30 minutes. 50 mL was dispersed into each square Petri dish. The seeds were then planted on the drug-free plates with a modified syringe and allowed to germinate and grow (standing vertically) for approximately six days in a lighted incubation chamber set at 25° C.

Drug Plate Preparation

The process for making the agar was the same above. However, the PTIO and ODQ were added to the liquid agar after autoclaving but before the agar had solidified. After solidifying, the plates were allowed to cool for two hours before the seedlings were transferred.

Transplantation

Seedlings, approximately six days old were transferred from their original drug free plates on to freshly made drug plates using forceps making sure the roots as straight as possible. Three seedling were placed vertically on each drug plate, but then the plate was turned 90 degrees so that the roots could reorient in a new direction, 90 degrees from the original growth direction. Plants were given an hour to adjust to the new plates before the initial 'zero-hour' photo was taken.

Images

All photos were taken using Dr. Anne Maglia's digital camera microscope. Pictures were taken of each seedling at one hour intervals for four hours. During this four-hour time-period, the plants were kept out of the growth chamber.

The camera magnification was 2.1 X . Adobe Photoshop was used to capture the images as well as create Figures 6 and 7. The reorientation angles were measured from the pictures using the software ImageJ. The diagram in Figure 1 was created using Microsoft Word. Graphs in Figures 2 through 5 and Figure 9 were created using Microsoft Excel. The images in Figure 8 were created using Paint.

Acknowledgments

Several people were involved or assisted with this project and many thanks are due to them. First, I'd like to thank our advisor, Dr. Marshall Porterfield and his graduate student Kacey Morris for their guidance and knowledge. I'd also like to thank my project partners Jennifer Jacobi and Jacob Elmer, whom without, late nights in the lab would have been extremely boring. Finally, I'd like to thank Dr. Anne Maglia and her graduate student Barb Banbury for letting us use their camera late to obtain our images.

References

1. Pagnussat GC, Lanteri ML, Lamattina L (2003) Nitric oxide and cyclic GMP are messengers in the indole acetic acid-induced adventitious rooting process. Plant Physiology 132: 1241–1248
2. Blancaflor EB, Masson PH (2003) Plant gravitropism: unraveling the ups and downs of a complex process. Plant Physiology 133: 1677–1690
3. Ottenschla¨ger I,Wolff P,Wolverton C, Bhalero RP, Sandberg G, Ishikawa H, Evans ML, Palme K (2003) Gravity-regulated differential auxin transport from columella to lateral root cap cells. Proc Natl Acad Sci USA 100: 2987–2991
4. Perbal G, Driss-Ecole D (2003) Mechanotransduction in gravisensing cells. Trends Plant Sci 8: 498–50

THE PROPERTIES OF BRIDGESTONE ECOPIA SOLAR CAR TIRES (FOR THE UMR SOLAR CAR TEAM)

Tessa C Russell
Department of Mechanical Engineering

Abstract
Much of the energy used by a solar car can be attributed to overcoming rolling resistance, and rolling resistance comes predominantly from the tires. The main goal of this project was to better understand the properties of the Bridgestone Ecopia tires used by the UMR Solar Car Team. Experiments were conducted to obtain this objective, measuring the vertical stiffness, lateral stiffness, and contact patch shape and area. As expected, with decreasing pressure and increasing load, the vertical and lateral deflections increased as well as the tire contact patch area.
The stiffness parameters of the tire, measured experimentally were used in an existing rolling resistance model for tires to measure quantitatively how load, pressure and tire misalignment affects the rolling resistance coefficient (C_{rr}) for the tires. With increasing values of the misalignment angle, the coefficient of rolling resistance increased. It was found that a tire can have a larger misalignment angle at higher loads and higher pressures. It was found that load and pressure had the same effect on the coefficient of rolling resistance. The main conclusion that can be reached from the C_{rr} results is that the tires should not have a misalignment angle greater than 1 degree to keep the C_{rr} down.

Introduction
Nearly 35% of the energy used by a well-designed solar car traveling at 56mph can be attributed to overcoming rolling resistance (1). This percentage increases with decreasing speed. The primary factor in rolling resistance is the tires. Therefore it is very important to understand the properties of the tires. There has been very little testing done on the Bridgestone Ecopia tires used by the UMR Solar Car Team. The main goal of this project is to better understand the properties of these Bridgestone Ecopia tires. There are two objectives to reach this goal. The first was to see how the tire deflected vertically with increased load. The second was to be able to better describe the coefficient of rolling resistance of the tires.

Experimental Setup and Procedure
For all experiments, one worn Bridgestone Ecopia tire and one new Bridgestone Ecopia tire, still with a sticker, were used. The following pressures were tested for each tire: 80psi, 100psi, and 120psi.

Tire Vertical Stiffness
The tire was placed in the Instron 5583 between the two compression platens. The Instron Merlin software was then programmed to conduct a compression test with a maximum load of 250lbs and a speed of 0.1in/min. The tire was then loaded per the program three times. The tire was rotated 60degrees for each run. Load and vertical deflection data was collected for each run.

Tire Lateral Stiffness
The tire was placed in the Instron 5583 between the two compression platens. A Linear Variable Differential Transformer (LVDT) was placed at the bottom of the tire, more specifically at the center of the tire wall, which was used to measure lateral deflection. The tire was then compressed to 200lbs. At each pressure, a 35lb lateral load was put on the tire three times. Before and after each lateral load, a lateral deflection was measured. Figure 1 displays the setup of the experiment.

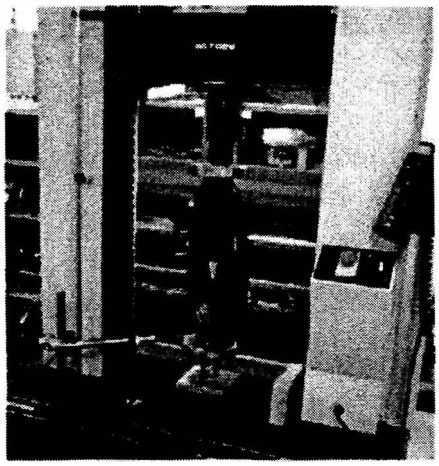

Figure 1: Experimental Setup

Tire Contact Patch

Before the tire was placed in the Instron 5583, three layers were placed on the bottom compression platen. The layers were as follows, bottom first: white computer paper, carbon paper, and 60 grit sandpaper. The tire was then placed in the Instron 5583 between the two compression platens. The tire was then compressed to 150lbs, 175lbs, 200lbs, 225lbs, and 250lbs. Elliptical imprints were made on each piece of white paper, and approximate measurements were taken for the two diameters of the ellipse. Three runs were conducted at each load.

Results and Discussion

Tire Vertical Stiffness

Once the data was collected, for each pressure a graph of load versus vertical deflection was created using Microsoft Excel. To create the graph, the total vertical deflection was divided by two since the measured vertical deflection was the deflection of two sides of the tire rather than one. Figure 1 shows the graph of load versus vertical deflection for the old tire at 80psi. As was expected, the vertical deflection increased with increasing load for each of the three runs.

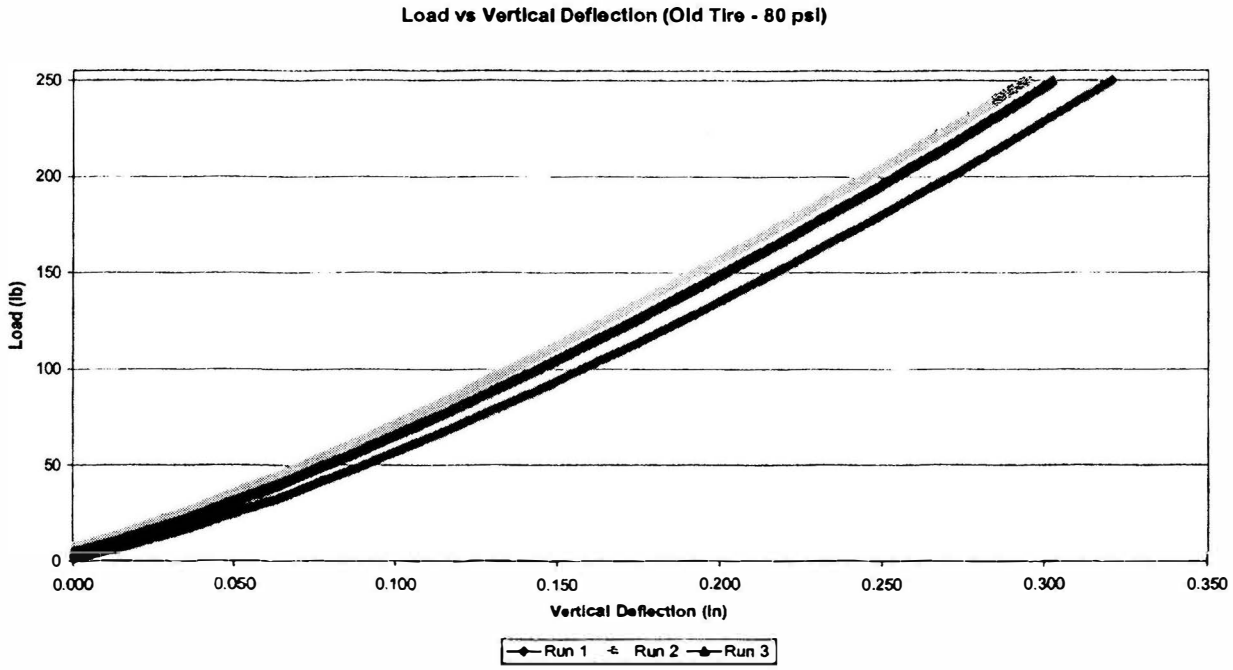

Figure 2: Load vs Vertical Deflection (Old Tire - 80psi)

Similar graphs were seen for pressures of 100psi and 120psi as well as for all pressure graphs for the new tire. As the pressure increased for both the old and new tire, the maximum vertical deflection reached decreased. Table 1 displays the average maximum vertical deflection at 240lbs for both the old and new tire at pressures of 80psi, 100psi, and 120psi.

Table 1: Maximum Vertical Deflection vs Pressure

Old Tire		New Tire	
Pressure (psi)	Deflection (in)	Pressure (psi)	Deflection (in)
80	0.296	80	0.280
100	0.232	100	0.238
120	0.206	120	0.225

It can be seen that as the pressure increases in both the old and new tire, the vertical deflection decreases. At a pressure of 80psi, the old tire deflected 0.016in more than the new tire, whereas at pressures of 100psi and 120psi, the new tire deflected more, 0.006in and 0.020in respectively.

Tire Lateral Stiffness

The difference between each before and after 35lb load measurement was averaged for the three runs of each tire. Then the data was averaged for both the old and new tire. Then a graph of lateral deflection versus pressure for the old tire, new tire, and both tires was created using Microsoft Excel (See Figure 3).

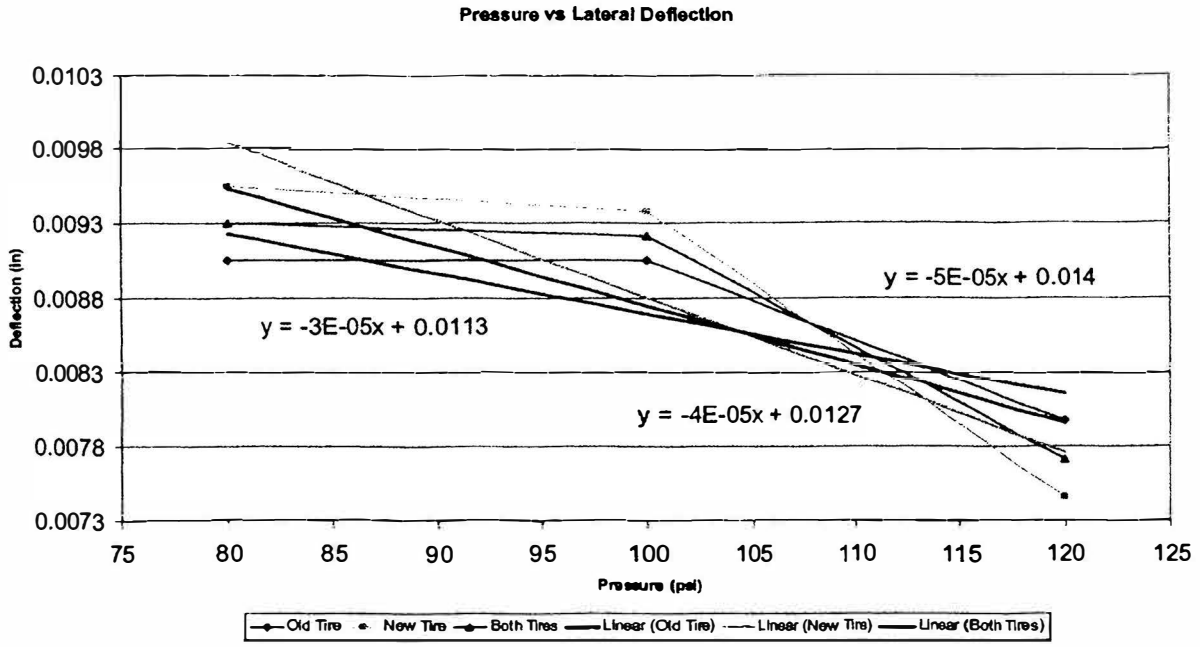

Figure 3: Pressure vs Lateral Deflection

A linear regression equation for the lateral deflection dependent on pressure was then found for data from the old tire, new tire, and both tires. The constants (C_1 and C_2) for the equation of both tires (Equation 1) are given in Table 2.

Table 2: Lateral Deflection Constants

C_1	C_2
-3.958E-05	0.012653

Equation 1: Lateral Deflection Dependent on Pressure

$$D = C_1 \bullet P + C_2,$$

The variables are described as follows: D = lateral deflection equation, P = pressure, and C_1 and C_2 are constants. This equation was used to formulate the lateral stiffness equation, k equation (Equation 2), which was used for the coefficient of rolling resistance analysis.

Equation 2: *k* Equation

$$k = \frac{3\ 5}{D} = \frac{35}{C_1 \bullet P + C_2}$$

The variables are described as follows: k = lateral stiffness equation, 35 = lateral load applied to the tires during the experiment, and D = lateral deflection equation (Equation 1).

Tire Contact Patch

Average elliptical diameters were calculated at each load from the three runs. For each pressure, plots of the contact patch were created, varying with load using Microsoft Excel.

Figure 4 shows the contact patch plot for an old tire at 80psi.

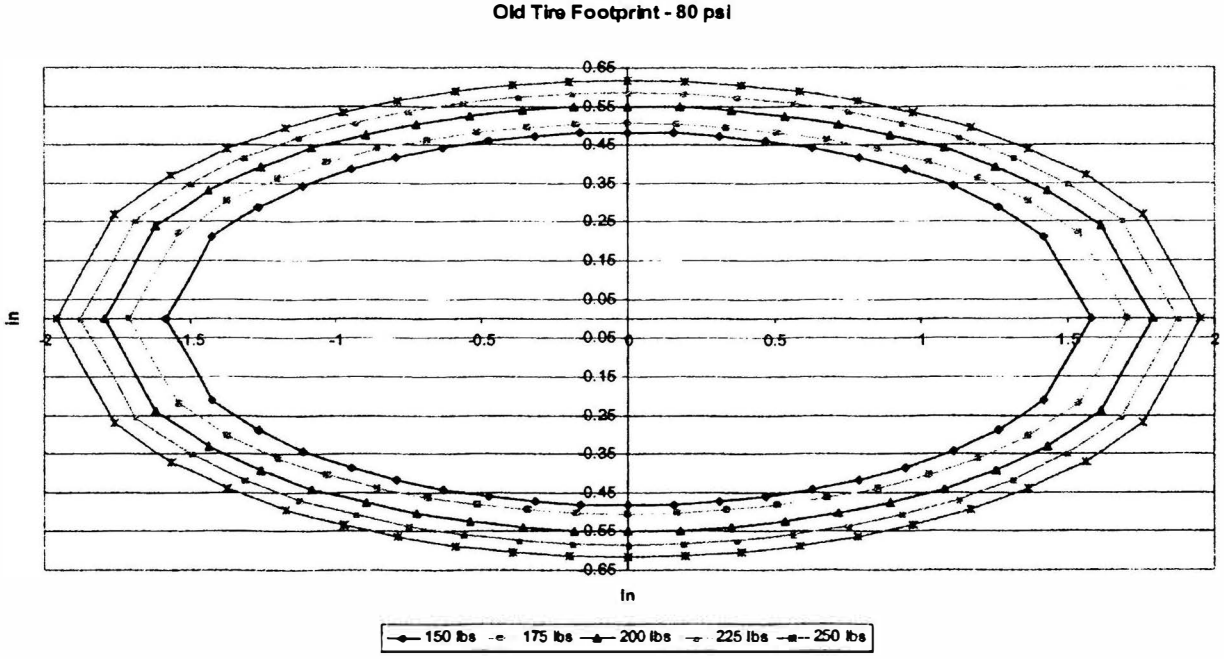

Figure 4: Old Tire Footprint - 80psi

Similar graphs were seen for pressures of 100psi and 120psi as well as for all pressure graphs for the new tire. As the load on the tires increased, the contact patches became larger. Table 3 displays the average a and b values for the contact patch of the old tire varying with pressure and load. The variables a and b are the elliptical diameters; a in the y-direction and b in the x-direction.

Table 3: Old Tire Elliptical Diameters

	Pressure - 80 psi		Pressure - 100 psi		Pressure - 120 psi	
Load	a	b	a	b	a	b
150	0.483	1.578	0.451	1.506	0.444	1.408
175	0.505	1.707	0.477	1.592	0.455	1.511
200	0.550	1.793	0.514	1.678	0.484	1.593
225	0.585	1.870	0.534	1.762	0.512	1.648
250	0.616	1.952	0.570	1.831	0.533	1.729

A table was created listing the average a and b values for the contact patch of the new tire varying with pressure and load (See Table 4).

Table 4: New Tire Elliptical Diameters

	Pressure - 80 psi		Pressure - 100 psi		Pressure - 120 psi	
Load	a	b	a	b	a	b
150	0.484	1.604	0.431	1.526	0.401	1.410
175	0.508	1.700	0.450	1.638	0.442	1.527
200	0.559	1.794	0.503	1.657	0.477	1.578
225	0.598	1.863	0.518	1.745	0.501	1.639
250	0.617	1.975	0.547	1.828	0.515	1.747

For the most part, the old tire elliptical diameters were greater than those of the new tire. A linear regression equation for the length of the contact patch dependent on pressure and vertical load, b equation (Equation 3), was found for both the old and new tire.

Equation 3: b Equation

$$b = C_1 \bullet P + C_2 \bullet W + C_3$$

The variables are described as follows: b = contact patch length, P = pressure, W = load, and C_1, C_2, and C_3 are constants.

Table 5 shows the values for the constants C_1, C_2, and C_3 for both the old and new tires.

Table 5: b Equation Constants

	C_1	C_2	C_3
Old Tire	-0.0051	0.0033	1.5151
New Tire	-0.0052	0.0032	1.5595

This b equation was used for the coefficient of rolling resistance analysis.

Rolling Resistance Coefficient (C_{rr})

For calculations of the rolling resistance coefficient, the flexible tire model (1) was used. The k (Equation 2) and b (Equation 3) equations from the lateral stiffness and contact patch experiments were used. The lateral motion of the tire can be attributed to flexing and/or sliding. There is a critical value δ_C, where the lateral motion of the tire is taken up either by flexing only or flexing and sliding. If the value of $b\sin(\theta) < \delta_C$, then the following equation (Equation 4) for C_{rr}' can be used.

Equation 4: C_{rr} Equation for $b\sin(\theta) < \delta_C$

$$C_{rr}' = \left(1 + \frac{kb\sin(\theta)}{W}\right) C_{rr}$$

The variables are described as follows: C_{rr}' = rolling resistance coefficient, k = lateral stiffness, b = contact patch length, W = load, θ = tire misalignment angle, and C_{rr} is explained by Equation 5.

Equation 5: C_{rr} Equation varied with Pressure

$$C_{rr} = 49.367\left(\frac{P}{100}\right)^{0.3072}\left[19 - \sqrt{19^2 - \frac{2299.7}{19.58 + (5975)(P)}}\right]$$

The variables are described as follows: C_{rr} = rolling resistance coefficient varied with pressure and P = pressure. If the value of $b\sin(\theta) > \delta_C$, then the following equation (Equation 6) for C_{rr}' can be used.

Equation 6: C_{rr} Equation for $b\sin(\theta) > \delta_c$

$$C_{rr}' = C_{rr} + \mu C_{rr} + \left(\frac{b\sin(\theta) - \frac{\mu W}{k}}{b\cos(\theta)} \right)$$

The variables are described as follows: C_{rr}' = rolling resistance coefficient, k = lateral stiffness, b = contact patch length, $\mu = 0.8$ (friction coefficient), W = load, θ = tire misalignment angle, and C_{rr} is explained by Equation 5. Equations 4 through 6 were used to create the following plots: C_{rr} versus theta, C_{rr} versus load, and C_{rr} versus pressure.

C_{rr} versus Theta

Two plots of rolling resistance coefficient (C_{rr}) versus the tire misalignment angle (theta) were created for both the old and new tire. The first plot, Figure 5, is the graph of C_{rr} versus theta for the old tire with pressure set at 100psi and constant load lines.

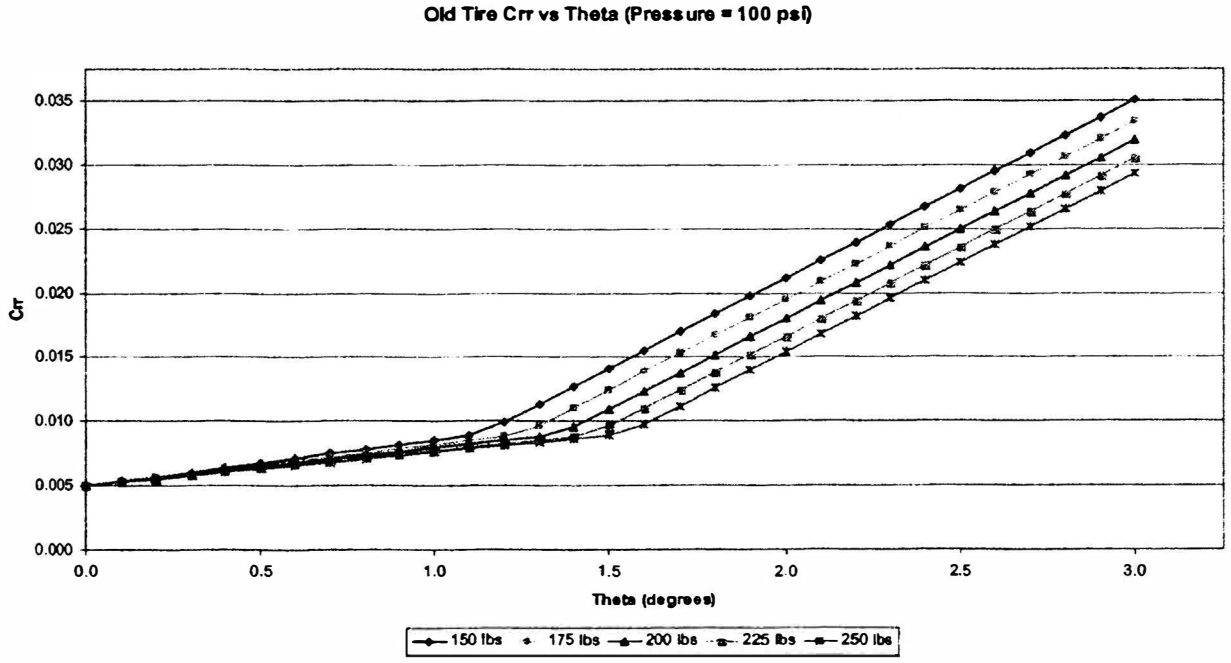

Figure 5: Old Tire C_{rr} vs Theta (Pressure = 100psi)

As can be seen, the C_{rr} increased with increasing values of the misalignment angle, theta. The slopes of these lines decreased with load. With a misalignment angle between 1 and 1.5 degrees, the slopes of C_{rr} versus theta lines increased. Essentially, a tire can have a larger misalignment angle at higher loads. A similar graph was seen for the new tire.

The second plot, Figure 6, is the graph of C_{rr} versus theta for the old tire with load set at 200lbs and constant pressure lines.

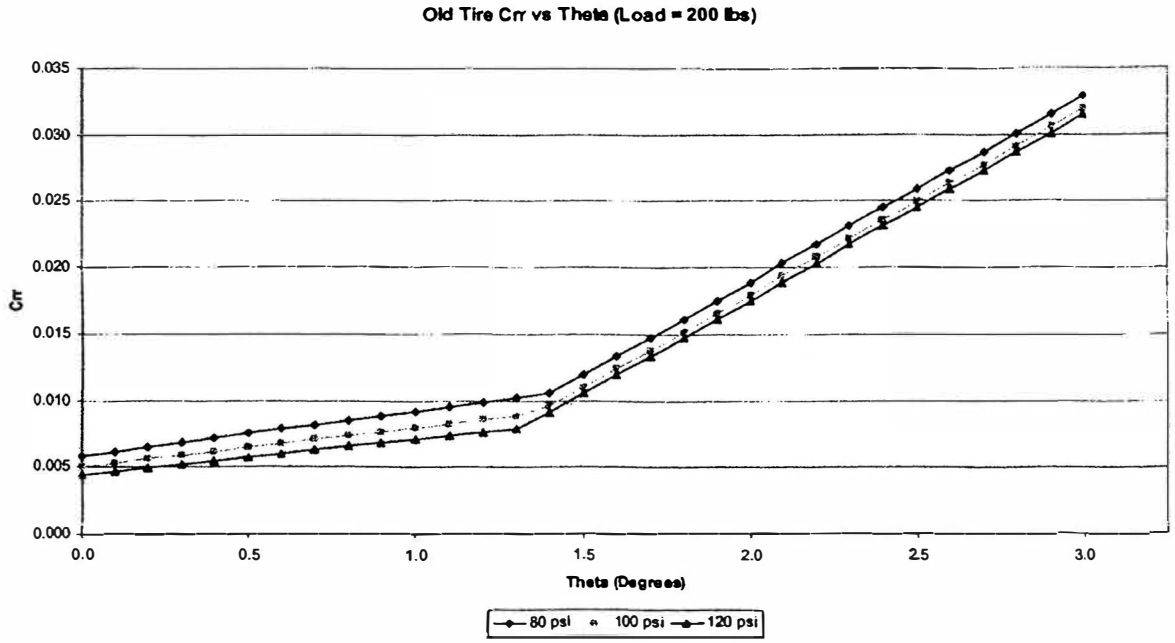

Figure 6: Old Tire C_{rr} vs Theta (Load = 200lbs)

As can be seen, the C_{rr} increased with increasing values of the misalignment angle, theta. The slopes of these lines decreased with pressure. With a misalignment angle between 1.25 and 1.5 degrees, the slopes of C_{rr} versus theta lines increased. Essentially, a tire can have a larger misalignment angle at higher pressures. A similar graph was seen for the new tire.

C_{rr} versus Load

Two plots of rolling resistance coefficient (C_{rr}) versus load were created for both the old and new tire. The first plot, Figure 7, is the graph of C_{rr} versus load for the old tire with a misalignment angle of 1 degree and constant pressure lines.

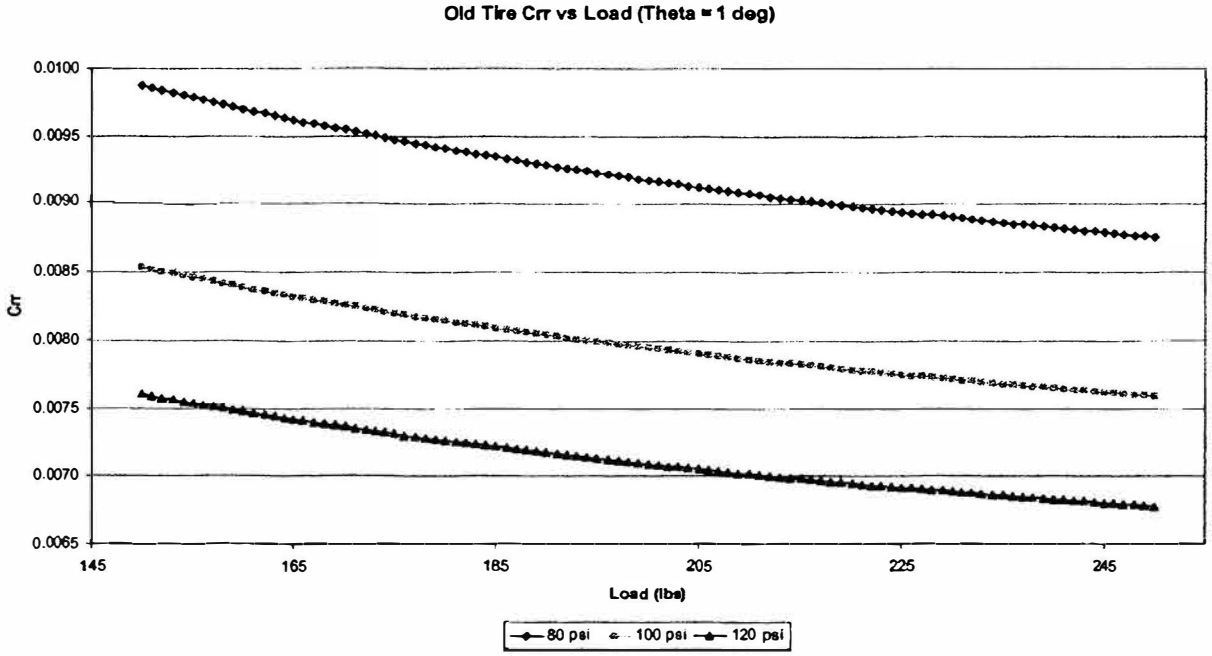

Figure 7: Old Tire C_{rr} vs Load (Theta = 1deg)

As can be seen, the C_{rr} decreased with increasing load and increasing pressure. A similar graph was seen for the new tire. The second plot, Figure 8, is the graph of C_{rr} versus load for the old tire with pressure set at 100psi and constant theta lines.

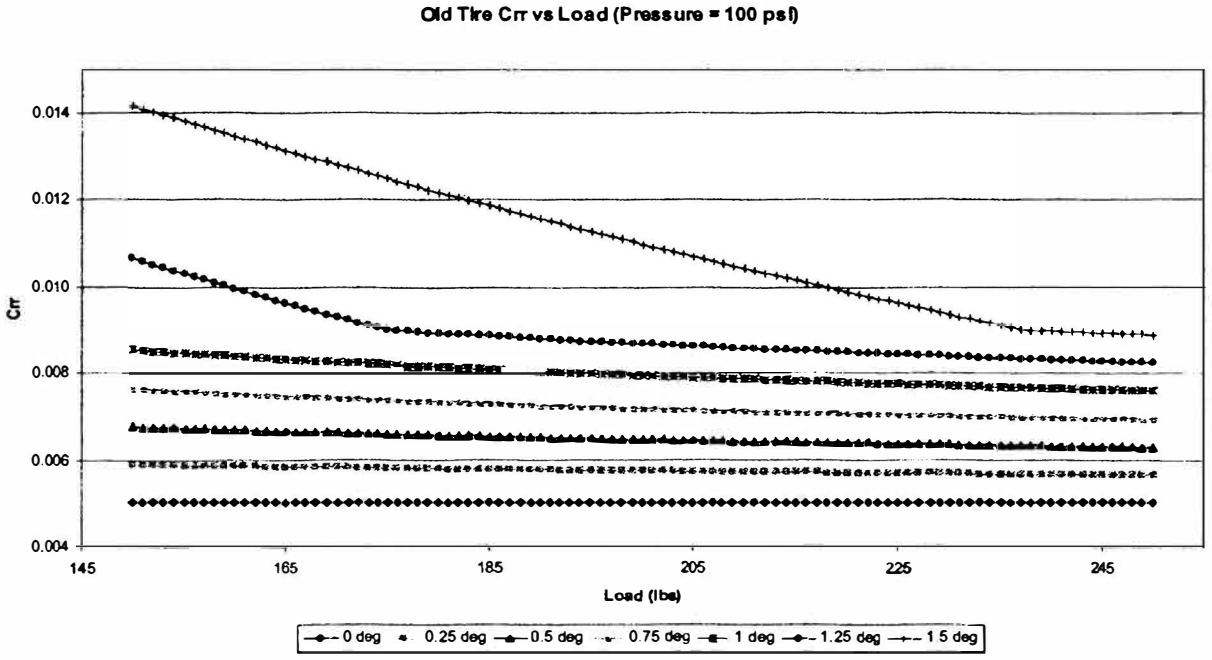

Figure 8: Old Tire C_{rr} vs Load (Pressure = 100psi)

As can be seen, the C_{rr} decreased with increasing load and decreasing values of the misalignment angle. For low values of misalignment angle, 0 to 1 degree, the C_{rr} values are fairly constant. For high values of

misalignment angle, greater than 1 degree, the C_{rr} lines have a very high decreasing slope. A similar graph was seen for the new tire.

C_{rr} versus Pressure

Two plots of rolling resistance coefficient (C_{rr}) versus pressure were created for both the old and new tire. The first plot, Figure 9, is the graph of C_{rr} versus pressure for the old tire with a misalignment angle of 1 degree and constant load lines.

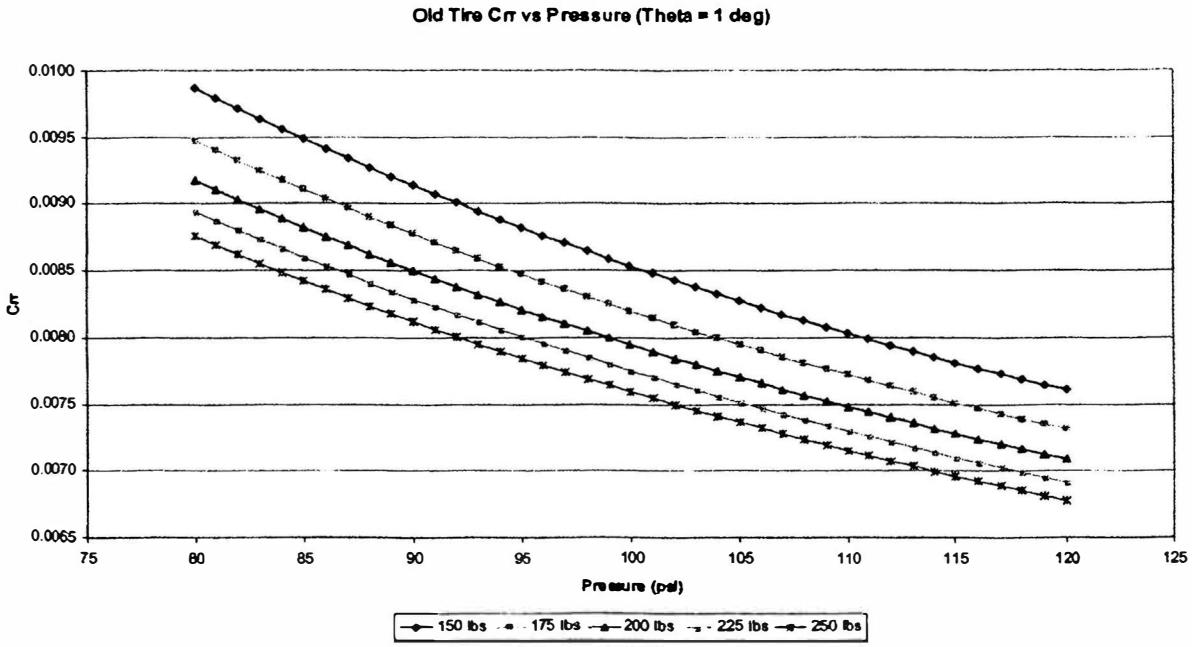

Figure 9: Old Tire C_{rr} vs Pressure (Theta = 1deg)

As can be seen, the C_{rr} decreased with increasing pressure and increasing load. A similar graph was seen for the new tire. The second plot, Figure 10, is the graph of C_{rr} versus pressure for the old tire with load set at 200lbs and constant theta lines.

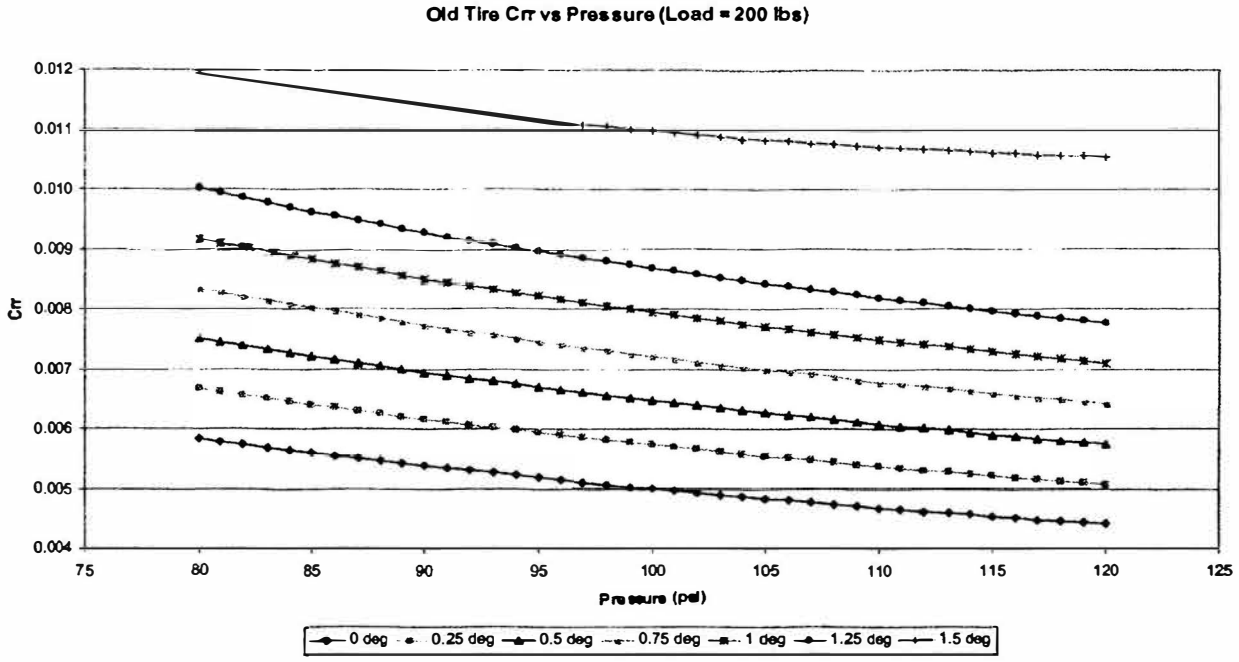

Figure 10: Old Tire C_{rr} vs Pressure (Load = 200lbs)

As can be seen, the C_{rr} decreased with increasing pressure and decreasing values of the misalignment angle. At misalignment angles above 1.25 degrees, there is a high jump in coefficient of rolling resistance. A similar graph was seen for the new tire.

Conclusions

The main goal of this project was to better understand the properties of the Bridgestone Ecopia tires used by the UMR Solar Car Team. Two objectives were realized through this project. The first was to see how the tire deflected vertically with increased load. The second was to be able to better describe the coefficient of rolling resistance of the tires. As expected, with decreasing pressure and increasing load, the vertical deflection of the tire increased. Also, with decreasing pressure and increasing load, the tire contact patch increased in size. The main conclusion that can be reached from the coefficient of rolling resistance results is that the tires should not have a misalignment angle greater than 1 degree to keep the coefficient of rolling resistance down.

Acknowledgements

I am especially grateful to my research advisor, Dr. Doug Carroll, the main faculty advisor for the UMR Solar Car Team. He gave me much needed advice, encouragement, and scientific insights. I would also like to thank Jeff Thomas, the Mechanics of Materials Lab Instructor, for helping me understand the inner workings of the equipment used for the experiments. And finally, I would like to thank the UMR Solar Car Team for allowing me to pursue this project.

References

1. Carroll, Douglas R. The Winning Solar Car: A Design Guide for Solar Race Car Teams. Pennsylvania: SAE International, 2003.

Reactivity Effect and Axial Flux Profile of Isotope Production Element

OURE Report 2005

University of Missouri-Rolla

University of Missouri-Rolla Reactor

Alfred L. Schovanez III

Submitted to Office of Undergraduate and Graduate Studies

Abstract:

Due to a continued increase for the demands of irradiation, new facilties to hold samples are needed. The IPE is an experimental facility at the University of Missouri-Rolla Reactor. The IPE is an isotope production element that uses pins, screws, and O-rings to keep a water-tight seal and hold samples in the reactor core. Since this element has never been tested in the last few years and no known data is on file on it, experimentation to find out how the IPE affects the core is needed. It was determined that reactivity testing and axial flux profile testing was needed. The reactivity testing was needed to determine how much reactivity would be added to the reactor and flux profile needed to determine the shape and intensities of the flux per unit length of the IPE. Testing has shown that the IPE is suitable for use in the UMR Reactor and has a maximum reactivity addition of around 0.25% which is well within safety limits of movable experiments at the UMR Reactor. Neutron flux profile testing has shown the distribution to be parabolic and that at the end of the tube compared to the middle section decreases to 50% the middle value.

Table of Contents

1. INTRODUCTION

1.1 What is the isotope production element?

The isotope production element (IPE) is an irradiation facility of the University of Missouri - Rolla Reactor (UMRR). An irradiation facility is a UMRR approved container used to irradiate samples with neutron or gamma irradiations. This container is the size of a normal fuel element, 3 inch by 3 inch cross section and it is three feet tall. A removable top uses O-rings to create a watertight seal. Inside the IPE, a hollow tube section allowed samples to be placed within the IPE. The top is secured onto the element's main body via screws and holding pins. The entire assembly is cladded in aluminum alloy and the filler material is graphite. Aluminum is used for economic considerations, good corrosion-resistance properties, and short half-life of 2.28 minutes. Graphite is used for its excellent neutron reflecting and moderating properties as well as its almost non-existent neutron absorption cross section. For further information on the IPE, see *University of Missouri-Rolla Nuclear Reactor Analysis Report* page 3-17 and Figure 15 on page 3-18.

Figure 1.1 Assembled Isotope Production Element

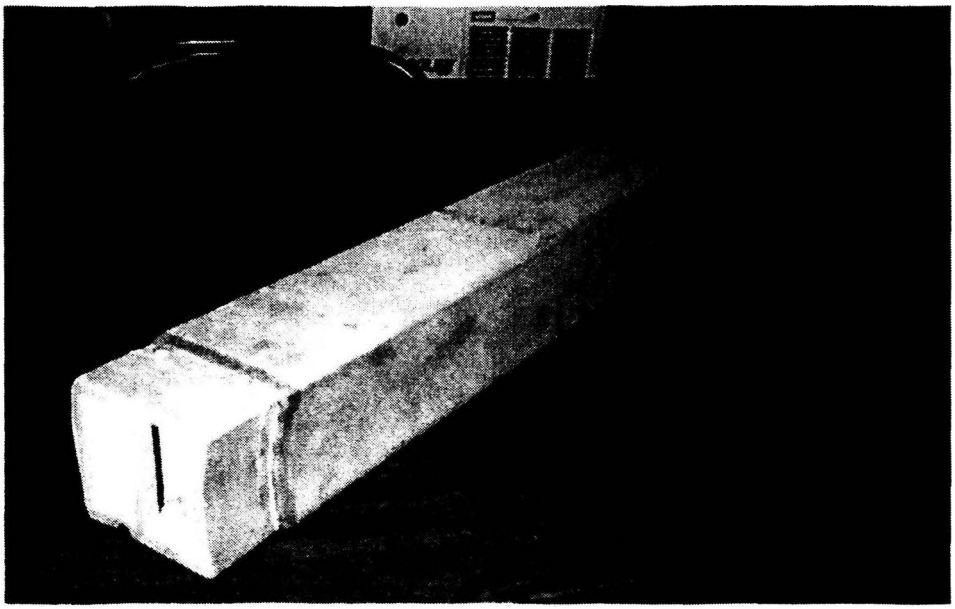

Figure 1.2 Disassembled Isotope Production Element

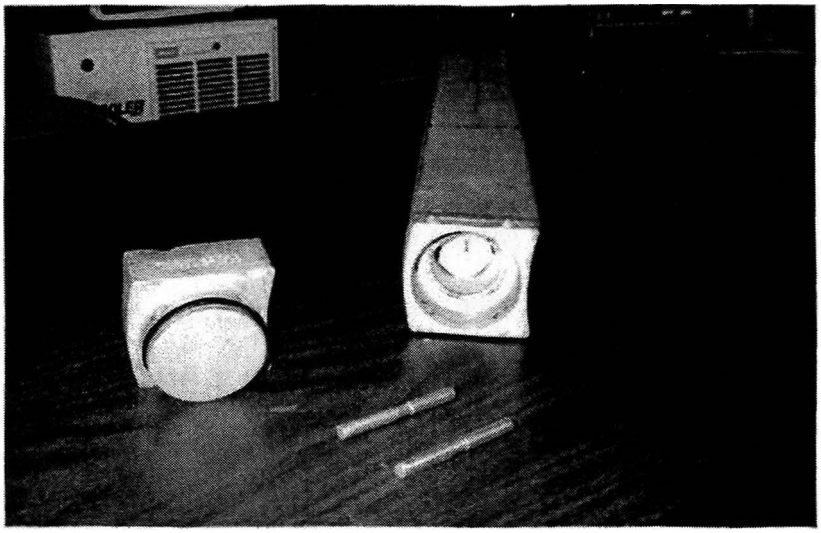

1.2 Why does it need to be tested?

The UMRR has listed the IPE as an approved experimental facility in the *Standard Operating Procedures* (SOP 206: §B). Due to years of disuse, data involving the effects of the IPE in the reactor core has either been lost or not at all taken. Technically, no testing has to be completed since the IPE is an approved facility, unless the IPE becomes a permanent core fixture as described in SOP 206 §C.4 and §C.5. However, the UMRR operates on the safety first principle. The primary concern, as outlined in the SOP 206, is reactivity addition to core when this experimental facility is installed.

Reactivity is defined as the deviation a reactor takes from criticality, usually measured in a percent. A critical reactor is a reactor that is at stable power; that means the neutrons created during the fission reaction is the same amount of neutrons being removed (absorbed by uranium) to create it. Positive reactivity is akin to adding more fuel to the fire, causing an increase in neutron population production per generation resulting in a condition called supercritical.

Negative reactivity is dosing down the fire metaphorically, thus causing a decrease in the neutron population after each generation and a decrease in power. Essentially, a nuclear reactor is controlled by changing reactivity to achieve a certain reactor condition.

Testing a reactivity addition of an experiment is very important for the safety of the reactor. If an inserted experiment adds too much reactivity, a large supercritical state could result exist causing a rampant power increase. A rampant power increase could compromise reactor safety features and limits. Therefore, a reactivity test would determine what the worth of experiment facility is and what effect it would have on reactor operations if installed.

2. PROCEDURE

2.1 Introduction to IPE Testing

Two tests were performed for the IPE. The first test was a reactivity test of the facility. The IPE was first placed into a core configuration, and then the reactivity worth was determined. This was repeated for several grid positions in the UMRR core. The second test was a core flux profile testing through neutron activation of a copper wire. The importance of the flux profile is to determine what the neutron flux is at various parts of the element and determine its distribution. The procedure for this was based on a NE 304 experiment entitled *Experiment VII: Measurement of Axial and Peripheral Flux Profile*. In addition, SOP 206 was followed for regulatory and precautionary purposes for both reactivity and flux testing.

2.2 Reactivity Testing

Reactivity testing involved comparing the critical rod heights of the reactor without the IPE and with the IPE installed in the core. Critical rod height is the height of the control rods that the reactor is critical at a certain power. As explained in the previous section, reactivity worth

(amount of reactivity the IPE adds to the core) of the IPE is important to determine. The importance of this is that if removal or installation of the IPE during operation, a situation did not occur where a rampant reactivity addition could compromise reactor integrity. Note that reactivity is denoted in terms of percent delta k / k.

The testing was performed when the IPE's hollow inner tube was filled with water and those positions that had a marginal core affect, defined as greater than 0.1% $\Delta k/k$ in the water filled mode. The IPE was tested in a water-filled mode for safety reasons. Since normally the IPE would be inserted dry-air-filled, it was important to determine that if the structural integrity of the IPE was compromised that the reactivity insertion was not so great as to cause a rampant power increase. A basic procedure was followed for both water and air-filled modes. The list shows in order the experiment was implemented.

1. The reactor started to a leveled power of 10 watts per SOP 103.
2. The critical rod heights of all four rods recorded to nearest tenth of an inch.
3. Reactor was shutdown by SOP 105.
4. The IPE inserted into a core position and reactor taken again to 10 watts.
5. Critical rod heights of all four rods recorded again to the nearest tenth of an inch.
6. The reactor was shutdown again by SOP 105.

Note that during the experiment, the neutron source was always inserted into the source tube. This experiment was performed on 9 core positions for the water-filled mode. Using the *Table 1: Integral Rod Worths Core 101W,* the reactivity worths of all four rods for when the IPE was installed and not installed was accomplished. By looking for the correct reactivity worth for the critical rod height and checking the corresponding column of rod worth, the rod worths were

added for all four rods for both rod heights. Then they were subtracted as shown from each other as shown in equation 2.1:

$$\sum_{i=1}^{4} \rho_{IPE\ critical\ rod\ height} - \sum_{i=1}^{4} \rho_{critical\ rod\ height} = \rho_{\text{reactivity worth IPE}}$$

The experiment was repeated three times for grid positions C3, C7, and C8 in the water-filled mode. Out of the nine core positions, only C3, C7, and C8 were repeated since those positions had the largest reactivity affect on the core and where the only positions tested for the air-filled mode. The reason why is that the air-filled mode would have less reactivity effect than the water-filled tube due to the nuclear properties of both modes. Figure 2.1 shows the actual facsimile of the core grid position in the reactor.

Figure 2.1: Core Grid Position

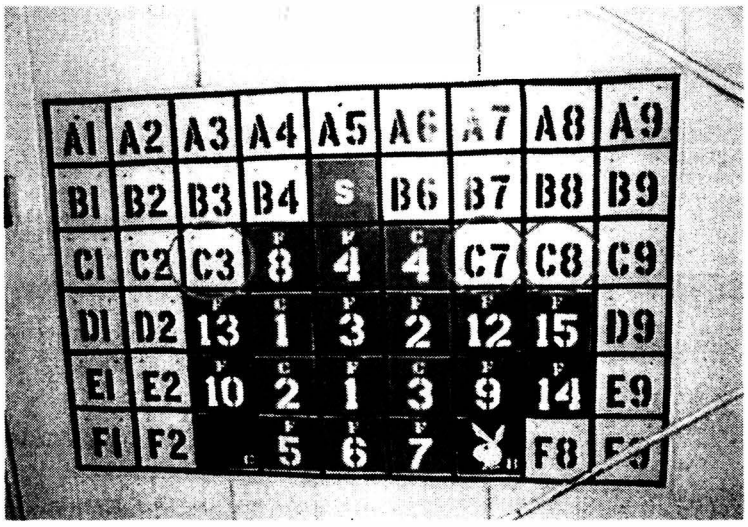

Note locations of C3, C7, and C8. Red squares designate fuel element, green squares designate control rod elements, 'S' designates neutron source, Playboy© Bunnies represent rabbit tubes, and white empty spaces indicated that core position is empty. In addition, see that C3, C7, and C8 are closer to the core than other positions thus more neutron radiation interacts at those locations. Finally, nothing below 'C' level is used for installation of experimental facility.

2.3 Flux Profile Testing

Neutron flux profile is the distribution of neutron activation density per vertical length of the IPE when the reactor is operating. It is quadratic with the maximum neutron activation density at the middle of the element and lowest at the IPE's ends. This is important when placing samples into the IPE to know what neutron exposure per unit length is and what the flux is through the entire length of element by relating it to the activity per inch of each piece. Copper wire was used because it has only two decay modes for the two isotopes Cu-63 and Cu-65. With a neutron absorbtion, these two isotopes become radioactive Cu-64 and Cu-66 which are both gamma ray emitters. Cu-64 has a half life of 12.7 hours and Cu-66 has a half-life of 5.1 minutes. Since after seven half-lives, an isotope is considered decayed away, the only isotope of concern for detection is Cu-64 because the wire was removed a little after two hours after the reactor was shutdown and seven half-lives is 35.7 minutes.

Using Irradiation Request Form (IRF) 05-01 based on IRF 95-37, the copper wire was irradiated at 500 watts for 10 minutes. The procedure for this is shown in the list below.

1. The IPE with copper wire was installed in core position C7.
2. The reactor was taken and leveled to 500 watts by SOP 103.
3. A timer was used to determine ten minutes of exposure.
4. The reactor was shutdown immediately after 10 minutes by SOP 105.

After several hours, the IPE was removed from the core, made sure no hazardous levels of radioactivity were present and the wire was removed. The wire's radiation is assumed to be of Cu-64 only since most of the Cu-66 has decayed away due to its short half-life. The wire was weighted in one-inch segments and taken to the sodium-iodide counter to be counted. A background check was taken every five counts. The entire segment was cut into 24 segments.

Each segment was weighed and activity counts was recorded in a Microsoft Excel datasheet. After, the material was picked placed on the hot bench to be disposed of properly. The experiment was also performed again on core position C3 in the same manner.

3. Reactivity and Core Flux Profile Results

3.1 Reactivity Results

The results for the water-filled data for the three core positions of primary interest C3, C7, and C8 is shown below. Note that the data is normalized to the reference core configuration of degrees Fahrenheit (21.11 Celsius). The reason for normalization to 70 degree Fahrenheit is to have a common point of comparison and since all of the rod worth tables are calculated in

Table 3.1: Reactivity of Water-Filled Void Tube at 70° F

Core Position	Trial 1: % Δk/k	Trial 2: % Δk/k	Average: % Δk/k	Standard Deviation:
C3	0.17132	0.16179	0.16656	0.0071
C7	0.39270	0.40977	0.40124	0.0122
C8	0.13967	0.10439	0.12179	0.0249

relation to that temperature. In addition, temperature affects reactivity in a linear proportion. Increasing temperatures causes a decrease overall reactivity for the UMRR. The first column is core position. Following the Core Position is Trial 1 and Trial 2, which are the reactivity worth of the IPE for both runs; the worth is done is % delta k over k. The fourth column is the average of the two trials and the standard deviation is calculated.

This next table is the reactivity worth of the IPE for air-filled mode. The results were repeated three times and the table follows that of Table 3.1. Again the first column is core

position, the second through fourth columns are the trial runs. The fifth column is the average of the three trial runs and the sixth is the standard deviation.

Table 3.2: Reactivity of Air-Filled Tube at 70° F

Core Position	Trial 1: % Δk/k	Trial 2: % Δk/k	Trial 3: % Δk/k	Average: % Δk/k	Standard Deviation:
C3	0.07494	0.03387	0.02764	0.04548	0.0257
C7	0.25914	0.24462	0.23838	0.24405	0.0114
C8	0.07974	0.02234	0.06819	0.05676	0.0303

3.2 Neutron Flux Profile Results

The results for the axial profile of the core positions are shown below. Notice how the graph is parabolic, which is expected for axial flux profile. Figure 3.1 shows the activity per gram versus wire length. The complete data is in Appendix B. The horizontal axis is length of wire with '0' inches being the top of the element's interior to '24' inches being the bottom of the element's interior. The vertical axis is activity per gram of the wire at that length. It is activity

Figure 3.1: Axial Flux Profile of IPE in C7

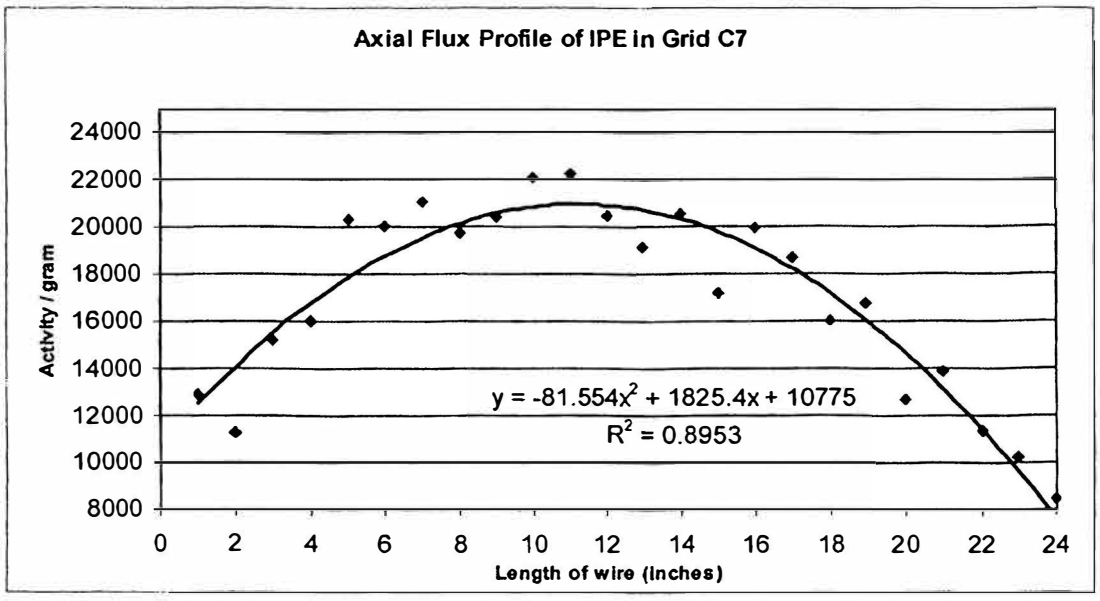

per gram as to normalize the data. This is done because mass is proportional to number density, which is proportional to activity. This information can be found in any nuclear physics text.

In addition note, that these values of activity were solved for the highest flux attained while at 500 watts for 10 minutes. This initial activity is solved for by back-solving using Equation 3.1.

$$A(0) = A(t)e^{\lambda t}$$

In this equation, A(0) is initial activity which is the unknown. A(t) is the detected activity in the sodium iodide detector taken 't' minutes after shutdown of the reactor. The λ is called a decay constant and equals the natural log of 2 over the half-life of the isotope in minutes. Through this, activity at the time of shutdown can be determined. To normalize, divide that activity by the weight of the sample (one through 24) in grams, then plot on an Excel spreadsheet. The second core position tested was C3. This profile is depicted in Figure 3.2 is presented in the same manner as Figure 3.1. Note that the flux is higher in C7 than in C3.

Figure 3.2: Axial Flux Profile of IPE in C3

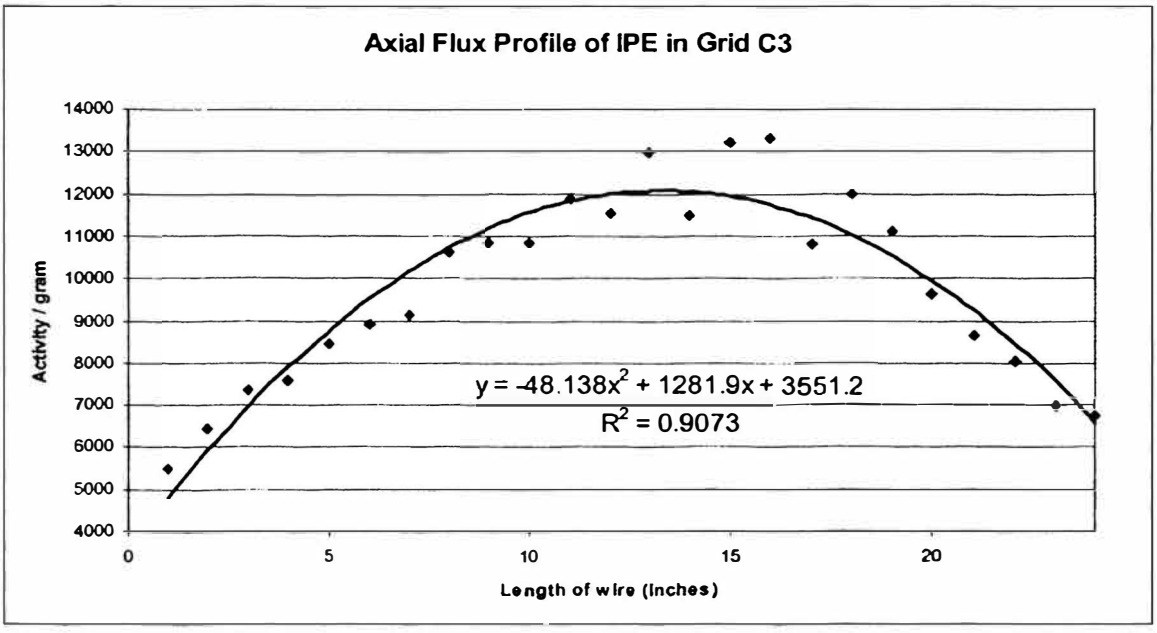

4 Abbreviated Discussion of Data

4.1 Implications on UMRR by Installation of IPE

According to SOP 206, there would be no problem in regards to installation if it were temporary. The IPE is already identified as a usable experimental facility that the UMR Reactor can use. If installed as a permanent fixture, excess reactivity and shutdown margin would have to be determined since C7 yielded a reactivity addition of greater than 0.2 % Δ k/k. According to the *Safety Analysis Reports Chapter 9.4*, the maximum reactivity change 0.4 % Δ k/k of a movable experiment. The air-filled tube would not violate this since its maximum reactivity change measured was 0.25914 % Δ k/k; granted if it were water-filled then it would violate it. The use of a water-filled tube as an experimental facility is of little chance. Since, the IPE would probably be removable; the IPE would be inserted into and out of the core via string instead of using the fuel-handling tool, since it would take less time, be more maneuverable, and require less staff assistance. An interesting follow up, as another OURE or NE 308 Reactor Lab, would be to calculate excess reactivity with the IPE(s) installed water-filled into the core. The purpose would be to see how they act as a reflector element since the IPE is made of carbon, which moderates and reflects well, would affect that parameter. This could be an inexpensive and potential way to increase excess reactivity levels in the core and to test to see how well graphite reflectors might improve excess reactivity.

4.2 Properties of the Neutron Flux Profile

The axial profile is parabolic and the equation in Figure generated could be used to determine intensities of neutron flux at different positions in the core. Taking the second derivative and setting it equal zero yields the peak flux intensity at 12.55 inches from the top. The intensities at the ends of the tube compared to the midsection are found by dividing the end

activity count divided by the one in the mid-section. Intensity of the neutron flux, falls to 45% to 50% of the mid-section value.

Added to this report is an example of the axial core flux of fuel element shown if Figure 4.1. This is an average axial flux profile of a fuel element. The same procedure and technique apply, but the facility differed. Note this is added strictly for comparison reasons only.

Figure 4.1: Example Core Flux Profile of Fuel Element

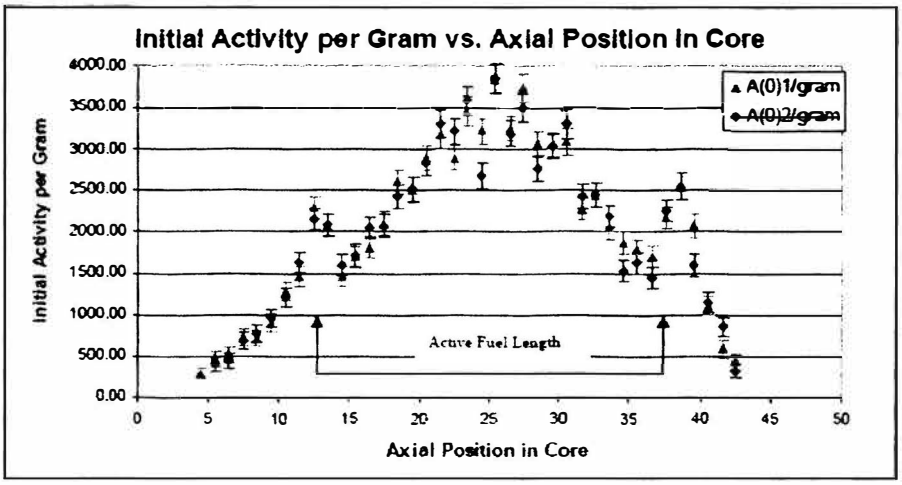

5. Conclusion

The IPE is an experimental facility that was tested for use as a possible experimental facility in the UMR Reactor. The IPE was tested for reactivity effects and the profile of the neutron axial flux. The IPE was found to have the most reactivity effect at C7 at 0.25914 % delta k/k. The flux profile was found to be parabolic and similar to a fuel element's profile. Position C7 was determined to have a higher flux value than C3. It was also determined that the flux intensity of a position was calculated to be 50% less at the ends that in the middle peak. Further experiments should investigate excess reactivity effects of the IPE to see if it increases excess reactivity and if so by how much.

6. Acknowledgments

Thanks for Dr. Tokuhiro for creation and guidance during this project. Special thanks to Reactor Manager Bill Bonzer for his assistance during the reactivity testing.

7. References

NE 304: Experiment Number 3: *Measurement of Axial Flux Profile.* Figure 1, page 8. October 23, 2003

University of Missouri-Rolla Nuclear Reactor Safety Analysis Report. Revision 1, 1988.

University of Missouri-Rolla Nuclear Reactor Standard Operating Procedure

Appendix A: Reactivity Testing Data

The data on Table A is the water-filled data for other positions that were not sequentially tested in the air-filled mode, since they have little reactivity effect (less then 0.05%). Position is the position in the core. Rod 1, Rod 2, Rod 3, and Reg. Rod are the critical rod heights for the reactor at 10 watts. The 'Start' position is the critical rod height with the IPE out of the core. Temperature is the pool water temperature. The % Δk/k is the reactivity worth of IPE which had a positive effect for all runs. Note that this stays the same for Tables A.1 to A.6.

Table A.1: Water Filled Data for Other Positions

Position:	Rod1:	Rod 2:	Rod 3:	Reg Rod:	$Water_T$	% Δk/k
Start:	22.4	22.4	22.4	11.3	76 F	------
A1	22.4	22.4	22.4	10.0	76 F	0.03293
A2	22.4	22.4	22.4	10.3	76 F	0.02540
B2	22.4	22.4	22.4	10.3	76 F	0.02540
C2	22.4	22.4	22.4	9.00	76 F	0.05633
B3	22.4	22.4	22.4	9.20	76 F	0.05165
B4	22.4	22.4	22.4	2.14	76 F	0.14469

Table A.2: Water Filled for C3, C7, and C8 Trial 1

Position:	Rod1:	Rod 2:	Rod 3:	Reg Rod:	$Water_T$	% Δk/k
Start:	21.0	21.0	21.0	21.7	74 F	-----
C8	21.0	21.0	21.0	13.9	74 F	0.13936
C7	20.0	21.0	21.0	6.4	74 F	0.39239
C3	21.0	21.0	21.0	12.60	74 F	0.17101

Table A.3: Water Filled for C3, C7, and C8 Trial 2

Position:	Rod1:	Rod 2:	Rod 3:	Reg Rod:	$Water_T$	% Δk/k
Start:	18.7	23.0	23.0	20.2	70 F	-------
C8	18.7	23.0	23.0	13.6	70 F	0.10439
C7	18.7	19.0	23.0	13.4	70 F	0.40977
C3	18.7	23.0	23.0	12.5	70 F	0.16179

Table A.4: Air Filled for C3, C7, and C8 Trial 1

Position:	Rod1:	Rod 2:	Rod 3:	Reg Rod:	$Water_T$	% Δk/k
Start:	23.0	23.0	23.0	9.0	70 F	---------
C3	23.0	23.0	23.3	3.9	70 F	0.07494
C7	23.0	23.0	20.2	4.2	70 F	0.25914
C8	23.0	23.0	22.1	7.1	70 F	0.07974

Table A.5: Air Filled for C3, C7, and C8 Trial 2

Position:	Rod1:	Rod 2:	Rod 3:	Reg Rod:	$Water_T$	% Δk/k
Start:	21.0	21.0	21.0	21.3	69 F	-----
C8	22.0	21.0	21.0	16.2	69 F	0.03418
C7	21.0	21.0	21.0	9.7	69 F	0.24493
C3	22.0	21.0	21.0	15.7	69 F	0.02265

Table A.6: Air Filled for C3, C7, and C8 Trial 3

Position:	Rod1:	Rod 2:	Rod 3:	Reg Rod:	$Water_T$	% Δk/k
Start:	21.4	21.4	21.4	11.3	69 F	-----
C8	21.0	21.0	21.0	13.4	69 F	0.02764
C7	20.0	21.0	21.0	6.4	69 F	0.23838
C3	21.0	21.0	21.0	12.6	69 F	0.06819

Appendix B: Axial Flux Testing Data

The data for the axial flux profile testing is present here in its entirety. Please note that height is in inches. Time is in minutes and the start time, time '0' was the shut down of the reactor. The first time is the time the count column was made and so on. Counts, activity, and activity per gram are in disintegrations per second. The reactor was shut down at 1334 hours and the first segment was tested at 1633 hours. For background counts, the same applies as above. The time is in minutes and is the minutes after shutdown the count was taken.

Table B.1: Flux Profile Data Position C7

Height :	Counts :	Time (minutes):	Activity:	Segment Weight:	Activity per Gram:
1	7115	179	8177	0.634	12897
2	7616	181	8782	0.780	11259
3	9865	183	11454	0.752	15232
4	9368	185	10887	0.680	16011
5	12227	188	14309	0.704	20325
6	12770	190	14981	0.748	20027
7	13106	191	15394	0.730	21088
8	12604	192	14810	0.750	19747
9	13056	195	15390	0.754	20412
10	12770	196	15063	0.682	22086
11	13451	198	15905	0.714	22276
12	12414	200	14690	0.718	20460
13	10937	203	12954	0.678	19106
14	12574	205	14950	0.728	20536
15	10304	206	12226	0.712	17171
16	12499	208	14900	0.748	19920
17	11420	210	13621	0.728	18711
18	9371	212	11161	0.696	16037
19	10788	214	12903	0.770	16758
20	6590	216	7817	0.616	12691
21	7464	219	8905	0.644	13828
22	6078	222	7234	0.636	11374
23	6223	224	7425	0.726	10227
24	6278	226	7506	0.888	8452

Table B.2: Background Counts

Background Counts:	155	178	182	180	165	200	164
Time Taken (min):	177	187	193	201	209	218	227

For Table B.2, the wire was irradiated in core position C3 for 10 minutes at 500 watts. The reactor was shutdown at 0921 and at 1336 the first testing began, which is 255 minutes after shutdown. This allowed for the other copper isotope to decay away. Background counts were taken at the start and end of the testing. In addition, background counts were taken every sixth sample. The averaged background counts were subtracted from the counts to calculate activity more precisely.

Table B.2: Flux Profile Data Position C3

Height :	Counts :	Time (minutes):	Activity:	Segment Weight:	Activity per Gram:
1	3232	255	3528	0.644	5478
2	3833	256	4294	0.666	6448
3	4405	258	5022	0.682	7364
4	4028	259	4549	0.602	7557
5	4516	260	5177	0.612	8459
6	4964	262	5751	0.646	8902
7	5073	263	5828	0.638	9136
8	6001	264	7022	0.662	10608
9	5995	265	7034	0.648	10855
10	5758	267	6743	0.622	10841
11	6487	270	7684	0.648	11857
12	7439	272	8912	0.774	11514
13	6034	273	7205	0.556	12958
14	5867	274	6996	0.608	11507
15	7123	276	8621	0.654	13183
16	7334	277	8910	0.670	13298
17	5453	278	6487	0.600	10811
18	6880	279	8346	0.696	11992
19	5955	281	7248	0.652	11117
20	4929	282	5923	0.614	9646
21	4833	284	5809	0.672	8644
22	4249	285	5054	0.628	8048
23	3722	286	4384	0.628	6980
24	3383	287	3944	0.586	6731

Table B.4: Background Counts

Background Counts:	367	506	479	388	346
Time Taken (min):	255	264	276	285	298

OURE REPORT

EMC investigations in Switch Mode Power Supply

Ashwin Shashindranath, Dr. David J. Pommerenke

July 1, 2005

Abstract

An experimental investigation on the radiated emissions caused by a high current switched mode power supply (SMPS) that supplies a CPU was performed. The emissions testing revealed data that could be used to predict causes of electromagnetic radiation from inside the computer. The noise sources identified included clocks on the motherboard, which was excluded for the purposes of this study. Testing concentrated on the SMPS and some theoretical ideas are proposed for better construction of the power supply.

INDEX

Background Information

There are requirements imposed by government agencies like the FCC in order to control the Electromagnetic interference produced by products. These FCC rules are contained in Title 47 of the code of Federal Regulations, of which Part 15 is of specific importance for the radio-frequencies devices. Some examples of these devices are digital computers whose clock signals generate radiated emissions in the 100 KHz- 30 GHz band.

Traditionally, the emissions have been dominated by clocks and digital signals. As a consequence of the reduced core voltages (approaching 1V) the VCC currents of the CPUs are approaching > 100 A. The currents are provided by a local step-down DC-DC converter. Driven by other design requirements, these DC-DC converters now produce significant emissions up to 1 GHz and start to be the main emissions source.

Test Setup

The testing was performed at the UMR EMC lab's semi-anechoic chamber. This chamber eliminates high outside ambient noise, and reduces the time needed to distinguish ambient noise from EUT emissions. The setup (Figure 1) included a Biconolog antenna which was capable of measuring between 30MHz – 5GHz. The signals were measured using a spectrum analyzer (Rohde and Schwarz FBEB series).

A PC having the SMPS and motherboard were taken for testing. In the first test the entire PC was run with 110V power and the radiated emissions from the PC was analyzed. This was to verify that the PC had in fact passed the FCC class B regulations and CISPR 22 B limits for Electromagnetic compatibility when it was sold.

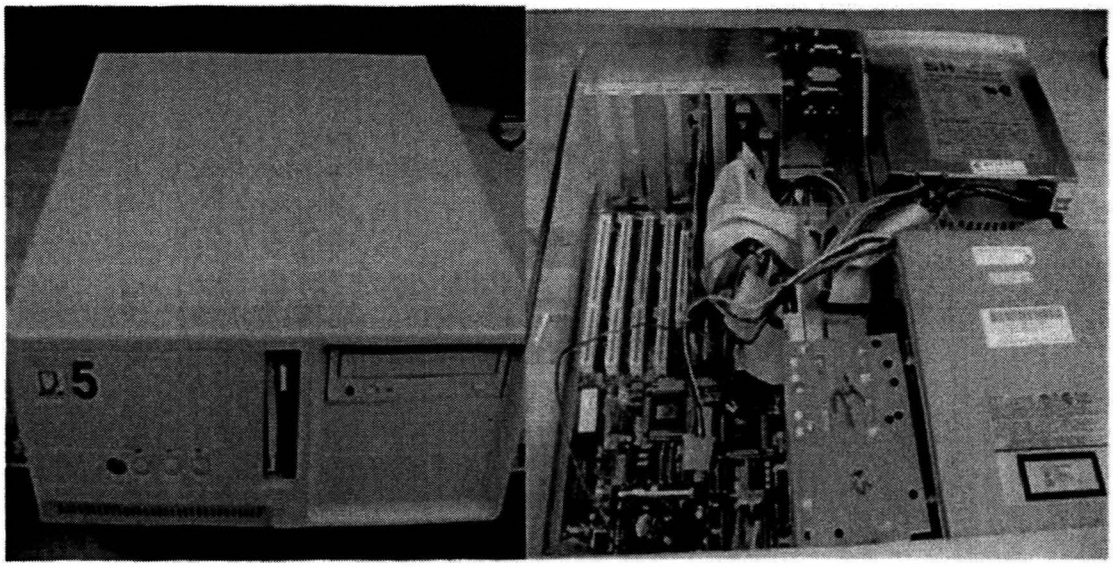

Figure 1: On the left, the computer under test. And on the right, case is opened.

Testing and Results

This initial testing was done to identify all the types of noises being emitted from a PC when the cover is opened. This testing would allow us to identify frequencies from the clocks which we are not interested in for this research. It would also allow us to identify the noise sources from the SMPS unit.

The test setup and the results are given below:

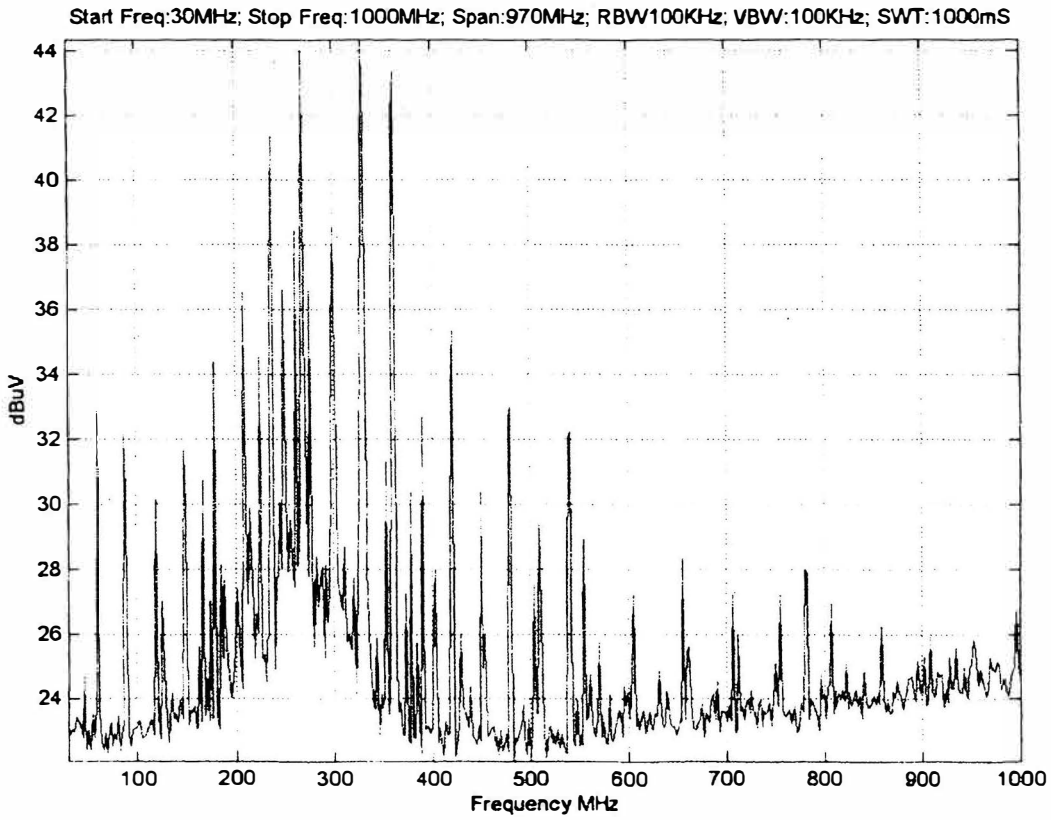

Figure 2: 30-1000 MHz Noise Spectrum.

From the figure above it is clearly evident that there is a 60 MHz and a 100 MHz clock inside the PC. We also observed some broadband noises around 330 MHz. We investigate further by turning everything off on the PC except the fan. This was done to make sure that the SMPS is being utilized by some component inside the PC.

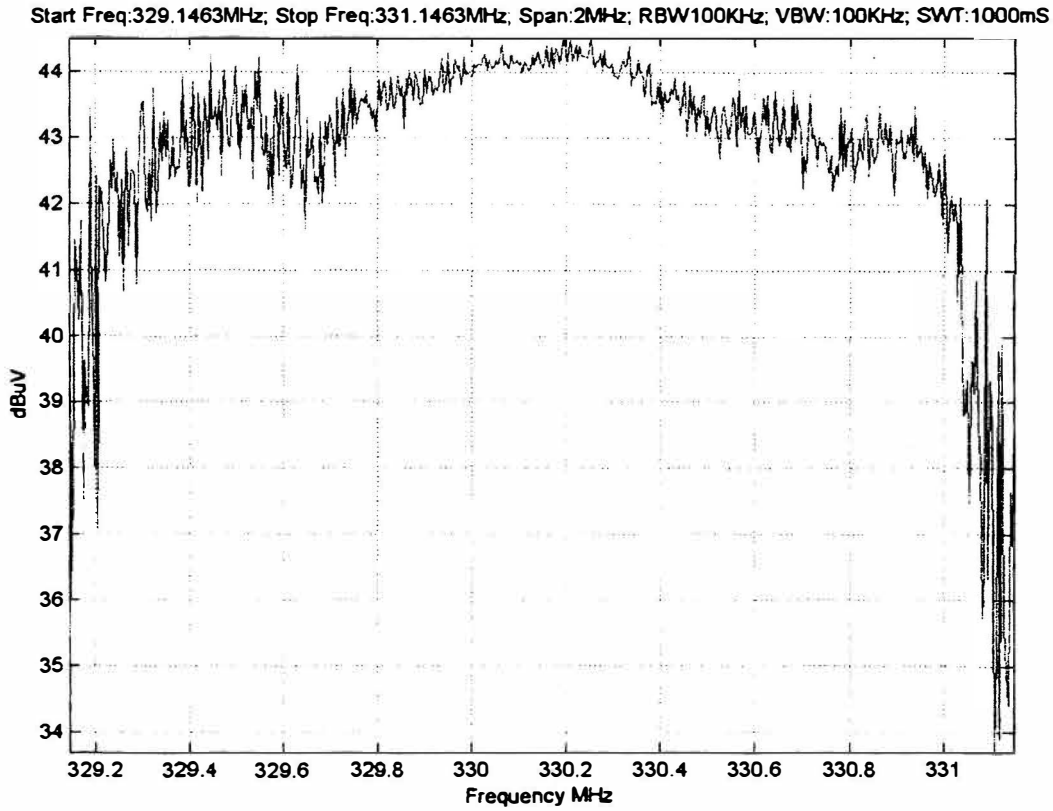

Figure 3:330 MHz broadband signal.

The above signal is observed around 330MHz and it confirms that the power supply is the cause of this broadband noise. A theoretical investigation of the main power supply was done.

CONSTRUCTION OF DC-DC CONVERTER

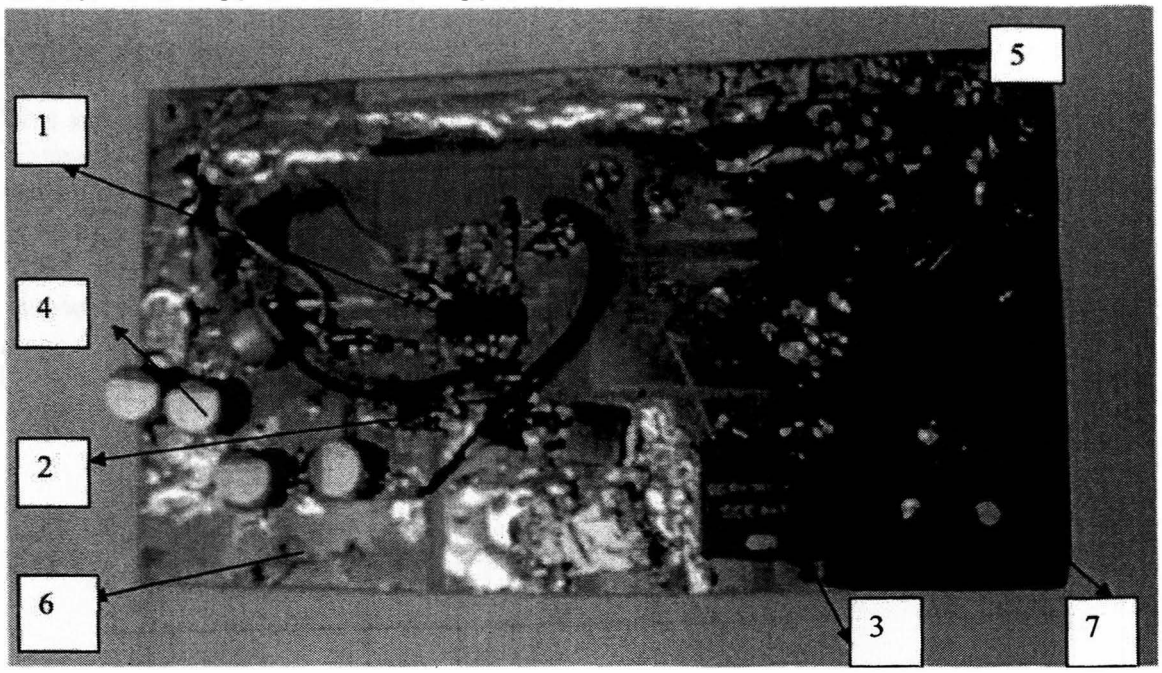

In this step a DC-DC converter board was constructed with Mr. Zhe Li's help. The board has the following components (labeled in the figure):

1. HIP6006 – N-channel MOSFET driver for a synchronous-rectified buck topology for microprocessor applications.
2. IRF7821 – Power MOSFET for high-frequency point-of-load synchronous buck converter application.
3. Inductor
4. Decoupling Capacitors – To reduce the noise level
5. Resistive load – To check the working of the DC-DC converter
6. Input voltage – 5V
7. Output Voltage

The board was constructed based on the following schematic from the manufacturer's website.

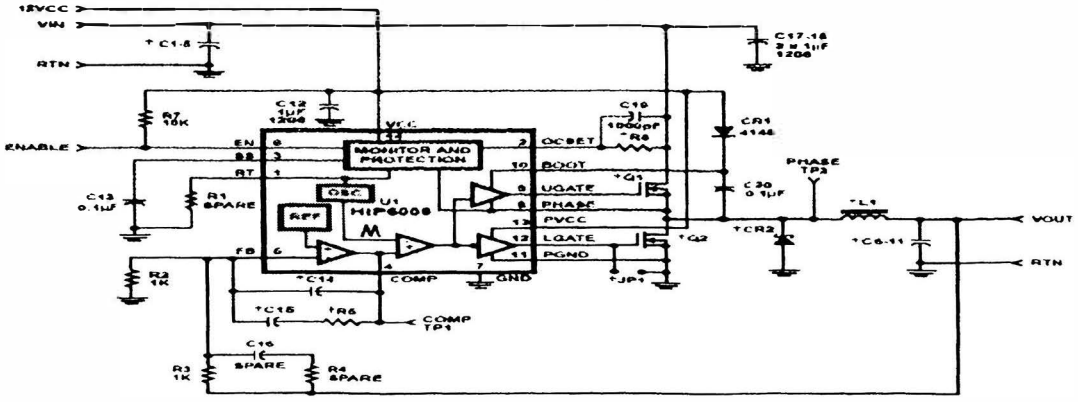

In the above circuit we modified our DC-DC converter to have a 200 KHz operating frequency for the HIP6006 (This is the default speed of the driver). The HIP6006 has options to increase this operating frequency by adding a resistor and capacitor at pin number 1. The output voltage can be adjusted in such a way that it is less than the input voltage or almost close to input voltage.

Due to some technical difficulties we were unable to check if this circuit was working right. We intended to do some near-field and far-field emissions testing, but since the circuit wasn't working and time constraints this will be considered at a future date.

Theoretical Investigations

A. Construction of the SMPS chassis:

Generally a SMPS has two main components. One component converts the AC to DC and is usually connected to the loads on the PC using cables. The output from this converter will have current flowing to the loads on these cables. These cables start acting as an antenna and are main sources of EMI noise. The second component is the control circuit section. The control circuit shouldn't be placed near the cables to reduce the electromagnetic coupling between them.

The case in which this whole circuit is placed inside is usually made of steel. Steel is effective shielding material of EMI noise. However during construction it has to be made sure that the case is water-tight i.e., it has to come together into one piece such that it won't let any water leak. Water is being used as an analogy to the EMI noise. Some effective ways to make sure that the shielding better are by using gaskets or by EMI fingers.

B. EMI considerations for Design and Topology

For economic purposes EMI has to be considered in the early stages of EMI design.The SMPS produces high-frequency noises as a result of its operations. In some parts of the circuit the di/dt and dv/dt is high and this results in a lot of EMI being caused by the SMPS. The saw-toothed shaped waveform is produced by the switching inverter which is what causes the high dv/dt. The current SMPS are using transistors with very fast rise times and fall times. They are approximately in 100 nano seconds range.

Therefore it is very essential to mount these transistors to minimize the area of radiating elements. There are also some parasitic components which influence the EMI of a power transistor.

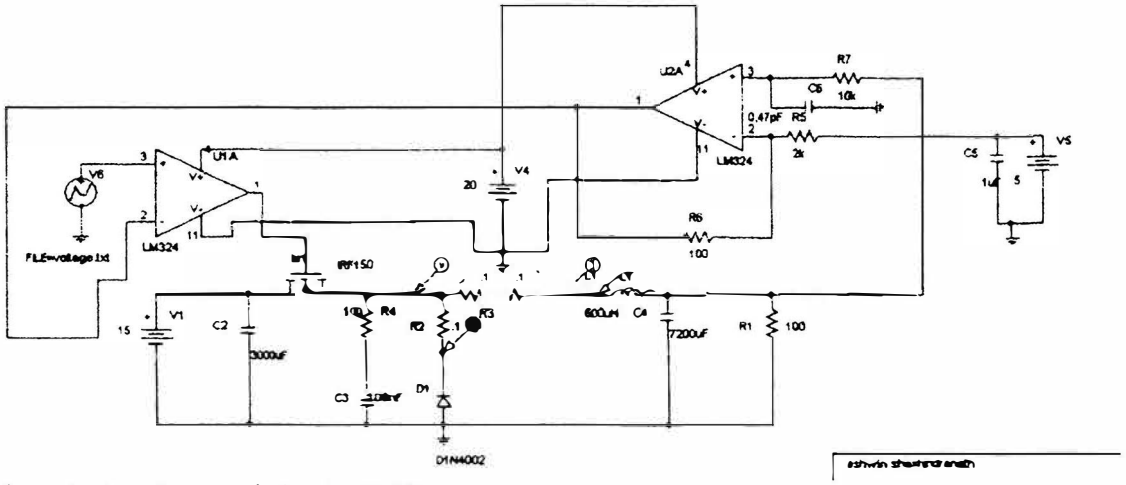

Figure 4: Buck-Booster design for SMPS.

Above is a possible theoretical Buck-Booster design that could be implemented to make a DC-DC converter for the SMPS.
Semiconductors like the MOSFET in the above circuit are strong sources for Differential-mode EMI. Good layout design will reduce the Differential-mode EMI. Good designs should make sure that the wires carrying a switching waveform (such as the saw-toothed shaped waveform) should be as close to each other as possible. RC snubbers can be used to reduce the ringing effect caused the L-C circuit. Good component selection will also reduce Differential-Mode EMI.

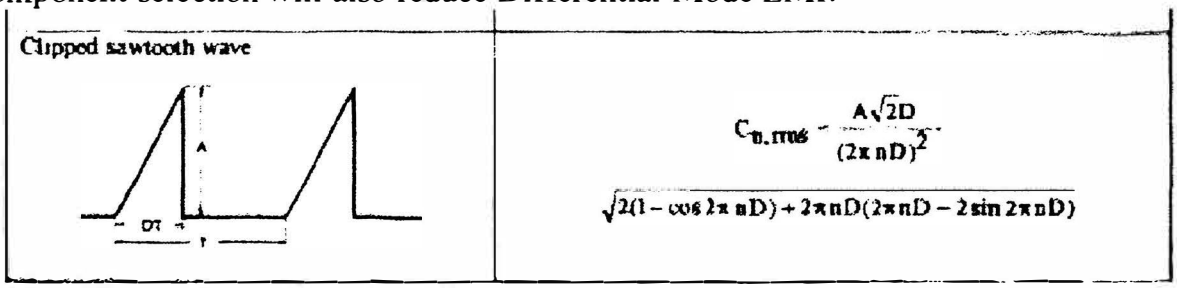

Figure 5: Clipped saw-toothed waveform of input current.

In figure 6 a method to dampen the effects of the fast risetime/fall times is shown.

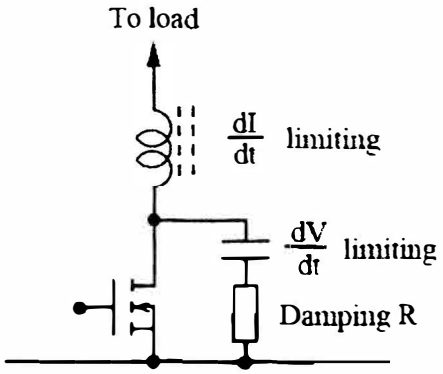

Figure 6: Adding L, C, R to slow the rising and falling edges of the current and voltage waveform.

Common Mode EMI:

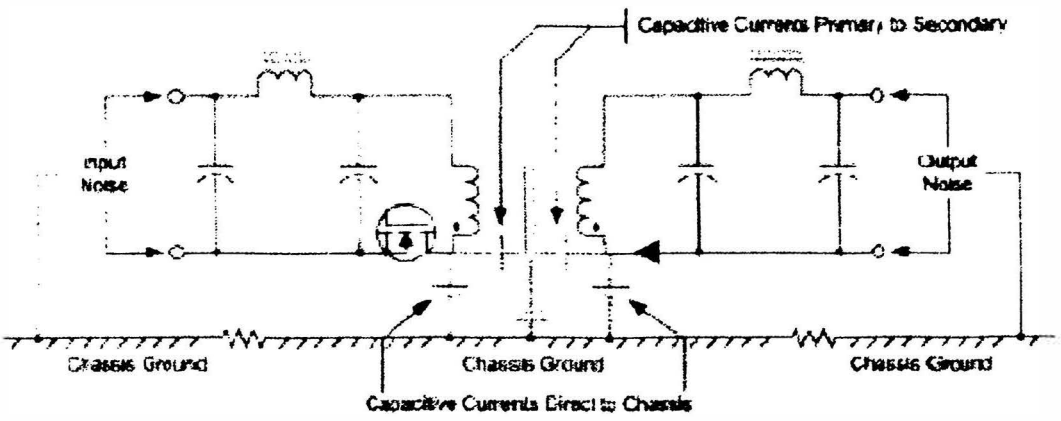

Figure 7: Capacitive current (i.e., currents associated with parasitics are shown).

The main reasons for common-mode EMI are the parasitic capacitances in the power transistor in the SMPS design. The parasitics which cause EMI are the collector to base and collector to heat sink capacitances. This can be minimized by reducing the stray capacitances between the circuit and the ground. It can also be reduced by proper component selection while building the circuit.

EMI Line Filter:

A good EMI line filter can be used to attenuate both common-mode and Differential-mode noises. Differential-mode noises can also be decreased by using X-capacitors and Common-mode noises can be decreased by using Y-capacitors.

Grounding

Ground plane should be as low resistance as possible. Single point grounding will help reduce the EMI.

Conclusion

Switch mode power supplies are notorious for creating Radio Frequency Interference and electromagnetic noise. The DC-DC converter that we constructed for microprocessor application didn't work as we expected. We hope to be able to work with in the future and make a good DC-DC converter with all the theoretical considerations taken intoaccount.

Low pass filters in the mains leads are vital to reduce conducted interference. Faraday screens between the transformer windings and around sensitive components, together with correct field canceling layouts on the circuit board, are also required to reduce electromagnetic noise and interference. The problems of smoothing of saw tooth current waveforms put a strain on capacitor design. The series inductance and resistance of standard electrolytic capacitors has a large effect on residual ripple and noise voltages at the outputs

Acknowledgements

I would like to thank my advisor, Dr. David J. Pommerenke, for his support and help in doing this work. I would also like to thank OURE for supporting the project. I would also like to thank my graduate supervisor, Mr. Zhe of the EMC laboratory for building the board.

References

1. **Switch mode power supplies: an EMI engineer's point of view**
Carter, T.;
Southcon/94. Conference Record
29-31 March 1994 Page(s):295 - 300

2. Introduction to EMC, Clayton Paul. Wiley Publishing

3. **Proper design of grounding for SMPS converters**
Perez, R.;
Electromagnetic Compatibility, 2000. IEEE International Symposium on
Volume 1, 21-25 Aug. 2000 Page(s):465 - 470 vol 1

4. Switched mode power supplies EMC analysis: near field modeling and experimental validation
Cristina, S.; Antonini, F.; Orlandi, A.;
Electromagnetic Compatibility, 1995. Symposium Record. 1995 IEEE International Symposium on 14-18 Aug. 1995 Page(s):453 - 458

Jeanne Shipman

Electric Spray Aerosol Generator

2004/2005 OURE

ABSTRACT

The 2004-2005 OURE research project was to devise and execute a test matrix specifically designed to evaluate the performance of the Electric Spray Aerosol Generator (ELSPRY). The first phase, for the 2003-2004 year, was to research the Electric Spray Aerosol Generator, and then to build it. This year there were two parts as well, the assembly and the testing, each of which had to be carefully monitored. The assembly of the parts also includes the testing of the individual pieces to ensure that all were working properly. This was key to determine if the ELSPRY was functioning properly.

INTRODUCTION

For the 2003-2004 OURE Project, the Electric Spray Aerosol Generator (ELSPRY) was to be built for the reason of replacing the nebulizer with something that would produce smaller particles. The nebulizer is only capable of producing particles greater than twenty nanometers in size, although smaller particles are often needed. In order to get particles less than twenty nanometers, a furnace has to be used. The furnace is not a reliable source of getting the small particles for two reasons. First, the furnace takes about four hours to heat to a suitable temperature, leaving no time to actually do what is needed. Second, the furnace can only produce aerosols from compounds that will sublimate at high temperatures yet not be decomposed at these temperatures. Cloud and Aerosol Science (CASL) would like to use a wider variety of compounds for challenge aerosols.

The ELSPRY is designed to work by first taking liquid solution, for example distilled water with NaCl, and putting it into a vial that sits in the pressure chamber. This chamber can hold large pressures; the vial chamber has been tested up to 55 psi. The capillary tube is grounded to the high voltage power supply, which allows the particles to become charged. The pressure pushes the liquid solution up through the capillary tube. At the end of the capillary tube, very small solution droplets are pulled from the capillary tube by an equal, opposite charge on an aluminum plate setting in front of the tube. The solution droplets are dried by an annular flow of dry, particle free air. The dried particles are then pulled through this aluminum plate and taken to the bipolar charger, which neutralizes the particles. This is where the particles exit the ELSPRY, and go on through the other parts of the system, where the particles will be counted and sized.

The first part of the project was to put the system together. The system needed to include, a high voltage power supply, a source of CO2, particle free house compressed air, filters, a Condensation Nucleus Counter, pumps, a ballast tank, a differential mobility analyzer (DMA), bipolar chargers, mass flow meters, and the ELSPRY. The DMA had to be re assembled for concentration vs. particle diameter testing. After all pieces of the system were pulled together, there was an amount of testing the parts to make sure that they were all working. We did this testing by generating commercially available standardized particles of known diameter (90 nm) of polystyrene latex (PSL) with the nebulizer and performing a size sweep to make sure everything was working well. The measured diameter was 103 nm, which is comparable to what we usually measure with other DMAs and the 90 nm PSL.

The next thing to be tested was the spray of the capillary tube, making sure the pressure chamber up through the capillary tube was working well. This proved to show that there was a leak in the pressure from the chamber, which was fixed with a sealant on the nylon ferrule. After doing this, the capillary tube flow was measured in respect to the pressure in the vial holder. The pressure was increased to find larger flows, showing the optimum pressure to be 5psig, giving a flow of 600 μL/min. The graph and some data are provided in appendix 1. This number needs to be lowered to be more similar to that shown in the journal article describing the commercially available ELSPRY, but that has not been achieved as of yet. Also, at the same time, there seemed to be a problem with the end of the capillary tube; the end was too flat to release the droplets off of the end, so they dripped off of the bottom of the tube, which incited another modification. The capillary tube was then shaped into a cone. This helped the droplets come off of the end of the capillary. Next, the 3rd piece of the ELSPRY was put together with the preceeding parts; this is the high voltage plate and its holder. Once this was placed on, it stopped the particles from going through, so this too had to be modified. It was originally 1/8 inch diameter, modified to ¼ inch diameter. While this piece was being modified, it was realized that the high voltage connection was not very well attached to the aluminum plate. So, while it was out, there were 2 new holes drilled to allow the high voltage wire to attach to the plate. This ensures that the high voltage wire will not fall out in the middle of an experiment, or in a move.

After all of the modifications and initial testing were accomplished, the system was ready to be tested for actual data. First, the pressure was changed; the ELSPRY works better, when all assembled, at around 45 psig. Next, the high voltage was increased

up to 6000 V. At 6000 V, however, there seemed to be a corona discharge, which caused an instability in the output concentration. The voltage was arcing from the tip of the capillary to the plate. Decreasing the voltage to 5000 V proved to not help the arcing problem. This needs to be looked at more in depth in the future; it has not been fixed. The DMA was then used to make size sweeps. Everything except DMA voltage was held constant. The voltage (AV) for the DMA ran from 12V to 6000V initially, showing that there is nothing trailing above 1000 V, and there seemed to be a peak at around 200 V. These size sweeps were continued back and forth through the DMA voltages. Also, there were backgrounds done to make sure that the particles that were being seen were not part of the background. The background proved to be insignificantly small, and not part of what was seen during the size sweeps. The data taken was then transferred to Gaussian curve fit in PEAKFIT.MCD, a MathCad application written by Dr Otmar Schmid, to compute the diameter selected by a DMA. This proved that there was a peak at around 25 nm. This is significantly smaller than the particles produced by a nebulizer, which are around 100 nm.

There still seams to be much to do with this instrument; all of the problems are not worked out yet. Also, there are some projects that are planned for shortly in the future. These include: using HNO_3 and sugar concentrations in the aerosol generator, varying the distance between the capillary and the high voltage plate, working on the pulsing of the high voltage (which may be fixed by the use of the HNO_3 in the solution in the vial), working on the overall stability of the concentration versus time, and finding the optimum of the flows of CO_2 and particle free house air, and the optimum high voltage.

ACKNOWLEDGMENTS

Thank you to Max Trueblood, Dr. Whitefield, Dr. Hagen, Shane Standley, and Max Alcorn, and Paul Bess.

REFERENCES

Chen, Da-Ren, Pui, David Y. H. (1995). "Electrospraying of Conducting Liquids for Monodisperse Aerosol Generation in the 4nm to 1.8μm Diameter Range." J. Aerosol Sci., 26, 963-977.

05321 CapTbFlow vs. Press - Electrospray.xls

Date	Time	dt (sec)	Drops	Press (psig)	Flow (drops/min)	Q-cc (cc/min)	Q-L (L/m)	Q-micrL (microL/m)
05321	1515	30	15	5	30	0.6	0.0006	600
		30	25	10	50	1	0.0010	1000
		15	30	20	120	2.4	0.0024	2400

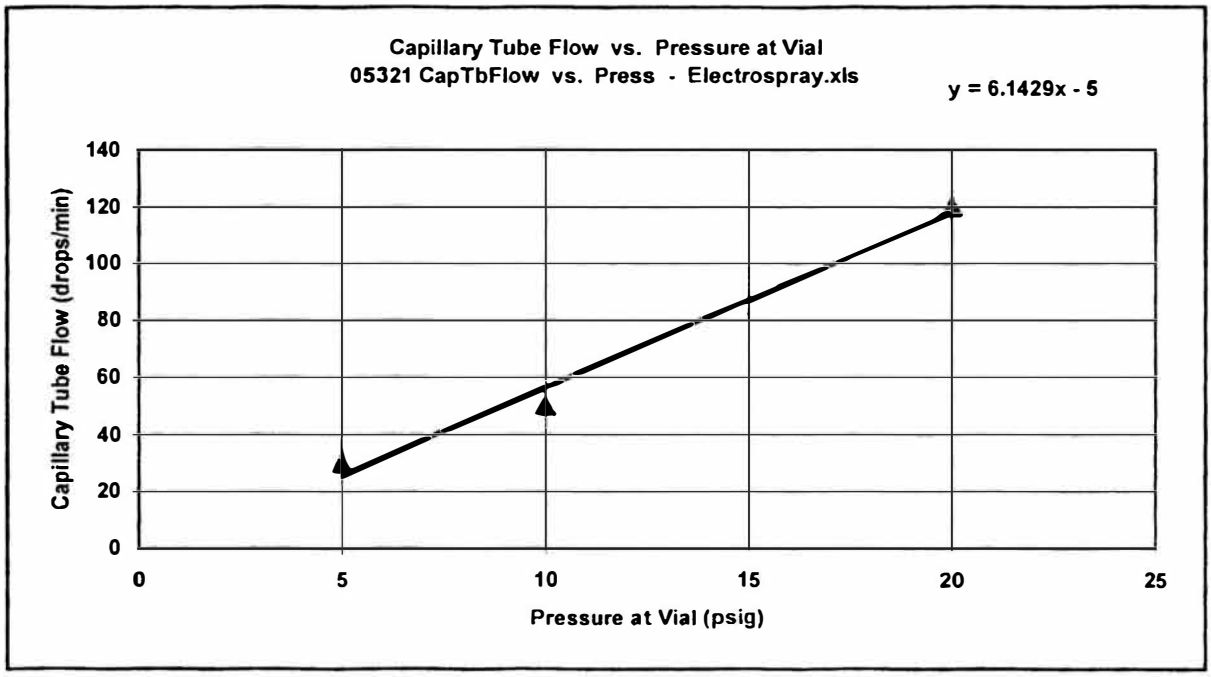

Gaussian curve fit: differential conc vs size

Data fr 05331 215p

The location of the maximum is: $Max_{gauss} = 25.3$ nm

Correlation coeff. r^2 $Rsqr_G = 0.797$

Root mean square deviation (normalized to maximum of diff. conc) $SD_G = 0.227$

$\sigma_{diffconc} = 12.12$ nm

$T = 293.2\,K$

$p = 972.2\,hPa$

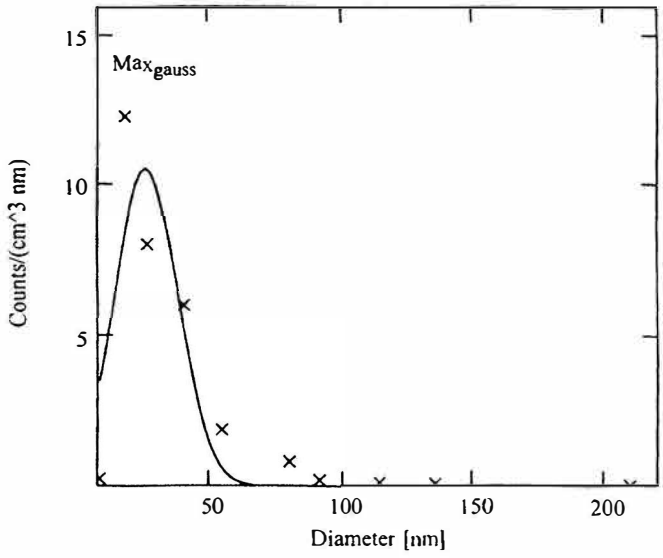

$\frac{\sigma_{diffconc}}{Max_{gauss}} = 0.478$

$Q_s = 24.522 \frac{liter}{min}$

$\beta = 0.056$

Gaussian curve fit: differential conc vs size

Data fr 05331 230p

The location of the maximum is: $Max_{gauss} = 29.6$ nm

Correlation coeff. r^2 $Rsqr_G = 0.896$

Root mean square deviation (normalized to maximum of diff. conc) $SD_G = 0.153$

$\sigma_{diffconc} = 8.10$ nm

$T = 293.2\,K$

$p = 972.2\,hPa$

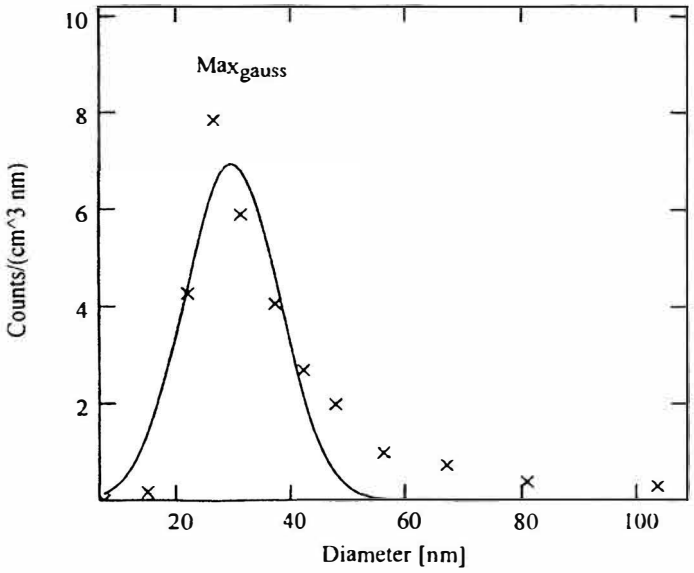

$\frac{\sigma_{diffconc}}{Max_{gauss}} = 0.274$

$Q_s = 24.522 \frac{liter}{min}$

$\beta = 0.056$

Gaussian curve fit: differential conc vs size

Data fr 05331 234p

The location of the maximum is: $Max_{gauss} = 24.4$ nm

$\sigma_{diffconc} = 10.08$ nm

Correlation coeff. r^2 $Rsqr_G = 0.903$

$T = 293.2\,K$

Root mean square deviation (normalized to maximum of diff. conc) $SD_G = 0.163$

$p = 972.2\,hPa$

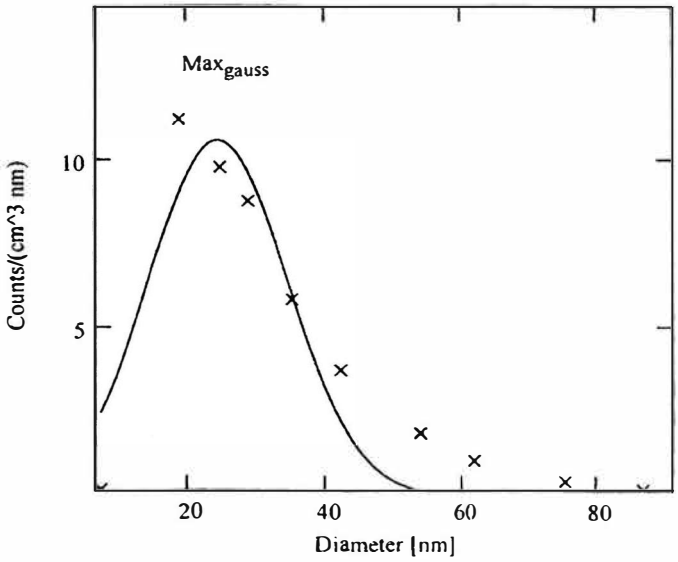

$\frac{\sigma_{diffconc}}{Max_{gauss}} = 0.413$

$Q_s = 24.522 \frac{liter}{min}$

$\beta = 0.056$

Gaussian curve fit: differential conc vs size

Data fr 05331 253p

The location of the maximum is: $Max_{gauss} = 196.9$ nm

Correlation coeff. r^2 $Rsqr_G = 0.795$

Root mean square deviation (normalized to maximum of diff. conc) $SD_G = 0.158$

$\sigma_{diffconc} = 58.05i$ nm

$T = 293.2\,K$

$p = 972.2\,hPa$

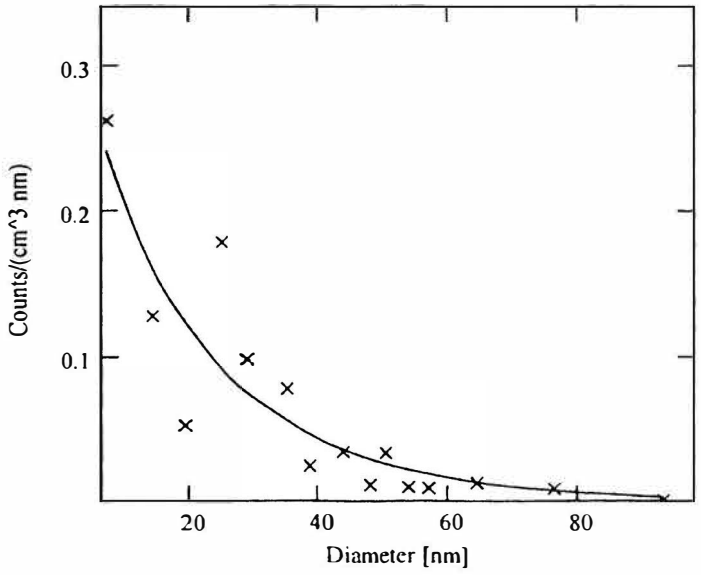

$\frac{\sigma_{diffconc}}{Max_{gauss}} = 0.295i$

$Q_s = 24.522 \frac{liter}{min}$

$\beta = 0.056$

INNER CYLINDER

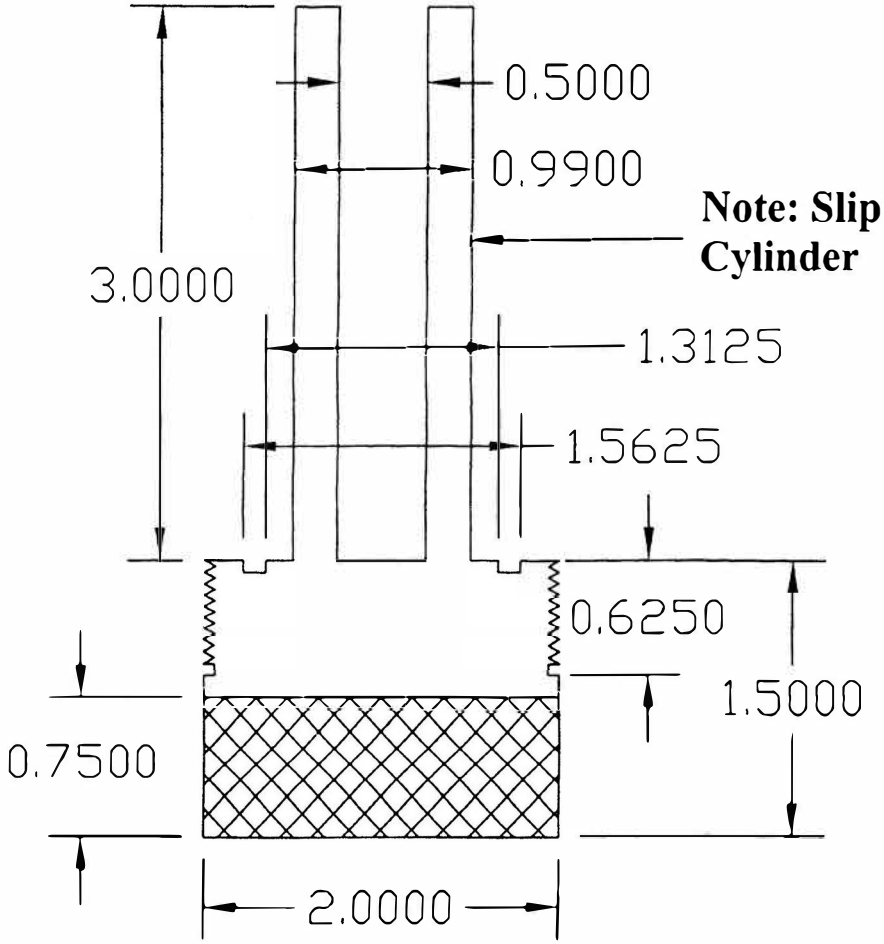

Note: Slip Fit into Outer Cylinder

Top View

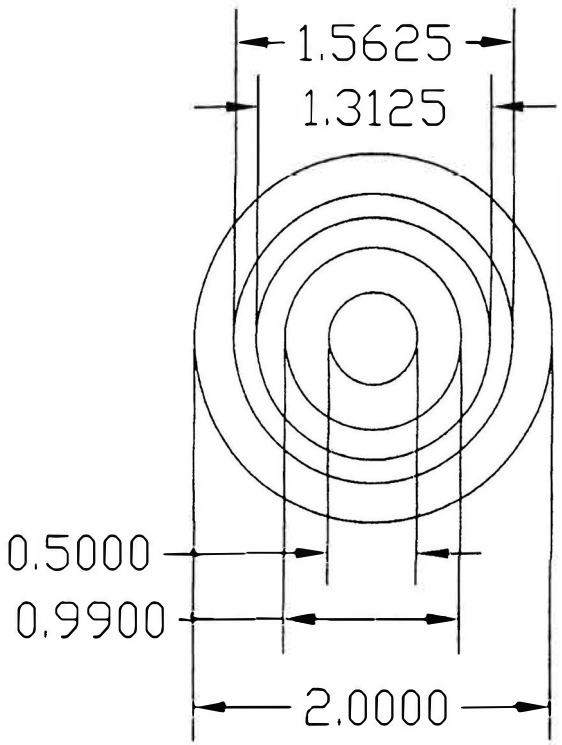

03731 DURE Vial Holder
Made by: Jeanne & Shane

OUTER CYLINDER

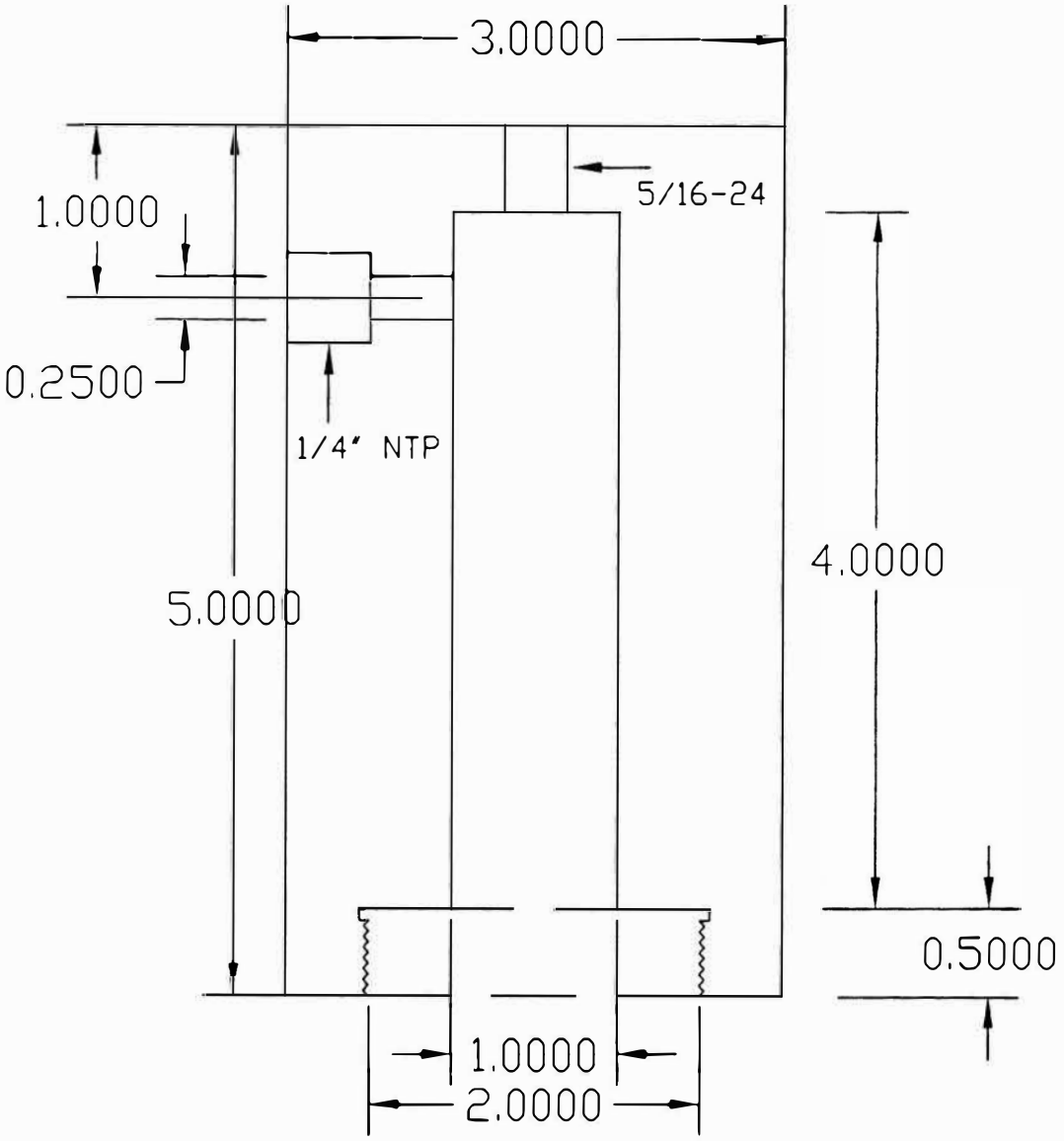

Bottom View

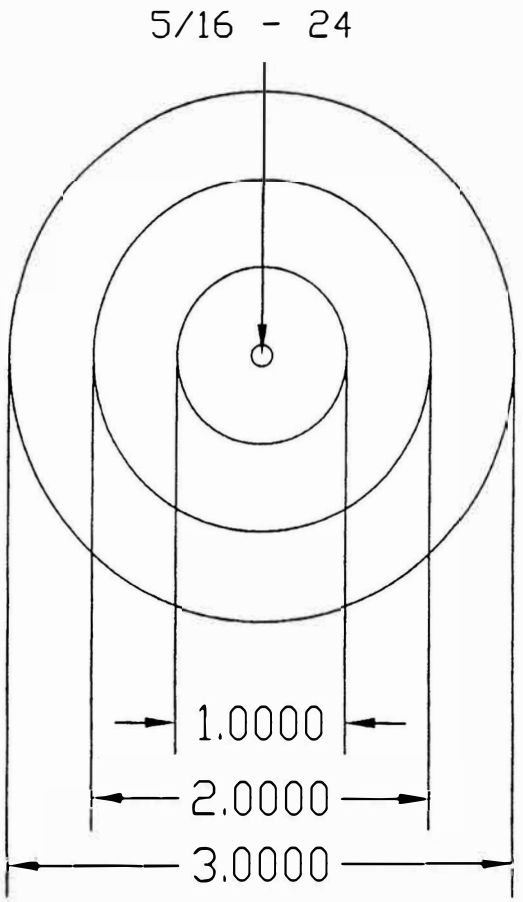

03801 OURE Outside of Holder
Made by: Jeanne & Shane

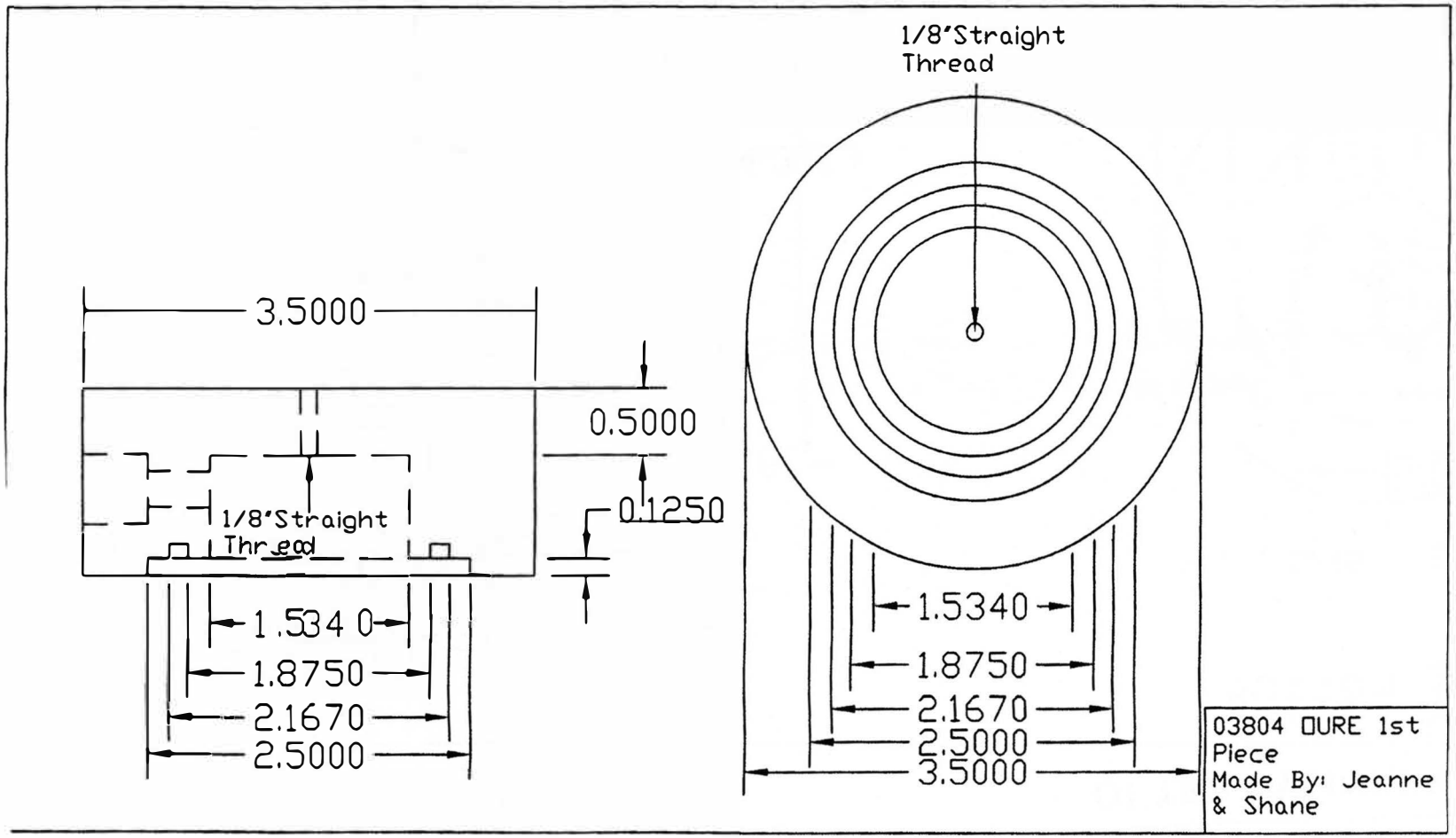
1/8"Straight
Thread
3.5000
0.5000
0.1250
1/8"Straight
Thread
1.5340
1.8750
2.1670
2.5000
1.5340
1.8750
2.1670
2.5000
3.5000
03804 □URE 1st
Piece
Made By: Jeanne
& Shane

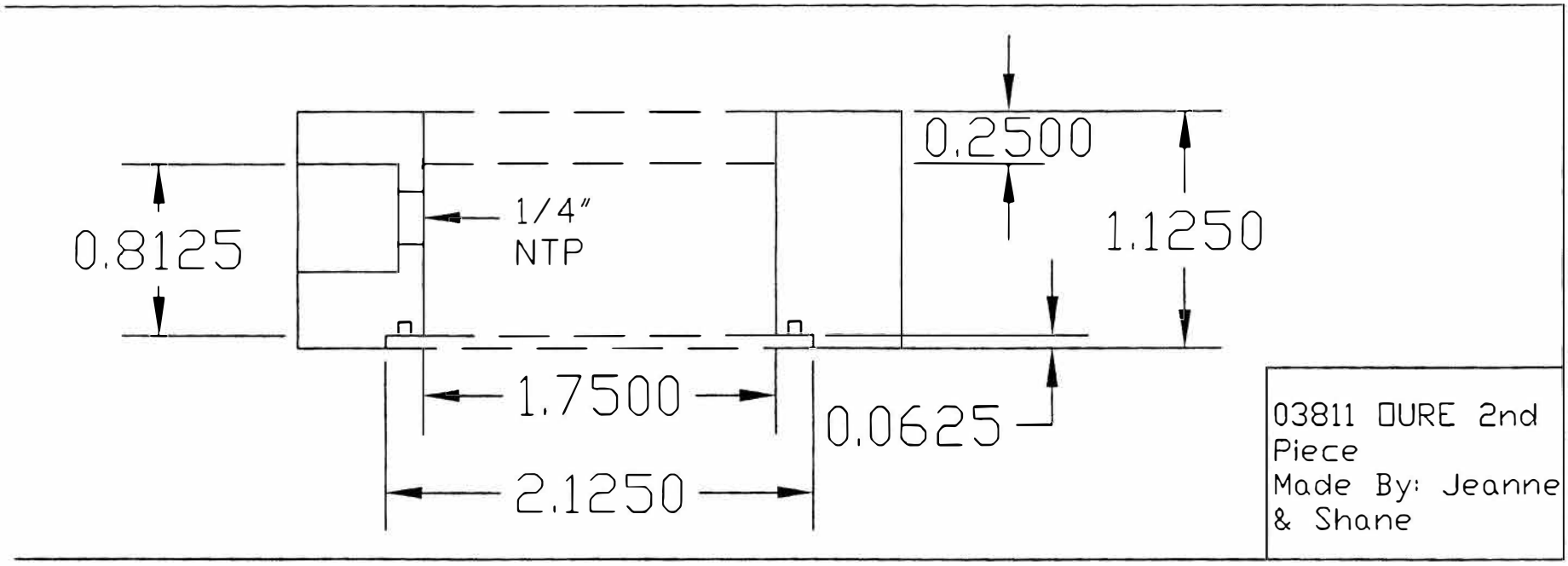
0.2500
1.1250
0.8125
1/4"
NTP
1.7500
0.0625
2.1250
03811 DURE 2nd
Piece
Made By: Jeanne
& Shane

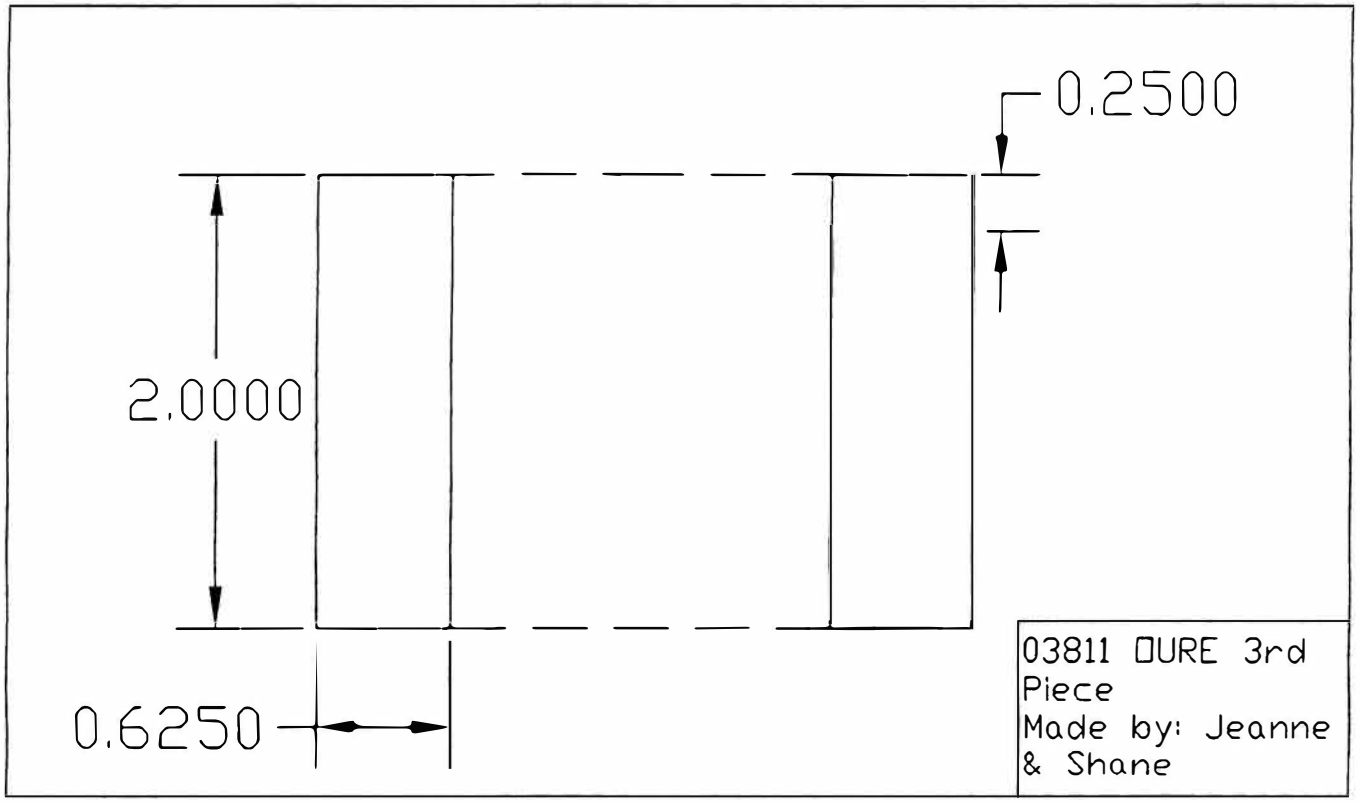
0.2500
2.0000
0.6250
03811 DURE 3rd Piece
Made by: Jeanne & Shane

A Hydrogen Economy

An OURE Report 2005
Submitted to Office of Undergraduate and Graduate Studies

Prepared by

Jeremy Snyder

Abstract

In 2003, MIT released "The Future of Nuclear Power," a study of the energy needs for now and the future. The report suggested several subsidies and a new "carbon tax." Also in 2003, President Bush made a State of the Union address that pledged more then a billion dollars towards hydrogen research and a move towards a hydrogen based economy. This report strives to tie together several hydrogen production methods and possible solutions for moving towards a hydrogen based economy. Background, production methods, and finally a revised carbon tax idea specifically aimed at jumpstarting hydrogen production are addressed in this report.

Table of Contents

1.0 Introduction

1.1 Background

President Bush declined to sign the Kyoto treaty, yet still pledged the United States to fight global warming and the production of greenhouse gases in the US. He designated over a billion dollars in his 2003 State of the Union Address towards development of hydrogen technologies. Whether there is an intended goal of reducing greenhouse emissions for purely altruistic environmental reasons, economic incentives, or a governmental mandate to change to a hydrogen based economy, this report addresses possible methods of altering the current course of hydrogen and energy production to some better alternatives.

MIT released "The Future of Nuclear Power," a study in 2003 of the course needed for nuclear power to head in for the future. It suggested "carbon tax" as a solution to energy needs for the future. There will be much opposition to the proposed tax from entrenched industries that will oppose any additional costs for any reason. If it is successful it will complement the recommendations from this report but it will be difficult to change to a perceived sheltering of the nuclear industry.

1.2 Scope of this Report

This report will focus on the current issues facing the United States. The report released by MIT addressed issues through a global viewpoint and though it is important to look at the global context for each of the current challenges, this report is not focused on addressing a solution that will work for every country. Some countries will have similar problems and similar solutions will work but regulatory issues and concerns over different technologies are resolved differently where they are found. By focusing on the issues in the United States, a more workable paradigm can be achieved for the energy needs of this country while not attempting to force a similar model to a different area that it would not be applicable in. For example, France produces roughly 80 percent of it's energy from nuclear power so a solution relying almost solely on nuclear power could be possible. But with the United States energy portfolio currently using only 20 percent

1.0 Introduction

1.1 Background

President Bush declined to sign the Kyoto treaty, yet still pledged the United States to fight global warming and the production of greenhouse gases in the US. He designated over a billion dollars in his 2003 State of the Union Address towards development of hydrogen technologies. Whether there is an intended goal of reducing greenhouse emissions for purely altruistic environmental reasons, economic incentives, or a governmental mandate to change to a hydrogen based economy, this report addresses possible methods of altering the current course of hydrogen and energy production to some better alternatives.

MIT released "The Future of Nuclear Power," a study in 2003 of the course needed for nuclear power to head in for the future. It suggested "carbon tax" as a solution to energy needs for the future. There will be much opposition to the proposed tax from entrenched industries that will oppose any additional costs for any reason. If it is successful it will complement the recommendations from this report but it will be difficult to change to a perceived sheltering of the nuclear industry.

1.2 Scope of this Report

This report will focus on the current issues facing the United States. The report released by MIT addressed issues through a global viewpoint and though it is important to look at the global context for each of the current challenges, this report is not focused on addressing a solution that will work for every country. Some countries will have similar problems and similar solutions will work but regulatory issues and concerns over different technologies are resolved differently where they are found. By focusing on the issues in the United States, a more workable paradigm can be achieved for the energy needs of this country while not attempting to force a similar model to a different area that it would not be applicable in. For example, France produces roughly 80 percent of it's energy from nuclear power so a solution relying almost solely on nuclear power could be possible. But with the United States energy portfolio currently using only 20 percent

nuclear power, no new nuclear power plants built in decades, and a long lasting stigma over Three Mile Island and Chernobyl, the solution will not be the same.

1.3 Intent

This report is intended to overview possible solutions needed to help develop a hydrogen based economy. Section 2 shows the push for development of hydrogen production and several obstacles that need to be addressed through several different means. There are several different solutions to each of these problems that are being discussed, but it was desired to include them to inform readers of additional issues that must be solved in addition to the main focus of the report.

The largest underlying reason to switch to a hydrogen fuel based economy is to help the environment – reducing carbon emissions, etc… Therefore the best solution is one that takes into account the most aspects in reducing those emissions – after all, there is little point in switching to a hydrogen fuel if the pollution is simply switched from a car exhaust to a smoke stack exhaust. Section 3 discusses several different methods of producing hydrogen with benefits and pitfalls to each.

In developing the new hydrogen based economy, new rules and regulations can be more easily assessed and implemented before production is in full swing then after. By mandating and regulating certain aspects, first movers will feel more confident that they won't have to spend millions of dollars in revising their production methods. They will also be able to determine from the earliest stage if they can compete efficiently in the market.

This report suggests a "carbon tax" that, while similar to one suggested in the MIT Study, is targeted and for a different intent. This tax is intended to level the playing field (offering incentives to lower emissions and offering help for risk taking first movers) while not eliminating or artificially encouraging any method over others.

2.0 The Hydrogen Push

2.1 President Bush's Plan

On January 30, 2003, President Bush made his state of the Union Address in which he declared a definite move toward a Hydrogen based economy to reverse the growing dependence on foreign oil. "President Bush is proposing a total of $1.7 billion over the next five years to develop hydrogen-powered fuel cells, hydrogen infrastructure and advanced automotive technologies...Through partnerships with the private sector, the hydrogen fuel initiative and FreedomCAR will make it practical and cost-effective for large numbers of Americans to choose to use clean, hydrogen fuel cell vehicles by 2020." [1]

The newest move towards a hydrogen economy is based upon several important issues, but mainly from reducing greenhouse gas emissions and reducing dependence on foreign oil.

i. Kyoto Accord

The Kyoto treaty was an attempt to lower the global emission of greenhouse gases to fight rising pollution and the possibility of global warming. The United States was the only country to not sign it – whether for better or worse is fiercely debated on both sides. However, President Bush still initiated programs to reduce greenhouse gas emissions in the US. Whether from mounting pressure from Kyoto treaty signatories or from similar belief but not bound by treaty, the US is pushing towards developing more of a hydrogen based economy.

ii. Foreign Oil

The push towards developing a hydrogen based economy can also be attributed towards an increased desire to be unbound from foreign oil supplies. As a commodity subject to world crises, the oil market is very volatile and seems to be steadily increasing in price. With gasoline prices slowly rising above $2.00 a gallon in the US, there is a greater push towards finding a cheaper alternative. With the vast majority of oil imported to the United States from foreign countries and most from the Middle East, the economy is at the mercy of foreign problems.

The possibility of oil production simply stopping is also a national security problem. If oil simply stopped being produced or delivered to the US for only a few days, the economy would suffer a massive shock at least on the order of 9/11 if not the size of the stock market crash of the 20s or even greater. With the recent terrorist attacks, there is an even greater desire to have an economy unbound by the whims of other countries and opposing peoples.

2.2 *Current Obstacles to Achieving a Hydrogen Based Economy*

There are several obstacles in place that are presenting roadblocks to building a hydrogen infrastructure. Industries currently build most facilities to produce hydrogen near where they are needed. This not led to the development of many things that will need to be addressed to conquer the problems posed by a hydrogen based economy.

i. Hydrogen Transport

Currently most hydrogen needed for extraction and industrial use is produced onsite. A safe, efficient method of transport is needed to get the product to the market – in this case the hydrogen to some sort of "Hydrogen station," similar to the current gas stations. There remains the question of how to transport this gas that is flammable.

ii. Prohibitive Costs

The Hydrogen used, whether for industrial or commercial purposes, must be cheap. That includes more efficient production methods, cheaper transport to needed locations, and more places and methods it can be produced from. It also includes costs that cannot be measured in dollars such as the effect on the environment and the ability to perpetually continue the production of hydrogen. There are also rare materials needed that greatly increase the cost of producing viable fuel cells for use in the average vehicle.

iii. Mass Production

The final goal of the hydrogen based economy is to replace gasoline driven vehicles with a hydrogen fuel based one. Whether it is complete replacement or a mix of different hybrid technologies remains to be seen but in order for a commercial economy to be created, it must be able to be used to replace or co-opt the millions of vehicles currently in use today. If the materials to produce or use in fuel cells or some part of the

vehicle that makes use of hydrogen is prohibitively expensive, it will prevent the mass production and distribution of vehicles to the public.

iv. Safety

Sadly, the most well known symbol associated with hydrogen is the Hindenburg. This has caused a stigma and fear against using hydrogen for simple things like powering a vehicle for everyday transportation. Hollywood movies have also presented a view of fuel cells as possible "mini-nukes." Some new designs emerging soon claim to be even safer then gasoline tanks, but further testing is required to prove the voracity of these claims. Regulating large stockpiles of hydrogen will be a challenge in the new economy because there still is a very real possibility of explosion.

3.0 Hydrogen Production Methods

3.1 Electrolysis

It is the simple method of passing an electric current through water. The Oxygen and the Hydrogen separate and are easily collected. The largest problem is the inefficiency associated with the process. There are far more efficient ways of directly creating Hydrogen without going through an intermediate step of producing electricity from power plants and then converting it to Hydrogen (with the associated energy loss). This would be a good approach when there is an over-abundance of electricity, produced at very little cost.

3.2 Steam Methane Reforming (SMR)

Steam Methane Reforming is the largest producer of hydrogen for most industries. It is relatively efficient and more inexpensive then many other methods. It is also a well studied and tried technology so there is a knowledge base experienced with production. There is some Carbon dioxide emission but it can be controlled with low resulting air pollution. The larger problem is the reliance on availability of natural gas. The United States has a limited supply of natural gas that has been facing price increases

for the last decade. A volatile market could destabilize the price and prevent a stable production at an acceptable price range when Hydrogen becomes more of a demand.

3.3 Coal Gasification

Coal contains a form of hydrogen that has been found to be extractable with a current cost slightly more then that of SMR. With some more development and research there is a possibility that it could present a good contributor to the hydrogen economy. The largest problem is the pollution that comes from mining and using the coal in both energy and hydrogen applications. The current goal is to reduce much of the emission of pollutants into the environment while this could simply be juggling the type of pollution until better methods are found and put into practice.

3.4 Biomass

There are several different ways of producing hydrogen through biological means, but they can fall into either gasification or a form of bio-synthesis.

i. Bio-gasification

Burning different biological products rich in hydrogen, such as wood chips and certain pieces of agricultural wastes, is a viable means of producing hydrogen. The technology has been researched, tested, and is currently in use world-wide in certain applications. Most of the opposition has been from the price, but it could become a competitive source of hydrogen if there is enough of an increase in the need for hydrogen.

ii. Bio-synthesis

There are many species that have different forms of photosynthesis that scientists have studied for years. There is a recently emerging technology that has allowed biologists to grow certain algae that can produce hydrogen. It shows promise, but has two large obstacles against helping the new economy. This bio-synthesis could have land requirements similar to that of Solar power that could make it prohibitive, but more importantly it is a developing technology. Since the knowledge base is just evolving, there is not enough information to know if it is a viable alternative for hydrogen production needs.

3.5 *Wind, Solar, and Similar Alternatives*

Electrolysis would be used to produce hydrogen from Wind, Solar, and Similar (such as Hydroelectric and Geothermal) power sources. They are pretty much infinitely renewable power sources that cause little damage to the environment in ways such as carbon emissions, waste storage, or some other undesirable effects (ignoring some possible problems with hydroelectric dams for the moment). The big problems come from expense and feasibility. These power plants cannot be placed anywhere near most of the areas that need them most and many are seasonal. Sunlight doesn't produce the same amount of energy throughout the year, rivers freeze over, and wind patterns change. They are also prohibitively expensive and most take large amounts of land. If it is attempted to use these as a power source for both energy and hydrogen production, they would be intermittent at best. No matter how environmentally friendly they can be argued to be, they cannot solve the energy production of current levels, let alone of the future with any current ideas given serious weight.

3.6 *Thermo-chemical*

Emerging high temperature techniques make it possible to more easily extract hydrogen at higher efficiency and without an intermediate step through power plant production. Promising experiments, designs, and demonstrations have shown the feasibility of high temperature extraction of hydrogen from high temperature nuclear power plants and certain other sources. The most promising is from a nuclear method, and the ramifications are discussed in the next section. As with other methods, there are still some obstacles: prohibitive costs in nuclear plant construction, public stigma towards nuclear facilities

4.0 The Nuclear Alternative

4.1 Power and Hydrogen Production

Currently, nuclear power accounts for approximately 20 percent of power produced in the US. If even a few of the recommended expansions from the MIT Study are implemented, a significant number of new nuclear power plants will be built. There are many designs that currently take advantage of the Thermo-chemical hydrogen production method mentioned in the last section to produce hydrogen as well as electricity. Hydrogen can be produced simultaneously with electricity, and can even be decreased or stopped when peak power demand is reached. With *no* carbon emissions, nuclear technology offers a well balanced production method that can become economically competitive if other issues can be overcome.

4.2 Waste

The largest obstacle to nuclear power seems to be the current NIMBY syndrome or "Not In My Back Yard." Much of the stigma over Chernobyl and Three Mile Island has faded in lieu of a good track record, increased education, more regulations, and better technology - but the worry over waste disposal continues. If several of the MIT Study recommendations, better and cheaper reprocessing technologies, or other creative solutions can be implemented, nuclear production will be a forerunner for developing the hydrogen economy.

5.0 Final Conclusions

5.1 Favoritism

In order for a solution to work, there must be a number of compromises made to most parties. In the MIT Study, a definite position of pro-Nuclear was defined, and a stance taken to force it to the fore. Whether right or wrong, it will likely be fought by industries currently enjoying influence in Congress. It is hard to justify suddenly changing position to actively subsiding new nuclear developments with a clear favoritism towards the nuclear industry. If such a tax is implemented it would grant nuclear power a position at the fore of the hydrogen production market. However, there is another solution that could make nuclear power a contender for the market, but not create an unbalanced solution that would be unacceptable to all parties. With President Bush's push towards a hydrogen based economy, all industries should be given a chance to be included. No method can be brushed aside or given wild advantages over their inherent benefits.

5.2 The Goal

The original goal in changing to a hydrogen fueled economy is to reduce emissions of Carbon dioxide and other pollutants. To this end, government should mandate certain hydrogen production emission standards so that the load is not simply shifted from where it is produced instead of reducing it. The best was to accomplish this would not only be an upper limit to emission standards, but a similar "carbon tax" to the one suggested in the MIT Study.

By creating this tax before an infrastructure is in place, there is reduced opposition to ground rules laid before companies begin moving towards production. This tax would also make it a fair competition. This would come from the inherent benefits and flaws from each method. Some methods still produce carbon and other pollutants and will have to bear a tax burden until they can develop cleaner technologies if they wish to compete in the industry. The tax would also provide funds for incentives such as grants to improve efficiencies and create new production technologies.

Subsidies and grants have historically been given for areas that are determined to be in the public interest or need that cannot be gained through the income received. They have also been offered in the development of new needed technologies. First movers and a variety of risk takers judged to have possible benefits should be awarded grants to begin development in the field. They would be valuable to test certain aspects of newer generation nuclear power plants that would lend invaluable experience and reduced construction costs to following reactors. Once a few new designs have been built, the MIT Study suggested that subsequent building costs would decrease and that should lend towards nuclear power becoming an economically competitive alternative.

The goal of the tax is to level that playing field and make the original movers into the field all competitive. Coal production methods will lose some of the lower cost advantage from emission problems until more environmentally friendly sequestering methods are developed. At the same time, solar power will benefit from no tax but suffer from inherent inefficiencies and costs.

5.3 Supplemental

The goal of this report was not necessarily to advocate a certain method, but to suggest a more level playing field that would allow them all to be economically competitive in a new hydrogen economy. Each method has benefits such as the low cost of coal or natural gas, the flexibility and stability of nuclear, and the nearly nonexistent pollution of renewables like solar power. By making nuclear power economically competitive in the hydrogen field, it also benefits to the energy production side, but does not gain an undue advantage from a demand from any interest group. Further research would reveal if some of the issues with nuclear or other production methods, as well as the hydrogen fuel issues can be resolved with a reasonable amount of research or money.

Acknowledgements

Dr. Tokuhiro has contributed a lot of his time and many helpful thoughts on the direction of this project. I greatly appreciate his patience and guidance towards creating a better report that will hopefully help find a solution to current energy and hydrogen needs.

References

1. Key Initiatives in the President's State of the Union Message, http://www.whitehouse.gov/news/releases/2003/01/20030128-14.html, Last Retrieved 3/22/05
2. Where Does Hydrogen Come From?, http://www.rmi.org/sitepages/pid557.php, Rocky Mountain Institute, Last Retrieved 3/22/05
3. Bush unveils US alternative to Kyoto protocol, NewScientist.com news service, Fred Pearce, http://www.newscientist.com/article.ns?id=dn1932, 09:50 15 February 2002
4. What is a Fuel Cell?, http://www.bullnet.co.uk/shops/test/hydrogen.htm, Last Retrieved 3/22/05
5. Hydrogen Production Using a Thermochemical Process Made Possible with the Use of a Ceramic Membrane, http://www.greatchange.org/bb-thermochemical_hydrogen.html, Last Retrieved 3/22/05
6. Nuclear Now, Peter Schwartz and Spencer Reiss, *Wired* (February 2005) pg 79-83 and 119-120
7. Economics and Environmental Effects of Hydrogen Production Methods, Greg Brinkman, Fall 2003, accessed at http://www.puaf.umd.edu/faculty/papers/fetter/students/Brinkman.pdf Last Retrieved 3/22/05
8. The Future of Nuclear Power, Ansolabehere, Deutch, et al, Copyright 2003

The Role of Regulatory and Liability Issues Stemming from the MIT Report, *The Future of Nuclear Power*

Christopher Speer

Abstract

With the nation's need for electricity and want for a cleaner environment increasing, nuclear energy seems to be an effective resource for meeting both those needs. MIT has recently released a paper entitled "The Future of Nuclear Energy" in which they propose the feasibility a large growth of the nuclear industry. However, their growth scenario fails to take into account several regulatory and liability issues that would arise with a large growth in the nuclear industry. Those issues must be understood before the nuclear industry can begin to grow. In this report, we attempt to clarify those issues.

Introduction

Currently there is an attempt underway to increase the nuclear capacity of the United States to meet the nation's ever-growing need for electricity. This movement finds its basis in the fact that nuclear power is an environmentally cleaner alternative to current coal-based and natural gas-based energy since it does not release any additional carbon dioxide into the atmosphere, thus reducing the greenhouse gas effect. Expansion of the nuclear industry would also ease the strain on the dwindling supply of fossil fuel and would help to ease the United States off of foreign oil dependence though the possibility to produce hydrogen for proposed hydrogen-fuel cell cars of the future.

The United States has 103 operational nuclear power plants, which supply approximately 20% of the nation's total electricity. Current legislation has been adequate up to now for dealing with any problems that have arisen since the birth of the nuclear industry in this country. However, with the nuclear industry poised to begin growing in the future, the question arises of whether or not the legislation currently in use will be enough to safely regulate the industry if it were to grow beyond its current capacity.

This is a question that must be answered before the nuclear industry is allowed to grow by any significant margin. Nuclear power is of a dual nature; properly regulated, it is a clean and

effective form of energy. However, if proper legislation is not present, it proposes a significant risk to the entire nation.

The MIT Growth Scenario

One recent publication that makes an attempt at answering the question of the ability of the US to sustain a large growth of the nuclear industry is the MIT report *The Future of Nuclear Power*. In order to explore the possibilities and pitfalls of a large expansion of the nuclear industry, the MIT report considers a growth scenario that would see the world have 1000 1gigawatt-electric nuclear reactors by 2050. Of these 1000 reactors, 300 of them would be in the US. Of the remaining reactors, 210 would be shared between Europe and Canada, 115 would be in developed East Asia, and 50 would be built in the developing world. For these reactors, the report assumes that a "once-through" fuel cycle will be utilized, rather than reprocessing of spent fuel. Although the report isn't completely in favor of it, it assumes that the geologic disposal of spent fuel would continue unless through future research a better solution is found. [1]

Global Growth Scenario

REGION	PROJECTED 2050 GWe CAPACITY	NUCLEAR ELECTRICITY MARKET SHARE 2000	2050
Total World	**1,000**	**17%**	**19%**
Developed world	625	23%	29%
U.S.	300		
Europe & Canada	210		
Developed East Asia	115		
FSU	50	16%	23%
Developing world	325	2%	11%
China, India, Pakistan	200		
Indonesia, Brazil, Mexico	75		
Other developing countries	50		

Projected capacity comes from the global electricity demand scenario in Appendix 2, which entails growth in global electricity consumption from 13.6 to 38.7 trillion kWhrs from 2000 to 2050 (2.1% annual growth). The market share in 2050 is predicated on 85% capacity factor for nuclear power reactors. Note that China, India, and Pakistan are nuclear weapons capable states. Other developing countries includes as leading contributors Iran, South Africa, Egypt, Thailand, Philippines, and Vietnam.

Figure 1 From MIT's "The Future of Nuclear Power" page 3 [1]

Current Legislation

There are two major pieces of US legislation that would be tested by a growth of the nuclear industry from its current level of 103 reactors; those same two pieces of legislation, if they fail, would mean that the nuclear industry as a whole would be placed in danger.

First among these is the Price-Anderson Act, which addresses the liability that nuclear power plants face in case of accidents. The Price-Anderson Act requires nuclear plants to carry the maximum liability coverage available to them from private insurers (currently $300 million) and creates a joint insurance pool from among the nuclear plants themselves, with each having to pay up to $100.6 million. These mandates create a total liability limit of $10 billion, past which state and federal governments are left to cover any excess costs. [2]

Next is the Nuclear Waste Policy Act of 1982. This Act, through its amendments, is what has established the federal government's focus on Yucca Mountain as a site for the geologic disposal of nuclear waste. It also establishes the Nuclear Waste Fund, which is the source of funding for any waste-related activities, including the construction of disposal sites and possibly to pay for any waste-transportation accidents. [3]

The MIT report makes mention of these two major pieces of legislation; however, it fails to adequately examine the effectiveness of these two pieces of legislation to sustain a large growth of the nuclear industry. If they were to fail under a large growth, the possibility opens up for the nuclear industry to be left without adequate liability coverage for accidents and without enough funding to create adequate waste disposal sites—two legislative concerns that are possibly the biggest that the industry as a whole faces.

The Price-Anderson Act

A total of $202 million dollars has been paid out of the insurance pool created by the Price-Anderson. Of that, $70.8 million is due to the 1979 accident at Three Mile Island. [4] With the total payment being only about 2.1% of the total liability coverage currently available to, not even half of that coming from the largest nuclear accident in US history, it seems that the liability limits set by the Price-Anderson act would be enough to support the MIT growth scenario.

However, rather than providing too little insurance, the MIT growth scenario shows that it may be providing too much. Supposing that each of the 300 proposed plants would pay the current-day requirements towards the insurance pool the availability of liability coverage from the pool in 2050 becomes:

300 reactors x $100.6 million per reactor = $30.2 billion dollars

This excludes even the liability coverage that nuclear plants must carry with private insurance companies. This means that the insurance pool alone could cover a Three Mile Island sized accident 426 times over. It would seem that the liability limits could easily be reduced and still provide adequate coverage, with the reduced limit corresponding to reduced cost per kilowatt-hour to the customer.

This analysis shows a flaw in assuming such a large growth scenario proposed by the MIT report. The growth scenario requires 4 reactors a year be built without any of the current 103 operational reactors being decommissioned. In fact, all of them will face the choice to decommission within the next 40 years. [5] This means that the growth scenario would require anywhere between 4 and 7 reactors be built every year on average in order to achieve the goal of 300 reactors by 2050. Even with the current legislation being streamlined for the approval to build new nuclear plants, this rate of construction seems very unrealistic. A more conservative estimate for construction of new nuclear plants would change the conclusion that the Price-Anderson Act provides an overabundance of liability coverage for nuclear accidents.

If the growth scenario proposed by MIT is cut in half to 150 commercial reactors by mid-century, the growth rate becomes a more realistic, although still optimistic, 1 to 3 new reactors per year, which more closely matches the nation's average of 2 per year since the first commercial nuclear reactor began construction in 1954. [6] Using current-day liability standards, it also cuts down the available insurance pool available for nuclear accidents to:

150 reactors x $100.6 million per reactor = $15.1 billion

This more conservative estimate decreases the overabundance of liability. When it is considered that this would be a peak for the insurance pool, and that possible accidents would have to be paid for along the way, it becomes apparent that it will be a long time before the Price-Anderson limits could be cut while still providing the same level of protection as is provided today.

However, because of the wording of the Price-Anderson Act, it is possible that the insurance pools and other reactor liability coverage will be the financial source for paying any damages that may occur due to future waste transport accidents. If America continues its push for a geologic depository at Yucca Mountain, Nevada for spent nuclear fuel, it means that spent fuel will have to be transported from the various current waste-holding facilities to Yucca Mountain. This creates an entirely new liability concern for the nuclear industry, as it will be their responsibility to pay the costs of such an accident.

If it is the case that the coverage created by the Price-Anderson insurance mechanisms will be applied towards waste transport accidents then the insurance limits should be increased. The possible $30 billion dollars from 300 reactors by the MIT Growth scenario may not even be enough coverage to pay back the costs of even a small number of waste accidents.

The Nuclear Waste Policy Act

The Nuclear Waste Policy At of 1982 mandates that each reactor pay into the Nuclear Waste Fund at the rate of one-tenth of a cent per kilowatt-hour of electricity produced. [3] At that rate, assuming a reactor running at an average of 90% of its total capacity, the total funding from each reactor

1000 MW x .9 capacity x 365.25 Days/Year x 24 hours/Day x 1000 kW/MW x .001$/KW-h = $7 889 400 per Reactor per year

Taking into account the number of reactors today, under the MIT Growth Scenario, and under the more conservative estimate, that makes the current annual budget of the Nuclear Waste Fund:

7889400 $/reactor x 103 reactors = $812 608 200 today
7889400 $/reactor x 300 reactors = $2 366 820 000 in 2050 under the MIT scenario
7889400 $/reactor x 150 reactors = $1 183 410 000 in 2050 under the conservative scenario

This funding is intended to be used to pay for the development, licensing, construction, and maintenance of a permanent waste storage facility, and for any costs involved with transporting waste to such a site. Currently, the United States plans on utilizing geologic disposal of spent nuclear fuel. The Office of Civilian Radioactive Waste Management estimates the total cost of Yucca Mountain to be $36.6 billion dollars over its lifetime of an estimated 117 years, meaning an average yearly cost of about $313 million. It is clear that the current funding level of the Nuclear Waste Fund can support a single Yucca Mountain site. However, the question is if this funding is enough to pay for the construction and maintenance of geologic disposal sites as they are needed.

There are several different volumes of spent fuel that could be held at Yucca Mountain. It will initially be cleared to hold 63 000 metric tons of commercial spent nuclear fuel. Over time, it may be cleared to hold up to 97 000 metric tons or even a maximum load of 119 000 metric tons. [7] The average 1 gigawatt nuclear plant produces 20 metric tons of spent fuel per year. Under the MIT growth scenario, this means that at maximum capacity the nuclear industry will produce the need for a new Yucca Mountain-sized depository every:

63 000 metric tons/Depository / (20 MTHM/Reactor/year x 300 Reactors) = 10.5 Years

If the total capacity of Yucca Mountain is increased from its starting capacity of 63 000 metric tons to its maximum possible capacity of 119 000 metric tons, the need for a new depository would become one ever 20 years, each of them potentially costing the same estimated $36.6 billion over their lifetime. Under the more conservative scenario, the need for new depositories decreases to one every 21 years in 2050 assuming the 63 000 metric ton capacity.

It would seem that under either scenario, the Nuclear Waste Fund would possibly be able to afford the continued construction and maintenance of new geologic disposal sites. However, this

fails to take into account the added possibility that the Nuclear Waste Fund would have to cover liability costs of waste transport related accidents. The wording of the Nuclear Waste Policy Act of 1982 makes this a possibility. If this is to be the case, the Nuclear Waste Fund would have to set aside a large portion of its annul budget to cover liability costs, and depending on what percentage that is, there may not be enough money left aside to afford the costs of constructing the waste disposal sites that would be needed in the future.

Conclusion

Many of the proposed routes for nuclear waste shipment to Yucca Mountain run near or through very populated areas. If an accident should at such a point, the cost of repairing possible damages and decontaminating those exposed areas would be very high. It seems self-evident that a large amount of funding should be set aside to pay for any such accidents. If the nuclear industry is to grow in the future, current legislation must be clarified to do so. Both the Price-Anderson Act and the Nuclear Waste Policy Act have mechanisms in them that can allow for the coverage of liability due to waste transport accidents. When looking a conservative growth scenario each of the two appears to be inadequate in order to pay for the costs it is intended to cover and to pay for the waste transport liability that they could potentially be required to sustain. Either one of those pieces of legislation, if they must cover waste transport liability on top of their own burden, will have to have their financial limits increased, most probably by a very significant amount. However, it is not necessary that each have the fees they charge to reactors be increased. Instead,

Figure 2 From Nevada state's website [8]

current legislation should be modified so that it is clear which of them is to cover waste transport liability, or an entirely new piece of legislation should be passed that would create an independent liability fund for waste transport accidents.

Without taking action to resolve this conflict between the Price-Anderson Act and the Nuclear Waste Policy Act of 1982, a large growth of the nuclear industry presents the distinct threat of a major waste transport accident without any funding to aid in the clean-up of the accident, or of reimbursement for damaged property. Without such liability funding, the threat of waste transport accidents should be more than enough to keep from allowing the nuclear industry to grow.

Acknowledgements

I would like to acknowledge and thank both Dr. Akira Tokuhiro and Jeremy Snyder for the assistance they provided me while producing this report.

References

1. *The Future of Nuclear Power*. retrieved Jan 23, 2005, from http://web.mit.edu/nuclearpower/pdf/nuclearpower-full.pdf
2. *Atomic Energy Act of 1954*. as amended, retrieved Jan 23, 2005, from http://www.nrc.gov/who-we-are/governing-lawes.htm
3. *Nuclear Waste Policy Act of 1982*. as amended, retrieved Jan 23, 2005, from http://www.nrc.gov/who-we-are/governing-lawes.htm
4. *Price Anderson Act Provides Effective Nuclear Insurance At No Cost to the Public*. retrieved Jan 23, 2005, from http://www.nei.org/index.asp?catnum=4&catid=319
5. *Reactor Decommissioning*. Retrieved Jan 23, 2005, from http://www.nrc.gov/reactors/decommissioning.html
6. *Shippingport Nuclear Power Station*. Retrieved Jan 23, 2005, from http://www.asme.org/history/roster/H047.html

7. *Yucca Mountain Science and Engineering Report, Revision 1*. retrieved Feb 5, 2005 from http://www.ocrwm.doe.gov/documents/ser_b/index.htm
8. *Nuclear Waste Transportation Routes*. retrieved March 19, 2005 from http://www.state.nv.us/nucwaste/states/us.htm

Reflection on the Learning Experience

1. I found that research of the nature that I have tried, dealing mostly with technical reports and federal legislation, is done online. This is because of the size of many of the documents that must be read. Few are under a hundred pages. It would be a waste of time and resources to print out each paper that needed to be read. Because of the complexity of the issues, having to take into account public acceptance, possible risk analysis, and logistics, many of the projections I came across were purely hypothetical.
2. I have very much expanded my understanding of the information available regarding nuclear power. Since most all of the information and reports are online, it is very easy to get a hold of information, to the extent that one is overwhelmed by the information available. It seems that because of the volume of information available, it is most efficient to look for very specific information, rather than to look for information regarding general concepts, so that the extraneous can be avoided.
3. Rather than the fundamentals of tangible experimental design, my research was focused towards examining hypothetical situations, and, to that extent, I've gained a large amount of knowledge. Through my research, I came across several hypothetical situations for waste transport accidents and for growth scenario problems, and had to analyze the probability of each occurring. I gained the knowledge of being able to recognize which of these scenarios presents a serious problem and should be examined, and which are, for all intents and purposes, impossible.
4. I have learned to interpret what is a distinct problem and what is not. Several issues came forth when I had to examine a large growth of the nuclear industry, and I needed to interpret which of these was a serious problem, and which were minor. After doing so, I had to determine what the magnitude of the problem presented, and what an effective method would be to resolve the problem.

OURE

SECONDARY REINFORCEMENT FOR FIBER REINFORCED POLYMERS REINFORCED CONCRETE PANELS

Reid Stephens, Jr.
Dr. John J. Myers

Center for Infrastructure Engineering Studies

University of Missouri - Rolla

1. Introduction

1.1 Background

Today's automobile population is increasing like never before. Due to the economic growth in developing countries around the world, exponential growth is inevitable. This increase in automobiles will bring new demands to the existing and future infrastructure system around the world. Because of the enormous amount of money invested in infrastructure, it is important that the product be as durable and long-lasting as possible.

A major issue with today's infrastructure and particularly bridges is corrosion of steel reinforcement within the concrete deck due to chloride penetration from deicing salts. Chloride ions mixed with water and oxygen leach into the structure through surface cracks and react with exposed steel rebar. This reaction creates rust and produces an increase in the original steel volume that causes the reinforcement to de-bond from the concrete and in turns causes delamination of the bridge deck and loss of structural integrity. This corrosion problem reduces serviceability life and in turn costs billions in rehabilitation and/or replacement.

There are generally two answers to this dilemma. One is to limit crack widths. Limiting the crack widths will help prevent the penetration of water, oxygen, and chloride ions from deicing salts into the bridge deck. Although cracks cannot be totally eliminated they can be controlled with proper reinforcement design. The goal is to replace the larger, less numerous cracks

that provide major exposure to reinforcement with smaller, more numerous cracks that restrict penetration.

The second solution is to find a suitable replacement for steel that will not corrode as easily and in turn will increase the serviceability life of the structure. Bridge deck deterioration shows that even epoxy-coated rebar, galvanized steel rebar, and cathode protection only delay corrosion instead of preventing the matter. One possible source for this replacement is fiber-reinforced polymers (FRP). FRP has been available for several decades and is advantageous because of its relatively lightweight and high-strength qualities. Even so, only since the 1990's has it been strongly considered as a replacement for steel reinforcement in highway bridge decks.

Several types of FRP exist, including glass (GFRP), carbon (CFRP), and aramid (AFRP). These different types of FRP all behave relatively similar, and have virtually the same advantages and disadvantages over steel reinforcement. The advantages and disadvantages of FRP reinforcement when compared to steel reinforcement are shown in Table 1 below. Looking at the comparison, FRP evidently seems to be a promising replacement for steel as reinforcement for concrete structures.

Table 1: Advantages and disadvantages of FRP over steel when used for concrete reinforcment

Advantages
Impervious to chloride ion and chemical attack
Tensile strength greater than steel
1/4th weight of steel reinforcement
Transparent to magnetic fields and radio frequencies
Electrically and thermally non-conductive
Disadvantages
Low modulus of elasticity
no yielding point before rupture
high initial cost
lack of familiarity within the industry

1.2 Scope and Objectives

This study deals with GFRP only and was performed in order to develop an empirical secondary reinforcement ratio for FRP based on experimental test data; more specifically to determine the optimum amount of GFRP to control cracking within a concrete slab. The current ACI guidelines for secondary reinforcement for FRP reinforced concrete are based on a steel reinforcement ratio of 0.0018 and account for the stiffness and strength of the FRP material by using a secondary reinforcement ration design equation. This design equation has no experimental data for backup and is considered excessive by many experts. Even the steel guidelines in ACI 318 for secondary reinforcement have little experimental data attributed to their basis. They are primarily the result of field observations over many years of structures that have yielded acceptable results. This research will hopefully aid the development of guidelines based on actual experimental validation of GFRP reinforced concrete specimens.

Currently, there is no standard test method to evaluate secondary reinforcement. Although previous research similar to this particular project has been attempted in the past, the mix design, specimen dimensions, and reinforcement ratio design combination are unique. Only Information on test setup and procedure from these studies was considered. The study is divided into two phases. Phase I will investigate the early-age effects of the various reinforcement ratios while Phase II deals with the later-age effects. Because

data is still currently being taken on this project, only Phase I observations are contained in this report. Phase II observations will come at a later date.

2. Literature Review

2.1 Cracking

As previously stated, exposure of reinforcement to weathering elements must be limited in order to prevent corrosion. One proven method is eliminating crack potential because cracks present a direct unrestrained path to the reinforcement. Cracking in concrete can be attributed to many different factors but they all correlate back to induced tensile strains as a result of deformation of the concrete. The typical factors affecting cracking in concrete include plastic shrinkage, drying shrinkage, and thermal shrinkage and expansion.

Plastic shrinkage cracks form soon after placement but before curing when the concrete is still in its plastic state. They result most commonly when the evaporation rate of water from the surface of the concrete exceeds the bleed water rate to the surface from the bottom of the slab. When this occurs, negative capillary forces are produced and cause the paste volume of the concrete to contract. This contraction of the paste induces tensile stresses that the still fresh concrete cannot support and results in cracking. Plastic shrinkage cracks can be minimized by controlling the evaporation rate of water from the concrete surface.

Besides plastic shrinkage cracks, drying shrinkage cracks also present a problem for reinforcement corrosion. Drying shrinkage occurs during the curing process and is a result of internal water loss from the hardened cement paste as

opposed to surface water loss. Factors that influence drying shrinkage cracks include cement composition, aggregate type, water content, and the mix proportions. Mix water left over from the hydration process is the main cause of drying shrinkage however. Adding no more water than just enough necessary to complete the hydration process will significantly aid with the prevention of drying shrinkage.

Thermal cracking is the result of deformations of the slab as a result of thermal gradients through its thickness. During a typical hot summer day the top surface of the concrete slab will become warm and expand as it is heated by solar radiation while the bottom surface remains cool and unchanged. This causes the slab to bow upward in a convex fashion. The opposite occurs at night when cool temperatures cause the top surface to contract. This slab deformation may be capable of producing stresses large enough to induce thermal related cracks. Also, while the slab is deformed it cannot adequately support traffic loads without cracking.

2.2 ACI 440

As discussed, most cracks form due to the high tensile stresses created by internal or external restraints produced by deformation of the concrete through shrinkage or temperature differentials. Using reinforcement will not eliminate cracks, and in some cases is thought to actually encourage cracking. However, the right design of reinforcement can distribute shrinkage strain along the bond of the bar and can produce several thin cracks instead of a few wide ones. This is

significant since finer crack widths result in less durability problems. Crack widths for FRP have more tolerance than for steel since corrosion is not an issue. The optimum amount of FRP to obtain acceptable crack width must now be determined. ACI 440 uses Equation 2-1 below to govern secondary reinforcement design for FRP.

$$\rho_{f,t} = 0.0018 \times \frac{60{,}000}{f_y} \frac{E_s}{E_f} \geq 0.0036 \qquad \text{(Equation 2-1)}$$

Equation 10-1 (ACI Committee 440-03)

"Due to limited experience, it is recommended that the ratio of temperature and shrinkage reinforcement given by Eq. (10-1) be taken not less than 0.0014, the minimum value specified by ACI 318 for steel shrinkage and temperature reinforcement. Spacing of shrinkage and temperature FRP reinforcement should not exceed three times the slab thickness or 12 inches (300 mm), whichever is less" (ACI Committee 440-03).

Notice that the equation uses the secondary reinforcement ratio for steel as its primary basis and factors in the ratios of strength and stiffness of the two materials to account for the properties of FRP. A limit of 0.0036 is provided to limit excessive amounts of reinforcement due to the stiffness of steel being much greater than the stiffness of FRP.

2.3 Previous Research

Studies regarding temperature and drying shrinkage reinforcement are scarce but available. Papers discussing plastic shrinkage are more available. An extensive foundation for this particular experiment was laid by Daniel Koenigsfeld and his work at the University of Missouri – Rolla with Dr. John

Myers, P.E. This project is an addition onto advancements already proven through his research. His work was considered during the design of the test specimen and the testing procedure.

3. Experimental Program

To simulate FRP reinforcement within a bridge structure a model having a similar behavior was designed. A total of five model bridge deck spans were cast; four of the spans containing different reinforcement ratios of GFRP reinforcement. A wide range of ratio values was implemented into the design. The fifth span was the control and contained steel reinforcement with the minimum allowed secondary reinforcement ratio. Each span's specific reinforcement design is shown in Table 2 below. The spans were joined at the end-sections in order to better control shrinkage during the experiment.

Table 2: Reinforcment design of individual spans

Slab #	Reinforcement Type	Bar #	Size of Bar	Number of Bars	Area of Bar	Total Area	Reinforcement Ratio
1	Steel	#3	0.375	2	0.11	0.22	0.0018
2	GFRP	#3	0.375	2	0.1307	0.2614	0.0022
3	GFRP	#3	0.375	3	0.1307	0.3921	0.0033
4	GFRP	#3	0.375	4	0.1307	0.5228	0.0044
5	GFRP	#4	0.5	3	0.2245	0.6735	0.0056

The five spans were eight feet long and two feet wide and were separated by a gap of three inches. Each slab thickness was four inches. Both the end sections of the specimen were four feet long, had a total width of eleven feet, and a thickness of eleven inches.

Throughout the testing period it was important to ensure that no shrinkage was allowed and that all deformation developed as cracks within the structure.

To account for this, eight tie rods were placed in each end section, extending through the entire thickness of the structure and on beneath the strong floor of the high-bay lab. The tie rods were tightened by a calibrated torque wrench with enough force to ensure no shrinkage but gently enough to avoid breaking up the concrete at the pressure point. Calculations for the torque wrench calibration can be found in the appendix. Figure 1 is a plan and side view of the testing specimen and may give a clearer picture of the design.

Figure 1: Plan and side view of specimen

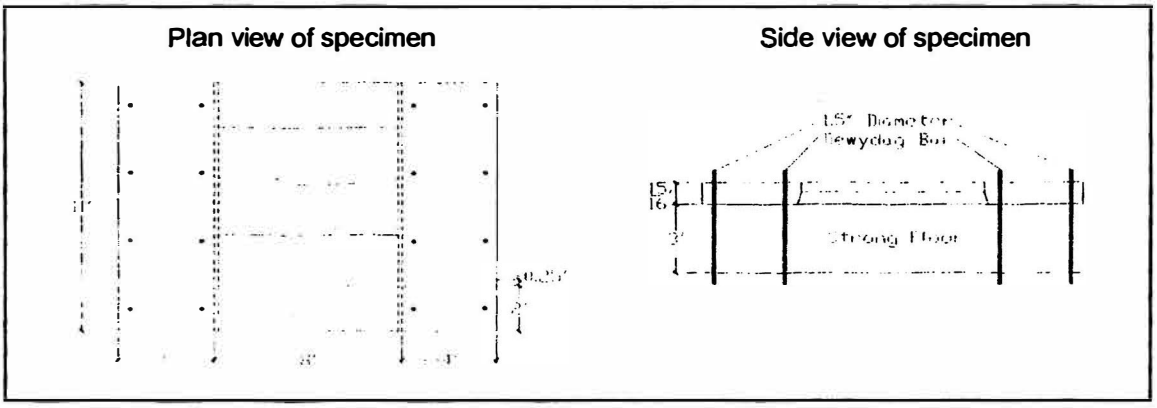

The concrete forms were entirely of wood fastened together with wood screws. It was manually manufactured within the high-bay lab. The reinforcement was held in place using three inch chairs. The chairs were nailed to the bottom support form to prevent movement during concrete placement. Reinforcement spacing was figured by evenly dividing the slab width by the number of reinforcing bars. Minimum concrete cover on the reinforcement was one inch. The reinforcement design can be seen in Figure 2 below.

Four strain gauges were located in each slab on the longitudinal reinforcing bars. This was done in order to verify throughout the study that the

concrete specimen was inducing shrinkage strain on the structure. Three strain gauges per slab would be sufficient to obtain the desired readings, however the fourth strain gauge per slab was added for the possibility of damaging one during the concrete placement.

Figure 2: Reinforcement design

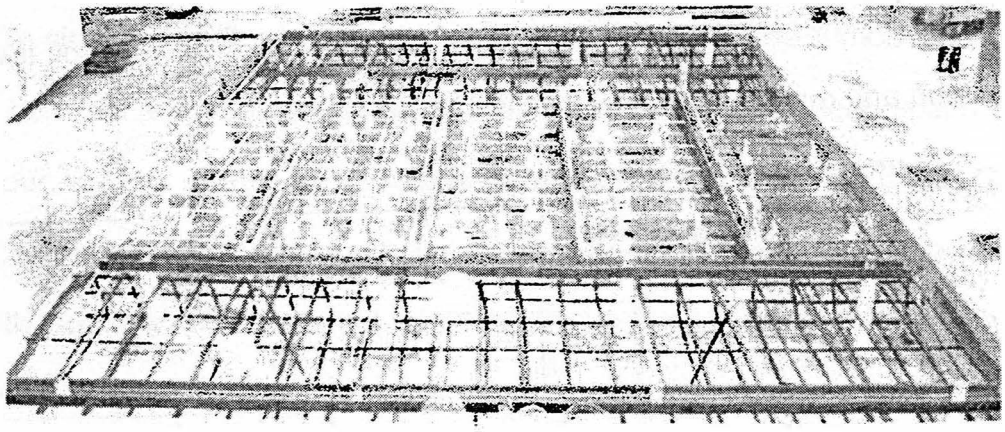

The concrete mix was a typical Missouri Department of Transportation bridge deck mix design. The specific design can be found in the appendix. The specimen took four men nearly three hours to cast. Cylinders and beams were cast along with the structure in order to perform strength tests throughout the duration of the experiment.

A few obstacles were encountered during and after the placement of the concrete and should be noted. As predicted above, the first problem during the placement was the damage inflicted on the two strain gauges in the spans. This most likely was the result from contact with the consolidation vibrator. Another problem encountered was the poor consolidation of some of the cylinders being cast for strength tests later on. This error is the cause of low strengths for two

cylinders. Other than these small occurrences the casting of the structure went well. A picture of the cast specimen is shown below in Figure 3.

Figure 3: Cast specimen

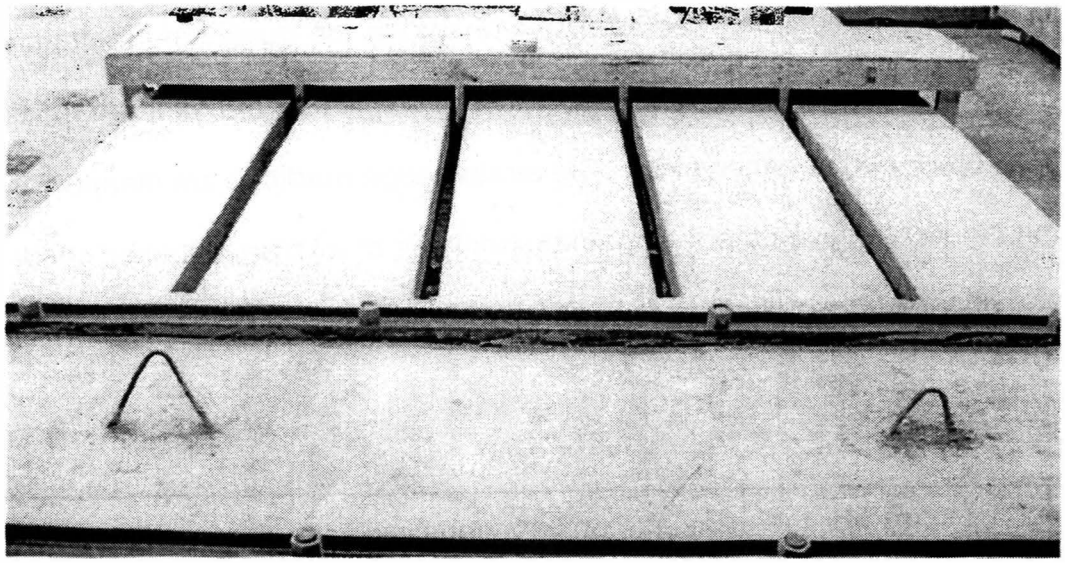

After the specimen was cast and sufficient strength was achieved the tie bars were tightened down. Because of the intricate design of the forms, their removal was not completed until several days after the placement. Because this study depends on shrinkage effects to determine the significance of the reinforcement and because late removal of forms can prevent shrinkage, this could prove to be the most critical error. As of now, no shrinkage cracks have formed in the specimen.

4. Experimental Results

Phase I which involves the short term observations of the experiment is complete and somewhat disappointing. To date, the only experimental results

gathered for Phase I are the strength breaks of the cylinders through twenty-eight days and strain readings on day 14. Data concerning cylinder breaks and strain readings can be found in the appendix. Since the mix design for the concrete is unique, no comparison can be made to ensure the quality of the concrete. The only assurance that the concrete is acceptable is that the strength gaining curve (see appendix) seems typical. The strain gauge readings are disappointingly low but are logical given the fact that no shrinkage cracks have formed. More results and observations will follow in Phase II of the study.

5. Summary

Phase I or the early-age observations of this project verified little from the results gathered to date. The concrete quality control seems to be adequate as determined from the cylinder breaks. It can be gathered that inadequate restraint of the structure was the result of no formation of shrinkage cracks. This could be accounted to the long amount of time required for form removal or an error in the tie rod tensioning in the end section of the structure. Phase II, later-age observations, will continue where Phase I ends and will hopefully encounter developments in cracking. Because cracking is critical to the basis of this project, if no self induced cracking occurs outside measures may need to be taken to induce cracking of the structure. These measures may include heating, wetting and drying, or loading the specimen. Again Phase II will determine what measures will be taken.

References

Koenigsfeld, Daniel. "Secondary Reinforcement for Fiber Reinforced Polymers Reinforced Concrete Panels." 2003

Mahmood, Hamid. "Cracking of Concrete Members Reinforced with Glass Fibre Reinforced Polymer Bars." 2002

Appendix

- Torque wrench data
- Strain gauge data
- Cylinder break data
- Mix design specifications

Torque Wrench Calculations

torque on wrench	Load Cell Measurements			
	Trail 1	Trail 2	Trail 3	Trail 4
0	0	0	0	0
10	38.90454	55.88107	45.97809	46.92124
15	55.17371	69.32082	56.58842	60.36099
20	69.32082	85.58999	69.32082	74.74388
25	82.76057	102.5665	80.6385	88.6552
30	98.32239	119.543	98.32239	105.3959
35	108.9327	130.1534	118.1283	119.0715
40	123.7872	142.8858	135.1049	133.9259
45	147.1299	161.277	154.9108	154.4392
50	171.18	176.8388	170.4726	172.8305
55	181.083	194.5227	197.3521	190.9859
60	196.6448	218.5728	219.2801	211.4992
65	215.7434	233.4272	232.0125	227.0611
70	232.7199	248.9891	252.5258	244.7449
75	258.1847	265.2582	264.5509	262.6646
80	273.0391	277.2833	286.4789	278.9338
85	296.3819	301.3334	310.529	302.7481
90	308.4069	320.432	321.8467	316.8952
95	326.0908	340.9453	343.7747	336.9369
100	344.482	364.288	358.6291	355.7997

Torque Wrench Calculations

$y = 3.4378x - 3.2091$
$x = (y + 3.2091) / 3.4378$

3 day

Compressive Strength =	4,090	psi
Tensile Strength =	409	psi
Torque to =	120	ft-lbs

7 day

Compressive Strength =	5,146	psi
Tensile Strength =	515	psi
Torque to =	151	ft-lbs

14 day

Compressive Strength =	5,970	psi
Tensile Strength =	597	psi
Torque to =	175	ft-lbs

Torque Wrench Calibration

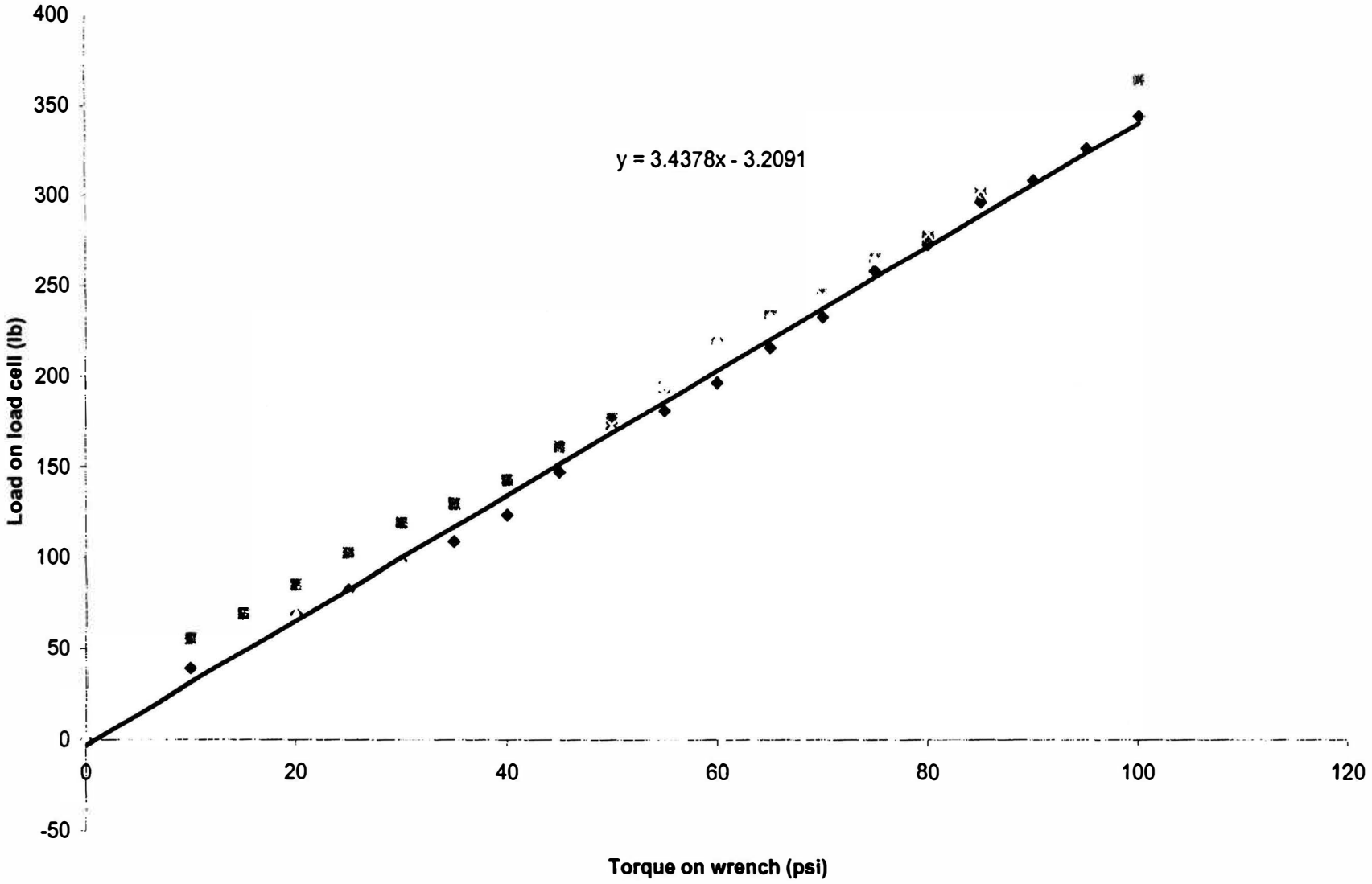

Strain Gauge Values

14 Day

Strain Gauge ID #	Micro Strain
1 - 1	1238
1 - 2	1116
1 - 3	---
1 - 4	642
2 - 1	1238
2 - 2	1004
2 - 3	552
2 - 4	606
3 - 1	361
3 - 2	409
3 - 3	101
3 - 4	824
4 - 1	1009
4 - 2	1000
4 - 3	1075
4 - 4	1546
5 - 1	1902
5 - 2	1368
5 - 3	1196
5 - 4	---

Cylinder Break Data

Diameter (inches)

	Day 1		Day 3		Day 7		Day 14		Day 28	
Cylinder #1	Diameter #1	4.000	Diameter #1	3.918	Diameter #1	3.929	Diameter #1	3.919	Diameter #1	3.923
	Diameter #2	4.000	Diameter #2	3.905	Diameter #2	3.919	Diameter #2	3.920	Diameter #2	3.923
	Avg.Diameter	4.000	Avg.Diameter	3.912	Avg.Diameter	3.924	Avg.Diameter	3.920	Avg.Diameter	3.923
Cylinder #2	Diameter #1	4.000	Diameter #1	3.922	Diameter #1	3.924	Diameter #1	3.919	Diameter #1	3.920
	Diameter #2	4.000	Diameter #2	3.930	Diameter #2	3.915	Diameter #2	3.840	Diameter #2	3.924
	Avg.Diameter	4.000	Avg.Diameter	3.926	Avg.Diameter	3.920	Avg.Diameter	3.880	Avg.Diameter	3.922
Cylinder #3	Diameter #1	4.000	Diameter #1	3.931	Diameter #1	3.925	Diameter #1	3.928	Diameter #1	3.926
	Diameter #2	4.000	Diameter #2	3.914	Diameter #2	3.918	Diameter #2	3.924	Diameter #2	3.926
	Avg.Diameter	4.000	Avg.Diameter	3.923	Avg.Diameter	3.922	Avg.Diameter	3.926	Avg.Diameter	3.926

Ultimate Compressive Strength (lbs)

	Day 1	Day 3	Day 7	Day 14	Day 28
Cylinder #1	28,230	48,135	64,350	71,820	72,345
Cylinder #2	29,715	50,955	59,190	70,785	81,615
Cylinder #3	29,475	49,005	62,940	66,390	78,660

Ultimate Compressive Stress (psi)

	Day 1	Day 3	Day 7	Day 14	Day 28
Beam #1	2,246	4,006	5,321	5,952	5,985
Beam #2	2,365	4,209	4,906	5,988	6,756
Beam #3	2,346	4,055	5,211	5,484	6,498
AVG =	**2,319**	**4,090**	**5,146**	**5,970**	**6,627**

Concrete Mix Design

-----Original Message-----
From: Myers, John (UMR) [mailto:jmyers@umr.edu]
Sent: Thursday, October 21, 2004 3:18 PM
To: Branham, Nathan Dale (UMR-Student); Cox, Jason
Subject: Mix Design
Importance: High

Here is a suggested mix design that is representative of MoDOT bridge decks:

Coarse Aggregate (3/4" max or smaller preferred; limestone) 1783 #/cy
Fine Aggregate (Natural river sand preferred) 1074 #/cy
Cement 728 #/cy
Water 320 #/cy
Add air entrainment to get ~ 5% air; perhaps ~ 3.3 oz/cy

Use enough water to attain target of 4" slump at placement. Perhaps less than 320 #/cy is needed to get the target slump so **do not** have the ready mix producer add all of the water at once unless he is checking the slump at the plant. Weight/measure any additional water added in the lab to make sure we have a very accurate w/c ratio for the report. Obtain the plant ticket and any material mil sheets they might have.

John J. Myers, Ph.D., P.E.
Assistant Professor and Architectural Engineering Program Coordinator
Dept. of Civil, Architectural and Envir. Engineering
The University of Missouri-Rolla
325 Butler-Carlton Hall
Rolla, Missouri 65409-0030
(V) 573-341-6618
(F) 573-341-6215
Email: jmyers@umr.edu
CArE Department Web Page
CIES Web Page

****
One of the Top 25 Civil Engineering Programs in the Nation
U.S. News
****

Tether Reel Mechanism for the MR SAT Project

Abbie Stewart
University of Missouri-Rolla
Dr. Henry Pernicka

The Missouri-Rolla Satellite (MR SAT) system is being designed and constructed by students at the University of Missouri – Rolla in order to give Aerospace Engineering students along with other majors practical experience in spaceflight concepts. The satellite system will consist of two tethered satellites that will eventually be completely disconnected and use a propulsion method to enter the chase phase of our mission. New design concepts are being used on this satellite including the possible use of a honeycomb-aluminum friction stir-welded structure and micro-pulse plasma thrusters for maneuvering. The research done this summer focused on the tether reel mechanism (TRM) including its initial deployment, unreeling/slowing down, and its final separation. The ideas for each mode of operation were put in trade studies to compare the feasibility and reliability of each concept. Two hovercrafts were also designed and built to test the TRM concepts in an environment that most closely resembled microgravity on Earth.

Introduction:

The NASA Goddard Space Center has been doing significant research in the benefits of using a Distributed Space System (DSS). This concept would send several smaller satellites into space to perform the function of one larger satellite. One area of research is in the tethered versus non tethered configuration of these satellite systems. With this in mind the MR SAT project team designed a mission that will allow both tether configurations to be tested. For the first phase MR SAT and its smaller counterpart MRS SAT (Missouri Rolla Second Satellite) will be formed into one satellite. Then in phase two they will separate along a ten meter tether. After remaining in this configuration for a few weeks the will finally disconnect completely in phase three of the mission. One of the greatest challenges to this mission concept is developing a mechanism that will separate the satellites, reel MRS SAT out to ten meters, decelerate her to a gentle stop at ten meters, and finally disconnect her completely from MR SAT. This is the challenge that was researched and will be discussed in this paper.

Satellite Separation:

A solenoid-magnet device was designed to separate the two satellites and disconnect the tether. The tether disconnect function will be discussed later. In its initial configuration MR SAT will have the Missouri Rolla Second Satellite (MRS SAT), another smaller satellite, tucked into the top of it. For the first phase of the mission MR SAT will need to release MRS SAT and allow her to reel out along a tether. One concept for this separation is the solenoid-magnet. A circular magnet will be attached to MR SAT and magnetically connected to a piece of iron on MRS SAT. The solenoid will be in the center of this magnet and when an electric pulse is sent through the solenoid will allow for the release of the magnet. This release will be due to the reverse of the poles in the magnet thus causing it to repel the iron as oppose to adhering to it. This design can be seen in Figure 1 below.

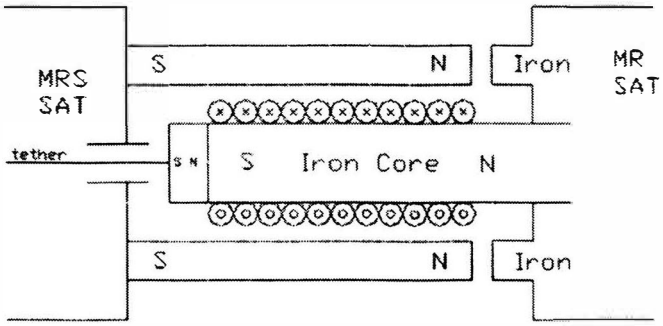

Figure 1

Another concept discussed by previous researchers was the use of springs for separation of MRS SAT. This concept posed several problems. The spring would have to be located at the exact center of MRS SAT in order to prevent her from spinning as she deployed. If multiple springs were used then they would all have to release simultaneously or it too could lead to spin. For these reasons this concept has nearly been discarded.

Trade Study Chart

Tether Separation

									Alternate Designs					
		Score						Weight	Score			Score		
Criteria	Units	0	1	2	3	4	5	1 to 4	Value	RS*	WS**	Value	RS*	WS**
Complexity		Very High	High	Mod high	Significant	Mod Accept	Accept	2	Mod High	2	4	Mod High	2	4
[redacted]	%	100	100-75	75-50	50-25	25-0	0	4	100-75	1	4	75-50	2	8
Development Time Required	Minutes	> 12	12 to 10	10 to 7	7 to 4	4 to 2	< 2	1	> 12	0	0	10 to 7	2	2
[redacted]	$	> 5000	5000-4000	4000-2000	2000-1000	1000-500	< 500	2	< 500	5	10	1000-500	4	8
Mass	kg	> 2	2-1.5	1.5-1.0	1.0-0.5	0.5-0.1	< 0.1	3	< 0.1	5	15	1.5-1.0	2	6
[redacted]								Weighted Score Totals			33			28

Figure 2

Tether deceleration:

One concept for the deceleration of MRS SAT as she is reeled away from MR SAT is to use a tapered tether design. The tether would be designed for one basic diameter and then during approximately the last meter of the tether it would gradually widen. The entire tether would deploy through a circular opening that would allow the initial width of the tether to move freely, but as the tether widened it would cause more and more friction to form on the tether eventually stopping it completely when the width of the tether exceeds the width of the whole it is traveling through. Companies that create tapered tethers were researched and after email discussions with these companies it was determined that this design would not be feasible due to the extreme cost of designing this type of tether.

Other concepts are being developed currently at the University of Missouri-Rolla by another team of students. These concepts along with the tapered tether concept are being compared (Figure 3) to see which will work best for the MR SAT mission.

Trade Study Chart

Tether Deployment Control

		Score						Weight	Alternate Designs											
									Active Control Trim			Trim with "Friction"			Tapered Tether			Spring		
Criteria	Units	0	1	2	3	4	5	1 to 4	Value	RS*	WS**	Value	RS*	WS**	Value	RS*	WS**	Value	RS*	WS**
		Very High	High	Mod High	Signif icant	Mod Accept	Accept	2	Mod High	2	4	Mod Accept	4	8	Mod High	2	4	Mod Accept	4	8
Risk of Rebound	%	>100	100-75	75-50	50-25	25-0	0	4	75-50	2	8	50-25	3	12	25-0	4	16	75-50	2	8
	minutes	>12	12-10	10-7	7-4	4-2	<2	1	12-10	1	1	7-4	3	3	7-4	3	3	4-2	4	4
Cost	$	>5000	5000-4000	4000-2000	2000-1000	1000-500	<500	2	4000-2000	2	4	1000-500	4	8	2000-1000	3	6	<500	5	10
	kg	>2	2.0-1.5	1.5-1.0	1.0-0.5	0.5-0.1	<0.1	3	2-1.5	1	3	0.5-0.1	4	12	0.5-0.1	4	12	0.5-0.1	4	12
					Weighted Total Score							43						42		

Figure 3

Tether disconnect:

The same solenoid-magnet configuration used to separate the satellites was used to disconnect the tether. A bar magnet was inserted in the center of the solenoid. It was attached to the tether connecting MRS SAT to MR SAT and to another piece of iron on MR SAT. The initial pulse of electricity through the solenoid will not affect the polarity of this magnet because it is on the inside of the solenoid instead of around the outside like the circular magnet. A secondary pulse will be sent through the solenoid in the reverse direction causing the polarity of the bar magnet to reverse and thus release the tether from MR SAT. This design is also shown in Figure 1 above.

Another concept for tether disconnect was the use of the same epoxy mentioned above. It was also discarded as an option for the reasons listed above. The trade study in Figure 2 was used for this portion of the mission as well.

Hovercraft:

It was decided that hovercraft would best simulate microgravity here on Earth and therefore would be the best method in testing both the TRM and other MR SAT applications. The hovercrafts were designed from a concept used at the University of Virginia, by Dr. Robert Tai [(1)]. This idea was modified to be of more use to the MR SAT project. The original hovercrafts

were designed to be circular, but since the MR SAT project has two satellites next to each other this design would not work. Therefore, two half circle hovercrafts were designed using the same method as the circular hovercrafts in order to allow the hovercraft to rest with a full side touching. They were constructed using quarter inch plywood cut in the semi-circle design. This plywood was then wrapped in thick plastic and sealed with duct tape. The center of the hovercraft was bolted in order to create a semi-circular pocket of air inside the plastic around the bolt. The air was provided by a cordless leaf blower that was connected to the hovercraft by a flexible plastic tube. Construction of these hovercrafts was done at a shop on the University of Missouri-Rolla campus. After significant testing, it was discovered that the hovercraft did not glide smoothly enough across a normal floor to truly simulate microgravity, so they had to be further modified. Most of the heavy-duty plastic wrapped around the plywood frame was removed and the wholes in the plastic on the bottom of the hovercraft were enlarged. Though they perform more proficiently now, they are still being modified in the hopes of further improving their performance. The original configuration of the semi-circle hovercrafts can be seen in Figure 5 below.

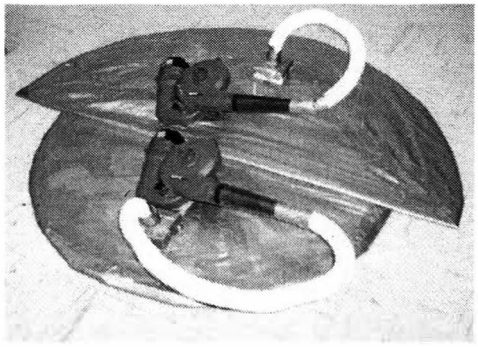

Figure 5

Conclusion:

Though the final decision has not been made on the TRM design, the research done over the summer was a good foundation for the future testing and research being done in this area. A prototype of the solenoid-magnet design is being built and will be tested with the new modified hovercrafts. The tapered tether idea has been discarded due the expense of creating this tether,

but other prototypes and ideas are also being tested currently. The final TRM is scheduled to be completed by the end of May 2005.

Acknowledgements:

The continued efforts of this design are being conducted by Everett Klapperich and Brian Peters at the University of Missouri-Rolla. They have taken my research from the summer and further developed a more complete model of the TRM design. The work done this summer was helped greatly by the efforts of Mike Ellebrecht who consulted on the Electrical Engineering aspect of the solenoid/magnet concept. The entire project was overseen by my advisor, Dr. Henry Pernicka, whose advice and assistance was invaluable to the research process.

References:

(1) http://www.vast.org/vip/HOVERCFT/instrctn/

Bioactive Glass Coatings for Adherence to Bone Tissue

By Wesley Trueblood
2/2/05
UMR Biological Sciences Department
OURE Final Paper

Abstract

The purpose of the experiments for this research project was to determine whether certain compositions of borate-based glasses are bioactive and can be used to bond titanium pins to bone. Two different major experiments were done. The first experiment was done to determine the bioactivity of the glass. The second experiment was done to simultaneously determine the bioactivity of the glass and determine whether or not the glass would bind to titanium and bone.

The majority of the research consisted of working with different compositions of borate-based glass, making glass pins, and coating titanium pins with the glass. The making and coating of pins was done in the Materials Research Center (MRC) at UMR. Various glasses were used and various synthesis techniques for the glasses were used.

The smaller but most important part of the research was done in the UMR animal lab. This part of the research involved performing surgery on rats to test the viability of the glass disks *in vivo*.

Introduction

Previous research has been done with bioactive glass. The research is mainly in the development phase and bioactive glass is not being currently used for commercial applications. The main differences between the established bioactive glass and the particular glass tested in this experiment is the chemical composition. Some established bioactive glasses have different amounts of borate with other chemicals.

The exact composition of the glass was not the focus of my research project. The synthesis procedure for the glass pins and the glass coating on the titanium pins was a trial-and-error procedure, and was mostly done by graduate students working in the MRC. The major focus of this paper will be the implanting experiments and the theory.

Theory

The potential of this research is that a type of glass could be developed that would improve the healing process for people who break bones and need to have titanium pins inserted into the bone. An ideal glass is one that can simultaneously bind to titanium and bone. The titanium pins can be coated with the glass and then inserted into the bone.

Once the pins are inserted, the glass should form a strong bond with the surrounding bone. The titanium pins themselves don't bond to bone as well as some other substances. One such substance that has been shown to improve bonding strength with bone is borate glass. This strong bond will speed the healing process by providing an indirect bone to pin bond.

Several other borate-based glasses have been shown to be bioactive – i.e. the glass provides a porous surface upon which biological tissues such as bone can permeate and proliferate. Prior to inserting the glass into a biological system such as the body of a rat, the glass needs to be soaked in bone marrow tissue.

Soaking the glass in bone marrow tissue requires a separate group of experiments to harvest the marrow stem cells and infuse the glass plates with them. The ideal conditions for inoculating the glass plates with cells can also be determined by practicing with some other types of bone cells instead of just marrow cells. The experiments for determining the conditions for inoculating the glass plates are discussed in the section titled "related experiments".

For the main experiments the marrow cells are taken from a live rat and cultured to keep them alive. The bone marrow tissue is taken from the femur of sacrificed rats, and it contains bone stem cells. Bone stem cells are generic cells that can develop into bone cells given the right biological environment. The porosity of the glass was an important aspect of the composition. The successful growth of bone on the glass required pores of a particular size.

Experiment 1

The first experiment's main purpose was to determine the right porosity and composition of glass to maximize the bioactivity. Two different types of borate glass were used, one called H12 and another called 45S5. Two different types of commercial bioactive glasses were also used to compare to the H12 and 45S5.

This experiment was repeated several times to test different compositions and porosities of the experimental glasses. Small disks were made for each type of glass, each about 3 mm thick and 2 cm in diameter.

Surgery was performed on the rats and the disks (which had been soaked in the bone marrow solution for 2 days) were inserted into the rats. The rats were shaved and put under anesthesia and four shallow incisions were made in the skin on their backs near the spine. The incisions were only skin-deep, because the disks needed to be inserted just underneath the skin.

The skin was separated from the fascia underneath by probing a small area on each side of the cuts with a blunt tool. Once a pocket was made, the disks were inserted underneath the skin in each of the four cuts. The wounds were then closed with staples and the disks were allowed to stay in the rats for 6 weeks. The rats recover fairly quickly from the wounds to the skin. They can walk around without much problem almost immediately after waking up from the anesthesia.

After six weeks the rats were sacrificed and the disks were extracted and analyzed. Eight rats were used for the initial experiment. The H12 disks showed about 50% of the amount of bone growth as the commercial disks. The 45S5 showed more bone growth than the H12, averaging about 75% of the growth on the commercial disks. The disks are analyzed for growth by placing them in a clear thermoset polymer solution and grinding them down into a thin section with a representative slice.

Experiment 2

The second experiment was to simultaneously affirm the bioactivity of the glass while testing the bonding capability of the glass to bone and titanium. The samples made were 16 small cylindrical plugs of either pure titanium, glass coated titanium, or pure glass plugs.

The pure titanium pins were used as a control to compare with the glass coated titanium pins. The pure glass pins were used to further assess the bioactivity of the glass. Eight rats were used again for this surgery.

The rats were put under anesthesia using isoflurane gas. The shin bone was used to test the glass for two reasons: it is easily accessible to surgery because there is very little muscle covering on the shin, so very little tissue has to be cut through to access the bone.

An incision was made in the skin of each of the shins of the rats. The incision leaves bare a small flat surface of bone where a small hole 2 mm in diameter was drilled out of the bone. One sample of the pins was inserted into each of the holes drilled in the bones. The rates generally recover quickly from this surgery. As with the subcutaneous implants, the rats can usually walk around easily immediately after waking up from the anesthesia. The wounds were stapled up and the pins were left in the tibia of the rats for 6 weeks. The rats were then sacrificed and the tibias of the rats were solidified in the polymer and ground down for analysis.

Related Experiments

For these experiments, porous glass disks are used to grow bone cells on. Bone cells migrate into the pores of the glass disks while the glass is soaking in the marrow solution. The marrow solution is made from the marrow cells taken from the femur of a live rat. Once the marrow cells are taken from the femur of a live rat, they are placed in a medium solution that contains plenty of nutrients for the cells to survive and replicate.

There are certain conditions that optimize the growth and inoculation of cells in the pores of the glass disks. The pore size of the disks is an important concern. If the pores are too big, there will be less total surface area for the cells to bind to the surface of the glass. When the pores are too small, the cells cannot migrate from the outer solution into the pores to attach to the surface of the disks. If the pores are the right size, the cells easily migrate into the pores and attach themselves to the large surface area of the disks. Marrow cells are difficult to attain because a live rat has to be sacrificed to get them.

To minimize the amount of rats sacrificed and still experiment with the pore size on the glass disks, different types of cells are used other than marrow cells. Other types of bone cells are approximately the same size as marrow cells and are much easier to obtain. In particular, some types of bone cancer cells can be grown in culture dishes in an incubator and used to experiment with the pore size of the glass.

Bone cancer cells tend to work well for this type of experimentation because they grow and replicate very quickly, so large colonies of them can be made in about a day. These cells are ironically called UMR cells. They tend to be very big and their colonies can be seen with the naked eye.

The following is an example of the experiments used to test for the correct pore size in the glass. A sample of the UMR cells are incubated in an oven until the cells form colonies and completely cover the bottom of the plate. Once the cells cover the plate,

they are "split". When the cells are incubated in the plates, they attach themselves to the surface of the plate. A chemical called trypsin is added to the cells. Trypsin causes the cells to detach from the bottom of the plate, and float in the fluid. A fraction of the total cells are taken off of the plate and put onto a new plate to form new colonies. In this way, large numbers of cells can be generated out of just a few cells.

Once a solution of the cells is obtained, the glass disks are immersed in the fluid with suspended cells. The suspended cells migrate into the pores on the disks and the cells are allowed to grow on the surface of the glass. In this way, many different disks with many different pore sizes can be tested to see which size pores are most conducive to cell growth.

Results and Discussion

Experiment 1 showed that the newly tested glasses did exhibit some bioactive behavior. The 45S5 pieces and the H12 pieces showed that after presoaking in bone marrow solution, and incubation under the skin of the rats, there was significant bone growth inside the pores on the large surface area of the glass. The pores not only provide a place for the bone stem cells to reside, but they also provide a large surface area to promote bone proliferation. The surface and chemical structure of the glass itself appears to aid in bone proliferation.

There were some design problems in the second experiment which prevented a proper analysis of the efficiency of the glass-titanium-bone interface. First, the porosity of the glass was somewhat difficult to control in the synthesis. If the pores were too big, the glass was unstable and in would easily crumble. If the pores were too small, the bone marrow solution wouldn't penetrate as easily and it reduces the efficiency of the bone growth.

The second problem occurred with the method of insertion into the rat's bone. The method involved using a small drill with only a 2 mm diameter bit. The hole was drilled in the shin of the rat, where there was little muscle cover (this reduces the amount of tissue destroyed on the rat, speeding its recovery). The bone at the shin position is pretty thin, and it is difficult to find the right spot to drill.

The entire length of the pins is only about 4 mm long. When the pins are inserted into the hole in the bone, it tends to come out after the wound is closed. This was the problem with three of the eight tested samples.

When the would was opened after six weeks to examine the adherence of the pins into the bone, the pin had actually come out of the hole and was resting along the shin just underneath the skin.

The samples that did stay in the bone adhered well and seemed to have made a good bond with the bone. Without having a good number of samples to analyze, however, it is difficult to say whether the glass coating on the pins provided and improved method of implanting titanium pins.

Conclusions

The first experiment confirmed that there is good reason to conduct further experiments on bioactive glasses. It showed that the new glasses tested, 45S5 and H12, exhibited bioactive behavior. In order for the glass to promote bone growth it is important to determine and comply with standards for the porosity and composition of the glass.

The design of the second experiment needs to be improved and optimized before any conclusions can be drawn about the viability of using bioactive glass to coat titanium pins before implanting them. The pins that were successfully implanted showed promise in bonding with the bone, however more experiments are necessary to confirm how well the implants work.

Kendra Waltermire
Sophmore
Biological Science

LEAD TOLERANT BACTERIA COULD BE THE FUTURE OF BIOREMEDIATION

Abstract

The contamination of soil, sediment, and water by toxic metals is a major problem worldwide, both environmentally, and economically. Microorganisms that are resistant to lead are rare in nature. Lead is toxic to most microorganisms and only a few have developed mechanisms to survive in this toxic environment. In this study, bacteria found in soil and water with high concentrations of soluble lead are isolated and characterized. I grew and isolated bacteria that are resistant to the lead found in the solid medium. A gram stain was used to characteristically determine the bacteria that were isolated. Four isolated bacteria were found. Three were found to be cocci in shape, and one was bacillus shaped. After continuation with this research, I hope to identify the four isolated bacteria and to further characterize the bacteria for future studies.

Introduction

Lead is mined every day from the environment and some lead gets deposited back into the soil or water. Lead and other residue separated in the preparation of mining is deposited back into the soil forming piles that can stretch for miles called tailings piles. St. Joseph State Park is found in the old "Lead Belt" of southeast Missouri where much of the nation's lead ore was extracted for more than a century. In 1972, the St. Joe Minerals Corporation ceased operations and subsequently donated the land to the state in 1976. The by-products of the lead mine at St. Joe State Park in Missouri were deposited in valleys causing the formations of many small lakes. The leftover lead from the tailings piles can react with the acidic rain and become soluble in the water. The soluble lead can run-off into the lakes causing lead poisoning to many animals, plants, and microorganisms. Lead poisoning is also a problem for humans. Lead poisoning attacks the nervous system causing vomiting, periods of stupor, higher blood pressure, being delirious, seizures and coma (2). The U.S. Environmental Protection Agency regulates drinking water for lead at 15 micro g/l, but this does not include the excess lead that is deposited into the water when soft, acidic drinking water wear down lead connectors, pipes, joints, and other fixtures that hold water that may contain lead (2). With the help of bacteria that can detoxify the lead, water treatment may become easier and more efficient.

Lead, the most common metal found at contamination sites, is the least studied of the metals (1). When lead and other organic compounds are released into the soil, the soil is considered cocontaminated. Cocontaminated soil is difficult to remediate because the metal is toxic, inhibiting the activity of the organic-degrading microorganisms (3). Most bacteria cannot perform this task because lead and other metals can inhibit enzymatic activities, disrupting membrane functions, and damaging nucleic acids (1). One reason may be that the energy requirements to maintain metal resistance and the organic degradation are too high (4). The microorganism cannot perform both activities along with environmental stress. The issue of cocontamination is serious. Approximately 37% of all contaminated sites in the United States contain metal and organic contaminants (4). By studying these microbes that have ability to resist and detoxify metals, environmental microbiologist can identify ways of cleaning up metal-contaminated systems (Roane, personal communication). Using these microbes to enhance the biological activity of the existing populations within a contaminated site is called bioaugmentation (3). Bioaugmentation of these wastes has been investigated in recent years as a safe and more environmental friendly alternative to chemical removal methods.

Kendra Waltermire
Sophmore
Biological Science

Materials and Methods

Field site. The sampling site for the water sample was taken from a well that near Monsanto Lake. The well contained groundwater that was surrounded by tailings. The water was monitored with an average pH of 8.12. The average temperature of the water was 11.98°C. The soil sample was collected from the center of the tailings pile with no lake nearby. A hole was dug about a foot or two down into the soil and I collected the sample from the lower, damper tailings. I gathered the samples at the sample site in sterile and cold conditions. The samples remained in an ice chest until further use in the lab.

I then mixed up a minimal broth containing .7g K_2HPO_4, .2g KH_2PO_4, .1g $(NH_4)_2SO_4$, .1g Glucose, .05g Sodium Citrate, .01g $MgSO_4 \cdot 7H_20$, and .01g $Pb(OAc)_2$ to produce 100mL of broth. I then added HCl until the pH was neutral (7.0). The broth was autoclaved for 15 minutes at 15 psi and 121°C. I made two different broths to grow separate soil and water samples. The broths were cooled to room temperature. I then added 1mL of the water sample to one of the broth flask. I added one scoop of the soil sample to the other broth flask. I allowed the bacteria to set for a week in room temperature to allow the bacteria incubation time.

I also grew the bacteria in a separate broth flask using Dr. Timberly Roane's recipe for the medium that she uses in her laboratory. Her recipe to make 200 mL of broth contained .1g Sodium Citrate, .2g Magnesium Sulfate, .2g Ammonium Sulfate, .2g Glucose, and .02g Sodium tripolyphosphate. I also added 2.04g of Potassium Hydrogen Pthalate as a buffer and .02g of $Pb(OAc)_2$ to introduce the lead into the broth. I then added NaOH until the medium has a pH of 6.5. The broth was autoclaved for 15 minutes at 15 psi and 121°C Using this same recipe with the addition of 3.0g of Agar, I made another 200mL for a solid medium that was used to isolate the colonies.

After incubation, I inoculated three of the solid agar plates with the bacteria growing in the Roane's broth containing the lead tolerant bacteria from the soil sample. I then inoculated three other solid agar plates with the bacteria growing in the Roane's broth containing lead tolerant bacteria from the water sample. After the bacteria grew for a week, I isolated the colonies on a new set of agar plates. After the isolated plates were allowed to incubate for another three days, I did a gram stain to characterize the bacteria.

Results

Once the bacteria began to grow in the minimal broth, I observed the results. A white, creamy bacteria colony had begun to grow in the soil sample broth, but none could be observed in the water sample. Once the Roane recipe was ready, I inoculated the broth with 1mL of water sample for the water broth and a scoop of soil for the soil broth. After four days in room temperature, white, creamy bacteria was noted in the soil sample, but there was no visible sign of bacteria in the water sample. In order to observe the bacteria, a wet mount was made from each sample and I viewed the bacteria under a microscope. Seeing that both samples contained bacteria, I inoculated three plates with the bacteria from the soil. I also inoculated another three plates with the bacteria from the water sample. I allowed the plates to sit five days in a 37°C incubator. I observed minimal bacteria as small white dots in the water sample plates. In the soil sample plates, I observed what appeared to be four different bacteria. The bacteria that I observed were a small white dot, creamy, film-like bacteria, tan/brown dot, and a large white dot. After isolation of these bacteria, I observed the bacteria on the plate. There were no visible bacteria on the plate that was inoculated by the small white bacteria from the water plates. All four bacteria from the soil plates were growing isolated from one another. I then used the gram

Kendra Waltermire
Sophmore
Biological Science

stain assay with the isolated bacteria for identification. The small white dot was gram positive and bacillus shaped. They were found clumped together or growing as individuals. The tan/brown dot was gram positive and cocci shaped. They were found in strains and clusters. The irregular, film-like bacteria were gram negative and cocci shaped. They were found growing in small clusters, chains, and as individual bacterium. What appeared to be an isolated colony of the large, white bacteria gave an incorrect result. Out of the three plates that the colonies were found, the soil plate 3 produced a gram positive while soil plate 1 and 2 produced a gram negative result. All of the stains showed a cocci shaped bacterium that was found in clusters. The bacteria had been growing for more than 48 hours which may have caused an invalid result. Further testing will be done to verify the results.

Soil			
Inoculated growth plates	Soil 1	Soil 2	Soil 3
Isolated plates	Soil 1	Soil 2	Soil 3
Bacteria growth	Brown, Large white, Film-like	Large White, Film-like	Brown, Large white, Small white, Film-like

Water			
Inoculated growth plates	Water 1-No growth	Water 2	Water 3-No growth
Isolated plates		Water 2-No growth	
Bacteria growth	None	None	none

Table 1. The table above gives the result of growth from beginning inoculation until isolation. After inoculation of the plates from the broth, the plates that contained water 1 and water 3 had no growth. Water 2 plate had minimal growth. After isolation, there were no bacteria colonies on the plate used to isolate the colony.

Gram Stain Results			
Bacteria	Soil 1	Soil 2	Soil 3
Brown-cocci	Gram Positive		Gram Positive
Small white dot-bacillus			Gram Positive
Large white dot-cocci	Gram Negative	Gram Negative	Gram Positive
Film-like-cocci	Gram Negative		Gram Negative

Table 2. The above gives the result of the gram stain assay in according to which plate the bacteria was isolated.

Discussion

While growing the bacteria, the pH was set slightly acidic. The acidity increases the lead bioavailability in the medium (1). Metals are generally considered biologically available and more toxic when they are soluble. Lead will readily precipitate out, especially when using inorganic phosphates (Roane, personal communication). Avoiding the inorganic phosphates helps to keep the lead more readily available.

After performing the gram stain test, I discovered that the large, white bacterium was not one but two different species, one gram negative and the other gram positive. The results of the gram stain assay may have formed an incorrect result because the bacteria were older than 48 hours from initial inoculation onto the plates. A bacterium's cell wall begins to break down after this time period causing opposite results of the true stain. In order for the gram stain to be considered correct, the bacterium must be stained no later than 48 hours after inoculation. I will try to re-isolate the bacteria again and perform another gram stain on the test to verify the results.

Kendra Waltermire
Sophmore
Biological Science

If the results are the same, I then will try to isolate the two different large, white cocci bacterium from the three soil plates. I will also try to reisolate the colony from the water 2 plate. Once I have isolated all of the bacteria, I will further characterize my isolates using different staining assays. I will run DNA sequencing on the bacteria. I will also perform some biochemical assays. After characterization and hopeful identification, I will test the lead tolerance of the bacteria and monitor the effects of the growth of the organism on metal solubility. This will test the physiological stress on the bacteria. Overall, these results support the brighter outlook for future bioaugmentation using lead tolerant and other metal tolerant bacteria.

Acknowledgements

I would like to thank Dr. Melanie Mormile for her guidance throughout all of my lab work. I would like to also thank Dr. Timberly Roane for all of her correspondence that has helped me to better understand lead tolerant bacteria and lab procedures.

References

1. Roane, R.M. (1998) Lead Resistance in Two Bacterial Isolates from Heavy Metal-Contaminated Soil. Microbial Ecology, New York
2. Andrews, Ph. D., R.D. Sandra L. (1991) Lead and Our Environment. MSU Extension Food and Nutrition Bulletin, Michigan Statue University
http://web1.msue.msu.edu/msue/imp/modac/e2416692.html
3. Pepper, Ian L., Gentry, Terry J., Newby, Deborah T., Roane, Timberly M., Josephson, Karen L. (2002) The Role of Cell Bioaugmentation and Gene Bioaugmentation in the Remediation of Co-contaminated Soils. Environmental Health Perspectives
4. Roane, T.M., Josephson, K.L., Pepper, I.L. (2001) Dual-Bioaugmentation Strategy to Enhance Remediation of Cocontaminated Soil. Applied and Environmental Microbiology AEM.67.7.3208-3215.2001

Structural Interpretations from High Resolution Aeromagnetic Data, Northwest Botswana

Daniel Wheaton

April 1, 2005

Abstract

High resolution aeromagnetic data collected over northwest Botswana has provided new insights into previously hidden geologic structures. Major antiformal and synformal structures have been recognized within the Kinabaran age Kgwebe meta-volcanics and other basement rocks. These structural features trend northeast-southwest agreeing with previously collected geologic field data and observed surface features. Further interpretation of the geophysical data has yielded relative dips of the fold limbs and indication of the direction of plunge. Folding extends both north and south of the Okavango Rift Zone for at least 100 – 200 kilometers. Further studies are being conducted to determine if these pre-existing geologic features exert structural control on neotectonic activity.

Introduction

There are two main purposes to this research. Primarily it is to interpret geologic structures based on geophysical data and determine what information can be obtained from such data. Secondly this research will be integrated with other studies to determine the role of existing geologic basement structures on neotectonic activity. Normally, geologic information is gathered through careful and intensive fieldwork. A geologist goes into the field with rock hammer, Brunton compass, and other tools to observe patterns and take samples and structural measurements from rock outcrops. Through traveling and various maps these small pieces are all combined to paint a larger, more complete geologic picture. However, circumstances are not always so kind. The northwestern regions of Botswana are one such place. It is a large area with very limited outcrops and many features are buried by more recent sedimentation. Borehole data in the area is also quite limited giving geologists only a very generalized picture of the area. So we turn to geophysical methods to do further investigations. Potential field methods such as gravity and magnetics allow us to look at the buried geology. These methods have already been used in the area (Kampunzu 1998, 2000) to delineate crustal blocks and regional features. Advances in technology have given us better tools to increase the quality of our data. The high resolution aeromagnetic data (250 meter line spacing) collected by the Geologic Survey of Botswana can be used to better delineate geologic boundaries as well as interpret structures.

The Ghanzi-Chobe belt of northwest Botswana (figure 1) extends from the Goha and Shinamba hills in the northeast to Mamuno in the southwest (Kampunzu 1998).

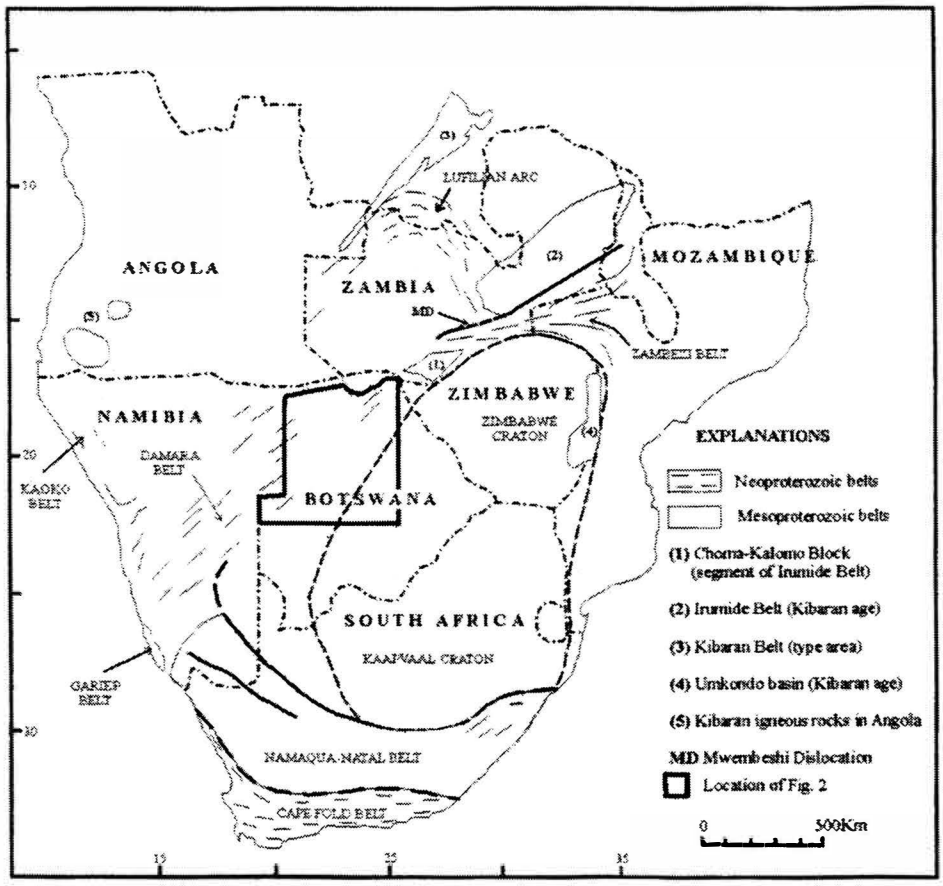
ANGOLA
ZAMBIA
MOZAMBIQUE
NAMIBIA
ZIMBABWE
BOTSWANA
SOUTH AFRICA
ZIMBABWE CRATON
KAAPVAAL CRATON
DAMARA BELT
KAOKO BELT
GARIEP BELT
NAMAQUA-NATAL BELT
CAPE FOLD BELT
ZAMBEZI BELT
LUFILIAN ARC
MD
(1)
(2)
(3)
(4)
(5)
EXPLANATIONS
Neoproterozoic belts
Mesoproterozoic belts
(1) Choma-Kalomo Block (segment of Irumide Belt)
(2) Irumide Belt (Kibaran age)
(3) Kibaran Belt (type area)
(4) Umkondo basin (Kibaran age)
(5) Kibaran igneous rocks in Angola
MD Mwembeshi Dislocation
Location of Fig. 2
0
500Km
10
20
30
15
25
35

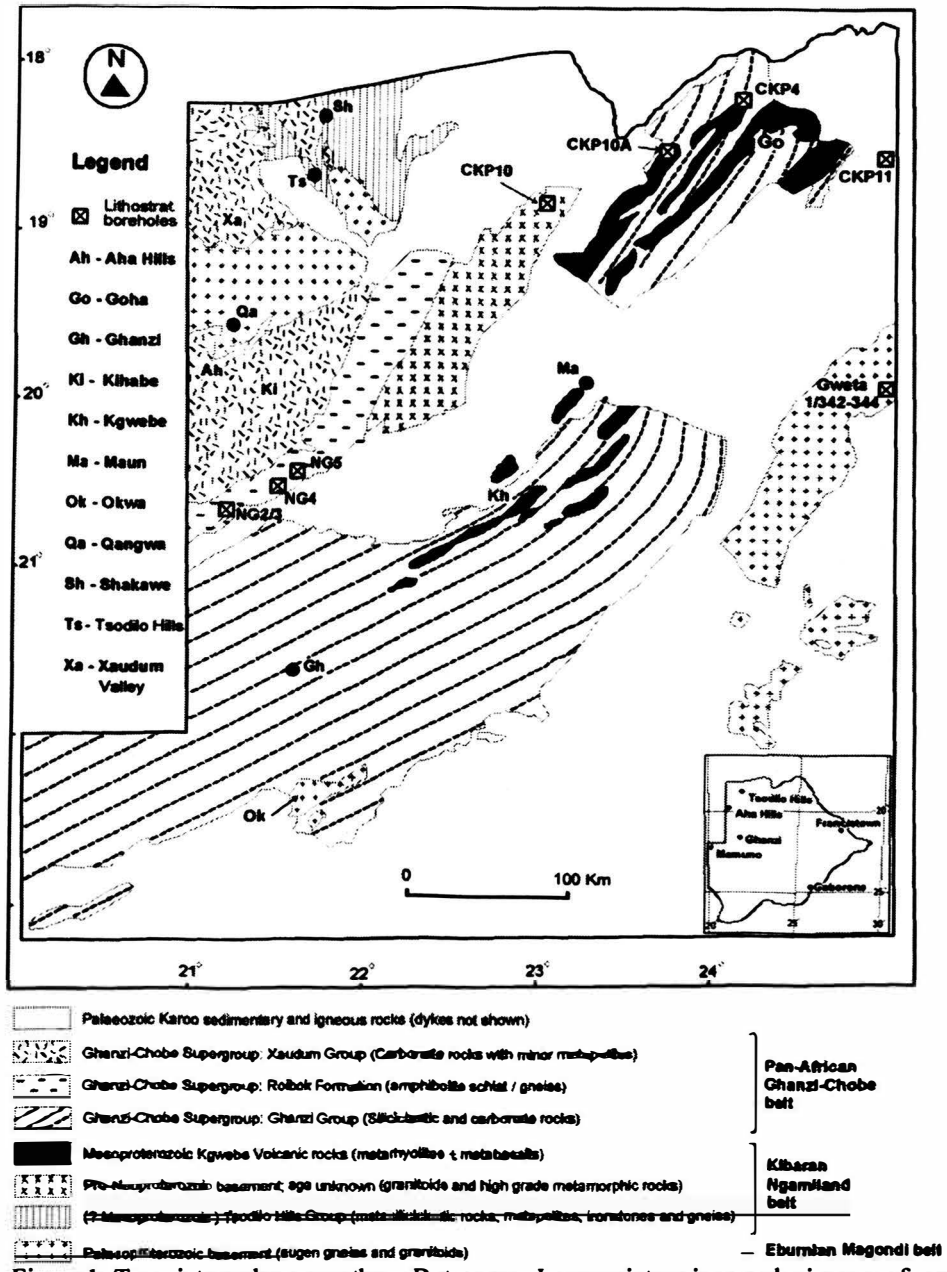

Figure 1: Top picture shows southern Botswana. Lower picture is a geologic map of northwest Botswana (after Kampunzu 2000).

It is part of the Neoproterozoic Pan-African belt system in southern and central Africa. Despite the fact that it is mostly covered by Phanerozoic strata, its boundaries have been well delineated with aeromagnetic data. The Okwa Group, a thick series of sedimentary deposits, namely sandstone, unconformably overlies the Kgwebe meta-volcanic rocks. The Kgwebe meta-volcanics make up part of the basement rock, the focus of this study. The Kgwebe meta-volcanics are primarily composed of meta-mafic and meta-rhyolite rocks. Clasts of the rocks are round in the overlying conglomerate and the rocks themselves have been correlated with meta-volcanics in Namibia which predate rifting thus making them part of the basement. The Kgwebe

meta-volcanic rocks form a series of hills trending northeast-southwest in the Ghanzi ridge and U-Pb zircon dating puts their age at 1106 +/- 2 million years. These meta-volcanic rocks were part of late Kinabaran magmatism so they are orogenic igneous rocks created by an extensional event that melted lower crustal rocks.

Methodology

In order to interpret structural features of the Ghanzi-Chobe belt in northwest Botswana high resolution (250 meter line spacing) aeromagnetic data was obtained from the Geologic Survey of Botswana. In this case, aeromagnetic data proved particularly useful because of the composition of the basement rock. The basement rock, which includes the Kgwebe meta-volcanics, is typically mafic in composition. These kinds of volcanic rocks generally contain magnetite and thus tend to have higher percentages of iron than other kinds of rocks. As volcanic rocks cool and crystallize the magnetic minerals they contain take on the characteristics of the earth's magnetic field. Once the rock cools below the Curie temperature it becomes magnetized based on those characteristics. This is called thermal remnant magnetization (Telford 1990). The sediment on top of the basement rock has very little in the way of magnetic minerals because they are weathered out. So using a magnetic data set allows us to strip away that top layer and view the geology beneath. The high resolution of this data set gives better detail making it uniquely qualified for viewing and interpreting buried structures.

Once the data is collected, a variety of computer software packages are available for processing. Processing for this project was done with Oasis Montaj Geosoft v6.01. There are numerous mathematical filters that can be applied to magnetic data in order to enhance certain features, observe different measurements, or get a different view. Several of these are important to this project, one being the first vertical derivative. This filter applies the first derivative to the magnetic anomaly in the vertical (z) direction providing the rate of change of the magnetic anomalies. It also serves to enhance the shallow anomalies (Geosoft Help File 2005). Filters are applied in the Fourier Domain. The first part of pre-processing is to remove the nth-order trend or mean from the gridded data. Next, the grid is expanded to prepare for the Fourier transform which uses either the Cooley-Tukey algorithm or the Winograd algorithm. The grid is then filled with dummies using maximum entropy to fill the new expanded dimensions such that the grid becomes smoothly periodic. The expanded and filled grid is converted from the time domain to the frequency domain by taking the integral of the series of gridded data values and multiplying them by e raised to the power of (iwt) and multiplying again by dt (where w is the wavenumber). Filters previously selected by the user are then applied to the Fourier transformed grid. The gridded data is put back into terms of wavelength (distance) by transforming it from the frequency domain back to the time domain. This is done by taking the integral of the filtered series of gridded data values and multiplying them by e raised to the power of (iwt) and multiplying again by dw. Dummy areas from the original grid are masked back onto the final filtered grid and the grid size is reduced to its original size. If a trend surface was removed during pre-processing, and if no high-pass filters was applied to the data, then the trend is added back to the output grid. Post-processing uses Boolean operations to deflate the filtered grid back to its original input size and then add the trend back into the grid.

Derivatives can also be applied in the x and y directions which becomes very important when doing Euler deconvolutions. The apparent depth to the magnetic source is derived from Euler's homogeneity equation (Euler deconvolution). This process relates the magnetic field and its gradient components to the location of the source of an anomaly (Geosoft Help File 2005).

The degree of homogeneity is expressed as a structural index which is a measure of the fall-off rate of the field with distance from the source. Euler's homogeneity relationship for magnetic data can be written in the form: $(x - x_o)\, dF/dx + (y - y_o)\, dF/dy + (z - z_o)\, dF/dz = N(B - F)$, where (x_o, y_o, z_o) is the source location whose magnetic field F is measured *at* (x, y, z); B is the regional value of the total field; and N is Euler's structural index. N is a measure of the rate of field change with distance. At each solution the Euler deconvolution process is applied. The user defines the structural index telling the program which shapes to look for. A least-squares inversion is employed to solve the equation for an optimum x_o, y_o, z_o and B. The program creates a database of information on all the anomalies that meet the criteria. The analytic signal filter also uses the derivatives, but to identify the edges of the magnetic source bodies on the map. This filter is the square root of the sum of the squares of the derivatives in the x, y, and z directions: analytic signal = sqrt (dx*dx + dy*dy + dz*dz). It is particularly helpful when remanence and/or low magnetic latitude complicates interpretation.

Besides filters, there are a few other tricks to processing data. Ternary diagrams present the user with one map that shows the information of three different maps simultaneously making shared features pronounced and contrasting different ones. Changing the color scheme of the maps also helps to better accentuate certain features and make contrasts more visible. Similar results can be obtained by changing the degree and direction of illumination.

Results & Discussion

Looking at a magnetic map (figure 2) is much like at satellite imagery, except that the colors indicate the strength of the magnetic source.

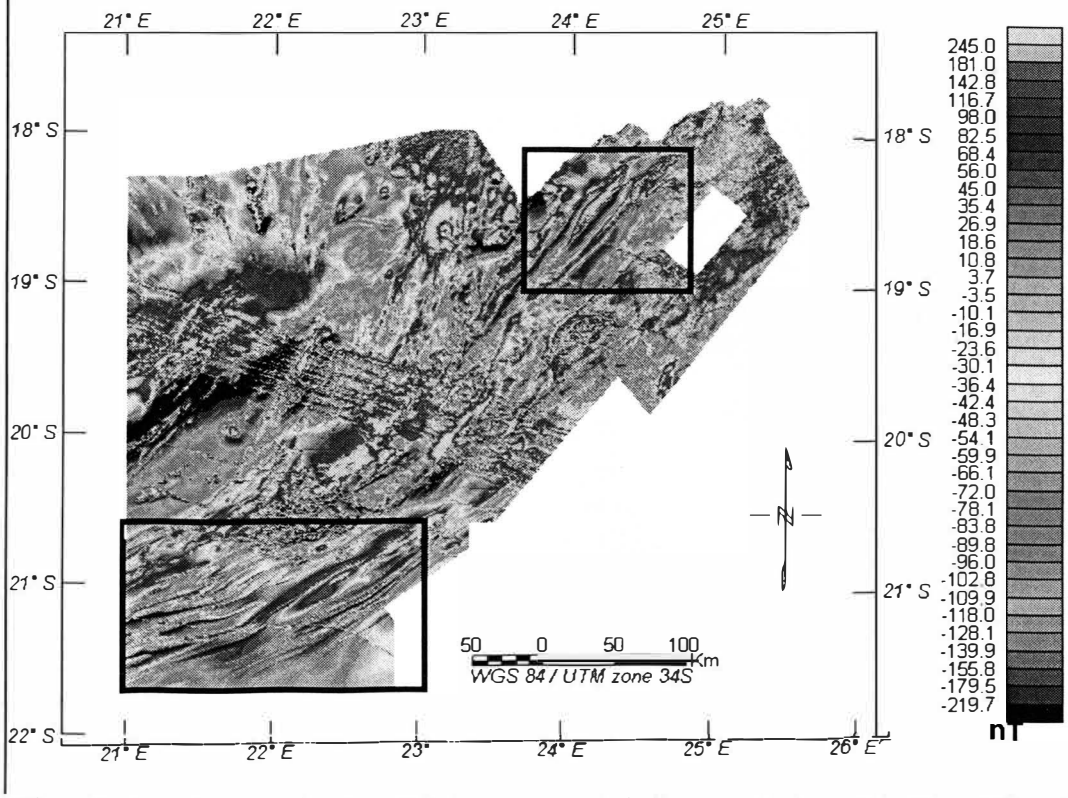

Figure 2: Magnetic map of northwest Botswana. Inserts indicate areas of research. The southern insert is shown in figures 4 and 7.

It was this similarity that first prompted the idea that the northeast-southwest trending magnetic anomalies were indeed geologic structures. It fits that if they are geologic structures that they should show up. The basement rocks, especially the Kgwebe meta-volcanic rocks, are much more magnetic than the overlying rock so any feature within should also show up. However, previous studies lacked the resolving power to differentiate these features. One may notice that the northeast-southwest trending structures, if traversed perpendicular to trend, alternate from high magnetic anomalies to low ones. This pattern was the first indication that these features were folds. This same pattern also emerged in the data after several filters were applied including the first vertical derivative and analytic signal. So, in order to view several maps at a time, the magnetic, first vertical derivative, and analytic signal grids were combined into one ternary diagram (figure 3). The same high alternating with low anomaly pattern can be observed on this map. One can also notice those areas where all three maps exhibit magnetic highs (black) or two maps exhibit highs (blue, bright green or red) seem to stand up off the map. On the other hand, areas of very low anomalies are subdued and seem depressed. Therefore, areas of magnetic highs are interpreted to be antiforms (hills in topographic expression) and areas of magnetic lows are interpreted as synforms (basins in topographic expression). These folded features can be better observed in the southern area of the map where they are prevalent as seen in figure 4. It can also be perceived at this scale that the smaller features mimic the larger ones; a very common characteristic of folding.

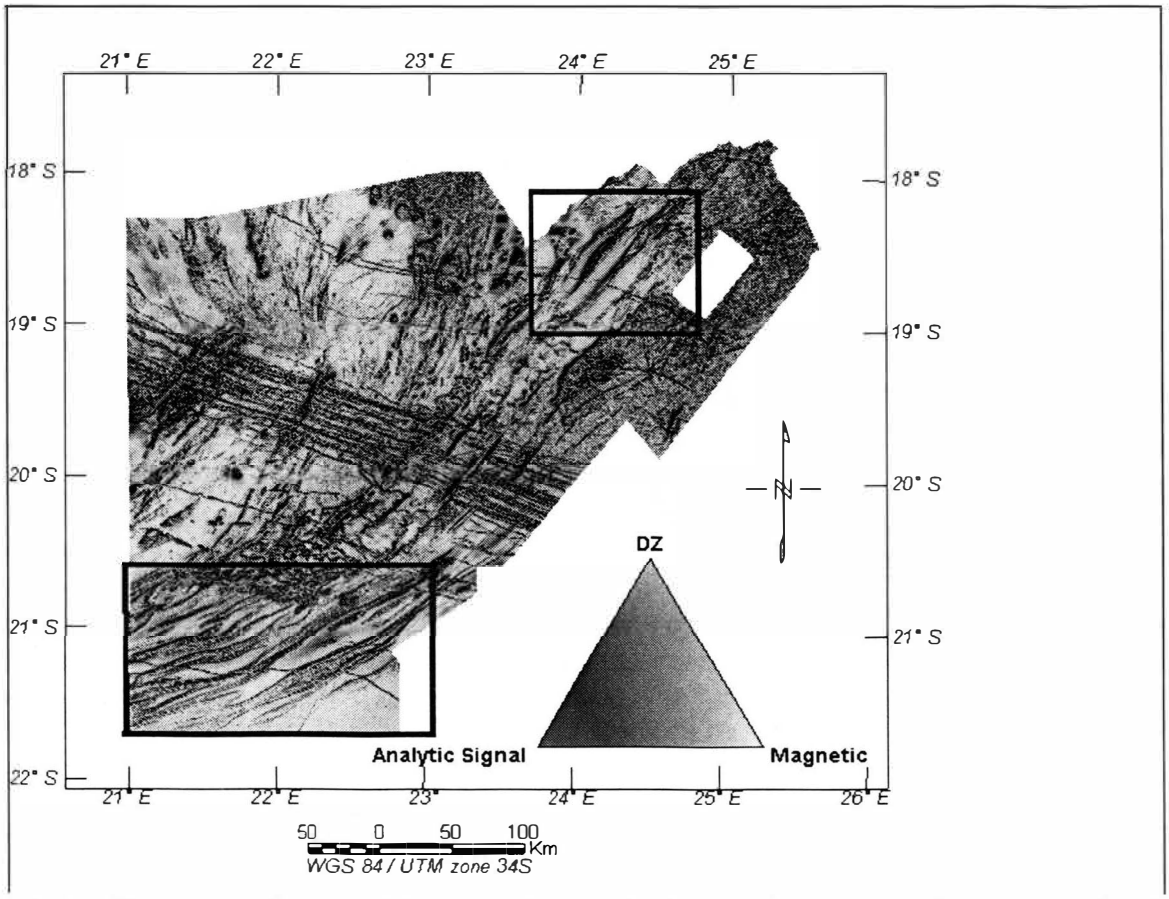

Figure 3: Ternary map of northwest Botswana. Inserts indicate areas of research. Southern insert depicts the area of figures 4 and 7.

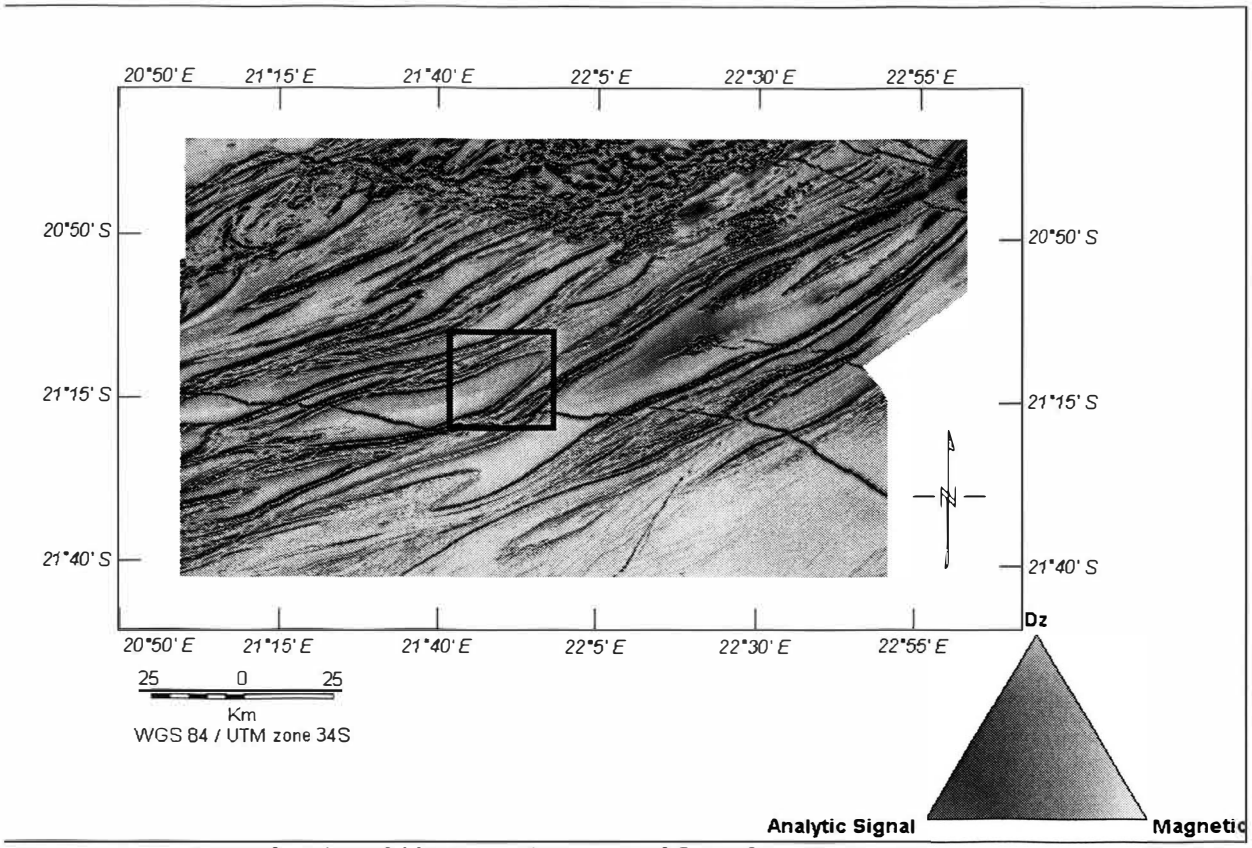

Figure 4: Ternary map of southern folds. Insert shows area of figure 5.

Figure 5A shows one area that was windowed out for Euler deconvolution. The structural index was chosen to detect cylinders, the closest approximation to a fold possessed by the program. Rocks can be folded or rolled up much like we do to magazines. One can observe that the Euler deconvolution symbols prefer to follow zones of magnetic highs contained on all three maps (figure 5B). The solution symbols also tend to form linear features. This could indicate one of several things or a combination thereof. First the solution symbols could be plotted along the limbs of the fold where the Kgwebe meta-volcanic rocks or other similar magnetic basement rock is found within the folds. Another possibility is that the solution symbols are being plotted along the peaks of the antiforms. Just as a hill changes elevation slowly at its base and more steeply as it nears its peak, if the peaks of the antiforms are more magnetic then the rate of change would increase as you neared the source until you were on the source where change would be essentially zero. This situation would very closely resemble a horizontal cylinder - which is exactly what the computer is looking for. This situation could also be produced if parts of the folds were more magnetic than others. A stronger magnetic source would produce a faster rate of change as one nears the source. This scenario, or a combination of the two, seems to be more probable given that it is highly unlikely that the bedrock should have

uniform magnetic strength. The delineation of the fold limbs is shown in figure 5C.

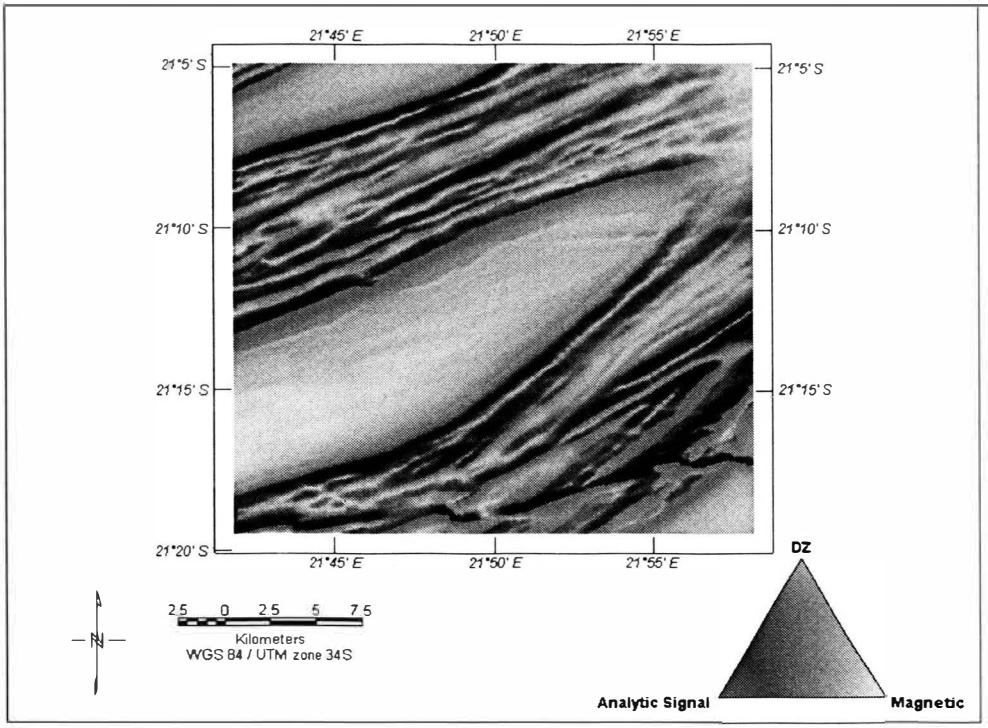

Figure 5A: Ternary map of an area of folding windowed out for Euler deconvolution.

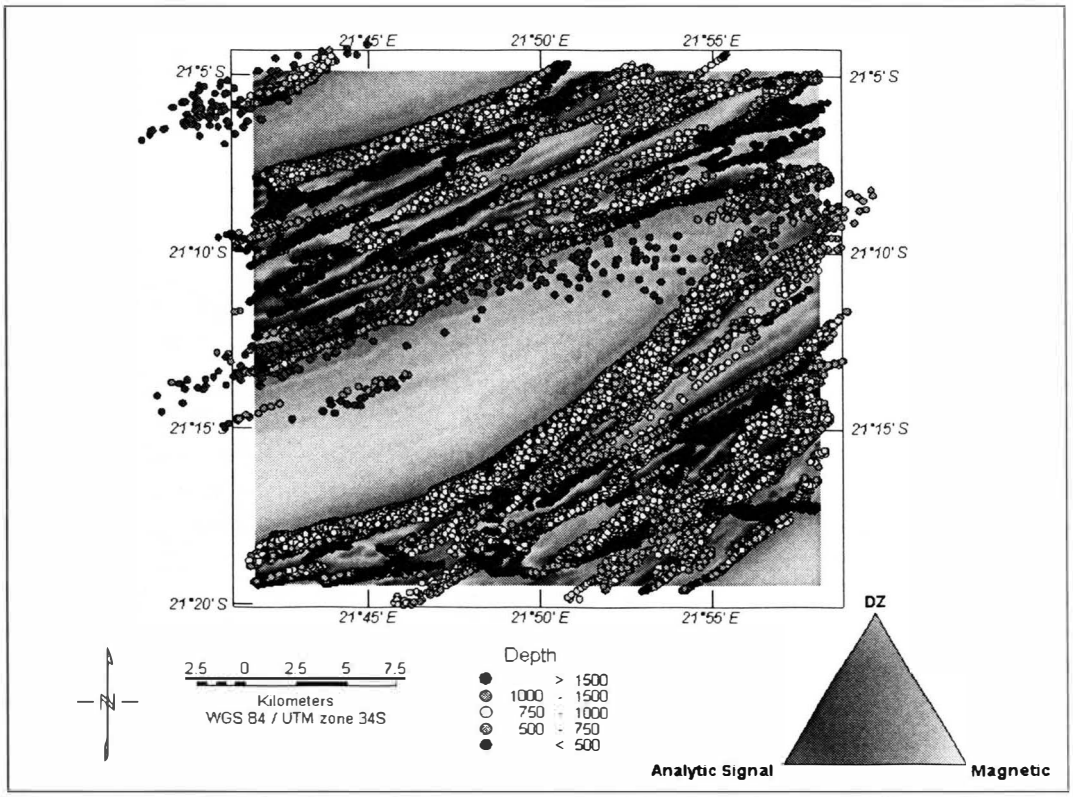

Figure 5B: Ternary map with Euler deconvolution depth to solution symbols plotted. Depths are in meters.

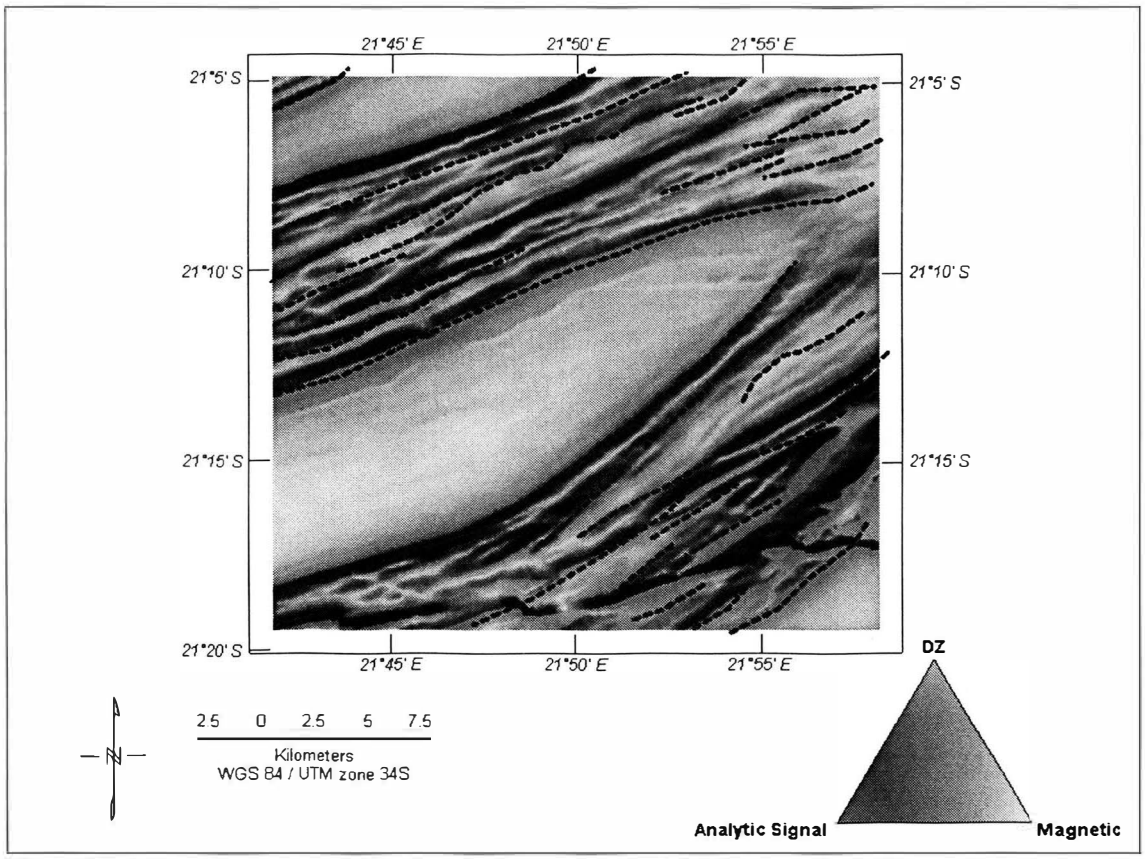

Figure 5C: Ternary map, dashed blue lines indicate interpreted fold limbs.

The Euler deconvolution supplies other important information as well. It can be seen from figure 5B that the deeper solutions follow the large center structure. To either side are more shallow solutions with deeper solutions on the other side again. The Euler deconvolutions symbols that indicate depth to source show the same pattern that the magnetic strength colors did. Not only that, but where magnetic strength was high the solutions were shallow while at low magnetic strengths solutions are deeper. Based on this, the large center feature is interpreted to be a synform. Yet the Euler deconvolution symbols can tell even more of the story. Notice how the very deep solutions are concentrated at the northeast end of the structure. This suggests that the synform plunges toward the northeast. Now, let us compare the limbs of our synform. The northern limb has solutions of 500 meters or less next to solutions of greater than 1500 meters. Meanwhile, the southern limb has solutions of less than 500 meters plotted next to solutions of 750 – 1000 meters. This would point towards the conclusion that our northern limb has a higher angle of dip than does the southern one. Also, now that the limbs of the fold have been outlined, it is possible to estimate the trend of the synform. Since this structure is interpreted as a synform, the adjacent feature should be antiforms. The adjacent features show shallower depths and stronger magnetic anomalies as expected. So, from the interpretation of one fold we may begin to interpret the features adjacent to it and so on throughout the area. With several smaller areas done, we can then backup and view the larger picture and begin to interpret the whole area, just a geologist would work his or her way up from outcrop scale to regional scale (figures 6, 7).

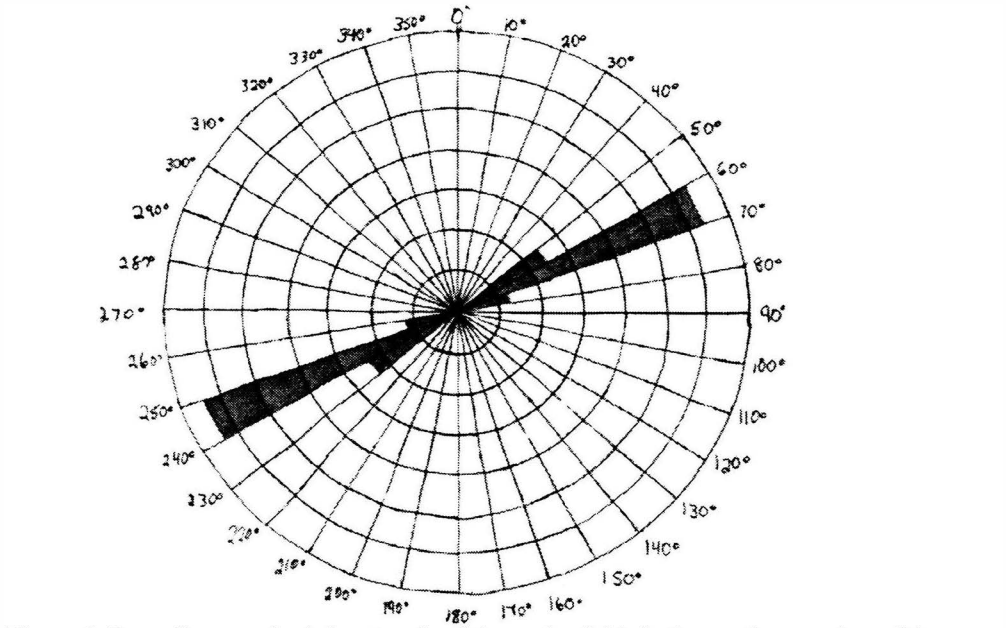

Figure 6: Rose diagram depicting trends of the major folds in the southern region of the map. Each circle is 10% of the total trends.

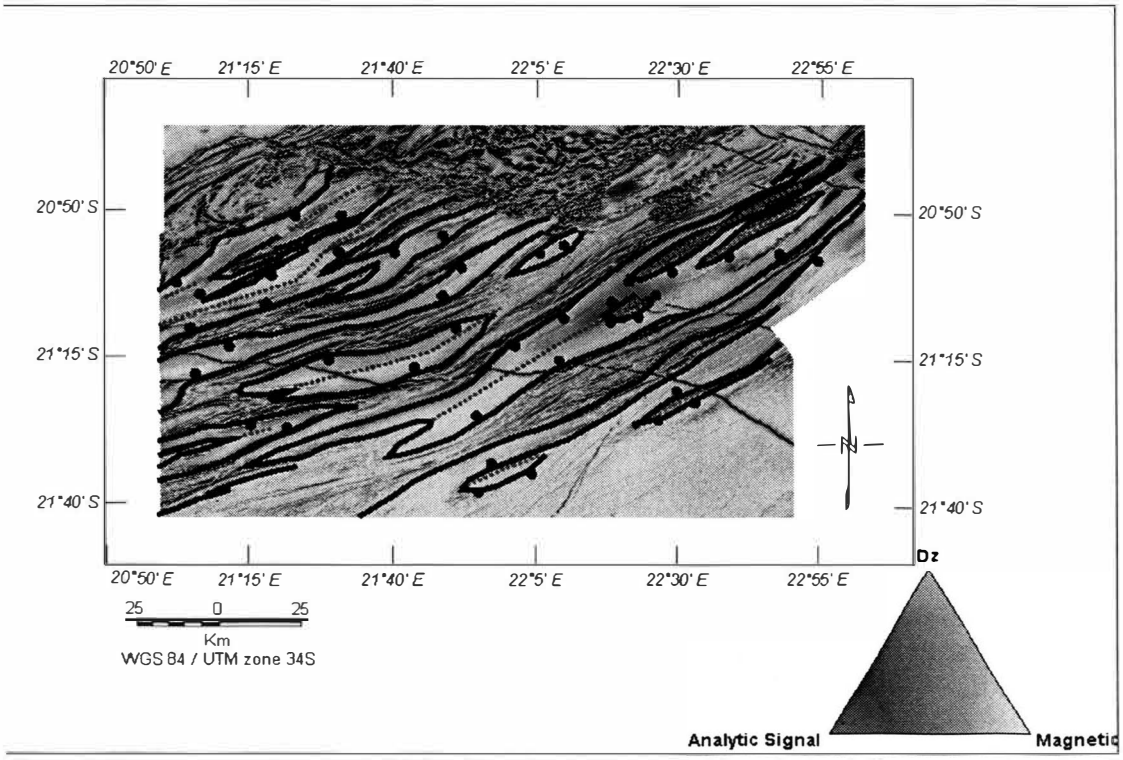

Figure 7: Ternary map of southern folds with major folds outlined in solid black lines, examples of trend in dotted red lines, and solid black circles indicate the direction of dip.

The first clues to the interpretation of northwestern Botswana were simple visual clues made by an eye with field and satellite imagery experience. Continued experimentation with various maps produced similar results. There are several ideas that are pertinent to this interpretation. First, what does stronger versus weaker magnetic anomalies mean? Well, to start, igneous and metamorphic rocks tend to have higher percentages of magnetic minerals giving them a stronger magnetic signal. Stronger magnetic potential also gives a faster rate of change near the source. In this case, the area is known to be made up of volcanic rock with overlying sediment. Volcanic rock also tends to be more resistant, so it lasts longer. This also means that as weathering occurs, the more resistant rock is left while less stable materials are eroded away so volcanic rocks frequently are raised up when compared to their surroundings. This puts them closer to the survey so they give a stronger signal, as seen in this survey. We would then expect that magnetic potential would be weaker from lower areas. It would also follow that these lower areas weren't as resistant and therefore had a different composition. It also makes sense that now these lower areas would be filled in by the overlying sediment which is magnetically weaker. Given that there is an unconformity between the basement rock and overlying sediment an erosional event resulting in just that is a possibility. Also, if these features are folds, then the oldest rocks should be at the core of the antiforms as this interpretation predicts. Folded layers of rock are further supported by the history of the region. The Kgwebe meta-volcanics were created by an extensional collapse brought on by a collisional orogeny. Continued stress after emplacement may have resulted in the deformation of rock and fold structures observed today. Besides just interpretation there is some data as well that backs up the interpretations. Satellite imagery in figure 8 presents features of differing elevation that are surface expressions of antiforms and synforms. Field evidence also demonstrates that the Kgwebe meta-volcanic rocks form hills trending northeast-southwest (Kampunzu 1998). As mentioned earlier, antiforms are frequently expressed as hills in the topography. Also, the trend of the hills matches that of the trends measured from the major folds within the basement rock. Furthermore data collected from the limited outcrops of the region shows that the dominant foliation of the rocks also matches this same trend as seen in figure 9 (Atekwana 2005).

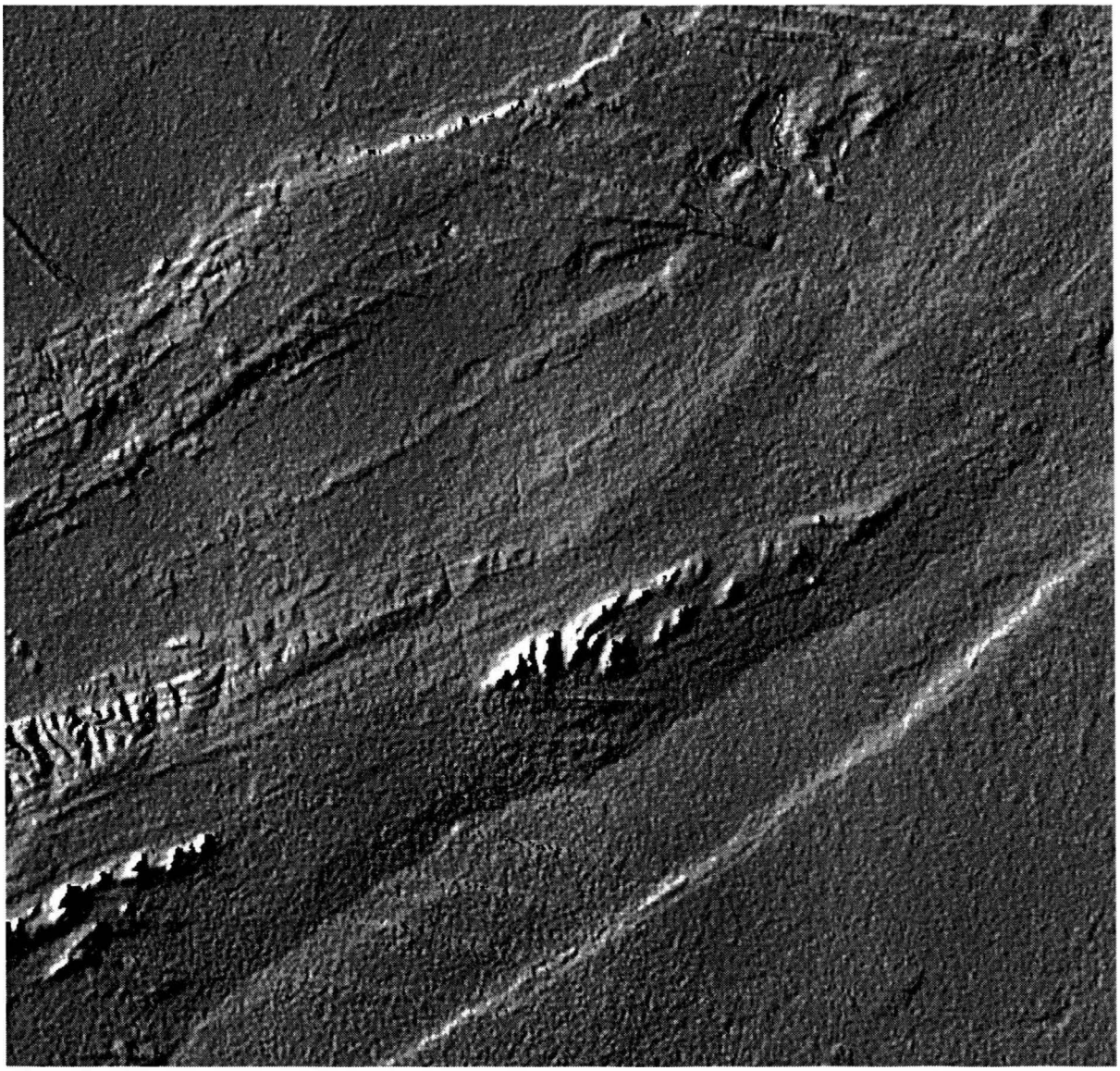

Figure 8: SRTM data from northwest Botswana showing surface expressions of antiforms and synforms.

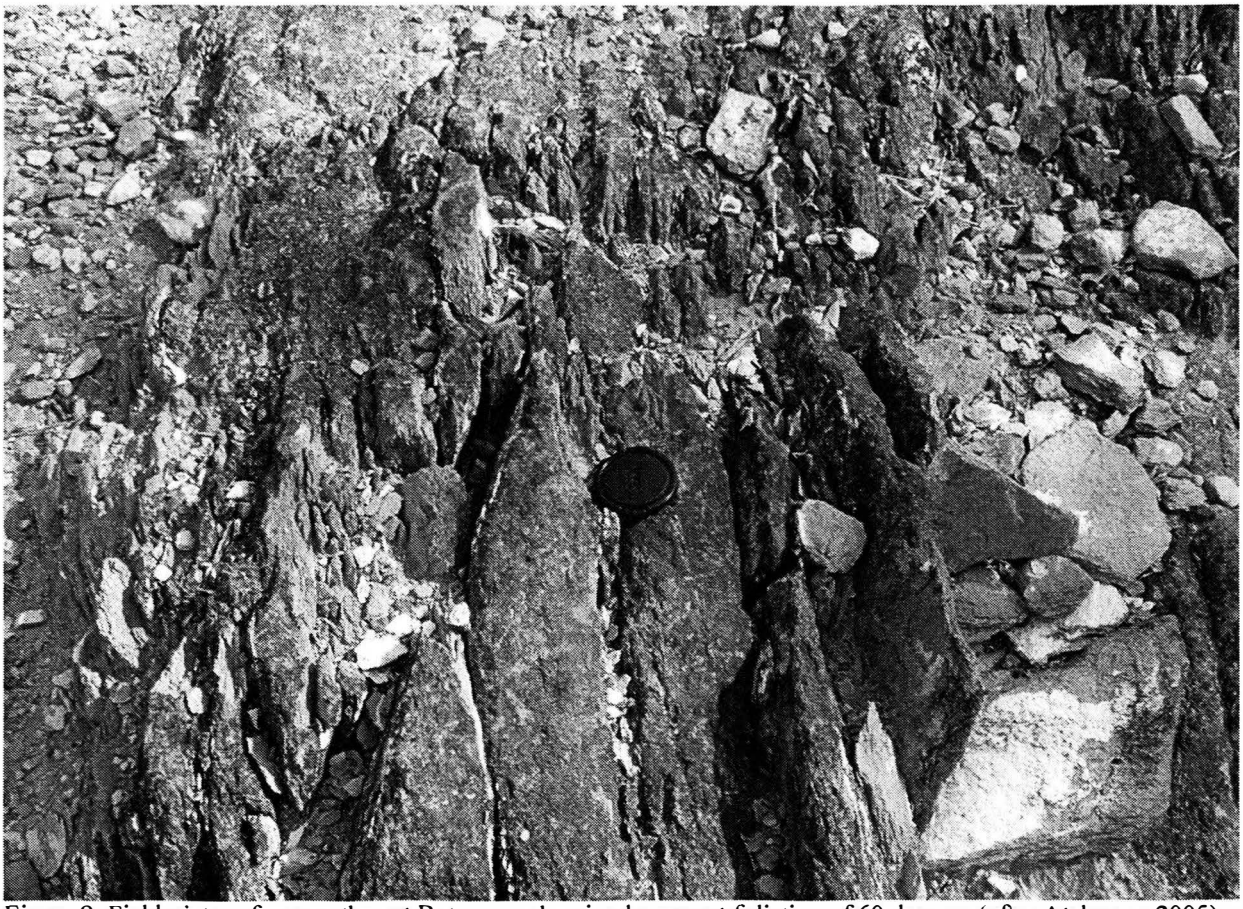

Figure 9: Field picture from northwest Botswana showing basement foliation of 60 degrees (after Atekwana 2005).

Conclusions

High resolution aeromagnetic data collected over northwest Botswana has provided a glimpse into the geology of a barely explored region. From this new information, northeast-southwest folds have been identified within the bedrock. The antiformal and synformal features extend at least 100 – 200 kilometers to the north and south of the Okavango Rift Zone. Relative dips of the fold limbs and indications of the direction of plunge have also been gathered from the geophysical data. This new information is important in several ways. First, it helps to unravel the geologic past of an area that has received little attention. It is also part of a larger project that will help determine if pre-existing basement structures influence modern rifting and other tectonic events. Finally it shows that geophysical data from magnetic studies can help in the structural interpretation of otherwise inaccessible areas.

Acknowledgments

I'd like to thank my advisor, Dr. Estella Atekwana for all her assistance and encouragement in this project. I'd also like to thank Dr. John Hogan for his insights into structural geology and the fresh ideas he brought to our meetings. Thanks to Baraka Kinabo for sharing his knowledge of Geosoft with me, and collaborating to make our projects better. Finally, the Opportunities for Undergraduate Research Experience (OURE) deserve a big thanks for providing the funding to help make this project possible.

References

Atekwana, Estella. Personal communication, March 2005.

Geosoft Help Files. Accessed March 2005.

Kampunzu, A. B., Armstrong, R. A., Modisi, M. P., Mapeo, R. B. M., 2000. Ion microprobe U – Pb ages on detrital zircon grains from the Ghanzi Group: implications for the identification of a Kibaran-age crust in northwest Botswana. Journal of African Earth Sciences, Vol 30 pg 579 – 587.

Kampunzu, A. B., Akanyang, P., Mapeo, R. B. M., Modie, B. N., Wendorff, M., 1998. Geochemistry and tectonic significance of the Mesoproterozoic Kgwebe meta-volcanic rocks in northwest Botswana: implications for the evolution of the Kibaran Namaqua-Natal Belt. Geology Magazine, Vol 135 pg 669 – 683.

Telford, W. M., Geldart, L. P., Sheriff, R. E. 1990. Applied Geophysics Second Edition. pg 67 – 84.

Thermal Insulation in Building Design:

A Comparison of Insulation Materials

By:

Patrick Williams

Department of Architectural Engineering
University of Missouri, Rolla
Rolla, MO 65409

Abstract:

In any type of construction, thermal inefficiency is a costly problem. Currently, we base our decisions on which insulation material to use based on R-values given by the manufacturers. Testing will allow a direct comparison of the actual insulating performance efficiency of materials and will prove or disprove the R-value as a reliable means of comparing their insulating properties. This project will test various construction and insulation materials to develop R-values in true building applications. The key areas investigated will utilize a test box built with varying insulation materials and a direct source of heat. Through this testing, the most energy efficient insulation material in a practical application will be discovered.

Introduction:

Energy is needed to enjoy the basic comforts we now take for granted. Therefore, energy conservation is paramount to maintaining our current quality of life. A vast majority of energy used in any building goes towards controlling the temperature and humidity of the air within. This is made possible by insulating the air within from the uncontrollable conditions outside. Insulation has the ability to slow down the rate of heat transfer from conditioned space to unconditioned space. Without insulation, it would be impossible to effectively heat or cool a home.

Most insulation is defined by its whole-wall R-value. This is a unit-less measure of the capacity of a material to impede heat flow. But does the R-value truly relate to actual insulation performance?

This investigation seeks to analyze the performance of several insulating materials and compare their results to their whole-wall R-values. Each material will undergo prolonged exposure to heat in a contained space. A test box will be constructed to house each insulation sample and control the exposure to heat. One side of the test box will be painted black and a 750 watt halogen bulb will apply heat. The investigation will seek to relate the rate of temperature change. A thermometer will be used to measure the temperature of the outside air and of the air inside the test box. The rates of temperature change for each insulation sample will be determined and compared.

The samples to be compared include formed plastic, Styrofoam, polystyrene foam, and structurally insulated panels (SIPs). Each sample will be cut to equal width and length, but the depth will vary according to the material. Logistic restraints prevent cutting the samples down to equal depths. Each sample has a unique predetermined R-value and this will be factored into the analysis.

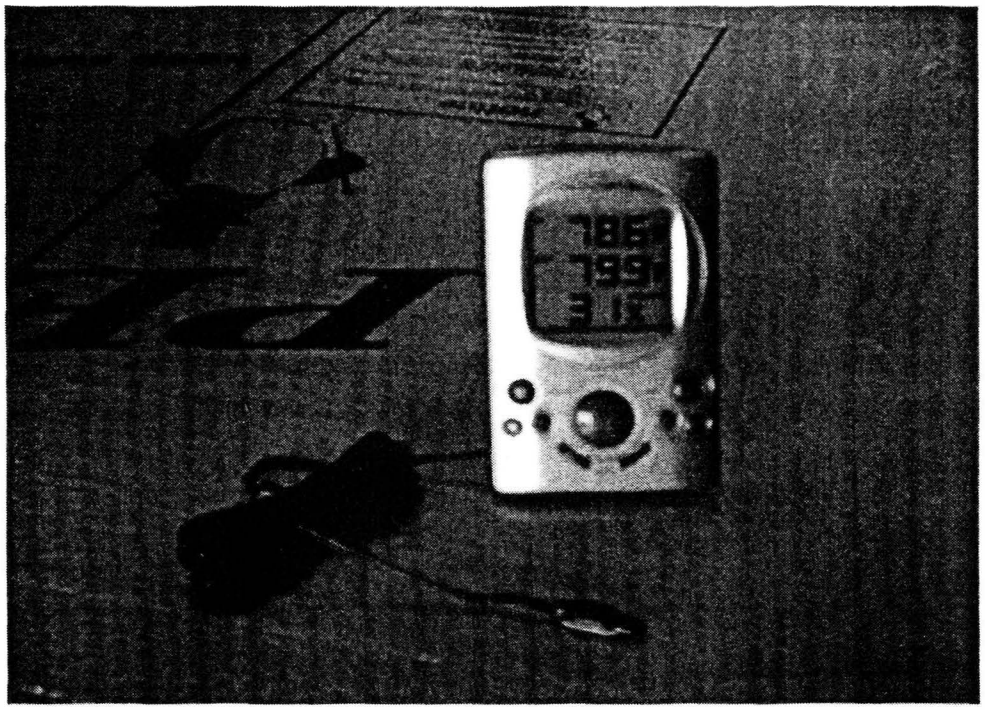

Figure 1: Thermometer with temperature probe

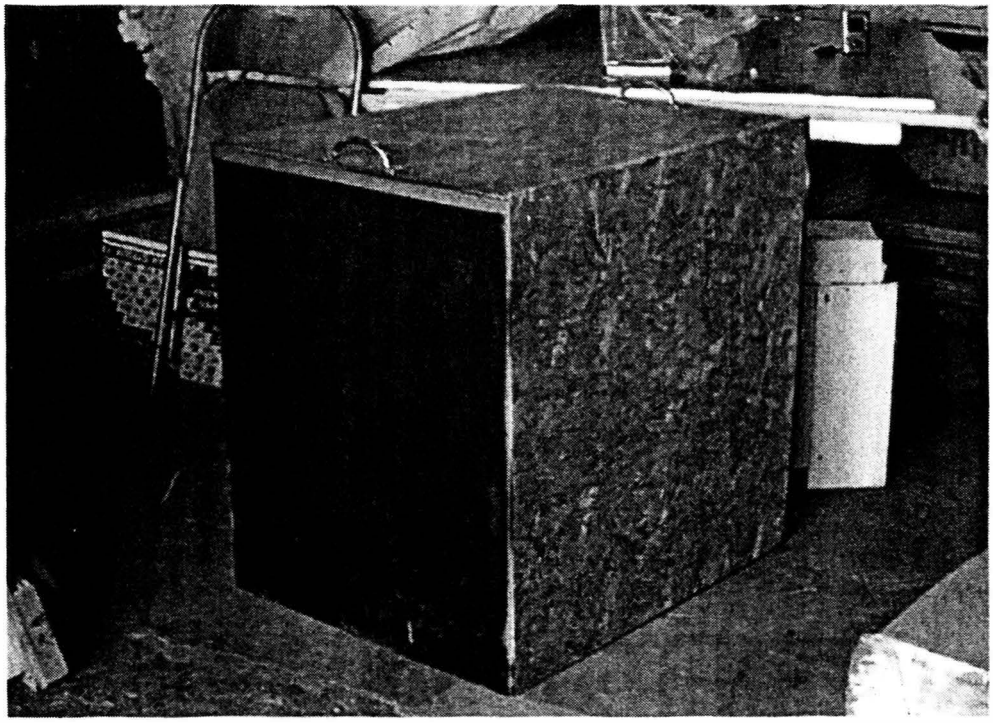

Figure 2: Test box with insulation stacked behind it

Results:

Control Group - Insulating Material: 1/4" Plywood Box

Time (minutes)	Room Temperature (°F)	Relative Humidity (%)	Box Temperature (°F)
0	81.3	31	79.5
1	81.3	31	79.5
2	81.3	31	79.7
3	81.3	31	80.2
4	80.8	30	81.3
5	80.8	30	83.1
6	80.4	30	85.3
7	80.4	30	86.7
8	80.4	30	88.0
9	80.4	30	89.8
10	80.4	30	91.2
11	80.4	30	92.5
12	80.4	30	93.4
13	80.4	30	94.6
14	80.4	30	95.5
15	80.4	30	96.1
16	80.4	30	97.0
17	80.6	29	97.7
18	80.6	29	98.4
19	80.8	28	98.8
20	80.8	28	99.3

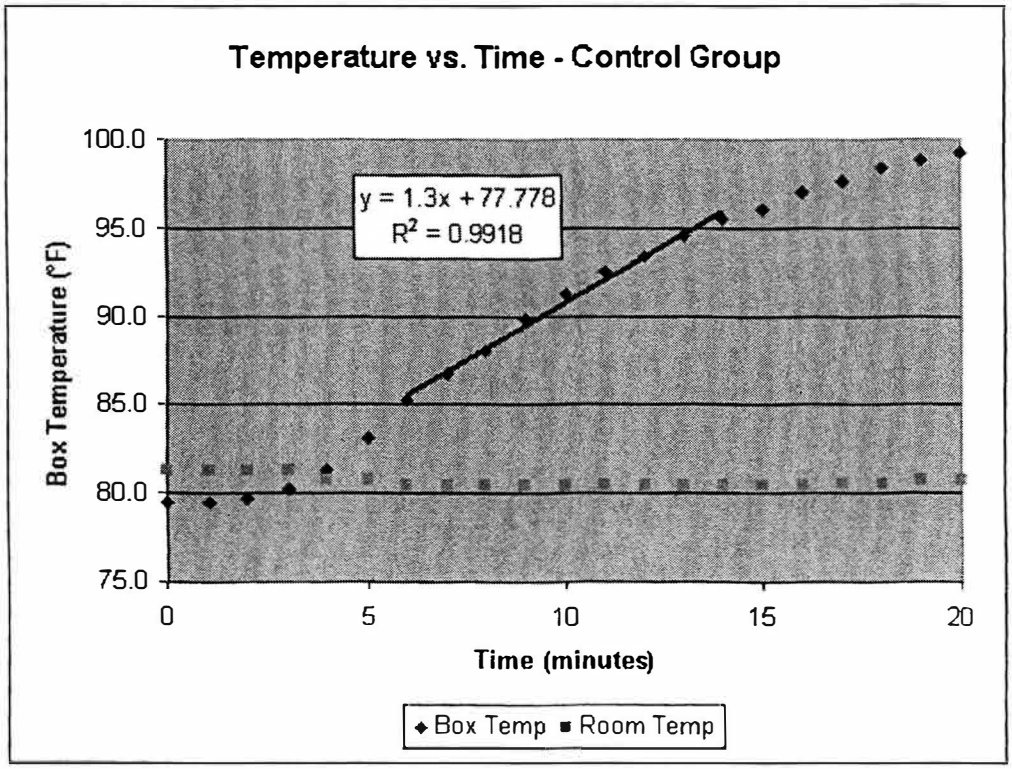

Test #1 - Insulating Material: Insulfoam R-tech Formed Plastic (2")

Time (minutes)	Room Temperature (°F)	Relative Humidity (%)	Box Temperature (°F)
0	81.5	28	79.0
1	81.5	27	79.0
2	81.5	28	79.0
3	81.5	29	79.3
4	81.7	29	79.5
5	81.7	29	79.7
6	82.0	29	80.4
7	82.2	29	81.3
8	82.2	29	82.2
9	82.2	29	83.1
10	82.4	29	84.0
11	82.6	29	85.1
12	82.6	29	85.8
13	82.6	28	86.7
14	82.6	27	87.8
15	82.6	28	88.3
16	82.6	28	89.2
17	82.6	28	89.8
18	82.6	27	90.5
19	82.4	28	91.2
20	82.6	28	91.6

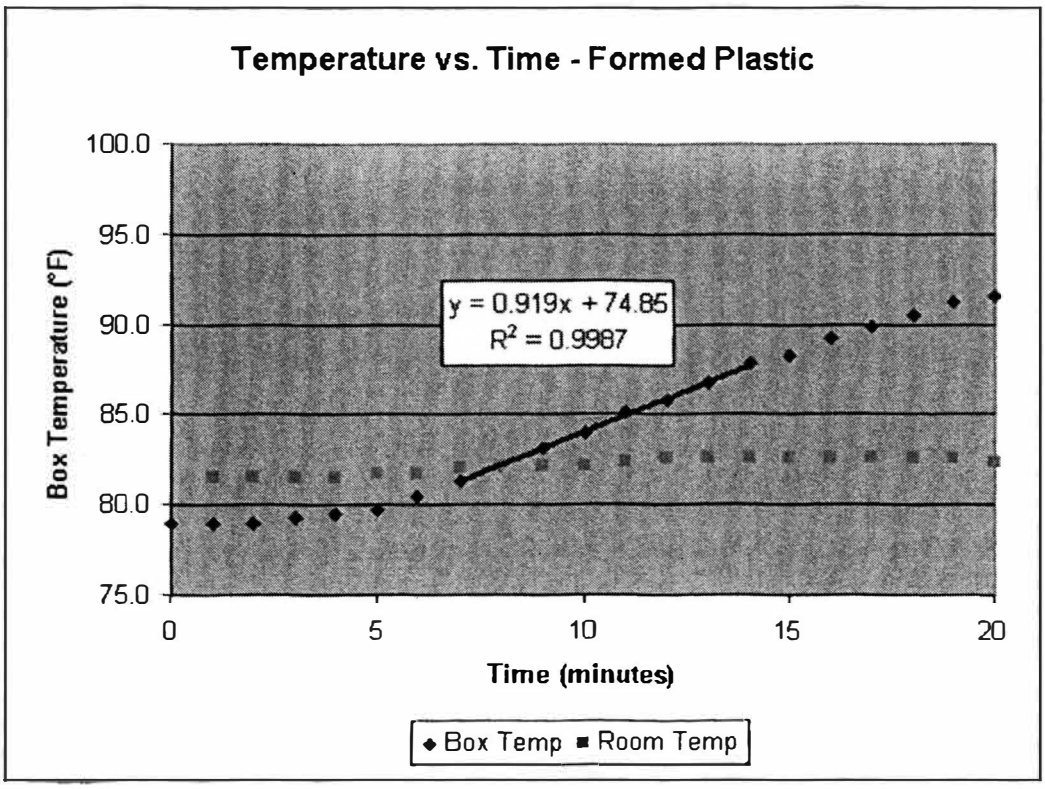

Test #2 - Insulating Material: Dow Styrofoam (1")

Time (minutes)	Room Temperature (°F)	Relative Humidity (%)	Box Temperature (°F)
0	81.3	28	81.3
1	81.5	28	81.3
2	81.7	27	81.5
3	81.7	28	81.7
4	81.7	29	82.2
5	81.7	30	82.9
6	82.0	30	84.0
7	82.6	30	85.6
8	82.9	30	86.0
9	83.1	30	87.4
10	83.3	30	88.7
11	83.5	30	89.6
12	83.5	30	90.7
13	83.5	30	91.9
14	83.5	29	92.8
15	83.3	29	93.4
16	83.1	29	94.3
17	83.1	29	94.8
18	83.1	30	95.2
19	83.1	29	95.9
20	83.1	29	96.4

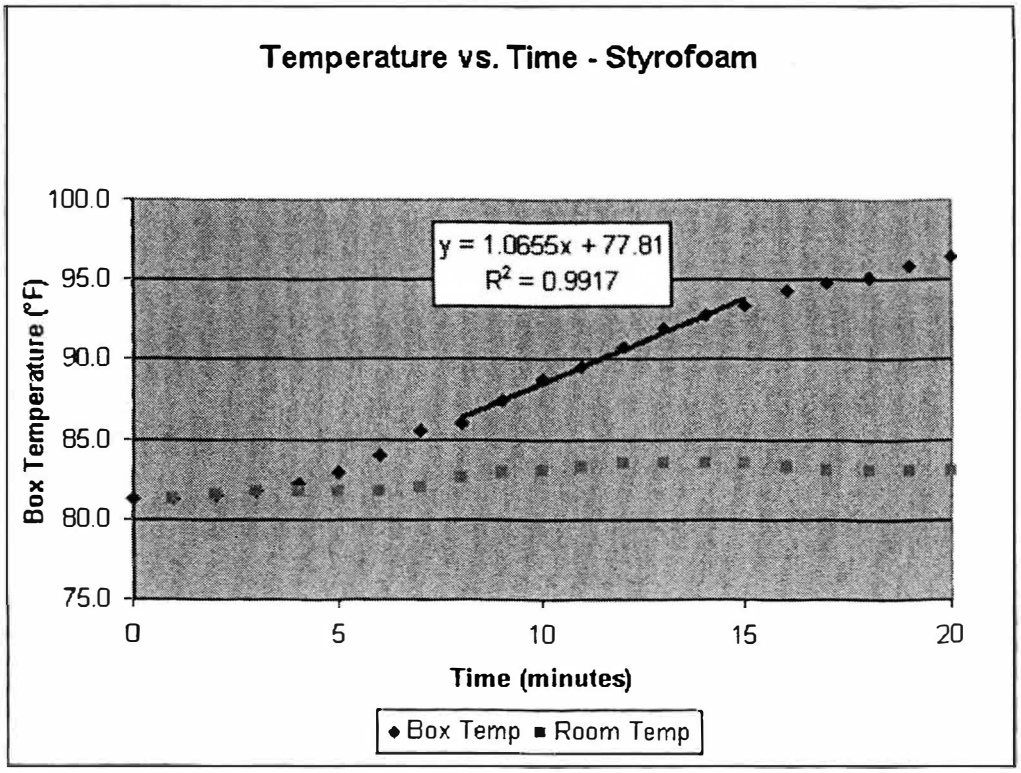

Test #3 - Insulating Material: Perma-R Polystyrene (1")

Time (minutes)	Room Temperature (°F)	Relative Humidity (%)	Box Temperature (°F)
0	80.5	28	79.5
1	80.7	28	79.7
2	80.9	27	80.3
3	80.9	28	80.9
4	80.9	29	81.7
5	80.9	30	82.9
6	81.2	30	84.0
7	81.8	30	85.0
8	82.1	30	85.9
9	82.3	30	87.1
10	82.5	30	88.4
11	82.5	30	89.5
12	82.5	30	90.7
13	82.5	30	91.9
14	82.7	29	93.1
15	82.5	29	94.1
16	82.3	29	95.5
17	82.3	29	96.4
18	82.5	30	97.0
19	82.5	29	97.5
20	82.5	29	97.9

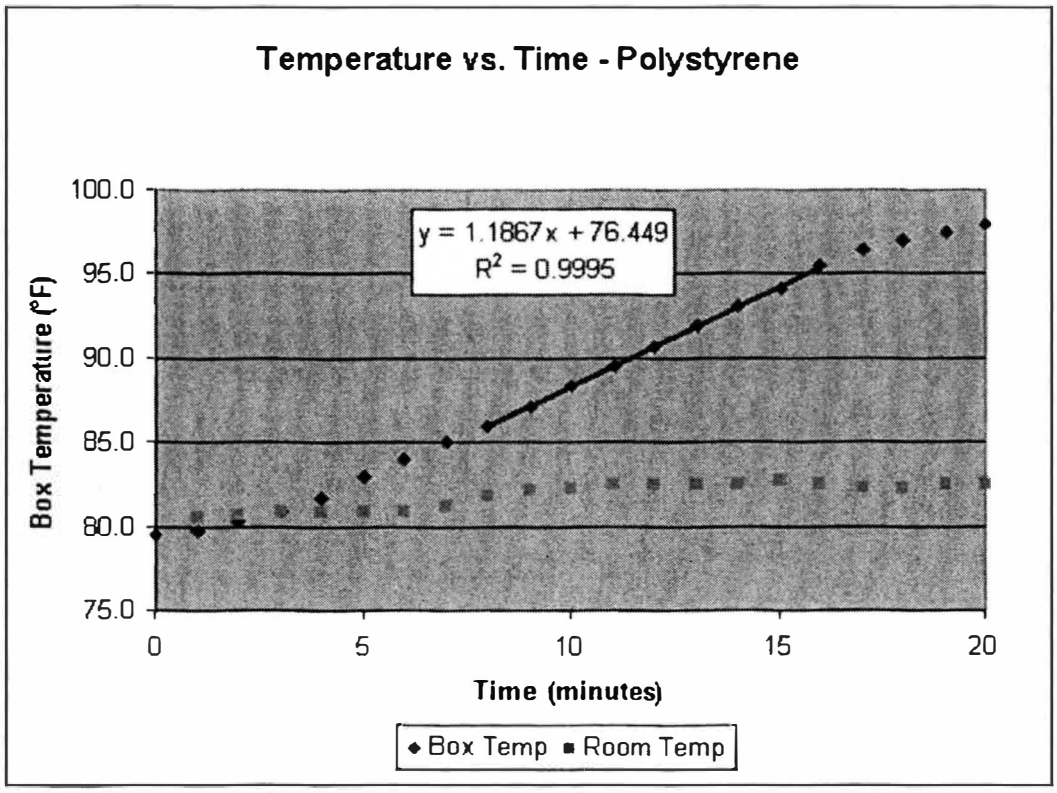

Test #4 - Insulating Material: Structurally Insulated Panel (6.25")

Time (minutes)	Room Temp (°F)	Relative Humidity (%)	Box Temp (°F)
0	80.8	30	79.3
1	81.3	30	78.9
2	81.5	30	78.4
3	81.7	30	77.6
4	82.2	30	77.0
5	82.6	30	76.8
6	82.6	31	76.8
7	82.6	31	76.8
8	82.9	30	76.8
9	83.1	30	76.8
10	83.3	29	76.8
11	83.1	29	76.8
12	83.1	28	76.8
13	83.1	29	76.8
14	83.1	29	76.8
15	83.3	29	76.8
16	83.3	28	76.8
17	83.1	29	76.8
18	83.1	30	76.8
19	83.1	30	76.8
20	83.3	30	76.8

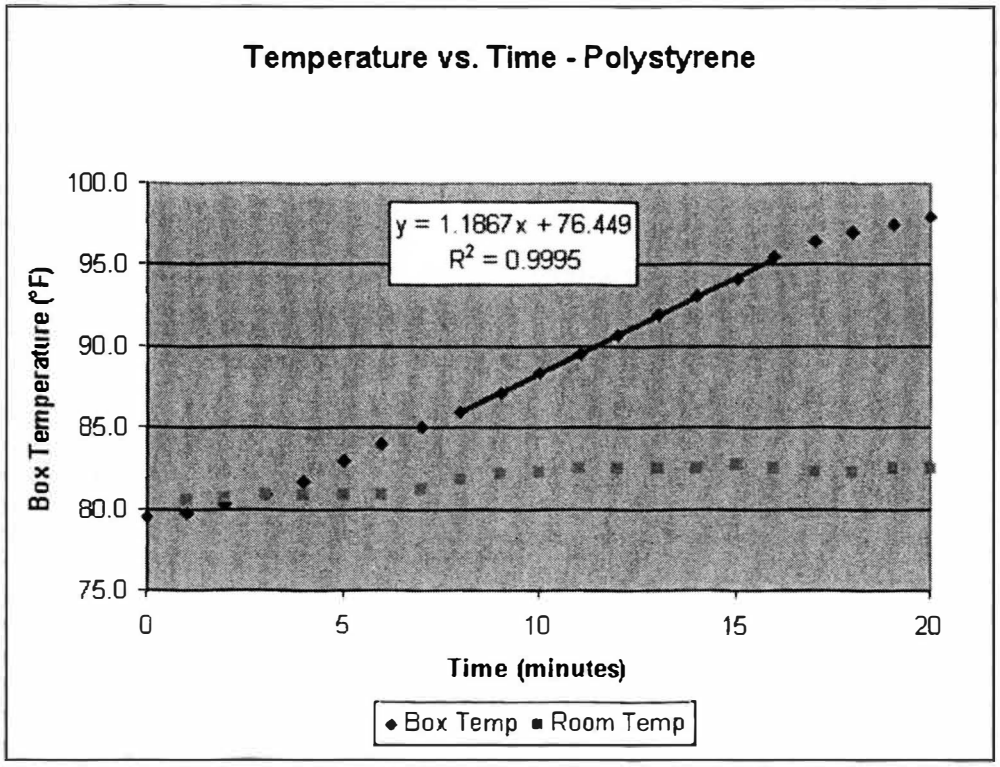

Analysis:

A brief examination of the graphs reveals that the thermal performance of each material varies significantly. To eliminate random error caused by fluctuating external temperatures, we focus solely on the difference in temperature with time.

The control test indicated a dT of 1.3 °F/s. The rest of the tests trended downwards from there, with the slope varying indirectly with the degree of the R-value. The SIP had the highest R-value, 40, and the temperature did not vary at all under the experimental conditions. Next came the Formed Plastic with an R-value of 7.8 and a dT of .919 °F/s. The Styrofoam had an R-value of 5 and a dT of 1.07 °F/s. The Polystyrene had the lowest R-value at just 3.9, and correspondingly had the highest dT at 1.19 °F/s.

The results indicate clearly that, as could be expected, the higher the R-value of a material the longer it takes heat to escape through it. This should be comforting to anyone wondering if high R-value insulation is worth the extra expense. One truly does get what they pay for when they insulate their homes.

Acknowledgement:

Robert B. Stone, Ph.D. – Research Advisor

References:

Oak Ridge National Laboratory (May 26, 2004). *Whole-Wall R-Values Explained.* <http://www.ornl.gov/sci/roofs+walls/whole_wall/rvalue.html> Accessed 11-12-2004

Porter SIPs (March 1,2004). *Introduction to SIPS.* <http://www.portersips.com/PANELS/introduction.htm> Accessed 11-12-2004

Colorado Energy (March 21, 2005). *R-Value Table.* <http://coloradoenergy.org/procorner/stuff/r-values.htm> Accessed 4-15-2005

Jones, Raymond P. Framing, Sheathing and Insulation. Albany: Delmar Publishers, 1964

Determination of Cadmium Nitrate Mass

Through Neutron Activation Analysis

Charles Williams
Department of Physics
University of Missouri-Rolla
Dr. M. Bertino, Advisor
April 1, 2005

Opportunity for Undergraduate Research Experience
Office of Undergraduate and Graduate Studies

Abstract

Neutron Activation Analysis is a method of determining the composition of a sample wherein the sample is irradiated, then measured through gamma ray spectroscopy. This method can also be used to determine the mass of a particular substance within an unknown sample by comparing the gamma ray spectroscopy results to that of known results and applying a predetermined linear relationship between known sample mass (or molarity) and the primary peak area form the gamma ray spectroscopy results. This relationship is what our project set out to determine for differing concentrations in a standard volume of Cadmium Nitrate solution ($CdNO_3$). We found a linear relationship to within an acceptable standard deviation, based on Molarities ranging from .001 to 1 Molar.

Introduction

Neutron Activation Analysis (NAA) is a method of sample analysis by which the composition of samples and relative concentrations of different isotopes within the samples can be determined. It relies on the principle that certain elements become radioactive when exposed to a source of neutrons. These elements then emit gamma rays at specific energies according to the particular isotope emitting. The gamma rays emitted are then analyzed through a process called gamma ray spectroscopy. Each isotope that is able to emit Gamma radiation will have a signature spectrum containing peaks, or elevated readings of gamma rays at specific energies. By comparing these peaks to data from known sources of radiation, one can reasonably deduce the composition of a particular sample. Also, by analyzing the area of a peak and subtracting out the background, a relation can be made between the corrected peak area and the mass of a particular element within a sample. This procedure can be very useful when analyzing unknown samples, but it is not a very simple procedure to set up. Establishing the relation between peak area and sample mass depends greatly on particular equipment, neutron flux, composition of the sample, and a standardized process.

The original aim of the project was to use NAA to determine the amount of Cadmium (Cd) picked up by gel samples washed in a Cadmium Nitrate solution, using a standardized process devised by Bren Phillips. It became quickly apparent that, to verify the results, a standard mass to peak area relation would be needed for Cadmium. Using set volumes and differing concentrations of Cadmium Nitrate ($CdNO_3$), Bren and I set out to build such a relation.

Discussion

Neutron Activation Analysis (NAA)

NAA was discovered in 1936 by Hervesy and Levi as a method to determine the presence of rare earth elements in rock samples[1]. The method uses a neutron source, usually a reactor, to excite an atom to a particular isotope. That isotope then emits gamma rays at specific energies, which are detected by the process of gamma ray spectroscopy.

Procedure

The procedure for the analyzation of a sample is as follows:

Sample Preparation

(1) A solution is made at a certain molarity of $CdNO_3$. We started the molarity of the samples in factors of ten (.01M, .1M, 1M) then began to fill in the gaps. A 1mL sample is placed in a 2mL plastic vial.

(2) Then place the small vial in one of the small zip-lock bags.

(3) Open the old rabbit vials used for the last round of irradiations and extract the centering jigs. The vials and all of the contents are hot so do your work handling the vials and the jigs on the hot bench.

(4) Place the centering jigs into new rabbit vials. Be careful to not contaminate the outside of the new rabbit vial while placing the centering jig in the vial.

(5) Place the small vial in the centering jig inside the rabbit vial and make sure it is firmly seated.

(6) Adjust the extra plastic from the small bag the 2 ml vial is in to act as packing when the lid is placed on the rabbit vial

(7) Close the rabbit vial lid and heat seal.

(8) Repeat steps (1) through (7) for all 6 vials

(9) Clean the outside of the rabbit vials with alcohol

(10) Label the vials with CdNO3 and numbers starting with the next number after the last vial that was irradiated.

(11) Check the calibration on the Ge detector and recalibrate if necessary.

(12) Irradiate the vial for 30 seconds at 2 KW, but be sure the power history of the reactor is not such that it will affect the instrumentation.

(13) When you hear the Nitrogen discharge to shoot the sample back up start a stopwatch.

(14) Remove the sample from the glovebox and take the 1-foot dose reading and report to the operator as required.

(15) Place the rabbit vial in the over pack with the centering sleeve inside.

(16) Place the over pack on the Ge detector by using the aluminum-centering jig and close the lid.

(17) Start a 10-minute live time count 2 minutes after the sample returned from the core.

(18) Save the spectrum and repeat steps (12) through (17) for all 6 samples

(19) Analyze the two peaks in the spectrum by calculating the net peak area using Equation 12.17 in Dr. Tsoulfanidis' *Measurement and Detection of Radiation* book[2]. This is also programmed in an Excel data sheet. This equation just takes a straight line from the background on each side of the peak and subtracts those counts. This step will be discussed in the next section.

(20) Make adjustments to the procedure to improve accuracy, such as decreasing the mass irradiated to increase power and irradiation time to prevent gamma flux from influencing instrumentation.

(21) Use the data collected to irradiate samples with unknown amounts of Cadmium in them and determine the amount.

Gamma Spectrum Analyzation

The method alluded to in Step 19 will be elaborated upon in this section. On the Gamma Ray Spectrum for Cadmium Nitrate, a peak will appear at 245 Kiloelectron-volts. This is the primary energy at which Cadmium emits gamma rays. There are other secondary energies that can be analyzed, but the peaks for these will be smaller, and therefore not as conducive to accurate results. For this study, only the peak at 245 keV will be analyzed.

To analyze the peak, the data must be separated into channels. Enough channels must be used on either side of the peak to include the background so that it may be subtracted from the original peak area. To determine the number of channels needed, the width of the peak at half of its maximum was determined. This number was defined to be э, and the uncorrected peak area was defined to be the summation of all the peaks within 3 times this number (3э), centered at the peak. An additional 1.5э on either side of this area determines the background. The average is taken over all of the background peaks, and that number times 3э is subtracted from the uncorrected peak area to yield the corrected peak area. (*figure 1*)[2]

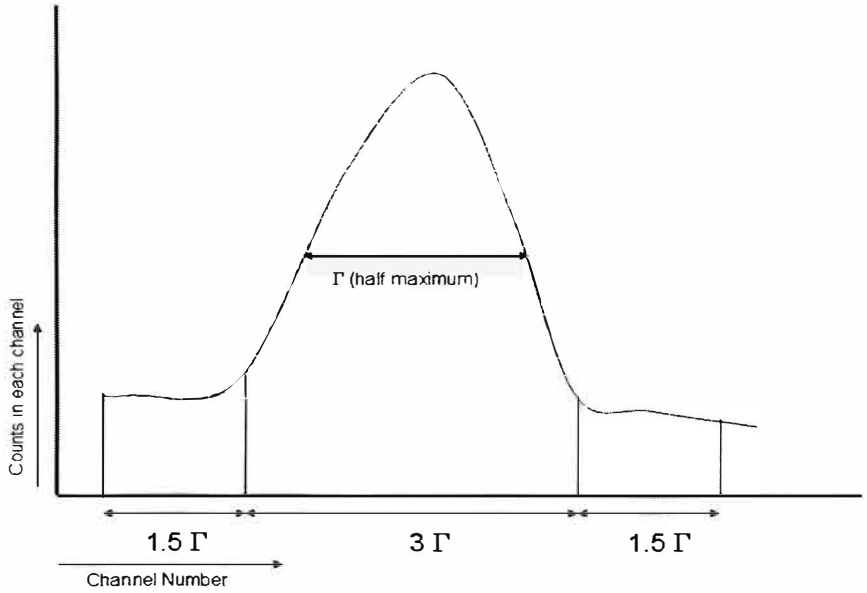

***figure 1*. Gamma Spectrum Analyzation**

Results

Several Samples were analyzed for each Molarity, and the average peak value was calculated for each. The standard deviations stayed below 4% for the most part. By graphing the average corrected peak areas for each molarity versus the molarity value, a linear relationship was discovered (*figure 2).* The data for the graph is shown in *table 1.*

Molarity of CdNO3	Average Corrected Peak Area (245 keV)
0.001	643.5
0.01	736.8
0.1	7117.4
0.25	18563.6
0.5	32336.9
1	54106.67

Table 1. Avg. Peak areas for Molarities of $CdNO_3$

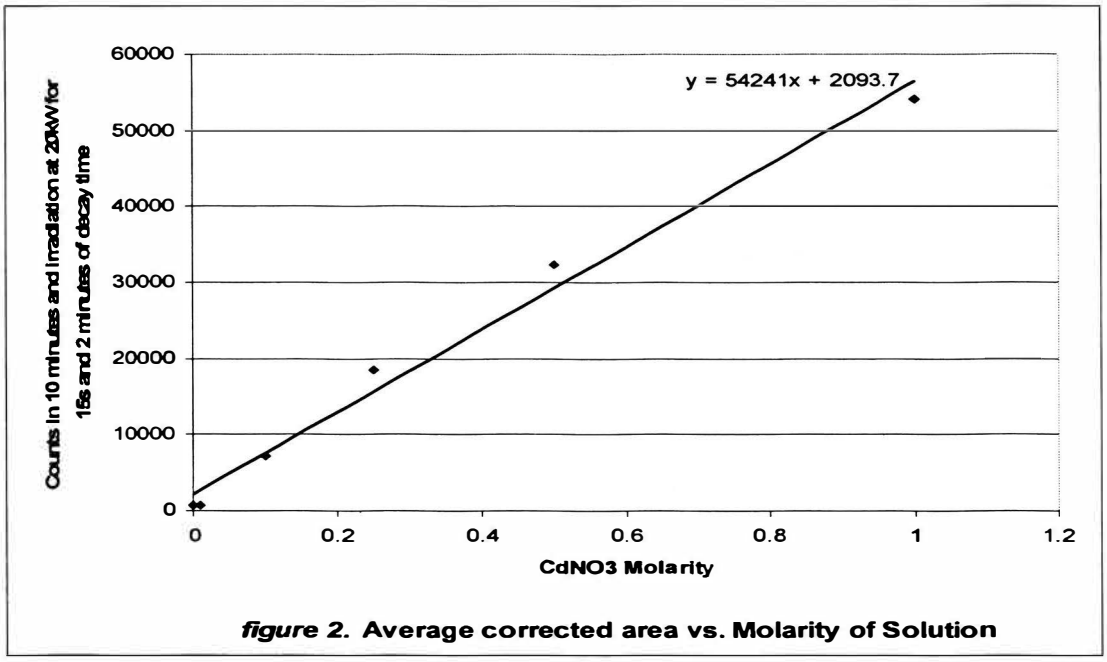

figure 2. **Average corrected area vs. Molarity of Solution**

The linear relationship inferred from our results is represented by the trendline on the graphed results in *figure 2*. The formula for this line is (approximately):

$$y = 54200x + 2100 \qquad \{1\}$$

More experimentation would be needed to reduce the uncertainty of this relationship for practical use, but the results are encouraging.

Conclusion

In conclusion we have shown a linear relationship between the molarity of Cadmium Nitrate and the peak areas of the Gamma Spectrum produced after an exposure time of 15 seconds, standardized, and a decay time of 2 minutes. This relationship will be useful when analyzing samples containing an unknown mass of Cadmium Nitrate. Unfortunately, preliminary experimentation has shown that additional substances irradiated with the $CdNO_3$, such as a silica aerogels severely alters the gamma spectrum results. Future experimentation will be needed to address this concern.

Acknowledgements

I would first like to thank my advisor, Dr. Massimo Bertino, for giving me the opportunity to gain valuable research experience under a watchful eye. I would also like to thank Bren Phillips, my lab partner, reactor operator, and technical expert for most of the project. Others I would like to acknowledge include Bill Bonzer and the staff at the UMR Research Reactor, and Harvest Collier.

References

[1] Michael Glascock, An Overview of Neutron Activation Analysis, http://www.missouri.edu/~glascock/naa_over.htm

[2] Nicholas Tsoulfanidis, Measurement and Detection of Radiation, Second Edition, 1995, Taylor and Francis

Relative Permeability of the Bluejacket Formation

OURE Research Project

University of Missouri-Rolla

Tanner Womack

April 28, 2005

ABSTRACT

Estimations of oil recovery from secondary or tertiary recovery processes require information about the flow characteristics of oil and other fluids present in the reservoir. When multiple fluids are present in the reservoir, they affect the flow of each other through the system. Relative permeability is a measurement of the flowing ability of a fluid in the presence of another fluid in a porous system.

Relative permeability curves have been generated for the Bluejacket sandstone reservoir located in Vernon County, Missouri. The relative permeability curves are based on core samples taken from the area.

I. INTRODUCTION

Heavy oil deposits found in Western Missouri are estimated to contain 1.5 to 1.9 billion barrels of oil in place. Eighty-eight percent of the oil is contained in the Warner and Bluejacket reservoir horizons[1]. Thick and concentrated oil deposits can be found at the southern end of the Forest City Basin in Vernon County[2]. Oil from the reservoirs flows into wells naturally, but flow rates are low due to the properties of the oil (18 °API, 1000 cp) and low reservoir pressures[3].

Thermal recovery attempts have been made in the area in the past with results ranging from poor to marginally successful from an economic standpoint[1]. The Petroleum Department at the University of Missouri-Rolla is experimenting with the use of microbial oil recovery as a viable economic means of recovering oil from the deposits. Microorganisms have demonstrated the ability to increase the mobility of crude oil in a reservoir[4]. The shallow depth of the reservoir allows horizontal fractures to be made in the formation due to the low confining stress. Horizontal fractures can be used to inject microorganisms into the formation in a well-distributed manner.

Relative permeability data is needed to model the oil flow in the reservoir with the water that has been injected into the formation due to the frac job and the microbial injection. Relative permeability would also be needed for waterflooding or other desired enhanced oil recovery methods.

In this study, relative permeability graphs for the two-phase flow of oil and water were generated using the Mohamad Ibrahim and Koederitz correlations. Porosity and wettability experiments were also performed to determine parameters needed for the correlations.

II. APPROACH

The relative permeability graphs were obtained using a program called *Relative Permeability Suite*, which was programmed by Dr. Leonard Koederitz. The program uses the Mohamad Ibrahim, and Koederitz relative permeability correlation to generate the values of relative permeability versus water saturation. The correlation is empirically based, because theoretical considerations to directly determine relative permeability are not as successful as empirical techniques[5]. The parameters needed for the correlation are porosity, absolute permeability, connate water saturation, residual oil saturation, formation type, and wettability. The porosity, absolute permeability, and wettability were experimentally calculated, while the other parameters were found in literature.

A. Average Effective Porosity

The average effective porosity was calculated directly from recent core samples taken from the Bluejacket reservoir. There were 16 core samples representing the reservoir across its 16 feet of net pay. The effective porosity represents the interconnected pore space in a system. The effective porosity was calculated by using a Helium Porosimeter to measure the grain volume and Vernier Calipers to measure the bulk volume (BV).

The Helium Porosimeter works by using helium to measure the volume of a cylinder. Helium easily penetrates the small rock capillaries, because of its small molecular size and mass[6]. Two readings are taken: The first one measures the volume of the empty cylinder, and the second measures the volume of the cylinder less the grain and unconnected pore volume. The interconnected pore space volume can be calculated from equation 2.1.

$$V_{grain} = V_{empty} - V_{sample} \quad \text{.....(2.1)}$$

The bulk volume is the total volume of a system. Vernier Calipers were used to measure the length, width, and height of the core samples. Multiple readings for each side were taken, and then they were averaged. The length, width, and height of the samples were multiplied to obtain the bulk volumes of the samples.

The effective porosity, which is the ratio of interconnected pore volume to total volume, can be calculated from equation 2.2.

$$\phi_e = \frac{BV - V_{grain}}{BV} \quad \text{.....(2.2)}$$

B. Absolute Permeability

Absolute permeability is a measure of the ability of a single fluid to flow through a porous medium[6]. This measurement is combined with relative permeability measurements to simulate a real world model of flow through porous media. Rajeev Gupta, a Master of Science candidate in the Petroleum Engineering Department, calculated the absolute permeability from the 16 core samples.

C. Wettability

Wettability is the tendency of a fluid to adhere to a solid surface in the presence of other immiscible fluids[7]. The molecules of the fluid are attracted to the electrical pull from molecules residing on the surface of the solids. In a reservoir, the rock formation has a natural in-situ wettability that results from the formation composition, minerals, and precipitates. This natural wettability can change when core samples are removed from the reservoir and exposed to the environment. The change occurs, because the composition of the surface molecules can become altered, resulting in different wettability characteristics.

The unconsolidated sands method is considered one of the best methods for determining wettability. It is a simple process that yields simple results. First, a thin layer of unconsolidated sand, which is saturated in the original crude oil, is spread on a microscopic slide. Next, droplets of water are placed on the sand grains. The interaction between the oil, water, and grains is observed, which leads to wettability classification[8].

D. Relative Permeability

Relative permeability represents the reduction in flowing ability of a fluid when multiple immiscible fluids are present. This representation is a dimensionless quantity that is used in conjunction with absolute permeability to obtain the effective permeability of a flowing fluid. The effective permeability is defined as the ability of a fluid to flow through a porous media when multiple immiscible fluids are present[4].

The relative permeability or flowing reduction is affected by the saturations of the fluids in place. Therefore, graphs are generally used to convey the relative permeability of each fluid at different fluid situations. Since the Bluejacket reservoir is two-phase (oil and water), the relative permeabilities of oil and water are plotted against water saturation.

The Mohamad Ibrahim, and Koederitz empirical correlations for estimating two-phase relative permeability in sandstone were obtained as a function of wettability[5].

Water-wet Wettability:

$$k^{\bullet}_{row} = 1 - 3.090996\, S^{\bullet}_{w} + 2.8670229 \left(S^{\bullet}_{w}\right)^{1.6} - 0.768952 \left(S^{\bullet}_{w}\right)^{2} \quad \text{.....(2.3)}$$

$$
\begin{aligned}
k^{*}_{row} = {} & 0.22120304\left(S^{*}_{w}\right)^{1.6} + 0.24933592\, S^{2}_{or}\frac{\left(S^{*}_{w}\right)^{3}}{\phi} \\
& + 21.370925\left(S^{*}_{w}\right)^{2}\left(S_{orw}\right)^{5} + 83.491972\,\phi^{4}\left(S^{*}_{w}\right)^{5}\left(S_{orw}\right)^{1.5} \\
& - 0.4562939\left(S_{wc}\right)^{3}\left(S^{*}_{w}\right)^{4} + 1161.07198\left(\phi^{2} S_{wc} S_{orw} S^{*}_{w}\right)^{2} \\
& - 8.7866012\left(S_{orw}\right)^{3}\left(S^{*}_{w}\right)^{2.3} \\
& + 0.00000578\left(S^{*}_{w}\right)^{3}\left(S_{wc}\ln k_{a}\right)^{10}\left(1 - S_{orw}\right)^{0.4} \\
& - 12.841061\left(S^{*}_{w}\right)^{2}\left(\left(\ln k_{a}\right) S_{wc}\right)^{3}\phi^{6}
\end{aligned}
\qquad \text{.....(2.4)}
$$

Intermediate Wettability:

$$
\begin{aligned}
k^{*}_{row} = {} & 1 - 2.985766\, S^{*}_{w} + 3.1548084\left(S^{*}_{w}\right)^{2} \\
& - 1.171486\left(S^{*}_{w}\right)^{3}
\end{aligned}
\qquad \text{.....(2.5)}
$$

$$
k^{*}_{rw} = 0.2441795\, S^{*}_{w} - 0.355058\left(S^{*}_{w}\right)^{2} + 0.5117625\left(S^{*}_{w}\right)^{3} \qquad \text{.....(2.6)}
$$

Two different test cases were considered.

- Case A – This case was considered to have water-wet reservoir characteristics. It is the more optimistic case, which would result in a more favorable mobility ratio.
- Case B – This case was analyzed assuming the reservoir has intermediate wettability characteristics. It presents a pessimistic view.

III. Results

A. Prerequisites

Determining values for connate water saturation and residual oil saturation preceded the relative permeability calculations. The connate water saturation and residual oil saturation were established from Rosiere's work as 24% and 33% respectively[9].

B. Average Effective Porosity

The average effective porosity was calculated by averaging the 16 calculated effective porosities. The results of the porosity testing are located in Table 3.1. The average effective porosity is 23.85%, which agrees with findings by Rosiere[9], Wells[1], and R. Blanc et al[10].

Table 3.1
Effective Porosity

Sample Depth	Chamber Volume Empty	Chamber Volume with Sample	V_{grain}	Bulk Volume		Porosity
	cc	cc	cc	mm	cc	
146	36.05	24.85	11.2	13557.02	13.56	17.39%
147	39.6	26.6	13	17257.79	17.26	24.67%
148	36.2	24.1	12.1	15896.32	15.90	23.88%
149	39.8	27.9	11.9	16205.55	16.21	26.57%
150	39.8	26.7	13.1	16692.73	16.69	21.52%
151	36.2	23.8	12.4	16031.92	16.03	22.65%
152	39.8	27.6	12.2	16660.95	16.66	26.77%
153	36.4	24.6	11.8	15931.98	15.93	25.94%
154	36.4	24.45	11.95	15160.40	15.16	21.18%
155	36.4	24.7	11.7	14910.16	14.91	21.53%
156	36.4	25.6	10.8	13945.91	13.95	22.56%
157	36.4	23	13.4	16372.30	16.37	18.15%
158	39.8	27.2	12.6	16667.60	16.67	24.40%
159	36.4	24.7	11.7	16718.92	16.72	30.02%
160	36.4	24	12.4	16322.42	16.32	24.03%
161	36.4	23.5	12.9	15570.61	15.57	17.15%
				Effective Average Porosity =		23.85%

C. Absolute Permeability

The average horizontal absolute permeability was calculated to be 163.10 millidarcys. The horizontal absolute permeability is the representation of the ability of a single fluid to flow horizontally through the reservoir. One hundred sixty-three millidarcys is an average permeability value. It is not exceptionally high or low.

D. Wettability

The rock grains showed some affinity for water. Water was observed displacing oil from the grains. The water also pulled away from the surface of the water bubble to saturate rock grains that were floating on it. If the grains had been strongly water-wet, the water would have distinctly displaced the oil from the grains, but the displacement was gradual and, in some instances, not complete. The grains appeared to exhibit weak water-wet to intermediate wettability. Complete observations from the wettability experiment are located at the back of the report (Figure 3.1).

These findings agree with by Rosiere[9] who found the Warner formation to exhibit intermediate wettability. The Warner formation is located 0-10 feet below the Bluejacket formation[1]. Heavy oil is present in both sandstone formations. Both of the oils have the same molecular composition, which means that the oil migrated into the reservoirs at the same time from the same source rock[10]. The similarities between the Bluejacket and Warner formations allow the wettabilities to be compared.

E. Relative Permeability Analysis

The relative permeability curves for Case A, water-wet wettability, are presented in Figure 3.2. The curve is summarized in tabular form in Table 3.1.

Figure 3.2
Water-wet Wettability

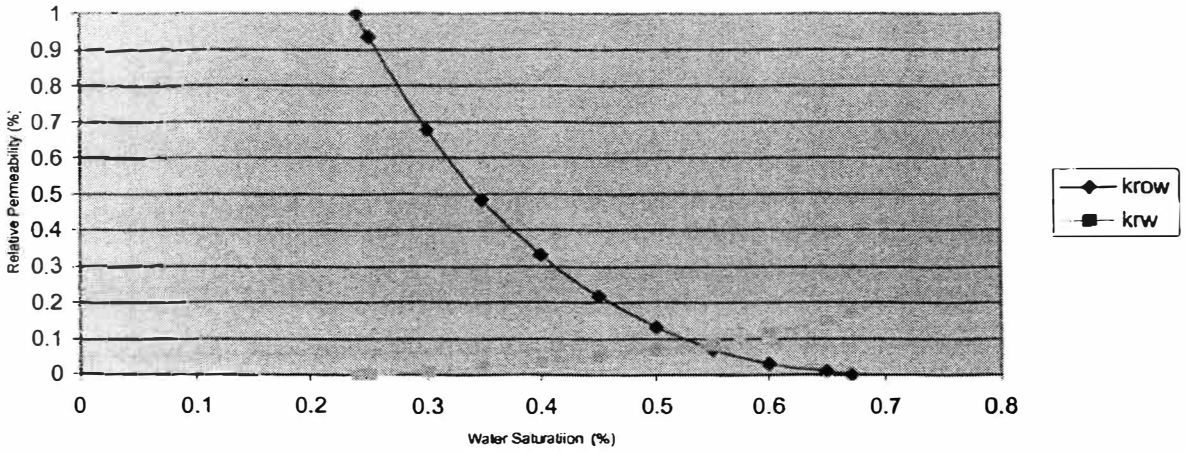

Table 3.1 Case A Water-wet		
Sw	**krow**	**krw**
0.24	1	0
0.25	0.93468	0.00054
0.3	0.67645	0.00838
0.35	0.48263	0.01991
0.4	0.33288	0.03334
0.45	0.21786	0.0484
0.5	0.13175	0.06571
0.55	0.07043	0.08669
0.6	0.03079	0.11354
0.65	0.01035	0.14937
0.67	0	0.16711

The relative permeability curves for Case B, intermediate wettability, are presented in Figure 3.3. The curve is summarized in tabular form in Table 3.2.

Figure 3.3
Intermediate Wettability

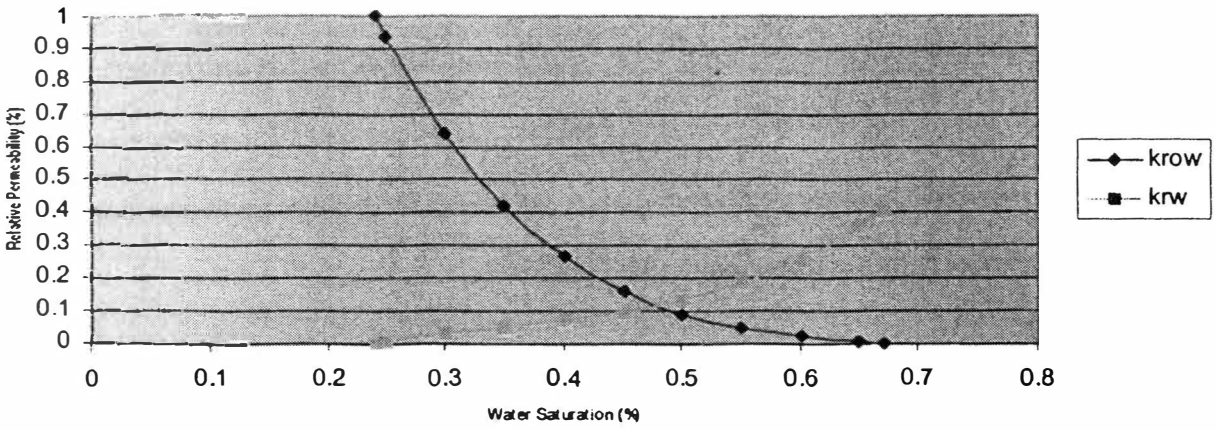

Table 3.2 Case B Intermediate		
Sw	**krow**	**krw**
0.24	1	0
0.25	0.93226	0.00549
0.3	0.64162	0.02855
0.35	0.42304	0.0478
0.4	0.26546	0.06806
0.45	0.15782	0.09418
0.5	0.08909	0.13096
0.55	0.0482	0.18325
0.6	0.02411	0.25587
0.65	0.00576	0.35365
0.67	0	0.40088

IV. CONCLUSIONS

1. The reservoir most likely exhibits intermediate wettability. Water-wet systems are preferred for enhanced oil recovery applications, because they allow for maximized recoverable reserves. Intermediate wettability systems can still be good candidates for enhanced oil recovery applications. Sometimes intermediate systems yield very favorable performances, but other times their oil recovery rate is not enough to be profitable.

2. Figure 3.3, the resulting two-phase relative permeability curve based on intermediate wettability, is a slightly pessimistic representation of the Bluejacket Formation. It should be used to obtain relative permeability values. Values taken from Figure 3.2, water-wet, could yield recoverable reserve estimates that are optimistically high and should not be used.

Figure 3.1

Unconsolidated Sands Method

Time	Water/Sand Grains
11:34	
11:35	Oil Migration not Heavy 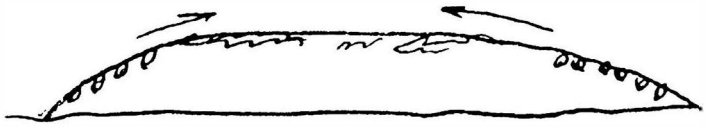
11:37	Grains Separating Light oil moving to center. 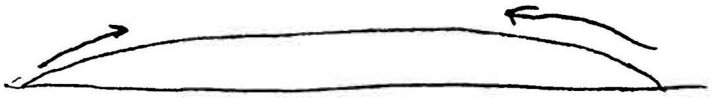
11:41	Water forming around grains on bubble surface. 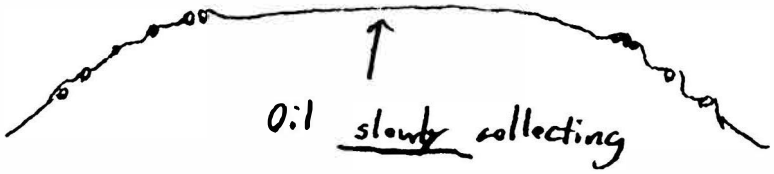
11:43	Oil drops forming. Sand grains separating. 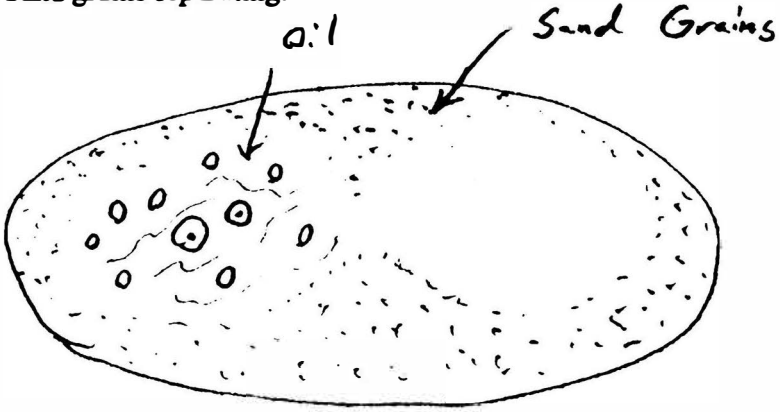

Figure 3.1 continued

11:46	Sand grains are well distributed on the bubble surface. As sand grains distribute, the bubble spreads out.

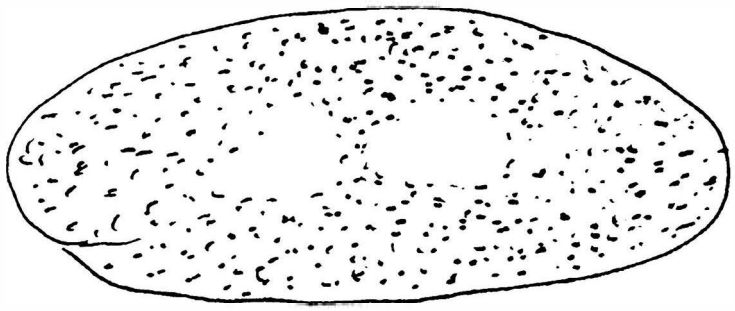

Process Continues	Water is adsorbing on to the surfaces of the grains. Fully saturating large clumps floating on surface.

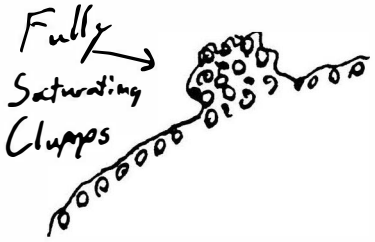

11:58	Water spreads to where the grains from experiment 1 are located after evaporation of water.

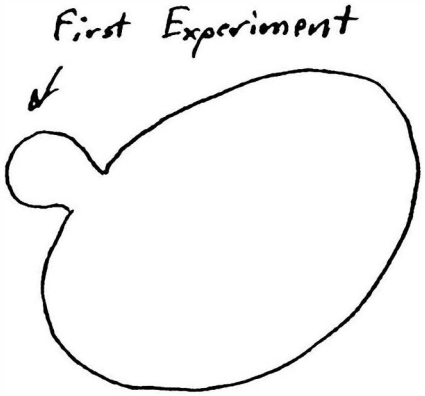

NOMENCLATURE

BV = Bulk Volume, cc
k_a = Absolute Permeability, md
$k^{\bullet}_{row}$ = Oil Relative Permeability, fraction
$k^{\bullet}_{rw}$ = Water Relative Permeability, fraction
S_o = Oil Saturation, fraction
S_{orw} = Residual Oil Saturation to Water, fraction
$S^{\bullet}_w$ = Water Saturation, fraction
S_{wc} = Connate Water Saturation
S_{wi} = Irreducible Water Saturation, fraction
V_{grain} = Volume of Rock Matrix, cc
V_{empty} = Volume of Space in Empty Cylinder, cc
V_{sample} = Volume of Space in Cylinder with Sample Present, cc
ϕ = Porosity, fraction
ϕ_e = Effective Porosity, fraction

ACKNOWLEDGEMENTS

I would like to thank my advisor, Dr. Shari Dunn-Norman, for valuable guidance, help, and encouragement throughout the research and preparation of this paper. I am also grateful to Dr. Leonard Koederitz for his assistance and advice.

Thanks are due to Rajeev Gupta who I assisted with the porosity research and who provided me with absolute permeability information.

Finally, I would like to thank my wife for her encouragement and support during the extent of this project.

BIBLIOGRAPHY

1. Wells, J. S. "Inventory of Heavy Oil in Western Missouri – Final Report." U.S. Department of Energy Report. 1979

2. Anderson, K. H. and Wells, J. S. "Heavy Oil in Western Missouri." *AAPG Bulletin*. 1968.

3. Dunn-Norman, S., Gupta, A., Summers, D. A., Koederitz, L. F. and Numbere, D. T. "Recovery Methods for Heavy Oil in Ultra-Shallow Reservoirs." SPE 76710. SPE Western Regional / AAPG Pacific Section Joint Meeting. Anchorage. Alaska. May 2002.

4. Koederitz, L. F., Harvey, A. H. and Honarpour, M. "Introduction to Petroleum Reservoir Analysis."

5. Mohamad Ibrahim, M. N. and Koederitz, L. F. "Two-Phase Relative Permeability Prediction Using a Linear Regression Model." SPE 65631. 2000 SPE Eastern Regional Meeting. Morgantown. West Virgina. October 17-19 2000.

6. Koederitz, L. F. "Core Analysis: Principles and Methods." *Petroleum Reservoir Laboratory Book*. University of Missouri – Rolla. 2001.

7. Craig, Forrest F. "The Reservoir Engineering Aspects of Waterflooding." Monograph Volume 3. New York. 1993.

8. Numbere, Daopu T. "Notes on Secondary Oil Recovery." University of Missouri – Rolla. 2002.

9. Rosiere, Darrell Wayne. "Relative Permeability Measurements for Thermal Applications to Heavy Oil Reservoirs in Western Missouri." Thesis. University of Missouri-Rolla. 1989.

10. Blanc, R., Coustau, H., Connan, J., Ebanks, W.J., and Roux, C. "A Multidisciplinary Approach to the Characterization of Heavy Oil Deposits From the Tri-State Area." Societe Nationale Elf Aquitaine. Pau, France.

Reflection of Learning Experience

1. **Describe your foundational understanding of how research is conducted in your discipline.**

   Research in the petroleum engineering field is conducted by identifying a problem and taking steps to solve the problem. The answer to the problem is sought in work previously done and published. If no answer is found, all literature pertinent to the problem is read. Research experiments are designed around the knowledge obtained from the literature review or knowledge from experts in the problem area. A research proposal is next made and funding is sought for the research. Finally the research is conducted, recorded, and submitted for peer review.

2. **How have you expanded your understanding of the informational resources available and how to best use them?**

   I have learned that petroleum research community is relatively small and helpful. Information is for the most part is easily obtained.

3. **Describe the knowledge you have gained regarding the fundamentals of experimental design.**

   The most important step in experimental design is to first review all of the information related to the problem being addressed.

Adhesion of an Axisymmetric Film onto a Rigid Substrate: Application to a MEM-RF-switch

Ming-fung Wong
Mechanical Engineering, UMR

Abstract

A solid mechanics model is constructed to discuss the mechanical aspect of a MEM-RF-switch. A thin circular membrane clamped at the perimeter is adhered to a rigid cylindrical flat punch. A tensile load applied to the punch causes an interfacial delamination. Once the contact circle shrinks to 0.1758 – 0.3651 of the punch dimension depending on the magnitude of the tensile residual stress on the film, a spontaneous delamination, or "pull-off", occurs and the film snaps from the substrate at a critical load and punch displacement. The theoretical model has significant implications in MEMS that involves active moveable films.

1. Introduction

MEMS (MicroElectroMechanical Systems) is a rapidly growing technology in microelectronics. It is a miniaturized version of the macroscopic machines, e.g. gyroscopes, liquid pumps, sensors, etc. One interesting application is in wireless communication devices [1] such as mobile phone, radar, and signal filters. In this paper, a specific radio frequency (RF) capacitive switch is investigated. The device comprises a beam, 'bridge', which is electrically grounded and mechanically suspended above an underlying dielectric film, 'pad', coated on a signal line as shown in figure 1. When the microswitch is in "off" state and the bridge in "up-state", the bridge-pad gap is at its maximum, the capacitance is minimal and the RF signal flows in the signal line. When the switch is activated by an

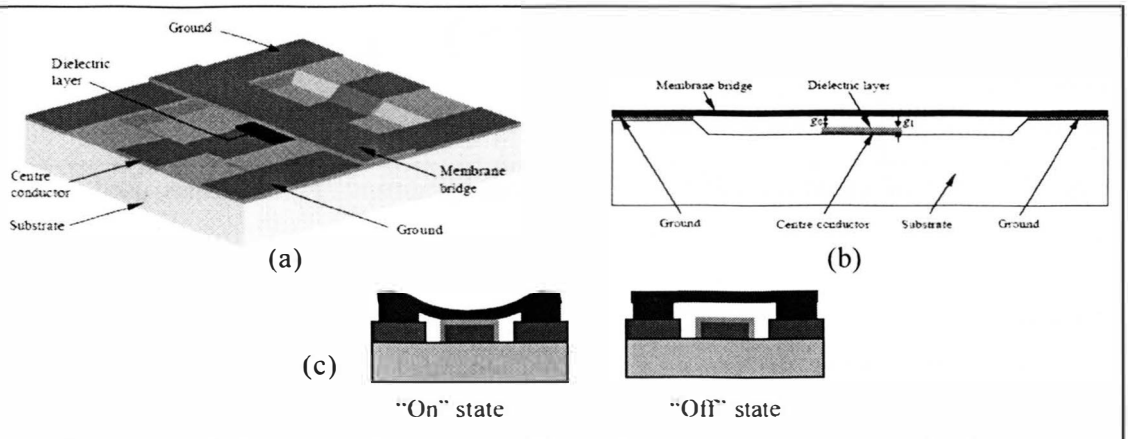

Figure 1. (a) 3-D model of a RF capacitive switch. (b) Cross section of a RF capacitive switch. (c) "On" and "off" states of the switch.

electrostatic attraction to "on", the bridge is pulled into contact with the underlying pad, resulting in a higher capacitance and signal switching occurs. Once the electrostatic force is turned off, the bridge is released and returns to its up-state. However, adhesion forces at the contact interface between the bridge and the dielectric film, coupled with intrinsic residual stress in the bridge, may hinder the capability of the bridge to break the contact, thus causing stiction failure. In theory, pad/punch interfacial adhesion energy and tensile residual stress on the bridge can affect the behavior of the performance of the capacitive switch, though studies in coupling of adhesion and residual stress are rare. Note that intrinsic residual stress arises from fabrication process, mismatch in coefficient of thermal expansion (CTE), and temperature rise during the switch operation.

Wan and Kogut [4] derived an elastic model for a flexible membrane with zero flexural rigidity such that only membrane-stretching is dominant. In this paper, the assumption is removed and the film is allowed to undergo plate-bending. A tensile residual stress is also incorporated into the new model. The coupling effect of interfacial adhesion and residual stress will be investigated.

	Actual Parameters	**Normalized Parameters**
Geometrical	$w(r)$ = deformation profile h = film thickness a = film / punch radius c = contact radius	$\xi = \frac{r}{a}$, $\zeta = \frac{c}{a}$, $\omega = \frac{w}{h}$ $\theta = \frac{\partial \omega}{\partial \xi} = \frac{a}{h}\frac{\partial w}{\partial r}$, $\theta' = \frac{\partial \theta}{\partial \xi}$,
Material	E = elastic modulus ν = Poisson's ratio κ = flexural rigidity = $\frac{E h^3}{12(1-\nu^2)}$ γ = interfacial adhesion energy ($J.m^{-2}$) σ_0 = tensile residual stress ($N.m^{-2}$)	$\beta = a\left(\frac{\sigma_0 h}{\kappa}\right)^{1/2}$ $\Gamma = \left(\frac{a^4}{2\kappa h^2}\right)\gamma$
Mechanical loading	F = applied external force w_0 = vertical displacement of punch	$\varphi = \frac{Fa^2}{2\pi\kappa h}$

Table 1. A list of variables and their corresponding normalized quantities used in this paper.

2. Theory

Figure 2(a) shows the cross-section of a clamped circular film and the external loading by a cylindrical flat punch. Upon an external load, the diaphragm deforms by plate-bending and membrane-stretching deformations. The constitutive relation (or mechanical response) $F(w_0)$ *without* delamination will first be derived before proceeding to the delamination mechanism.

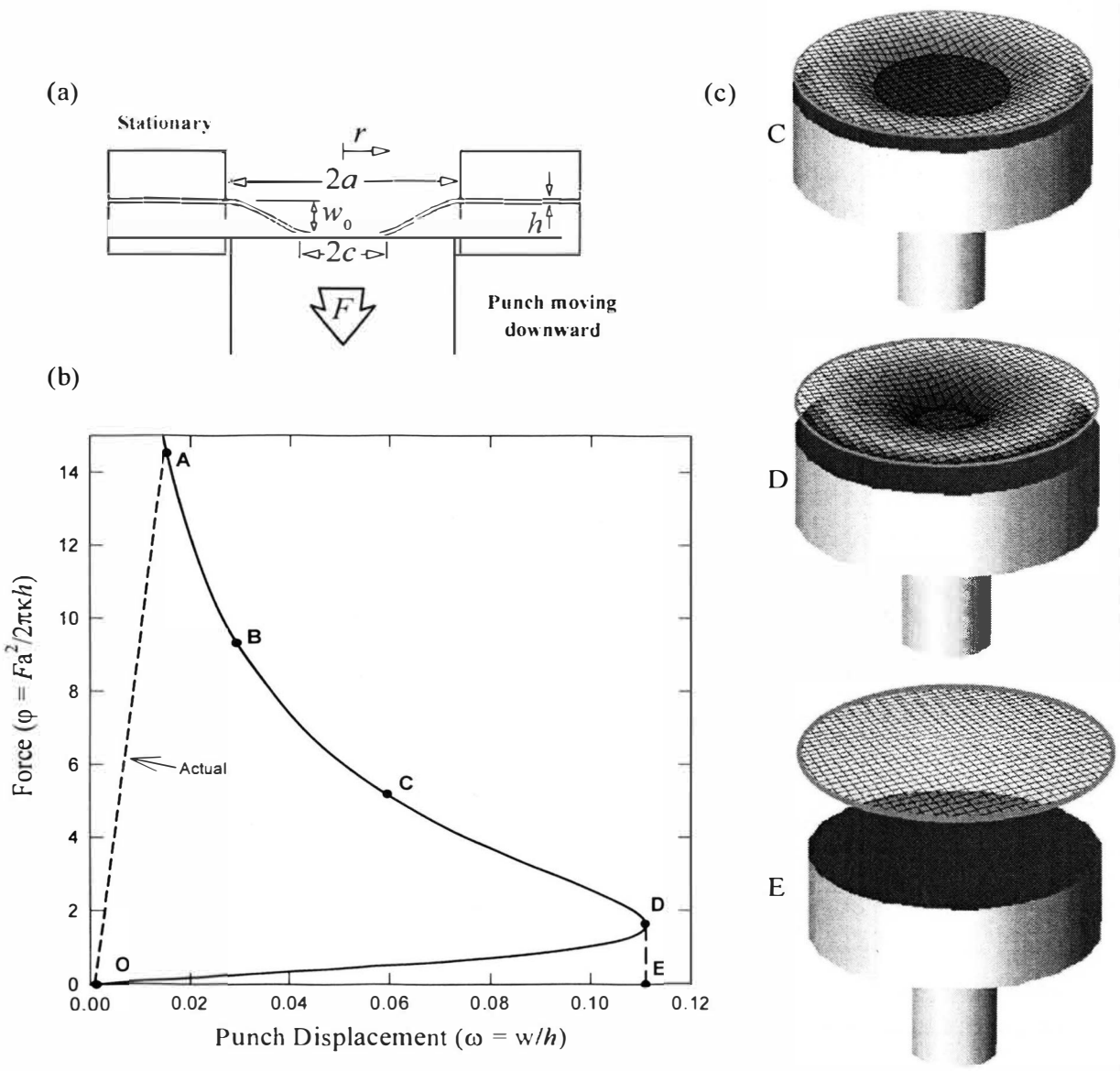

Figure 2. (a) The rigid film attached to the punch with interfacial adhesive energy. A tensile load is applied to the punch resulting in deformation and delamination of the film. (b) Constitutive relation for delamination. At O, the film is in full adhesion contact with the punch. Delamination begins at A, continues to B, then C, before "pull-off" occurs at D. The external load then drops to zero at E. (c) 3-D sketch of the delamination process.

2.1 Constitutive relation without delamination

For a film with non-zero κ and a tensile membrane stress σ_0, the deformed profile is governed by the von Karman equation.

$$\underbrace{\kappa\,\nabla^4 w}_{\text{plate-bending}} - \underbrace{\sigma_0 h\,\nabla^2 w}_{\text{membrane-stretching}} = \underbrace{F\,\delta(r)}_{\text{central external load}} \qquad (1)$$

where $\nabla^2 = \frac{1}{r}\frac{\partial}{\partial r}(r\frac{\partial}{\partial r})$ is the Laplacian operator in the polar coordinates, and the Dirac delta function, $\delta(r)$, denotes the central external load. The RHS of (1) is the mechanical input and the LHS the deformation. The profile gradient, $\theta = (a/h)(dw/dr)$, can be directly derived from (1), yielding

$$\xi^2\frac{\partial^2\theta}{\partial\xi^2} + \xi\frac{\partial\theta}{\partial\xi} - (1+\beta^2\xi^2)\theta = \xi\varphi \tag{2}$$

with boundary conditions, $\theta(1) = \theta(\zeta) = 0$ since the gradient at the clamped perimeter and the contact edge must vanish. Equation (2) is the modified Bessel equation [8] which gives

$$\theta = \varphi\left[C_1\, I_1(\beta\xi) + C_2\, K_1(\beta\xi) - \frac{1}{\beta^2\xi}\right] \tag{3}$$

where I_n and K_n are the n^{th} modified Bessel functions of the first and second kind, and C_1 and C_2 are constants to be fit to the boundary conditions:

$$C_1 = \frac{\zeta K_1(\beta\zeta) - K_1(\beta)}{\beta^2\zeta(-I_1(\beta\zeta)K_1(\beta) + I_1(\beta)K_1(\beta\zeta))} \quad \text{and} \quad C_2 = \frac{I_1(\beta) - \zeta I_1(\beta\zeta)}{\beta^2\zeta(I_1(\beta)K_1(\beta\zeta) - I_1(\beta\zeta)K_1(\beta)}$$

The profile is found by integrating θ with respect to ξ to give

$$\omega = \frac{\varphi}{\beta}\left\{C_1\left[-1 + I_0(\beta\xi)\right] - C_2K_0(\beta\xi) + C_3 - \frac{\log\xi}{\beta}\right\} \tag{4}$$

with the integration constant $C_3 = \dfrac{I_1(\beta)K_0(\beta) - \zeta I_1(\beta\zeta)K_0(\beta) + \left[I_0(\beta)-1\right]\left[K_1(\beta) - \zeta K_1(\beta\zeta)\right]}{\beta^2\zeta\left[I_1(\beta)K_1(\beta\zeta) - I_1(\beta\zeta)K_1(\beta)\right]}$.

The central displacement of the diaphragm, or equivalently, the vertical displacement of the punch is given by $\omega_0 = \omega(\zeta)$. The *linear* constitutive relation, $F(w_0)$ or $\varphi(\omega_0)$, can thus be found such that $\varphi \propto \omega_0$ as is obvious in (4). The presence of a residual stress stiffens the film such that the apparent elastic modulus increases.

2.2. Constitutive relation with delamination

The delamination mechanics is derived for a finite punch-film interfacial adhesion as follows. Once the tensile load exceeds a certain threshold, delamination begins. An energy balance method is adopted here. For an incremental decrease in contact radius, the total energy of the punch-film system is given by

$$dU_T = dU_P + dU_E + dU_S \tag{5}$$

where $U_P = Fw_0$ is potential energy, $U_E = \int F.dw_0$ elastic energy stored in the film, and $U_S = = \gamma(\pi c^2)$ is the surface energy with γ the adhesion energy at the punch-film interface ($J.m^{-2}$). It can be shown that (5) requires

$$\gamma = -\frac{F}{2}\left[\frac{dw_0}{d(\pi c^2)}\right]_{F=\text{constant}} \quad \text{or} \quad \Gamma = -\frac{\varphi}{2}\left[\frac{d\omega_0}{d(\zeta^2)}\right]_{\varphi=\text{constant}} \tag{6}$$

Substituting (4) into (6) leads to

$$\varphi = \sqrt{\frac{f_1(f_2+f_3-f_4)}{8\beta^3\zeta^3\left[I_1(\beta\zeta)K_1(\beta)-I_1(\beta)K_1(\beta\zeta)\right]}}\,\Gamma \tag{7}$$

where $f_1 = -I_1(\beta)\left[K_0(\beta)-K_0(\beta\zeta)\right]-\left[I_0(\beta)-I_0(\beta\zeta))K_1(\beta)\right]$

$f_2 = \beta\zeta\left[I_0(\beta\zeta)+I_2(\beta\zeta))(K_1(\beta)-\zeta K_1(\beta\zeta)\right]$

$f_3 = I_1(\beta)\left[\beta\zeta\, K_0(\beta\zeta)-2K_1(\beta\zeta)+\beta\zeta\, K_2(\beta\zeta)\right]$

$f_4 = I_1(\beta\zeta)\left[\beta\zeta^2 K_0(\beta\zeta)-2K_1(\beta)+\beta\zeta^2 K_2(\beta\zeta)\right]$

The delamination process is illustrated in Figure 2b and 2c for a fixed adhesion energy $\Gamma = 1$ and zero residual stress $\sigma_0 = 0$. Delamination follows the trajectory OABCDE. When a load is first applied to the punch, delamination begins at A. A decreasing load is needed for the delamination to proceed along BCD. At D, $(d\varphi / d\omega_0) = (dF / dw_0) = \infty$, the delamination becomes unstable, the contact circle shrinks spontaneously to zero and the film snaps from the punch. This is known as the "pull-off" event in literature. The critical values of φ^*, ω_0^*, and ζ^* at "pull-off" can be measured experimentally, yielding the adhesion energy and residual stress. Note that the branch DO is a direct result from the mathematical energy balance, but is not physically accessible.

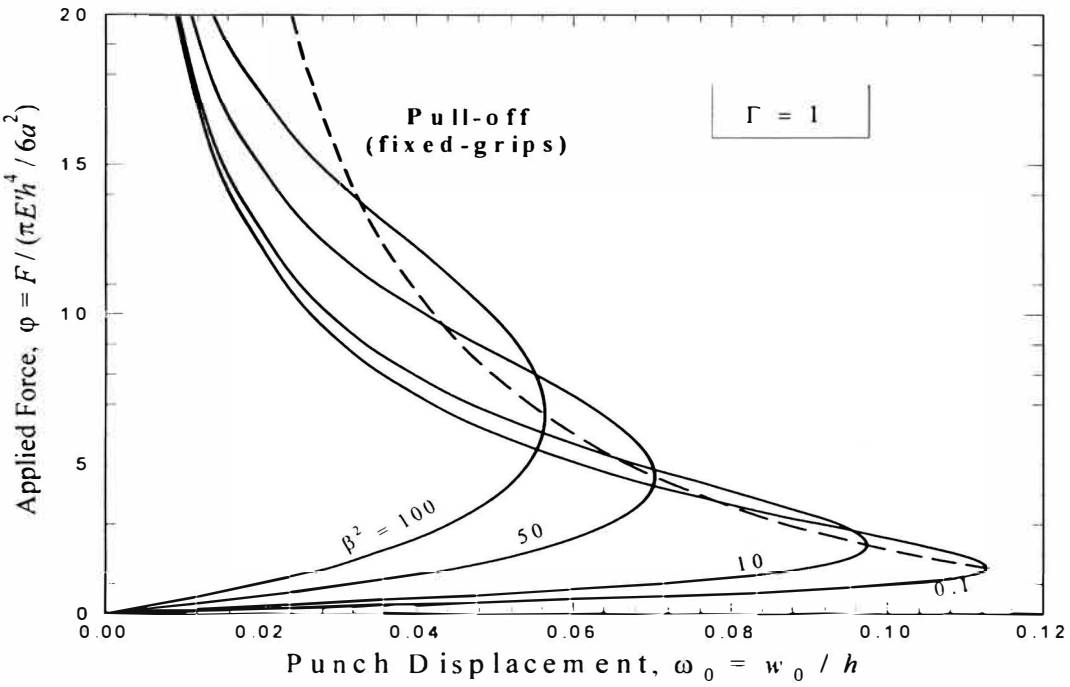

Figure 3. Delamination process is controlled by the coupling of adhesion energy and residual stress. At a fixed adhesion energy ($\Gamma = 1$), the residual stress shifts the "pull-off" event to a larger applied force and a smaller punch displacement.

Figure 3 shows the effect due to residual stress (β_0 or σ_0) at a fixed adhesion energy. The "pull-off" event occurs at a larger external load (φ^*or F^*) and smaller punch displacement (ω_0^* or w_0^*) as a result of the residual stress stiffened membrane. Figure 4 shows the corresponding changes in contact radius (ζ^* or c^*) as a function of residual stress. At small σ_0, the adhesion energy is the dominating factor in the delamination mechanics and ζ^* approaches 0.1785. This contact dimension increases as σ_0 augments. At large σ_0, the residual stress prevails and ζ^* approaches 0.3651.

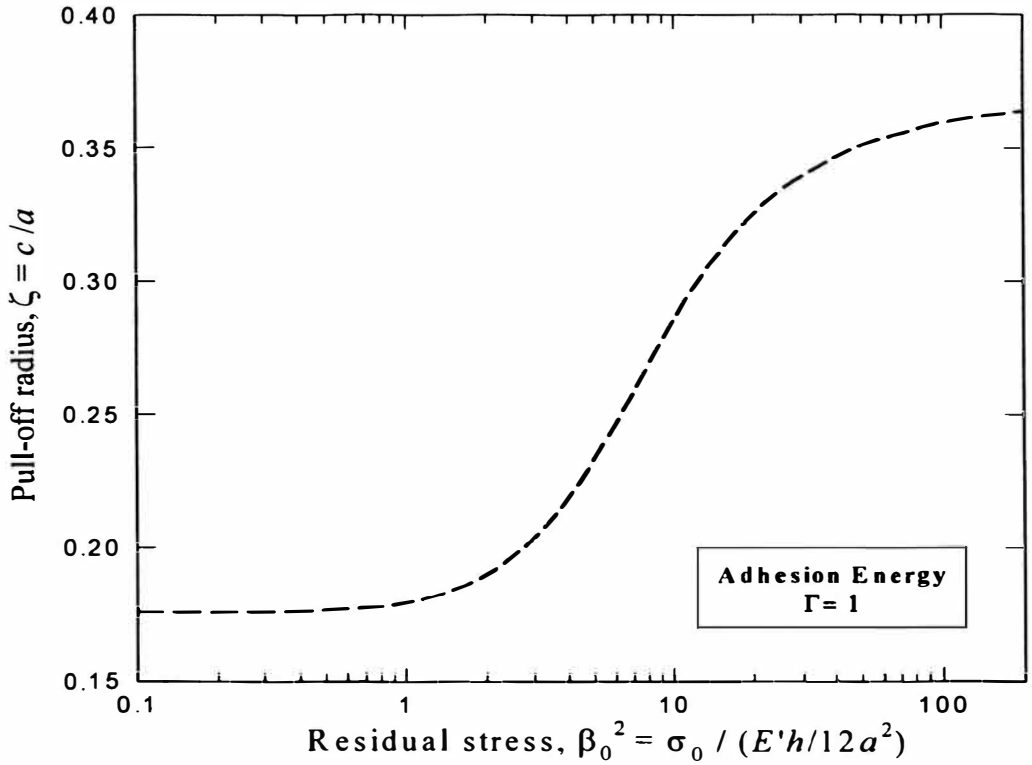

Figure 4. The pull-off radius increases as tensile residual stress increases. At small residual stress ($\beta^2 < 2$), the pull-off radius approaches 0.1758. After a transition around $\beta^2 = 10$, the pull-off radius approaches 0.3651.

Discussion

In designing a RF MEMS, according to figure 4; if a high bounce-back required, a highly preloaded film has to be made very close to the bottom plate; if a reasonable distance between the film and bottom plate, the film can be less preloaded, but the short side would be smaller contact area between the film and the bottom plate and there might be some bad effect on the circuit performance.

High residual stress does not have to be a good design as well, in figure 3, it shows that high residual stress film require a bigger force to pull it toward the punch. In reality, high residual stress result in high current flow in pad for higher electrostatics energy and a series of operation and mechanical issues. For example, higher current result in higher heat generation which lead to heat transfer concern; bridge fatigue with high residual and short operation lift is resulted. However, all these reality issues have not be a concern in this research paper, further study will be done alone these lines.

Conclusion

A mathematical model is constructed to show the delamination mechanics of a stiff circular membrane adhered to a rigid punch. The constitutive relations are derived for situations with and without delamination using an energy balance method. The residual stress in the membrane has a significant effect on the mechanical behavior of the punch-film system. The trends and graphs given here will have significant impacts on the design and fabrication of many MEMS devices, especially those involve moveable circular or rectangular membranes.

References

[1] J.-M. Huang, A.Q. Liu, C. Lu, J. Ahn, Mechanical characterization of micromachined capacitive switches: design consideration and experimental, Sensors and Actuators A 108 (2003) 36-48.

[2]P.M. Osterberg, S.D. Senturia, M-test: a test chip for MEMs material property measurement using electrostatically actuated test structures, J. Microelectromech. Syst. 6 (2) (1997) 107-108

[3]P. Osterberg, H. Yie, X. Cai, J. White, S. Senturia, Self-consistent simulation and modeling of electrostatically deformed diamphragms, in: Proceedings of the Micro Electro Mechanical Systems Workshop, MEMs'94, Oiso, Japan, 1994, pp.28-32

[4]K.T. Wan, L. Kogut, The Influence of Residual Stress on Micromachine Stiction: ASME/STLE International Joint Tribology Conference. (2004) TRIB 2004-64333.

[5]Abramowitz, M. and Stegun, I.A., *Handbook of Mathematical Functions*(National Bureau of Standards, John Wiley, New York, 1959).

Opportunity of Undergraduate Research Experience to me

The project I worked on for this undergraduate research program is about thin film mechanics. In this research, I learned the relationship between the tensile residual stress to the performance of the film. The idea of this research came from the similar situation in MEMs device. However, my professor Dr. Wan from Mechanical Engineering Department gave me a brain shock on how a single knowledge being applied into so many different kinds of study. Thin film mechanics behavior is not only the major issue of the performance of MEMs devises, it also affects the performance of our eyes, the behavior of normal cells and malfunction cells, and etc. Even today progression of this research is still far from entering any specifics field, the reference and information I read greatly furnished my knowledge.

The source of my information is mostly came from Dr. Wan previous papers and related papered from library journal resource. Some of the information came from meeting with different professors in other fields. For me, reading is boring but not understanding, so I compared different papers and my research, then found out why that information related to my research. This why I understood the information a lot better and information research became a fun part of the research. On the other hand, talking to other professors was fun too. They were always doing something that I never heard of and somehow related to my research. One of them was Dr. Ravi in Washington University in St. Louis. He was an eye doctor. I learned the membrane rigidity of the lens related to the performance of the eyes. In conclusion, I think absorbing knowledge is not the best way to learn. Instead, understanding the relationship of the knowledge to my work is the best use of knowledge.

The experience from this research is not just about the book, it also improved my technical writing skill and learning skill. Technical writing would help me better express my idea to other people and better skill of learning gives a new way to understand the world of knowledge. I think I gained life time benefit from this research experience.

Solar Science

A study of the 2002 UMR/RTI competition solar house

Chris Wright

Abstract

The purpose of this report is show the progress as where it stands for the setting up, collection, and analysis of data on the uses and efficiencies of the 2002 UMR/RTI competition solar house. Sensors were set up and configured to record data every minute on appliance and photovoltaic loads, temperature inside and outside the house, solar radiation, light levels, and net metering information. Temperature stratification, solar panel efficiency, and total house loads are some of the analysis that has been done with this data. I have also used the software donated by Campbell Scientific, Inc. to set up a real time web display of the sensors in the house, which can be viewed at http://solarhouse1.dnsalias.net. The final goal is to make the first of its kind solar house research facility and make the data readily available to the general public.

Introduction

This research originally started to compare the efficiency and comfort level of a forced air heating system versus a radiant floor heating system. The goal was to verify that the radiant floor system that is going to be installed in the 2005 solar house is a better choice by power usage and comfort level. This project has since then gone much further. The National Renewable Energy Laboratory (NREL) has gotten involved and a small team of UMR students received a grant from the Environmental Protection Agency (EPA) to expand this research to analyzing power loads and lighting levels in the house. There were over 20 sensors installed and the now the complete workings of the house are being monitored, recorded, and attempting to be made readily available.

Procedure

The first part of the project was to install the sensors and data logger for the collection of the data. Campbell Scientific, Inc. and Vaisala have generously donated sensors and software used for this project. My advisor and I installed three temperature and humidity sensors inside the house at different height levels for the temperature and humidity stratification of a forced air heating system inside the house. The original idea was to compare this data of the forced air heating system to radiant floor heating system data collected from the 2005 UMR/RTI competition solar house, now being constructed on campus. Due to construction restraints the house is not as far along as originally thought, so data is not able to collected yet. After the sensors were installed the data logger had to be programmed to store the data every so often. By the time we got most of the bugs worked out we had caught the eye of NREL and they donated more sensors for our project and helped with the programming of the datalogger. Now there are 12 watt nodes measuring the AC power loads on the house, 4 temperature and relative humidity sensors measuring inside and outside the house, and 8 sensors measuring the voltage and current of the DC loads on the house. (see Appendix 1 for photos)

Results

The AC loads include the furnace, heat pump, hot water backup, roof circulator pump, heat trace tape, communications, clothes washer, dishwasher, and miscellaneous with a previous collection on the microwave and programming for the home office and cooktop pending the ability to

obtain more sensors. The total loads into and out of the house are also being measured to determine the total power bought and total power sold back to the power company. The house sells back the energy it makes over and above what it uses, which is called net-metering. DC loads being measured are the refrigerator, amount of power the solar panels are making, and the power that is used to keep the batteries charged.

LOADS	Total Energy Used (Wh)	# of days/years kWh	38.5722 kWh/day	0.1057 kWh/year	$/yr @ $0.10/kWh
Furnace	1673066.10	1673.07	43.37	15831.84	$1,583.18
Heat Pump	274.50	0.27	0.01	2.60	$0.26
Hot Water Backup	119818.25	119.82	3.11	1133.81	$113.38
Roof Water Pump	11169.38	11.17	0.29	105.69	$10.57
Heat Trace Tape	267131.63	267.13	6.93	2527.80	$252.78
Cooktop	290.25	0.29	0.01	2.75	$0.27
Communications	31591.87	31.59	0.82	298.95	$29.89
Clothes Washer	28628.18	28.63	0.74	270.90	$27.09
Dishwasher	2228.51	2.23	0.06	21.09	$2.11
Lights and other	118151.23	118.15	3.06	1118.04	$111.80
Microwave	10230.34	10.23	0.27	96.81	$9.68
Refridgerator	21878.97	21.88	0.57	207.04	$20.70
TOTAL	2284459.19	2284.46	59.23	21617.31	$2,161.73
TOTAL without communications and heat trace		1985.74	51.48	18790.56	$1,879.06

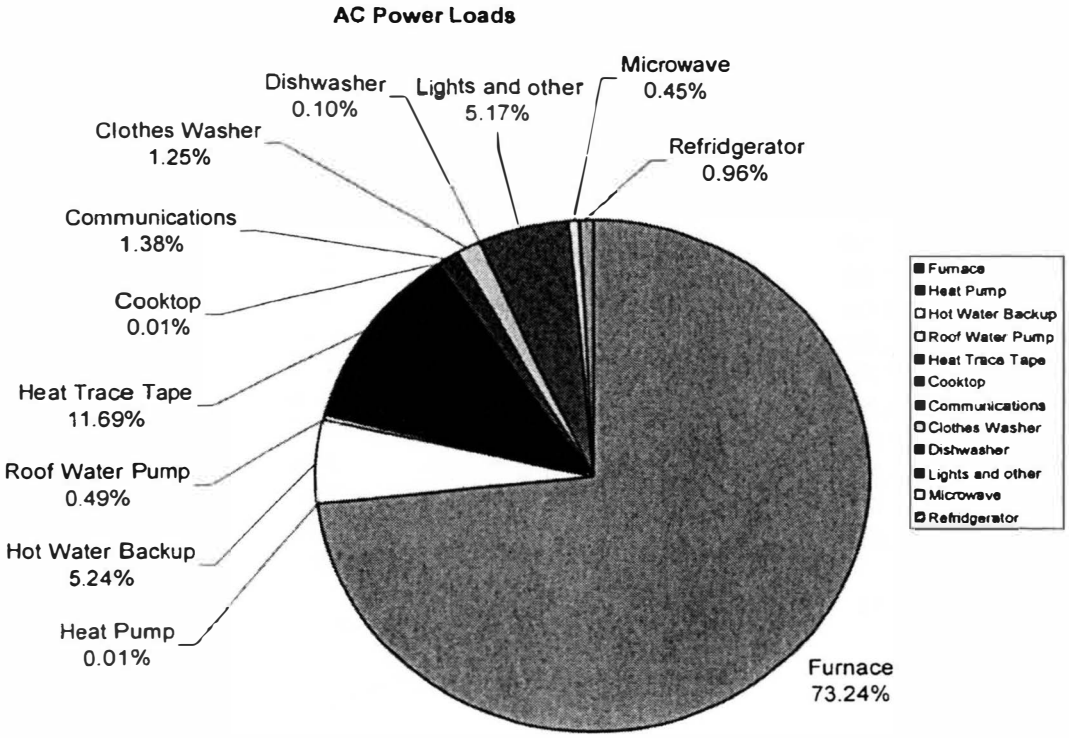

The table above shows the measured total energy used and cost of appliances during the month of February and March of 2005. The data is not complete in that the total number of minutes of data that has actually been recorded only adds up to 38.5722 days. This is only 65 % of the actual time in the months recorded. The pie chart shows the percentages of the total loads or the whole system. The furnace being over 73% of the entire energy usage is a very costly part of the house. This cannot just be turned off since it is the heat for the residents. The radiant floor heating system that is being installed in the 2005 competition house will not use electricity at all. This system will use hot water to heat the house. This system will greatly reduce the cost of living in the house.

The relative humidity in the house decreases with increasing height from the floor. It is mainly consistant between 20% and 50%. Regulations for the 2005 Solar Decathlon which the UMR/RTI solar house team is competing restricts the humidity to 40% to 55% (http://www.eere.energy.gov/solar_decathlon). While the data was taken during the winter and the outside air is very dry, this comfort zone could be improved. The average change in relative humidity is 2.59% per meter which decreases with height. Below is a sample of the humidity data.

		0.7620		1.9558		1.1938
Average inside Relative Humidity	Difference between High and Middle Relative Humidity	Relative Humidity change per meter measured between high and middle sensors	Difference between High and Low Relative Humidity	Relative Humidity change per meter measured between high and low sensors	Difference between Middle and Low Relative Humidity	Relative Humidity change per meter measured between middle and low sensors
40.33	-1.70	-2.23	-7.10	-3.63	-5.40	-4.52
40.50	-1.60	-2.10	-7.40	-3.78	-5.80	-4.86
40.53	-1.70	-2.23	-7.40	-3.78	-5.70	-4.77
40.60	-1.60	-2.10	-7.40	-3.78	-5.80	-4.86
40.53	-1.60	-2.10	-7.50	-3.83	-5.90	-4.94
40.60	-1.50	-1.97	-7.50	-3.83	-6.00	-5.03
40.53	-1.50	-1.97	-7.30	-3.73	-5.80	-4.86
40.47	-1.60	-2.10	-7.30	-3.73	-5.70	-4.77
40.47	-1.60	-2.10	-7.30	-3.73	-5.70	-4.77
40.50	-1.60	-2.10	-7.40	-3.78	-5.80	-4.86
40.53	-1.70	-2.23	-7.40	-3.78	-5.70	-4.77
40.53	-1.70	-2.23	-7.40	-3.78	-5.70	-4.77
40.43	-1.60	-2.10	-7.20	-3.68	-5.60	-4.69
40.47	-1.70	-2.23	-7.20	-3.68	-5.50	-4.61
40.50	-1.50	-1.97	-7.20	-3.68	-5.70	-4.77
40.57	-1.60	-2.10	-7.30	-3.73	-5.70	-4.77
Average	-0.33	-0.43	-5.65	-2.89	-5.32	-4.46
			Average Relative Humidity change per meter:		-2.59	

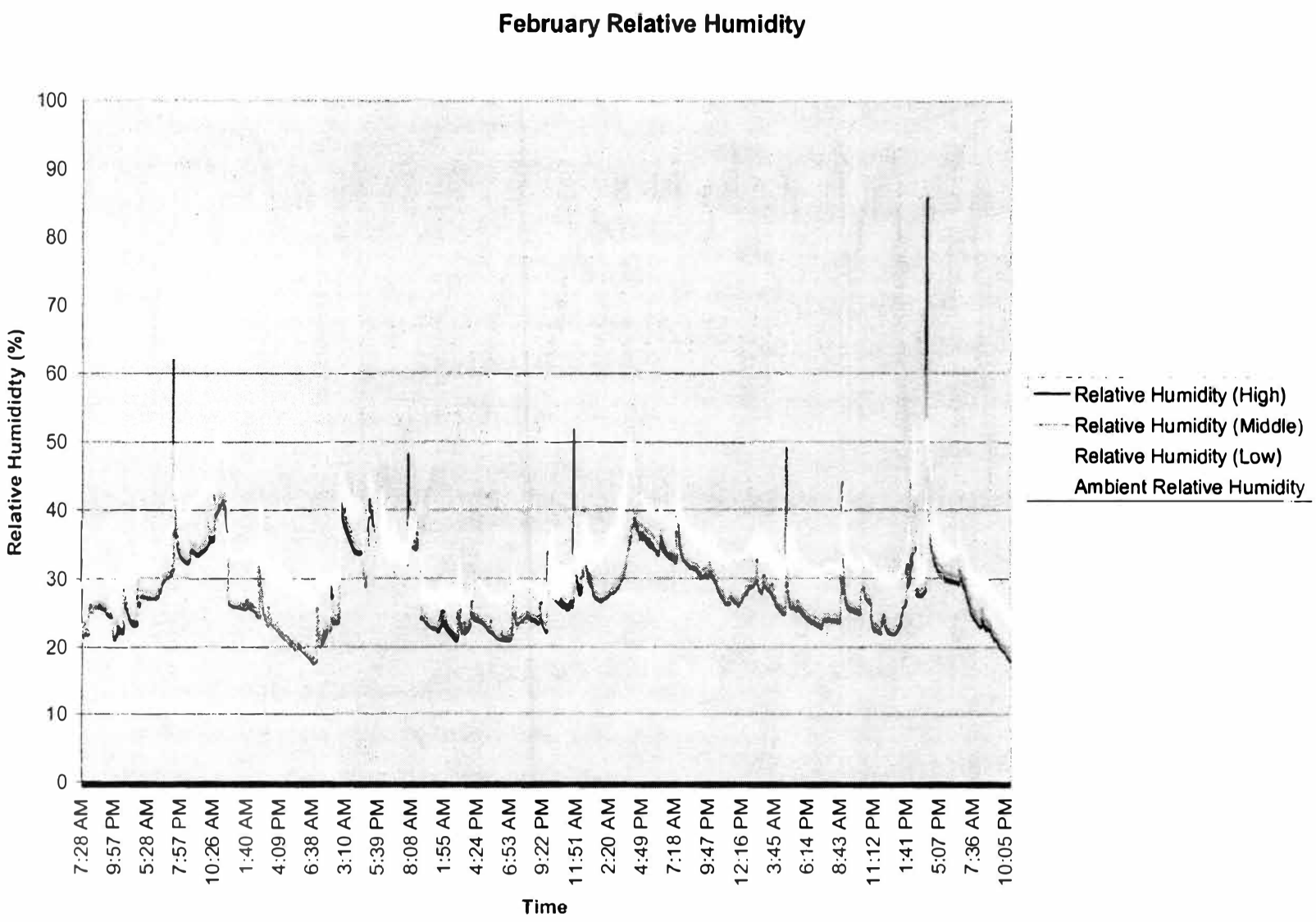
February Relative Humidity
Relative Humididty (%)
100
90
80
70
60
50
40
30
20
10
0
7:28 AM
9:57 PM
5:28 AM
7:57 PM
10:26 AM
1:40 AM
4:09 PM
6:38 AM
3:10 AM
5:39 PM
8:08 AM
1:55 AM
4:24 PM
6:53 AM
9:22 PM
11:51 AM
2:20 AM
4:49 PM
7:18 AM
9:47 PM
12:16 PM
3:45 AM
6:14 PM
8:43 AM
11:12 PM
1:41 PM
5:07 PM
7:36 AM
10:05 PM
Time
Relative Humidity (High)
Relative Humidity (Middle)
Relative Humidity (Low)
Ambient Relative Humidity

The above graph is the Relative Humidity inside and outside the house during the month of February. The relative humidity inside the house generally increases when the relative humidity outside decreases. This pattern is unexpected since the outside humidity affects inside humidity whenever doors are opened or just by air infiltration. The relationship is probably due to the differences in temperature since it is relative to the amount of vapor the air can hold instead of absolute humidity. Relative humidity is expected to increase with a decreasing air temperature since the amount of water in the air stays the same, but the amount the of water the air can hold decreases.

		0.7620		1.9558		1.1938
Average inside Temperature	Difference between High and Middle Temperature	Degree change per meter measured between high and middle sensors	Difference between High and Low Temperature	Degree change per meter measured between high and low sensors	Difference between Middle and Low Temperature	Degree change per meter measured between middle and low sensors
73.30	1.34	1.75	3.50	1.79	2.50	2.09
73.30	1.34	1.75	3.50	1.79	2.50	2.09
73.27	1.34	1.75	3.60	1.84	2.60	2.18
73.30	1.34	1.75	3.50	1.79	2.50	2.09
73.27	1.34	1.75	3.60	1.84	2.60	2.18
73.33	1.47	1.93	3.60	1.84	2.50	2.09
73.30	1.34	1.75	3.50	1.79	2.50	2.09
73.30	1.34	1.75	3.50	1.79	2.50	2.09
73.27	1.34	1.75	3.60	1.84	2.60	2.18
73.30	1.34	1.75	3.50	1.79	2.50	2.09
73.30	1.34	1.75	3.50	1.79	2.50	2.09
73.30	1.34	1.75	3.50	1.79	2.50	2.09
73.27	1.34	1.75	3.60	1.84	2.60	2.18
Average	1.18	1.54	7.68	3.92	6.80	5.70
			Average degree change per meter:	3.72		

This chart is a sample of the analysis of the temperature stratification in the 2002 solar house with the forced air heating system. The average degree change per meter is 3.72 degrees F increasing as the height increases. This value is in error because the spot chosen for the location of the sensors is directly on a seem that joins two modules. This is bad positioning because there is air flow through the floor where the seem is and this affects the reading of the temperature sensors especially the lowest one. The average temperature change in meters is almost 4 or above when it is measured with the low sensor.

The graph below has a relationship between the outside temperature and the inside temperature. As the outside temperature increases the inside temperature has a very subtle change toward the same direction. The reason for this is that temperature is measured on an absolute scale as opposed to relative. As the outside temperature increases the infiltration into the house will bring in a higher temperature than previously and will lessen the load on the heater.

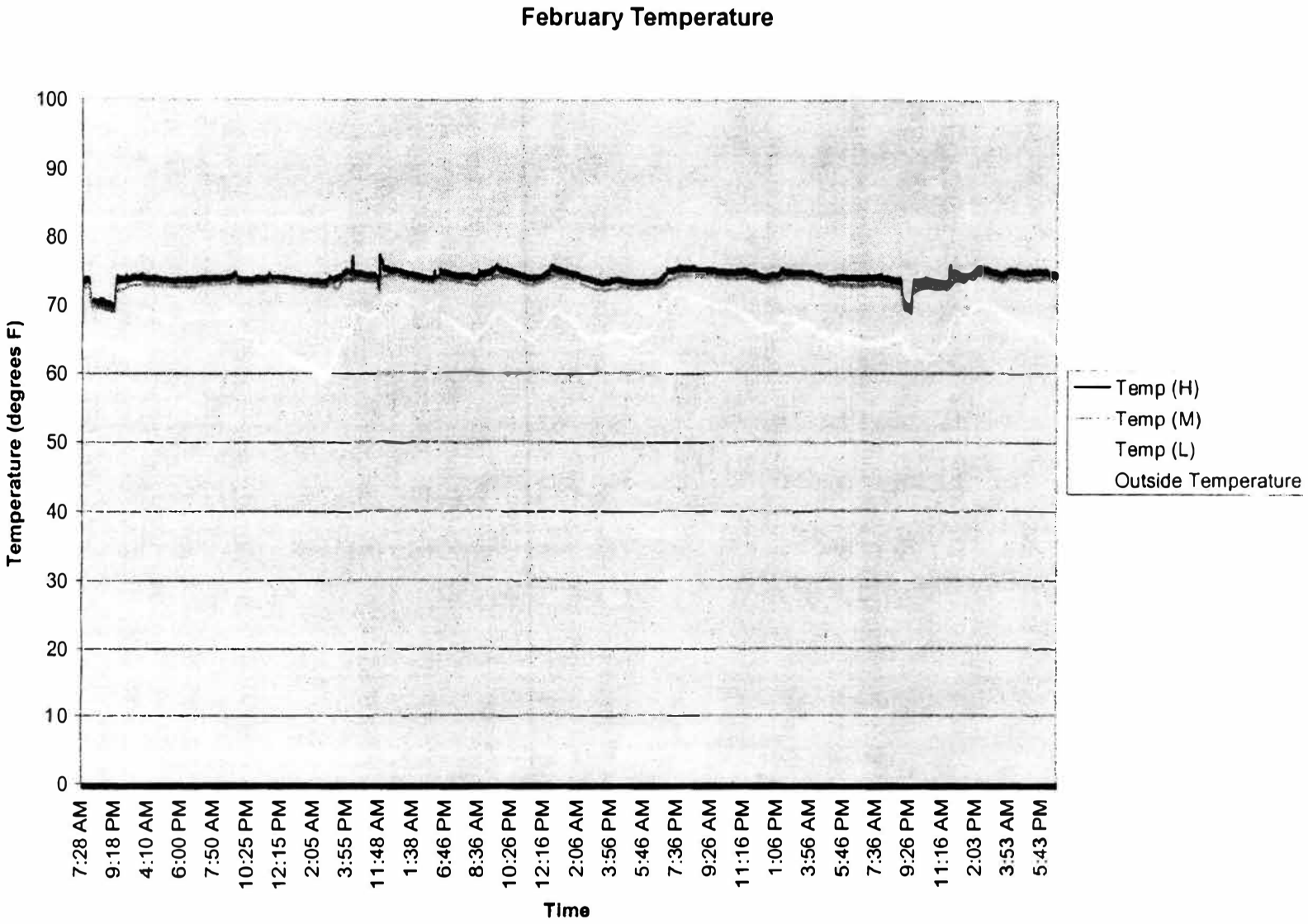
February Temperature
Temperature (degrees F)
100
90
80
70
60
50
40
30
20
10
0
7:28 AM
9:18 PM
4:10 AM
6:00 PM
7:50 AM
10:25 PM
12:15 PM
2:05 AM
3:55 PM
11:48 AM
1:38 AM
6:46 PM
8:36 AM
10:26 PM
12:16 PM
2:06 AM
3:56 PM
5:46 AM
7:36 PM
9:26 AM
11:16 PM
1:06 PM
3:56 AM
5:46 PM
7:36 AM
9:26 PM
11:16 AM
2:03 PM
3:53 AM
5:43 PM
Time
Temp (H)
Temp (M)
Temp (L)
Outside Temperature

The power output from the solar panels is also being measured, but also with error. The solar radiation sensor or pyranometer, which measures the available sunlight, seems to be set up incorrectly. The sensor is on a vertical post on the top of the roof. It is the highest part of the house so that it is never shaded by any other part of the house. The data seems to be getting more negative with the increasing light. It also seems to read -6999 instead of -600. The reference insolation that the data is being compared to is 2820 watts per square meter per day for February and 3520 watts per square meter per day for March which was found on http://Apricus-solar.com. The measured February average is -935.492 which is in absolute terms over 1800 watts difference and the March average is over 5 million off. (see Apendix 1 for data tables)

Conclusions

Some problems I am running into and in the process of working them out is first of all the lack of a radiant floor heating system to compare data. Another is the lack of knowledge about the software and programming and trying to figure out the programming language. There are breaks in the data which was found to be places when the computer did not have an account running. This problem has hopefully been addressed by never logging out of the system. The largest load in the house was found to be the heater in the months of February and March. Without the heater using electricity the power consumed would decrease by more than 70%. This is huge especially when dealing with a solar house attempting complete self-sufficiency. The sensor that measures the available sunlight was found to be configured wrong which shows a percent error of over 1000%.

Acknowledgements

Jeff Birt – Advisor
Helped with the installation, programming, and troubleshooting of the project

Mike Wassmer – NREL
Helped with the installation, programming, and troubleshooting of the project

Campbell Scientific, Inc.
Donation of sensors and software

Vaisala
Donation of sensors

References

http://www.eere.energy.gov/solar_decathlon
http://apricus-solar.com

Appendix 1

Data Tables

Solar Collection

Date	Average Solar Radiation from Apricus-Solar.com (Wh/m^2)	Measured Solar Radiation (Wh/m^2)	Array Area (m^2): Array #1 Energy (Wh)	5.004 Array #2 Energy (Wh)	Array #1 Measured Energy per Area (Wh/m2)	Array #2 Measured Energy per Area (Wh/m2)	Array #1 Efficiency	Array #2 Efficiency	Array #1 Percent Error	Array #2 Percent Error
1-Feb	2820.00	-857.376	6924.939	-1.333	1383.881	-0.266	-161.409	0.031	-50.926	100.009
2-Feb	2820.00	not complete								
3-Feb	2820.00	no data								
4-Feb	2820.00	no data								
5-Feb	2820.00	no data								
6-Feb	2820.00	-1056.456	1622.544	1374.868	324.249	274.754	-30.692	-26.007	-88.502	-90.257
7-Feb	2820.00	not complete								
8-Feb	2820.00	not complete								
9-Feb	2820.00	-705.960	829.008	640.456	165.669	127.989	-23.467	-18.130	-94.125	-95.461
10-Feb	2820.00	not complete								
11-Feb	2820.00	not complete								
12-Feb	2820.00	no data								
13-Feb	2820.00	no data								
14-Feb	2820.00	-2035.584	8790.514	8215.033	1756.698	1641.693	-86.299	-80.650	-37.706	-41.784
15-Feb	2820.00	not complete								
16-Feb	2820.00	not complete								
17-Feb	2820.00	-1298.016	9013.653	9109.306	1801.290	1820.405	-138.773	-140.245	-36.124	-35.447
18-Feb	2820.00	-1283.112	8951.096	8779.547	1788.788	1754.506	-139.410	-136.738	-36.568	-37.783
19-Feb	2820.00	-270.504	1028.240	828.608	205.484	165.589	-75.963	-61.215	-92.713	-94.128
20-Feb	2820.00	-1322.496	6540.405	6479.003	1307.035	1294.765	-98.831	-97.903	-53.651	-54.086
21-Feb	2820.00	-1084.104	2100.704	1803.931	419.805	360.498	-38.724	-33.253	-85.113	-87.216
22-Feb	2820.00	-426.264	3341.766	4465.967	667.819	892.479	-156.668	-209.372	-76.318	-68.352
23-Feb	2820.00	-543.888	153.682	116.502	30.712	23.282	-5.647	-4.281	-98.911	-99.174
24-Feb	2820.00	-173.232	232.846	88.280	46.532	17.642	-26.861	-10.184	-98.350	-99.374
25-Feb	2820.00	not complete								
26-Feb	2820.00	no data								
27-Feb	2820.00	not complete								
28-Feb	2820.00	-1104.408	5288.147	5320.156	1056.784	1063.181	-95.688	-96.267	-62.525	-62.299
February Average	2820.00	**-935.492**	**4216.734**	**3632.333**	**842.673**	**725.886**	**-90.078**	**-77.594**	**-70.118**	**-74.259**
1-Mar	3520.00	-238.320	9481.110	9844.288	1894.706	1967.284	-795.026	-825.480	-46.173	-44.111
2-Mar	3520.00	-156.240	9459.961	9522.821	1890.480	1903.042	########	1218.025	-46.293	-45.936
3-Mar	3520.00	-905.904	9459.067	9032.063	1890.301	1804.969	-208.665	-199.245	-46.298	-48.722
4-Mar	3520.00	not complete								
5-Mar	3520.00	-1859.184	9220.746	9553.475	1842.675	1909.168	-99.112	-102.688	-47.651	-45.762
6-Mar	3520.00	-1232.208	8041.035	8456.476	1606.921	1689.943	-130.410	-137.148	-54.349	-51.990
7-Mar	3520.00	-1600.416	3485.107	2857.957	696.464	571.135	-43.518	-35.687	-80.214	-83.775
8-Mar	3520.00	-674.952	8957.102	8157.217	1789.988	1630.139	-265.202	-241.519	-49.148	-53.689
9-Mar	3520.00	-1237.032	6746.224	7908.855	1348.166	1580.507	-108.984	-127.766	-61.700	-55.099
10-Mar	3520.00	not complete								
11-Mar	3520.00	not complete								

12-Mar	3520.00	not complete								
13-Mar	3520.00	-9206657.640	4384.464	3918.990	876.192	783.171	-0.010	-0.009	-75.108	-77.751
14-Mar	3520.00	not complete								
15-Mar	3520.00	no data								
16-Mar	3520.00	-50093328.600	9196.290	8389.355	1837.788	1676.530	-0.004	-0.003	-47.790	-52.371
17-Mar	3520.00	not complete								
18-Mar	3520.00	no data								
19-Mar	3520.00	no data								
20-Mar	3520.00	not complete								
21-Mar	3520.00	-4937445.216	5709.000	4653.981	1140.887	930.052	-0.023	-0.019	-67.588	-73.578
22-Mar	3520.00	-1733624.424	1897.333	1603.441	379.163	320.432	-0.022	-0.018	-89.228	-90.897
23-Mar	3520.00	-1149188.712	1298.214	1062.225	259.435	212.275	-0.023	-0.018	-92.630	-93.969
24-Mar	3520.00	-12246728.112	3797.209	3057.503	758.835	611.012	-0.006	-0.005	-78.442	-82.642
25-Mar	3520.00	-1836443.088	2116.030	1742.353	422.868	348.192	-0.023	-0.019	-87.987	-90.108
26-Mar	3520.00	-1691325.912	1882.412	1572.300	376.181	314.209	-0.022	-0.019	-89.313	-91.074
27-Mar	3520.00	-2012685.360	2212.785	1847.740	442.203	369.253	-0.022	-0.018	-87.437	-89.510
28-Mar	3520.00	-66602251.560	10633.827	########	2125.065	2199.098	-0.003	-0.003	-39.629	-37.526
29-Mar	3520.00	-57287404.368	9201.411	8767.573	1838.811	1752.113	-0.003	-0.003	-47.761	-50.224
30-Mar	3520.00	not complete								
31-Mar	3520.00	no data								
March Average	3520.00	**-5414088.003**	**6216.593**	**5984.067**	**1242.325**	**1195.857**	**-0.023**	**-0.022**	**-64.707**	**-66.027**

Minimum, Maximum, Average, and Sum of all Sensors

SENSOR	MIN	MAX	AVERAGE	SUM
Relative Humidity				
Relative Humidity (High) (%)	16.20	85.80	26.75	1485755.70
Relative Humidity (Middle) (%)	16.50	62.40	27.08	1503921.60
Relative Humidity (Low) (%)	19.30	53.40	32.40	1799526.00
Outside Relative Humidity (%)	15.00	97.40	67.20	3732327.20
Temperature				
Temperature (High) (degrees F)	69.28	78.90	74.41	4132813.32
Temperature (Middle) (degrees F)	68.63	75.50	73.53	4084179.40
Temperature (Low) (degrees F)	59.02	72.60	66.73	3706501.72
Outside Temperature (degrees F)	18.96	77.80	42.68	2370416.09
Light				
Pyranometer (W/m^2)	-6999.00	0.05	-257.12	-14281379.85
Photometer #1	-6999.00	182.40	-5267.90	-292599992.99
Photometer #2	-6999.00	-1470.00	-6998.64	-388732390.00
Battery				
House Battery Voltage (V)	48.32	58.35	54.02	3000253.43
House Battery Current (A)	-101.50	75.00	0.14	7772.91
House Battery Power (W)	-5020.00	4059.00	7.81	433702.35
House Battery Energy (Wh)	-16.70	10.19	0.73	40808.38
Solar Panels				
Photovotaic Array #1 Current (A)	-0.27	48.17	4.79	266188.41
Photovoltaic Array #2 Current (A)	-0.19	36.39	4.47	248136.29
Photovoltaic Array #1 Power (W)	-15.52	2609.00	258.96	14383787.86
Photovoltaic Array #2 Power (W)	-10.70	1971.00	241.30	13402689.81
Photovoltaic Array #1 Energy (Wh)	-0.26	43.48	4.32	239729.80
Photovoltaic Array #2 Energy (Wh)	-0.18	32.85	4.02	223378.16
DC Fridge				
Fridge Current (A)	-0.85	2.76	0.44	24318.57
Fridge Power (W)	-46.12	147.80	23.63	1312737.98
Refridgerator Energy (Wh)	-0.77	2.46	0.39	21878.97
Appliances				
Furnace Energy (Wh)	0.00	85.00	30.12	1673066.10
Heat Pump Energy (Wh)	0.00	1.50	0.00	274.50
Hot Water Backup Energy (Wh)	0.00	72.80	2.16	119818.25
Hot Water Circulator Energy (Wh)	0.00	0.38	0.20	11169.38
Cooktop Energy (Wh)	0.00	18.00	0.01	290.25
Heat Trace Energy (Wh)	0.00	6.75	4.81	267131.63
Communications Energy (Wh)	0.00	1.13	0.57	31591.87
Clothes Washer Energy (Wh)	0.00	19.50	0.52	28628.18
Dishwasher Energy (Wh)	0.00	10.50	0.04	2228.51
Office Energy (Wh)	0.00	0.00	0.00	0.00
Microwave Energy (Wh)	0.00	24.00	0.18	10230.34

Miscellaneous Critical Loads (Wh)	-2.31	30.32	2.13	118151.23
Datalogger				
Logger Voltage	13.06	13.61	13.30	738876.40
Logger Temp	48.08	93.10	70.38	3908950.91
Reference Temp	47.08	90.10	67.97	3775590.91
Total House Energy				
Critical Load Energy (Wh)	0.00	115.00	5.62	312152.15
Sum of Critical Loads (Wh)	0.00	89.44	3.49	194000.92
Purchased Utility Energy (Wh)	0.00	190.00	37.97	2109045.00
Sold Utility Energy (Wh)	0.00	65.00	3.06	170160.00
Energy In (Wh)	-0.12	204.49	46.28	2531855.49
Energy Out (Wh)	0.66	201.53	44.81	2488839.31

Difference between purchased and sold utility energy (kWh):	-1938.89

Appendix 2

Photos

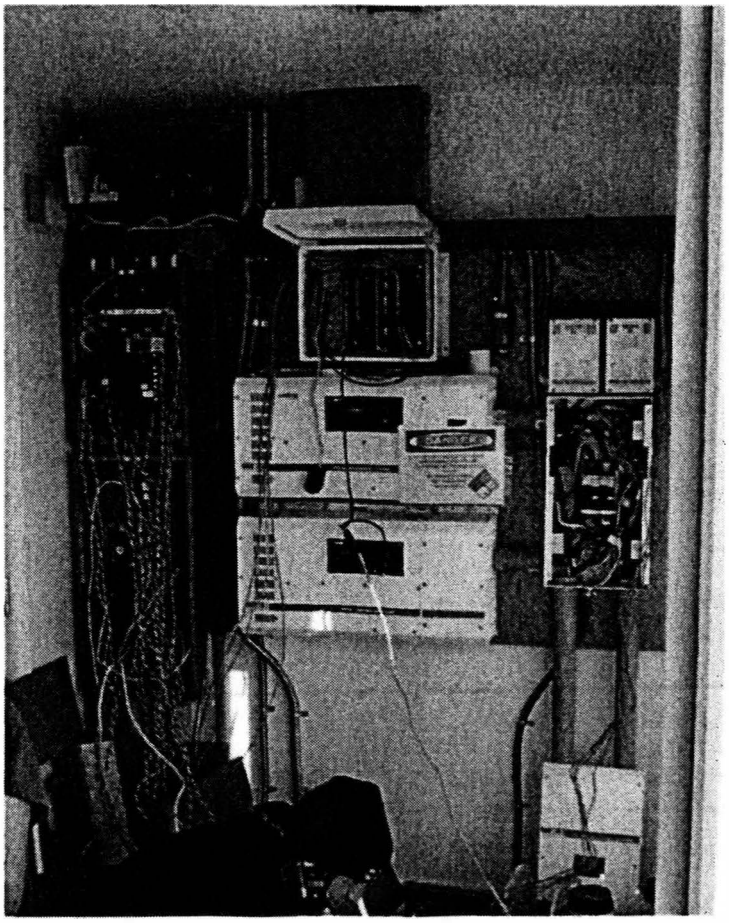

This shows the installation of the sensors. The Campbell Scientific datalogger is in the top center box, the DC load sensors in the right box, and the AC wattnodes are connected in the two electrical panels on the left.

(The NREL representative, Mike Wassmer is in the bottom of the picture)

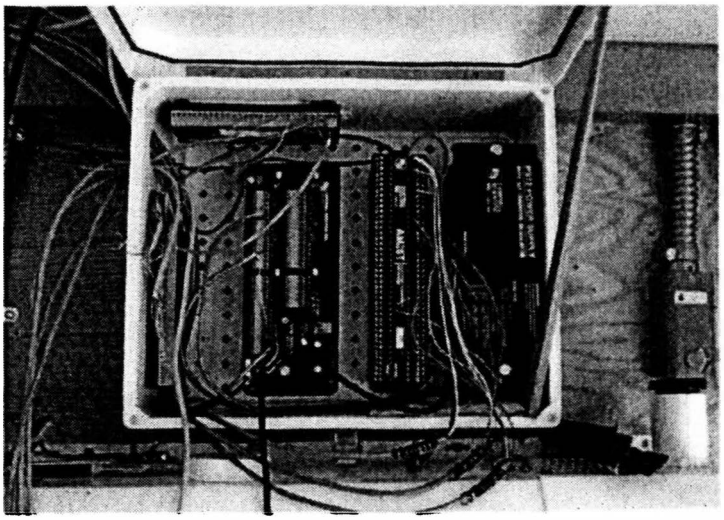

This is a close up picture of the Campbell Scientific datalogger and multiplexer with all the wires running to it.

This is a photo of the 2002 UMR/RTI competition solar house. The pyranometer is in the middle of the two modules, sticking up above the rest of the house.

These are the temperature and humidity sensors in the 2002 house.

An Overview of Security Issues in a Digital City

Bonnie Yates, Department of Information, Science and Technology, School of Management & Information Systems, University of Missouri – Rolla, Rolla, MO 65401, email: bjyrg7@umr.edu

Faculty Advisor: Dr. Bih-Ru Lea, School of Management & Information Systems, University of Missouri – Rolla, Rolla, MO 65401, email: leabi@umr.edu

Abstract

This paper addresses what a digital city is, the advantages a digital city provides and how security must be considered when developing and deploying a digital city. Digital cities provide a dynamic living space that cannot be founded on static technology. Instead it must have its foundation on dynamic technology. Included in dynamic technology is security, which is a common thread among digital cities. Without proper security, digital cities cannot expand to their full potential.

1. Introduction

Digital Cities are not just about globalizing businesses and earning companies more profit. It is also about creating rich information spaces for everyday life. Security is becoming a focal point for designing, developing, and deploying software security [10]. Security is the one common thread that runs through most of the articles available on digital cities. Security must be a high priority in order for Digital Cities to become fully functional and to be used as they are intended. While the Internet makes research and businesses global, life is inherently local. The Internet is no longer just for universities and businesses; but is now becoming a fixture in everyday life [3]. Each digital city has its own goal and uses different means in obtaining those goals.

This paper addresses what a digital city is, the advantages a digital city provides and how security must be considered when developing and deploying a digital city.

2. Digital City Overview

What is a digital city? A digital city is the virtual representation of a physical city, such as a real city, town or village, on the Internet through applications of advanced information and communication infrastructure [5]. For example, Digital City Kyoto establishes a strong connection and representation to physical Kyoto, as shown in Figure 2-1 [1].

Citizens of a digital city can share knowledge, experience and mutual interests [3]. Services offered by a digital city include all kinds of information about the real city [5], possibilities for communication and social interaction [5], access to social environments, community services, municipal information and e-commerce [4], and opportunities to engage in

business transactions, personal ambition, and social activity [2]. AOL Digital City focuses on local information for each city it represents, as shown in Figure 2-2. If you want to visit a particular city, such as New York City, access AOL's digital cities home page at www.digitalcity.com and choose New York. From there you can locate local information such as shopping, commerce, hotels, the yellow pages, and the like.

Figure 2-1. 3D Digital City Kyoto

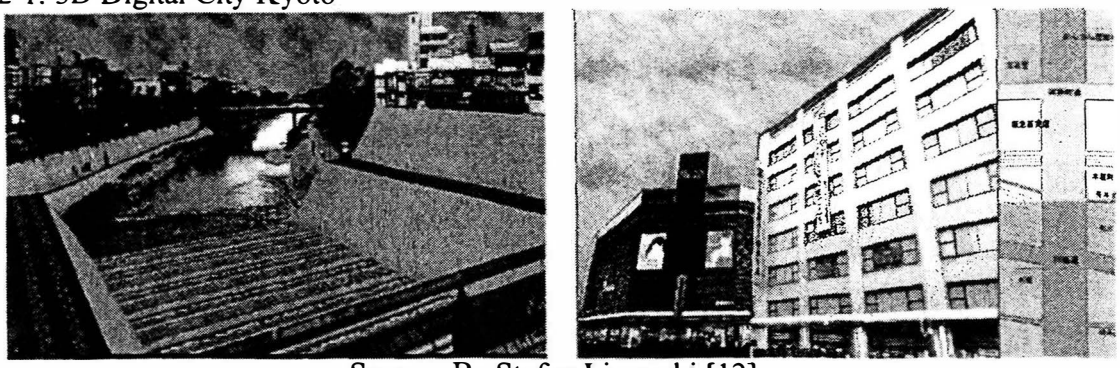

Source: By Stefan Lisowski [12]

Figure 2-2. AOL Digital Cities (www.digitalcity.com)

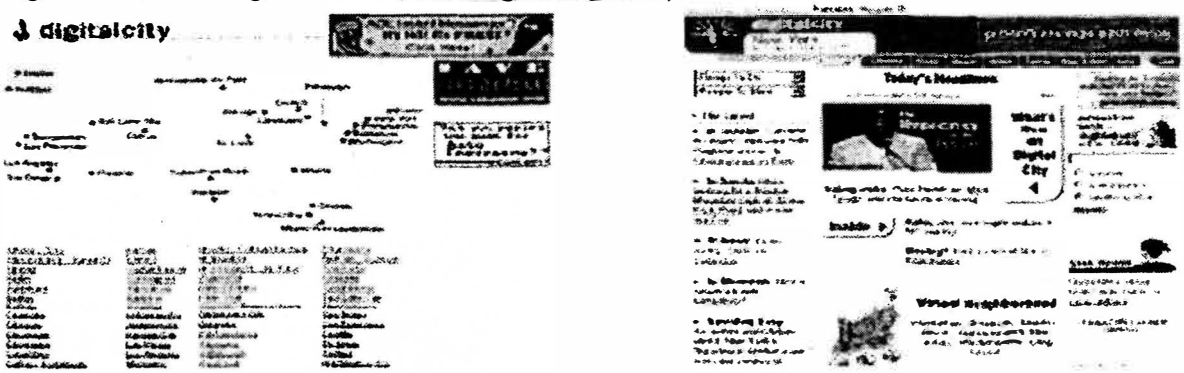

Digital city is a virtual place where people can go to meet other people, not just from their geographical area but from around the world. They are able to develop relationships, share mutual interests, offer advice, and exchange solutions to problems. Therefore, citizens of a digital city are able to participate in social interaction, economic and commerce activities and have the opportunity to improve their everyday life. The Virtual Helsinki project (http://www.hel.fi/infocities/) is one of these examples [13]. The project was named Helsinki Arena 2000 and was a four year project which began in 1996. An example of Virtual Helsinki is depicted in figure 2-3. Virtual Helsinki was an attempt to put all the municipality's public services online. It gave the citizens of physical Helsinki the ability to view public areas in real time, access online services, make purchases and place video phone calls through their personal computers [11].

Figure 2-3 Virtual Helsinki

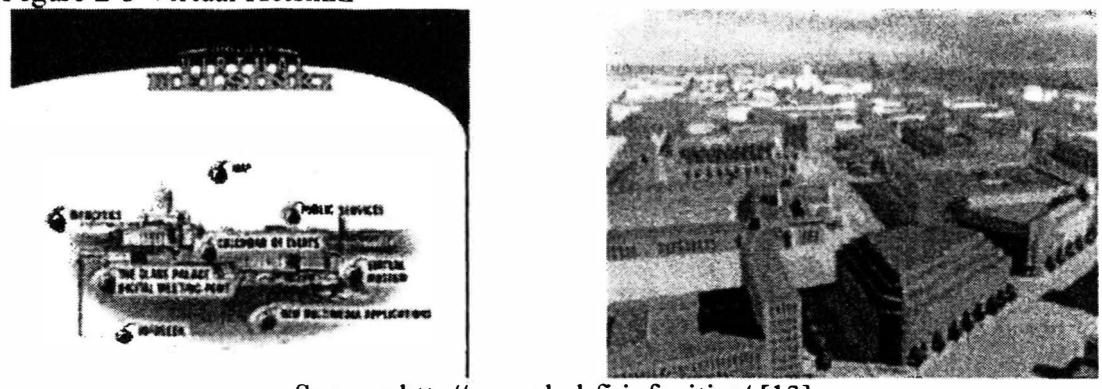

Source: http//www.hel.fi.infocities/ [13]

The advantages of a digital city encompass several aspects. The digital city provides social interaction, economic and commerce activities, and the ability to improve the efficiency of daily life.

With social interaction people are able to share experiences and knowledge with each other, to make recommendations, and to discuss a wide range of topics. It also enables people to get to know other people and to seek out affiliation, companionship, and support [24]. Digital cities can also strengthen family ties by providing a means of communication. A site with local everyday life eventually becomes a nexus linking residents to visitors from overseas [12]. Digital City Kyoto, Virtual Helsinki, and AOL's digital cities are just a few of the well-known examples in existence. Each digital city has something different to offer depending on what they want to accomplish. For example, Digital City Kyoto was developed as a social information infrastructure; AOL collects both tourist and shopping information of a corresponding city and provides for local advertising opportunities for vertical markets; and Virtual Helsinki was developed so that their residents could do anything in the virtual city that can be accomplished in the physical city, which not only encompasses social interaction but also provides opportunities to improve the efficiency of everyday life.

The success of these cities indicates that people need these services for their everyday life. Residents of Helsinki are able to access their municipal public information services online [11]. In this virtual city, if you forget your friend's phone number, all you have to do is logon to your computer, take a stroll down the 3D version of the street in which they live on, and ring the virtual doorbell. AOL makes information retrieval convenient and easy so those who either live in the area or perhaps those wanting to visit the area can get access to hotels, entertainment, restaurants, and so on.

Digital cities also provide opportunities for economic and commerce activities. According to the Census Bureau of the Department of Commerce, the fourth quarter U.S. retail e-commerce was $18.4 billion (adjusted) and $21.4 billion (unadjusted) [25]. These figures indicate that digital cities, such as AOL's Digital Cities, are providing site visitors with the opportunity for economic activities. More and more people are doing their shopping online

through digital cities rather than trying to run "all over town" trying to find what they are looking for.

3. Important Issues involved in a Digital City

In addition to technological problems, non-technical problems have also been encountered. A dynamic living space cannot be founded on static technology [12]. It must be founded on dynamic technology, constantly moving and changing. The research gaps identified are currently based on dynamic technology and include international focus, government involvement and security.

3.1 International Focus

Digital cities give us the ability to overcome the geographical limitations. In these environments, we can meet people who have different cultural backgrounds and living in different geographical areas. Since digital cities create regional information spaces in the Internet, cross-cultural communication becomes an essential issue [7]. Intercultural interactions in daily life become necessary if digital cities are to thrive.

There are two essential reasons for discussing cross-cultural and intercultural communication in the context of digital cities. First, almost all cities are becoming 'melting pots,' meaning that citizens are becoming more diverse. A digital city can play a major part in building a bridge to cross the cultures. Second, a digital city will represent a real city on the Internet. Millions of people are using the Internet to visit different cities and countries; therefore, cross-cultural and intercultural communication must be supported, even though the main purpose of digital cities is to support the everyday life of local residents [12].

Two major issues to resolve are copyright infringement and mistranslations. For example, both the United States and England speak English. However, some of our words, even though they are spelled the same, have a different meaning.

3.2 Government Involvement

The main question is: should government be responsible for providing Internet security measures or should it be a combination of government, those who are developing the digital cities, or someone in between. The growth of computer-based crime has led to criminalization of certain behavior on the Internet: throughout the 1990s there was growing law enforcement attention and legislation relating to abuses of computers in both private and public sectors [14].

The public's concern over privacy and security is growing as the Internet grows. The evidence is mounting and the necessary remedy just might be a protective framework that includes legislative provisions. In the information society and economy, law, like location, will still matter [9].

3.3 Security

There are several types of security measures available today. Will it be adequate as technology changes? Practically speaking, the security of most sites on the Internet today rests on four key pieces [18]:

1. Firewalls that partly insulate servers (and a company's intranet systems) from the public Internet
2. Secure Sockets Layer (SSL) for encrypting sensitive data, such as credit card numbers and other billing information
3. Passwords to authenticate individuals
4. System hardening, to decrease the likelihood of a break-in.

Enterprises today can no longer afford to consider security only after the application has been constructed: irreparable security compromises may have already been exposed, and fixing such problems requires tremendous effort and resources [10]. Users rely on a digital city to provide the security they require. Just as we have social laws in physical cities such as peeping-tom laws, digital cities should introduce social guidelines that provide the security people need to feel comfortable about joining the information space [13]. A range of technologies is going to be needed in order to keep up with the Internet which is dynamic and changing everyday. Some of the ranges may include encryption, authentication, password controls, and firewalls. Since the Internet is dynamic, threats change, business needs change and technologies change. Ongoing research and analysis are needed to keep up to date with potential attackers [13].

A single-dimensional security approach is no longer sufficient. A multi-dimensional approach is now required to discourage the ever-more-sophisticated threats that a digital city can face [6]. A multi-dimensional security approach uses a range of security measures to ensure a comprehensive security system.

Security generally falls into three categories: prevention, detection, and response. Prevention comes in the form of a firewall. A firewall helps to prevent unwanted and unauthorized communication into or out of the network, and to allow an organization to enforce a network security policy on traffic flowing between its network and the Internet [15]. A firewall enables employees who need to access the Internet to perform their job, do so with confidence. Firewalls are like a fence around a house, they are a necessary part of the overall security, alone however, it is insufficient to provide the necessary security for a digital city. Another problem with using firewalls only is that this setup does not provide protection from the people the FBI says are responsible for most computer and network crime: employees already on the inside of the network [6].

One form of detection is a server scanner. Like door alarms and motion detectors in a building, intrusion and misuse detection devices add an important dimension to Internet security [6]. Response can include the shutting down of log-in accounts or sending an e-mail message to the appropriate administrators. A response is like alarms on a building that sound off and also call the police and building manager. In addition to sounding an alarm, sending an e-mail message, or transmitting a message pager, misuse and anomaly detector systems can take

defensive actions such as shutting down a log-in account, shunning connections from an attacker's Internet address, and replacing damaged files [6]. Unfortunately, there is no one program that can provide all three layers of the multi-dimensional security system. Usually one program will cover only one or two aspects of security.

4. Security and the Digital City

In the U.S., alone, nearly 300 virtual cities, representing their counterpart physical cities, have emerged over the past five years. They provide a range of services to city inhabitants and plenty of others, including those wishing to do business over the Internet [2]. With the addition of new Internet users on a daily basis, the number and variety of information that is transmitted on computer networks has increased. At the same time, the number of security attacks and aggressors has also increased. This incipient number of threats over the information systems forces us to make an effort to improve information systems security and its communication [17]. Users must feel confident that their personal information is kept secure, if not; they are less likely to use the Internet.

Webster's Dictionary defines security as a safeguard, protection, feeling secure, freedom from fear, doubt, and the like [8]. However, it is most commonly defined as "keeping the wrong people out, while letting the right people in" according to Avolio [1998]. Initially, the Internet was used primarily by both the government and academic community. Today, it is an indispensable business tool involving millions of users in nearly every country on the planet [6]. Security, particularly Internet security, is vague terms that may mean various things to different people [15].

The impact of not having proper security can be devastating. For example, the Federal Bureau of Investigation was forced to take down its Internet site after hackers began an attack against it. It remained inaccessible for several days, along with the site for its National Infrastructure Protection Center, which helps investigate computer crimes [22]. Another example is a series of distributed denial-of service attacks interrupted service at many high-profile sites, including Yahoo!, CNN, and eBay. These attacks have disrupted businesses with direct costs for cleanup, indirect costs through lost productivity, and, in some cases, lost revenue [18]. There seems to be no end to these types of stories. Complex attacks are not only performed by hackers but also because of simple mistakes. For example, a programmer at Northwest Airlines turned their encryption program off to make changes in the code. The programmer forgot to turn the encryption program back on and gave access to thousands of credit card numbers to anyone who logged onto their Web site. Security must be provided well if digital cities are to be used to their full potential. In addition to security, privacy and trust must be addressed.

Another issue related to security is the privacy concern. Privacy is usually interpreted as the unauthorized collection, disclosure, or other use of personal information as a direct result of electronic commerce transactions [21]. Privacy is better thought of as a personal space that is free from impedance by other people and businesses. If individuals feel that their personal information is not kept private, they are unlikely to visit, and do business, in digital cities. Therefore, free flow of information should equal the benefits that citizens receive from that free flow of information. In order for privacy to be protected, several aspects must be aggregated.

Some people believe that the government should be responsible for protecting their security. On the flip side of the same coin, others believe that if digital cities are regulated by the government they will not be able to grow and expand. A balanced approach to regulation may gain majority support within a country, but we question whether regulation can be established internationally, at least in the near future [22]. Therefore, Wang, et. al, propose that the government, business and individuals are the three main parties should be involved in dealing with security issue [21]. Government should promote strong privacy laws for both the public and private sectors; establishing independent privacy commissions to oversee the implementation of these laws; educating the public about privacy issues; encouraging business self-regulation. On the other hand, businesses need to promote self-regulation for fair information practices. Finally, individual should adopt privacy enhancing technologies, such as network and information security tools.

5. Conclusion

Each digital city has its own goal. AOL's digital cities aim at growing their business in so-called vertical markets. Helsinki is planning the next generation metropolitan network. In Kyoto, a social information infrastructure for urban life is being tested [1]. In all of these cities, security must be addressed in order to build digital cities that are reliable. It is often stated that one of the most obvious characteristics of virtual communities is that they are restricted by geographic or time "borders."

Security not only affects whether users will participate in a digital city but also to what extent they participate in it. If a user feels that proper security measures are not available, the likelihood they will participate in the digital city is slim. A secured digital city would therefore enhance the advantages of participating in it. For example, if a consumer feels confident in the security measures available in a digital city, they are more likely to participate in various activities.

One area of debate concerning security measures is who should be responsible for providing those measures. There are those who feel that the government should be responsible for providing the laws for security measure while others do not want the government involved. They believe that the government would stifle the expansion of the digital city. However, the author feels that the security should be a shared responsibility among the participants, business or the digital city providers, and the government in order to fully realize the anticipated advantages of participating in a digital city.

6. Acknowledgement

I gratefully acknowledge OURE for providing the opportunity to expand my horizons through research. I would like to thank Dr. Bih-Ru Lea, my faculty advisor and mentor, for her support, encouragement and guidance.

Reference

[1] Ishida, Toru; 2002; "Digital City Kyoto," Communications of the ACM, Vol. 45 (7), pages 76 – 81.

[2] Sairamesh, Jakka; Lee, Allison; Anania, Loretta; 2004, "Information Cities," Communications of the ACM, Vol. 47 (2), pages 29 – 31.

[3] Akahani, Jun-ichi; Isbister, Katherine; Ishida, Toru; 2000, "Digital City Project: NTT Open Laboratory," CHI 2000, pages 227 – 228.

[4] Ferguson, Donald; Sairamesh, Jakka; Feldman, Stuart; 2004, "Open Frameworks for Information Cities," Communications of the ACM, Vol. 47 (2), pages 45 – 49.

[5] Van den Besselaar, Peter; Tanabe, Makoto; Ishida, Toru; 2002, "Introduction: Digital Cities Research and Open Issues," Digital Cities II, Springer-Verlag Lecture Notes in Computer Science.

[6] Avolio, Frederick M.; 1998, "A Multi-Dimensional Approach to Internet Security," Putting it Together, pages 15 – 22.

[7] Ishida, Toru; Akahani, Jun-ichi; Hiramatsu, Kaoru; Isbister, Katherine; Lisowski, Stefan; Nakanishi, Hideyuki; Okamoto, Masayuki; Miyazaki, Yasuhiko; Tsutsuguchi, Ken; 1999, "Digital City Kyoto: Towards A Social Information Infrastructure," Cooperative Information Agents III, pages 34 – 46.

[8] Guralnik, David (Ed.); 1971, Webster's New World Dictionary of the American Language, page 539.

[9] Clarke, Roger; 1999, "Internet Privacy Concerns Confirm the Case for Intervention," Communications of the ACM, Vol. 42 (2), pages 60 – 67.

[10] Wang, Huaiqing; Wang, Chen; 2003, "Taxonomy of Security Considerations and Software Quality," Communications of the ACM, Vol. 46 (6), pages 75 – 78.

[11] Geary, James; 1998, "Digital Cities," Time.com, Vol. 151 (26).

[12] Ishida, Toru; 2004, "Activities and Technologies in Digital City Kyoto," www.digitalcity.gr.jp/DigitalCityKyoto20040601.pdf.

[13] Ishida, Toru, Isbister, Katherine; 2000, "Understanding Digital Cities," Digital Cities: Technologies, Experiences and Future Perspectives, Springer-Verlag Lecture Notes in Computer Science, Vol. 1765.

[14] Blumenthal, Marjory; Clark, David; 2001, "Rethinking the Design of the Internet: The End-to-End Arguments vs. the Brave New World," ACM Transactions on Internet Technology, Vol. 1 (1), pages 70–109.

[15] Oppliger, Rolf; 1997, "Internet Security: Firewalls and Beyond," Communications of the ACM, Vol. 40 (5), pages 92-102.

[16] Cranor, Lorrie Faith; 1999, "Internet Privacy," Communications of the ACM, Vol. 42 (2), pages 29-31.

[17] Sierra, J.M.; Ribagorda, A; Munoz, A, Jayaram, N.; 1999, "Security Protocols in the Internet New Framework," IEEE, 0-7803-5247, pages 311-317.

[18] Treese, Win; 2000, "Living on the Internet Plateau," Putting It Together, Vol. 4 (3), pages 9-11.

[19] Xiao, Lu; 2002, "Digital City Examples," http://filebox.vt.edu/users/lxiao1/Digital%20City%20Examples1.ppt

[20] Stotlterman, Erik; 1999; "Technology Matters in Virtual Communities," SIGGroup Bulletin, Vol. 20 (2), pages 7-9.

[21] Wang, Huaiqing; Lee, Matthew; Wang, Chen; 1998, "Consumer Privacy Concerns about Internet Marketing," Communications of the ACM, Vol. 41 (3), pages 63-70.
[22] Dekleva, Sasa; 2000, "Electronic Commerce: A Half-Empty Glass?" Communications of AIS Vol. 3, (18), pages 1-99.
[23] Sproull, Lee; Patterson, John F.; 2004, "Making Information Cities Livable," Communications of the ACM, Vol. 47 (2), pages 33 – 37.
[24] Girgensohn, Andreas; Lee, Allison; 2002, "Making Web Sites Be Places for Social Interaction," Communications of the ACM, pages 136 – 145.
[25] Scheleur, Scott; King, Carol; Shimberg, Michael; 2005, "Quarterly Retail E-Commerce Sales 4th Quarter 2004," United States Department of Commerce News, http://www.census.gov/mrts/www/ecomm.html

Abstract

The premise of this research is the ability to use electricity to detect skin cancer. The study considers the electrical characteristics of the skin and skin cancer – that is, its ability to resist electrical current and store electrical energy – at both low and high frequencies. Low frequency measurements are taken using an impedance spectrometer in the frequency range of 1 kHz to 1 MHz. High frequency measurements are taken using a network analyzer in the 300 MHz to 3 GHz frequency range. A probe is used on each machine that either passes a small electrical current through the skin or looks for an electrical reflection from the skin surface. Using the input and output signals of the probe, data can be formed about the impedance of the skin. Using preliminary impedance data, 85% to 100% of the tumors in a test set were correctly diagnosed.

I. INTRODUCTION

Skin cancer is the deadliest form of cancer, with almost one million new cases reported each year in the Americas. The current detection of skin cancer is rudimentary at best—a biopsy is taken of a suspect lesion, a lesion that is detected visually by certain patterns in the skin. Once the lesion is large enough for one to question whether or not it is malignant, the tumor has already grown a fair amount. Currently, the best way to defeat cancer is to detect it early. Therefore, by incorporating a new method of detection that is quick, easy and accurate, skin cancer can be detected early so the patient has a much better chance of defeating the disease.

Two different types of cancer were investigated: basal cell carcinoma (BCC) and melanoma. Melanoma is the deadliest form of skin cancer. With current techniques in dermatology, certain forms of skin cancer (like BCC) have a high cure rate (better than 95%) if detected and treated early. With the help of a local dermatologist, patients that were identified as having possibly cancerous lesions were asked to have measurements taken in the lab for data analysis. Then the patients had a biopsy taken of the lesion and a pathological examination of the lesion was performed. Results of the pathological analysis were compared to data obtained in the study.

II. DATA COLLECTION TECHNIQUES

Two different instruments were used to take data on each lesion. One instrument was the impedance spectrometer. This apparatus measured impedance at low frequencies—from 1-1000 kHz. Data points were recorded following a logarithmic scale in the range of frequencies. A probe was used to obtain data, which is shown below in figure 1. Before the data was taken, the skin was soaked with a 0.9% saline solution. This increased the conductivity of the top layer of skin. The total size of the probe was about 10 mm. There were two source electrodes that injected current into the skin. The source electrodes varied the current between each other such that different skin depths could be measured. A guard electrode separated the source and sink electrodes so that surface currents were reduced. The other electrode was the sink which took in the current injected by the source electrodes. The impedance spectrometer then used this data to plot the impedance magnitude and phase. Then the data points were analyzed and plotted to determine the diagnosis of the lesion.

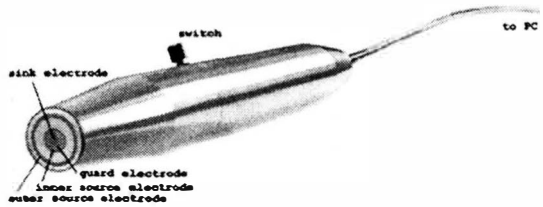

Figure 1: Impedance Spectrometer Probe (picture taken from [1])

The second method used a network analyzer to obtain data. The probe used with the spectrum analyzer was very small—about 2 mm in diameter. A breakdown of the probe is shown in figure 2. It was essentially an open-ended coaxial probe which measured the reflection

coefficient of the medium, which in this case was skin. Using this equipment, impedance measurements in the frequency range of 0.3-3 GHz were taken (this is in the microwave spectrum). The method used with the spectrum analyzer to take data was slightly different than that of the impedance spectrometer. Instead of injecting current, the probe sent microwaves into the skin and then measured the reflected waves. Using the difference between the output and reflected waves, the impedance can be calculated to some extent.

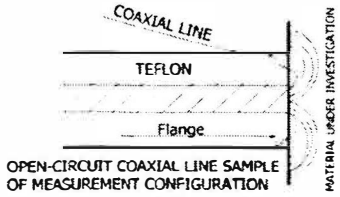

Figure 2: Breakdown of Probe Used to Measure Impedance at Microwave Frequencies (picture taken from [2])

Comment [d1]: Please reference Pratik's thesis
Dr. B – I don't have Pratik's thesis, I took this information off of one of your research proposals, which doesn't have the information on the paper. Please provide the information on his thesis so I can include it in the reference section.

For both probes, there were essentially three places in the vicinity of the lesion where readings were taken. These three regions are shown in figure 3 below. Position A was the first position, where the probe was placed directly on the center of the lesion. For most lesions, the impedance spectrometer covered the whole lesion. With the microwave probe (because of its small size and the speed with which measurements could be taken), several measurements were taken at different parts of the lesion. The next location, position B, was right on the periphery of the lesion. This position was used so that part of the lesion could be on the sink of the probe with the sources just on the outside of the lesion. Using this location, the goal was to be able to characterize the boundary of the lesion. Then the last location, position C, was totally off of the lesion and generally was about 1 cm away from the lesion. By taking these measurements, the normal skin (in this measurement) was compared to the data collected on the lesion. Most measurements were taken more than once—the low frequency measurements were taken twice at each location and the microwave measurements were taken four times at each location.

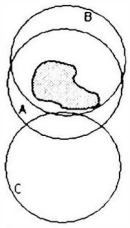

Figure 3: Three Basic Probe Positions for Measurements (picture taken from [1])

III. RESULTS

The primary function of this OURE project was to measure impedance data on patients. This data is analyzed in a variety of ways to determine the potential of these measurements to be used as a diagnostic tool for skin cancers. For example, in a previous study by this group, data

that was taken from each patient was broken down into four different impedance parts: magnitude index (MIX), phase index (PIX), real-part index (RIX) and imaginary-part index (IMIX). Different results were obtained when measuring cancerous lesions, benign lesions and normal skin. The data shown below in figure 4 was a set of basal cell carcinoma lesions [1]. The graphs are box and whisker plots. In these plots, the boxed areas represent where 50% of the data collected was observed. The line in the boxes indicated the median value. The area above the line in the box represented 25% of the data above the median, while the area below the line in the box represented 25% of the data below the median. The boxes were shaded dark to light, which represented BCC, benign and normal skin data (respectively). Whiskers extend above and below the boxes to the maximum and minimum values, respectively. From these plots, one can see that for the MIX, PIX, and IMIX data the values generally tend to be lowest in a region containing BCC. Benign lesions also had lower values than normal skin, but were higher than the BCC regions.

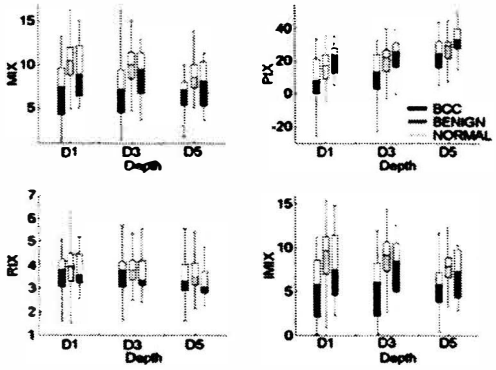

Figure 4: Box and Whisker Plots of MIX, PIX, RIX, and IMIX Data for Basal Cell Carcinoma, Benign and Normal Skin Areas (graphs taken from [1])

A statistical analysis of the probability that values were similar was also conducted [1]. Using the Wilcoxen signed rank test, the significant difference can be determined. If the probability of similarity was less than 0.05, then the values were considered significantly different. Table 1 shows all the values computed against each other. BCC stands for basal cell carcinoma, NOR stands for normal skin, BEN stands for benign lesions, and NS means not significant. Most of the values at all depths were not greater than 0.05 when comparing basal cell carcinoma to normal or benign lesions. The only exception to the rule was at depth 5 where no significant difference between normal skin and basal cell carcinoma was found.

		Depth		
		1	3	5
MIX	BCC & NOR	**0.0000007**	**0.0000018**	**0.000012**
	BCC & BEN	**0.0027**	**0.0032**	**0.037**
	NOR& BEN	NS	NS	**0.041**
PIX	BCC& NOR	**0.042**	**0.008**	NS
	BCC & BEN	**0.0001**	**0.0001**	**0.0003**
	NOR & BEN	**0.014**	**0.034**	**0.028**
IMIX	BCC & NOR	**0.0000037**	**0.0000017**	**0.000006**
	BCC & BEN	**0.0012**	**0.0018**	**0.026**
	NOR & BEN	NS	NS	NS
RIX	BCC & NOR	NS	NS	NS
	BCC & BEN	NS	NS	NS
	NOR & BEN	NS	NS	**0.015**

Table 1: Probability of Similarity Between Impedance Measurements (taken from [1])

The depth of the measurements did not change the index values very much. Values differed from skin type to skin type, but the relative difference between normal, benign and basal cell carcinoma remained.

The median values (as seen in figure 4) signified a decent difference between the benign, normal, and basal cell carcinoma skin. However, there was some overlap in the measurements. A clearer cut solution would be desirable. Since the low frequency probe was so large, more than likely normal skin was included in the measurements along with the lesion. For example, if a lesion was 2 mm in diameter it would only cover 4% of the area underneath the probe. If a smaller probe could be obtained and used, a smaller amount of error may be observed.

By using the microwave probe, data was taken on a more precise basis because the probe was small. At this time, not enough data has been compiled using the microwave equipment to support any conclusions as to whether or not the data was more accurate. Possibly a two-fold solution could result, where low impedance readings could be taken in conjunction with microwave readings and together a more accurate analysis can result.

IV. DISCUSSION OF RESULTS

There were significant differences between normal, benign and cancerous lesions. These differences need more research on why they occur and what relation they may have to cancerous properties of the skin. Some possible differences may occur because basal cell carcinoma lesions have more blood flow in them than normal skin or benign lesions. Because of the excess liquid, the impedance of the lesion area would be different than that of surrounding normal skin. Also, the top-most layer of skin above the basal cell carcinoma lesion has more water content and is thinner than normal skin. This would change the impedance measured in the lesion area as well. Usually the nuclei of cancerous lesion cells are larger than that of normal skin, which could affect impedance measurements. These differences seemed to cause a variation in the impedance of the skin as a function of frequency.

Other research that has been made on electrical impedance of the skin suggested that the impedance of the skin was different depending on age and where the impedance was measured on the subject [3]. The subjects that were studied had a fairly wide range of ages and the cancerous lesions occurred mainly in the head and neck while benign lesions tended to be elsewhere. By taking the error (by statistical means) in the normal skin impedance values for both cancerous and benign lesions, there was very little difference in values. Results of the statistical analysis can be found in Table 2 [1]. This suggested that the area and location of the lesion did not make very much difference in the patient set that was tested.

	MIX	PIX	IMIX	RIX
Average values, patients with BCC	10.2±3.0	11.8±15.9	8.7±3.8	4.4±1.6
Average values, patients with benign	10.5±3.6	12.6±17.9	9.2±4.1	4.4±1.8
Probability of similarity	0.74	0.87	0.68	0.95

Table 2: Mean and Standard Deviation of Impedance Measurements on Normal Skin (table taken from [1])

The impedance data taken at low frequencies was also analyzed using neural network techniques [4]. Impedance data of basal cell carcinoma lesions was measured over the whole range of 1-1000 kHz using the impedance spectrometer. Using neural networks, the impedance data was split into training and test sets, such that the network would not be able to memorize the data. After running the sets, the network was able to correctly classify all the lesions, both benign and malignant, with 100% accuracy. Normal skin data was used to form a base for comparison of benign and malignant lesions. This indicated that low frequency impedance tests could precisely identify basal cell carcinoma.

Another type of analysis used incorporated statistical methods [5]. The likelihood ratio test was the method used in the analysis. A sample test data set was constructed using the magnitude, phase, real and imaginary parts of impedance. Most of the results of the tests were generated using a round-robin approach. When using this analysis, the benign and basal cell carcinoma lesions were classified with 100% accuracy as well.

V. CONCLUSION

By taking measurements of electrical impedance of the skin, a reasonable amount of difference can be seen between normal skin, benign lesions, and cancerous lesions. Measurements of patients were taken at multiple frequencies using different types of equipment. Using the spectrum analyzer, impedance was measured using microwave frequencies (0.3-3 GHz). The impedance spectrometer took data in the range of 1-1000 kHz. After analyzing data taken from patients with both benign lesions and basal cell carcinoma, the benign and malignant lesions were classified with 100% accuracy using both statistical analysis and neural networks. These results were very promising, but more test data is needed to make a more definite conclusion of how to detect cancerous lesions over a wide range of skin types. If such data was obtained and a more detailed analysis was performed, then an instrument could be developed. This instrument would allow doctors and/or nurses to immediately test numerous suspicious

lesions in the office. Lesions could be tested quickly and identified early before the cancer develops so that there is a better chance of curing it. This would greatly improve the chance of defeating skin cancer for the patient and reduce the number of deaths associated with this disease.

Acknowledgements

The help and direction of the research advisor, Dr. Daryl Beetner of the University of Missouri-Rolla Electrical and Computer Engineering Department, was greatly appreciated in this research. Two research assistants also helped with this research, Deepak Narayanswamy and Kundan Chand, were of great help with taking measurements and analyzing data. The knowledge of Dr. W. Van Stoecker in the field of dermatology was a great help in the experiments. The patients from his clinic that volunteered for these experiments were also appreciated.

References

[1] Beetner D, Kapoor S, Manjunath S, Zhou X, Stoecker W: Differentiation Among Basal Cell Carcinoma, Benign Lesions, and Normal Skin Using Electrical Impedance, *IEEE Transactions on Biomedical Engineering*, 50(8): 1020-1025, 2002.

[2] Gupta K, "Detection of Skin Cancer Using Electrical Impedance, An electrical Model of Skin, and Statistical Methods," M.S. Thesis, University of Missouri - Rolla, 2004.

[3] Nicander I, Nyren M, Emtestam L, Ollmar S: Baseline electrical impedance measurements at various skin sites – related to age and sex, *Skin Research and Technology*, 3: 252-258, 1997.

[4] Dua R, Beetner D, Stoecker W, Wunsch D, "Detection of Basal Cell Carcinoma using Electrical Impedance and Neural Networks," *IEEE Transactions on Biomedical Engineering*, 51(1): 66-71, 2004.

[5] Gupta K, Beetner D, and Stoecker W, "Diagnosis of Basal Cell Carcinoma Using Electrical Impedance: A Statistical Approach," *World Congress on Medical Physics and Biomedical Engineering*, 2003.

Synthesis and characterization of Mercury vapor Coordination Species Using 1,3-Benzenedioethanethiolate (BDET)

Elizabeth Zuchek and Dr. Harvest L. Collier*

University of Missouri – Rolla MO 65401, USA

Submitted April 1, 2005

Abstract

Mercury is a major pollutant in the air today. Some possible chelators that have been used are British anti-Lewisite (BAL) 2,3-dimercaptopropanol, dimercaptosuccinic acid (DMSA), dimercaptopropanesulfonic acid (DMPS), and 1,3-benzenediamidoethanethiolate (BDET). All contain two thiol groups, which 'capture' the heavy mercury element. Due to their structure, they all differ in how well they bind to the mercury atom. BDET is the most recent and efficient chelate used. Statistics show that coal-fired power plants are the nation's largest mercury polluter. Steps have been taken to lower the emission of this toxic metal by the Clean Air Act. However, recently The Bush Administration's Air Pollution Plan undermines the act. It delays the expectations and plans of the Clean Air Act by 10 years [1].

Introduction

Mercury has been a well-known hazard ever since the mad hatter cases in 1950 [2]. The heavy metal (also known as 'quick silver') affects the brain and nervous system and could sometimes lead to death. Much of the mercury that the average person has in his/her body is through the consumption of foods. The most common food that is contaminated with mercury is fish. Mercury has been a serious problem for years, but lately the Clean Air Act has been trying to control mercury pollution. The existing Clean Air Act states that mercury pollution will be down to 5 tons per year by 2008, from the current pollution of 48 tons per year [3]. Recently President Bush set forth a plan that will weaken the Clean Air Act.

Since most mercury pollution comes from coal-fired power plants, many businesses have been trying to reduce their production of mercury before the end of the decade. The main goal of this research project was to try to find a faster, more efficient, easier way to detect the amount of mercury that is being burned off in coal. One method that was looked at was to take a common chelator, specific to mercury, and polymerize it so it works similar to pH paper. Although the interaction would be would be vapor-solid state rather then

*Department of Chemistry, University of Missouri - Rolla, 246 Schrenk Hall, Rolla, MO 65401, USA

liquid-solid state interaction. The following is a discussion about mercury pollution today, different chelators of mercury, and a possible chelator that could be used.

Regulation of Mercury

The nations largest mercury polluters are coal-fired power plants. They produce about one third of the mercury in the air [3]. The mercury vapors contaminate lakes, rivers, soil, and streams, thus producing serious health risks. At this time the Environmental Protection Agency (EPA) is required by law to issue "maximum achievable control technology" (MACT) standards for coal-fired power plants by the end of 2007 [3]. Currently the Clean Air Act (CAA) has a plan to reduce mercury pollution. If MACT is installed into most coal-fired power plants then mercury should be reduced from 48 tons per year to 5 tons a year by 2008. However, President Bush has just recently brought a plan that would weaken the progress of the CAA by 10 years! President Bush's plan would allow for 26 tons per year by 2010 and 15 tons per year by 2018 [1].

Another major difference would be that the CAA would require mercury reductions in *each* power plant, where Bush's plan would allow unrestricted emissions trading. Meaning that businesses would be allowed to buy their way out of the plan. The business would simply buy mercury emission 'credit' from other businesses instead of reducing the amount of mercury being emitted. This would lead to very toxic 'hotspots' and worsen the problems in that specific area.

Mercury Removal

Both plans require that mercury be controlled. One way that mercury is being removed from the fumes caused by coal burning uses a regenerable sorbent. It allows mercury to be recovered and recycled by triple distillation. The sorbent was developed by ADA Technologies and the entire process is called "Mercu-Re process" [4]. The process allows noble metals to repeatedly sorb and desorb mercury compounds at flue-gas conditions. This system has mercury removal effectiveness above 95%, regardless of the chemical form of the mercury [4]. The types of mercury forms are methylmercury ($HgCH_3$), mercuric chloride ($HgCl_2$), mercuric oxide (HgO), and elemental mercury (Hg). Methylmercury is the form that is very toxic and contaminates most fish. Although this technique is very effective, it is costly and takes up a great amount of space. ADA Technologies expect the cost of their system to be $866,000 per year for a 250 MW plant [4].

Chelators

A chelator is a molecule that binds to a metal ion by at least two functional groups to form a stable complex. This stable complex is known as a chelate. The first chelator, British anti-Lewisite (BAL, Figure 1A), was used for the removal of the arsenical war gas Lewisite. Due to its low solubility and horrible smell dimercaptopropanesulfonic (DMPS, Figure 1B) was produced. DMPS had better solubility and was nearly odorless. Later dimercaptosuccionic acid (DMSA, Figure 1C) was introduced with approximately the same properties of DMPS [5].

DMPS and DMSA were originally used for chelation therapy. Chelation Therapy is the removal of mercury from the body. They work fairly well, but are unable to remove mercury from the brain due to lack of access. Another problem with both complexes is that they tend to form different species other then DMSA-Hg complex (Figure 1D) and DMPS-Hg. Possible species may include $Hg_2(DMSA)_2$, $Hg_3(DMSA)_3$, or the similar species with DMPS [5]. These species would bear high negative charges and would not be very stable. Also for a drug to be effective for chelation therapy, it must bind effectively all by itself (without any additional molecular entity) [5]. Studies have shown that these chelators are somewhat effective, but not the best option.

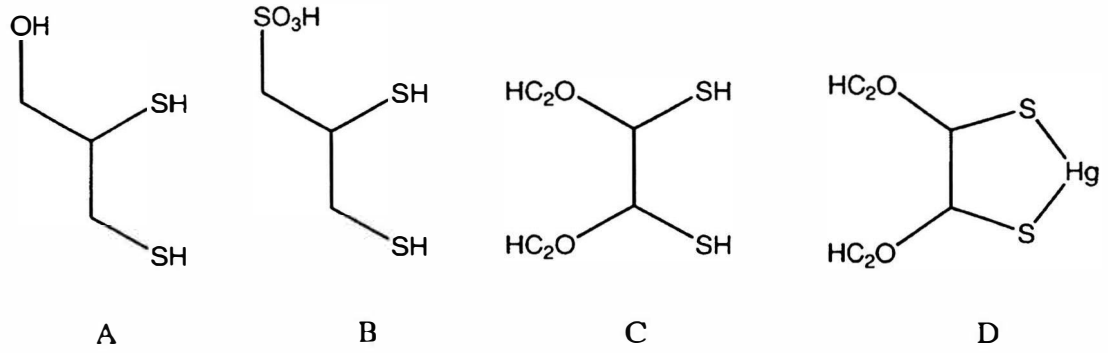

Figure 1
(A) BAL, (B) DMPS, (C) DMSA, (D) DMSA-Hg complex.

A recent complex has been developed that seems to 'trap' the mercury element more effectively. The complex is called 1,3-benzenediamidoethanethiolate (BDET, Figure 2 & Figure 3). Studies have shown that it has a high affinity for soft heavy metals such as: Cu^{+2}, Cd^{+2}, Mn^{+2}, Pb^{+2}, Hg^{+2}, and Zn^{+2}. When it binds to one of the metals the species formed precipitates out. The complex is stable under low and high pH and strongly oxidizing conditions [6].

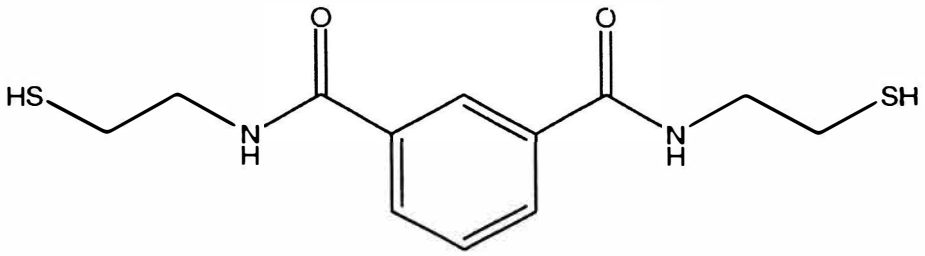

Figure 2
The stick model of BDET

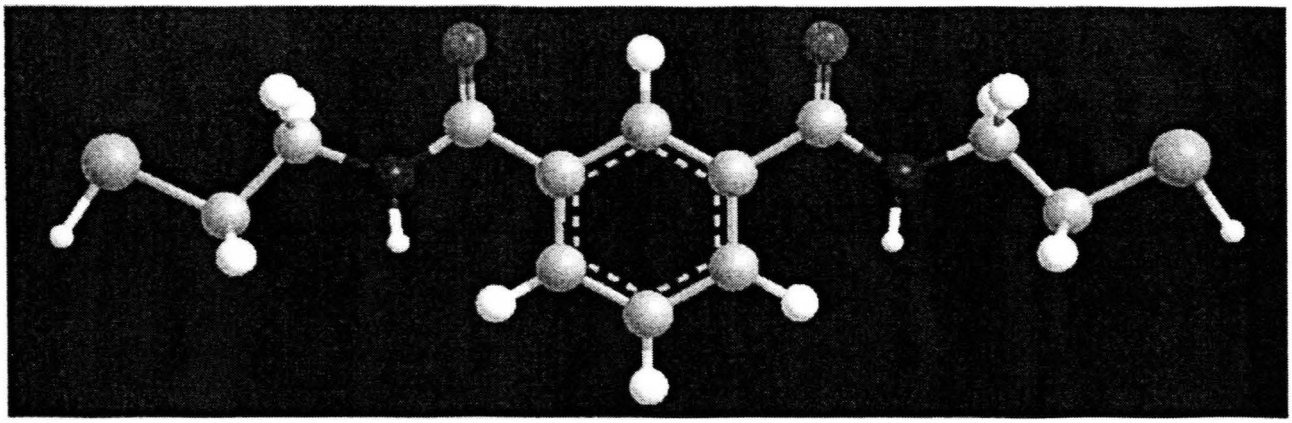

Figure 3
A ball and stick model of BDET complex. Carbon = light grey, Hydrogen = white; Oxygen = red; Nitrogen = blue; sulfur = yellow

When the mercury element binds to BDET, it will most likely form the structure shown in Figure 4 & Figure 5. The benzene ring will arrange itself so that the complex formed will be stable. The reaction that takes place has the following equation [7]:

$$C_{12}H_{16}N_2O_2S_2 + M^{2+} + 2H_2O \rightarrow C_{12}H_{14}N_2O_2S_2M\downarrow + 2H_3O^+$$

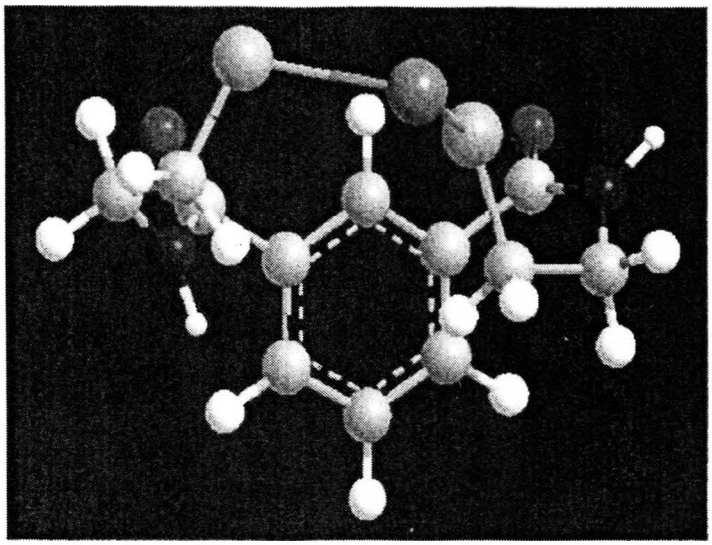

Figure 4
A side view of BDET- Hg complex. The color scheme for the atoms is the same as what was used in Figure 3 with Mercury = dark grey.

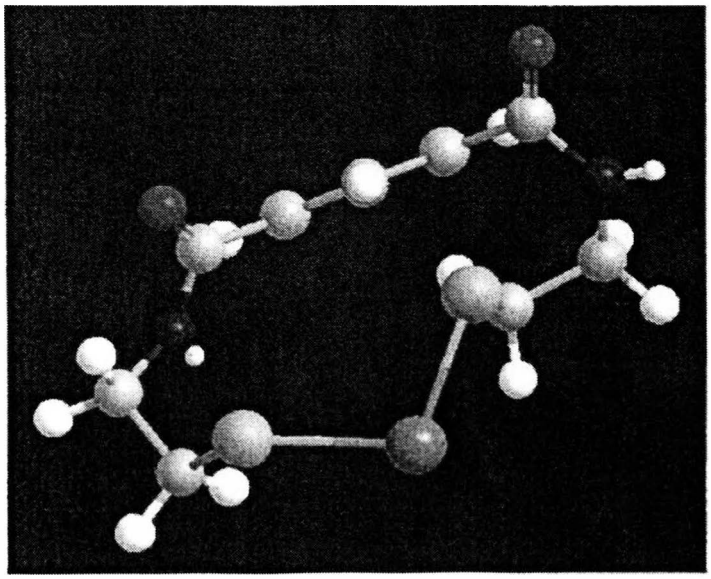

Figure 5
Top view of BDET-Hg complex. Showing the orientation of the benzene ring.

Allowing BDET to bind to a polymer (Figure 6) and still be effective is the next step in the research of this species. Still to be investigated is the mercury vapor interaction with the solid form of BDET. A possible problem would be whether or not the BDET being bound to a polymer will affect it from moving its side 'arms' to capture mercury.

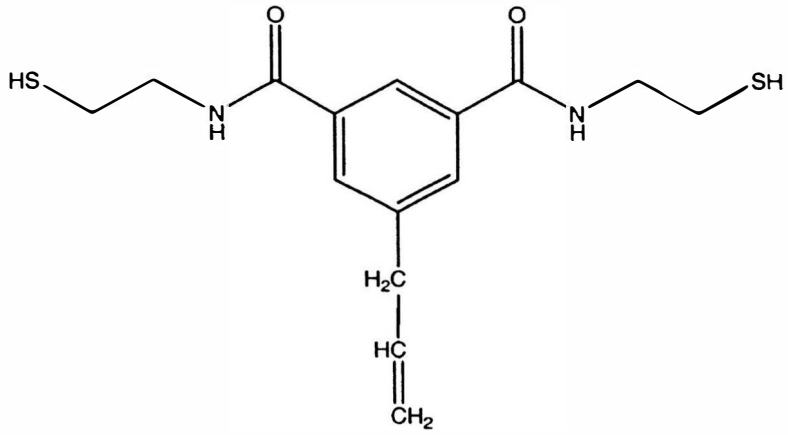

Figure 6

Conclusion

Even though mercury has been a well-known poison to humans and the environment, the control and pollution of the harmful element has just begun. Many steps have been taken to help limit and lower the emissions of mercury from coal-fired power plants, but President Bush's plan seems to dilute the CAA's plans for the future. In either case, steps have been taken to produce the best way of detecting and removing mercury from the vapors of the burning coal. However, since BDET is a fairly new compound, future studies are still to come to produce more information on the application and use of BDET.

Acknowledgement

The work and research was supported by Opportunities for Undergraduate Research Experiences (OURE) at the University of Missouri – Rolla. I would also like to thank Prof. Harvest Collier for his guidance and help throughout the year.

References

[1] http://www.nrdc.org/air/pollution/fclearsk.asp Natural Resources Defense Council: *The Bush Administration's Air Pollution Plan*
[2] Howell, Charles D.; *The Mad Hatter and the Sacrificial Lamms* http://www.redlandsfortnightly.org/howell83.htm
[3] http://www.cleanairnow.org/cleanairnow.asp?id2=10874&id3=cleanairnow& Clean Air Now: *No More Mercury: Fact Sheet*
[4] Turchi, Craig S.; Stewart, Robin M.; Broderick, Thomas E.; Albiston, Jason; *Removal and Recovery of Vapor-Phase Mercury from Flue Gas Using Regenerable Sorbents* ADA Technologies, Inc.
[5] George, Graham N.; Prince, Roger C.; Gailer, Jurgen; Buttigieg, Gavin A.; Denton, M. Bonner; Harris, Hugh H.; Pickering, Ingrid J.; *Mercury Binding to*

the Chelation Therapy Agents DMSA and DMPS and the Rational Design of Custom Chelators for Mercury Chem. Res. Toxico., 17 (8), **2004**, 999 – 1006.
[6] Matlock, Matthew M.; Howerton, Brock S.; Van Aelstyn, Michael; Henke, Kevin R.; Atwood, David A.; *Soft metal preferences of 1,3-benzenediamidoethanethiol* Water Research 37, **2003**, 579 – 584.
[7] Matock, Matthew M.; Howerton, Bock S.; Atwood, David A.; *Irreversible precipitation of mercury and lead* J. Hazardous Materials 84 (1), **2001**, 73 – 82.